



Esta sección no está terminada. Siquieres puedes echarle un ojo para ver la estructura y cómo encaja con el resto pero no merece la pena revisarla en detalle en el estado actual.

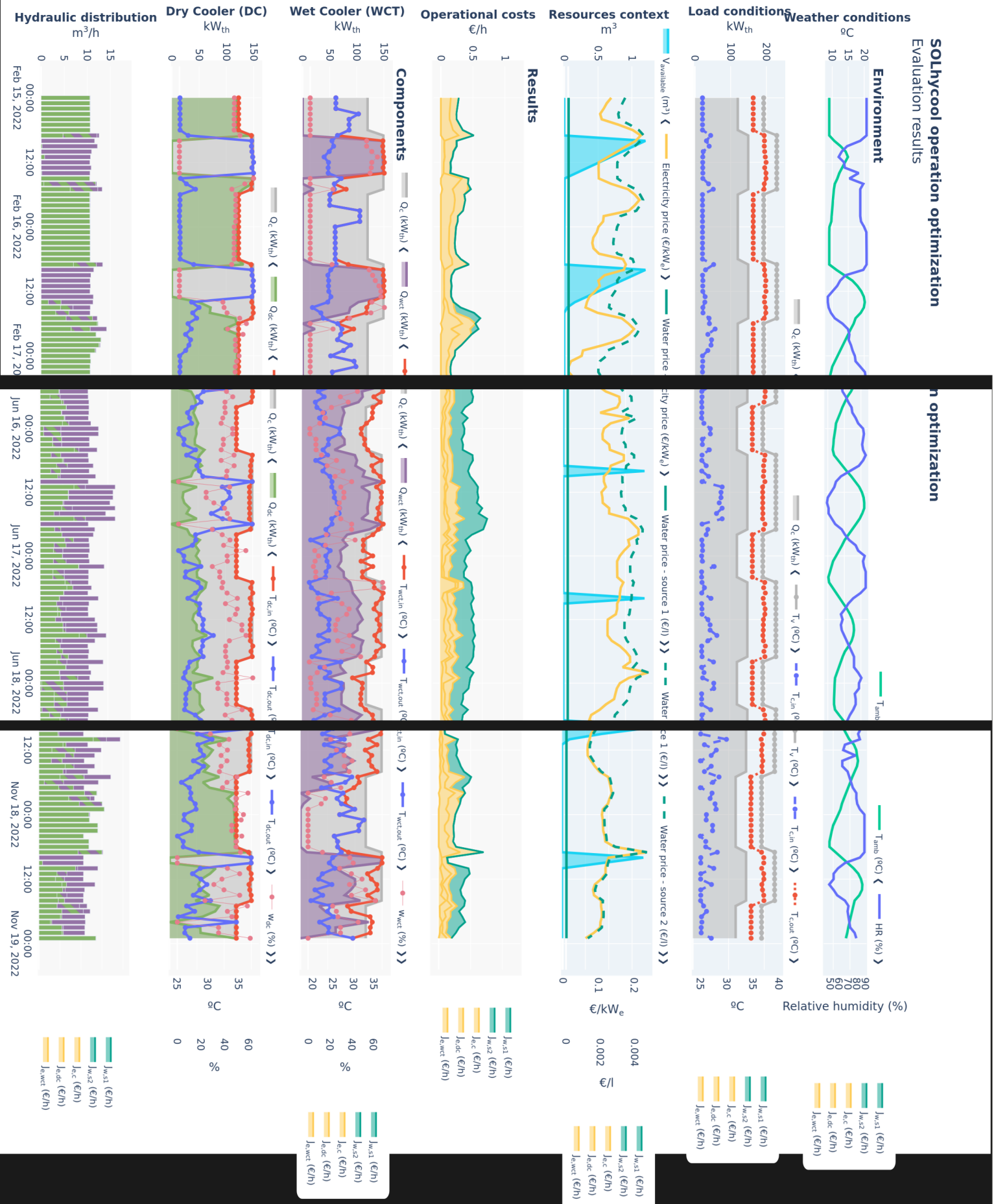
asd what is going on

What is thiiis

1. adjust
2. asdasd

SOLhycool operation optimization

Evaluation results



Model 0.1: Test

$T_{cc,out}, C_e, C_w, T_{c,out} = \text{combined cooler model}(q_c, R_p, R_s, \omega_{dc}, \omega_{wct}, T_{amb}, HR_i, T_v, \dot{m}_v)$
 $T_{cc,in} = T_{c,out}$
 $T_{dc,in} = T_{cc,in}$
 $q_{dc} = q_c \cdot (1 - R_p)$
 $q_{wct,p} = q_c \cdot R_p$
 $q_{wct,s} = q_{dc} \cdot R_s$
 $T_{dc,out}, C_{e,dc} = \text{dc model}(q_{dc}, \omega_{dc}, T_{amb}, T_{dc,in})$
 $q_{wct}, T_{wct,in} = \text{mixer model}(q_{wct,p}, T_{cc,in}, q_{wct,s}, T_{dc,out})$
 $T_{wct,out}, C_{e,wct}, C_{w,wct} = \text{wct model}(q_{wct}, \omega_{wct}, T_{amb}, HR, T_{wct,in})$
 $T_{c,in}, T_{c,out} = \text{condenser model}(q_c, \dot{m}_v, T_v)$
 $q_{cc}, T_{cc,out} = \text{mixer model}(q_{wct}, T_{wct,out}, q_{dc}, T_{dc,out})$
 $C_e = C_{e,dc} + C_{e,wct} + C_{e,c}$
 $C_w = C_{w,wct}$

As can be seen in Model 0.1, the counter is working.

Problem .1: Test

Hello, here is some text without a meaning. This text should show what a printed text will look like at this place. If you read this text, you will get no information. Really? Is there no information? Is there a difference between this text and some nonsense like "Huardest gefburn"? Kjift – not at all! A blind text like this gives you information about the selected font, how the letters are written and an impression of the look. This text should contain all letters of the alphabet and it should be written in of the original language. There is no need for special content, but the length of words should match the language.

$$\min_{\mathbf{x}, \mathbf{e}; \theta} J = f(\mathbf{x}, \mathbf{e}; \theta) = f(x)$$

with:

- Model name model

$$out_1, out_2 = f(in_1, in_2, \dots, in_N)$$

- Decision variables

$$\mathbf{x} = [x_1, x_2]$$

- Environment variables

$$\mathbf{e} = [e_1, e_2, \dots, e_3]$$

- Fixed parameters

$$\theta = [\theta_1 = X, \theta_2 = Y]$$

subject to:

- Box-bounds

$$\cdot x_1 \in [\underline{x}_1, \bar{x}_1]$$

- $x_2 \in [\underline{x}_2, \bar{x}_2]$
- Constraints
 - $|out_X - out_Y| \leq \epsilon_1$
 - $out_X \leq out_Z - \Delta Z$

As can be seen in Problem .1, the counter is working.

TL;DR

test test

Problem: Test

$$\min_{\mathbf{x}, \mathbf{e}; \theta} J = f(\mathbf{x}, \mathbf{e}; \theta) = f(x)$$

with:

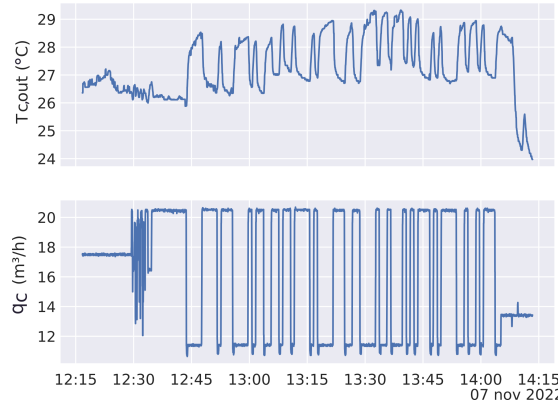
- Model name model
 - $out_1, out_2 = f(in_1, in_2, \dots, in_N)$
- Decision variables
 - $\mathbf{x} = [x_1, x_2]$
- Environment variables
 - $\mathbf{e} = [e_1, e_2, \dots, e_3]$
- Fixed parameters
 - $\theta = [\theta_1 = X, \theta_2 = Y]$

subject to:

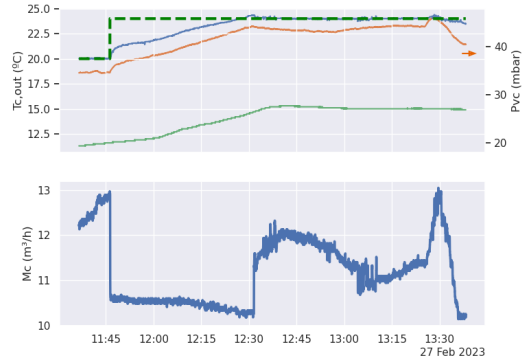
- Box-bounds
 - $x_1 \in [\underline{x}_1, \bar{x}_1]$
 - $x_2 \in [\underline{x}_2, \bar{x}_2]$
- Constraints
 - $|out_X - out_Y| \leq \epsilon_1$
 - $out_X \leq out_Z - \Delta Z$

the heat definition of efficiency

In process heat driven system, plants that produce the same final product, the most efficient one that uses the least amount of heat. While given two plants that produce the same amount of waste heat, the one is the one that produces given that heat.



(a) Dynamic identification by means of PRBS signal



(b) Controller application results

Figure 2: Condenser outlet temperature control implementation. To tune the controller, the system was excited with a PRBS signal. An ARX model ($n_a = 20$, $n_b = 4^{\text{th}}$ order fit) using the *System Identification* toolbox in MATLAB, which allowed to extract the first-order dynamic with which the controller.

The kaobook class

PhD Thesis

**Towards optimal resource management in solar thermal applications:
desalination and CSP**

Juan Miguel Serrano Rodríguez

August 17, 2025

University of Almería

The kaobook class

Disclaimer

You can edit this page to suit your needs. For instance, here we have a no copyright statement, a colophon and some other information. This page is based on the corresponding page of Ken Arroyo Ohori's thesis, with minimal changes.

No copyright

 This book is released into the public domain using the CC0 code. To the extent possible under law, I waive all copyright and related or neighbouring rights to this work.

To view a copy of the CC0 code, visit:

<http://creativecommons.org/publicdomain/zero/1.0/>

Colophon

This document was typeset with the help of KOMA-Script and \LaTeX using the kaobook class.

The source code of this book is available at:

<https://github.com/fmarotta/kaobook>

(You are welcome to contribute!)

Publisher

First printed in May 2019 by University of Almería

The harmony of the world is made manifest in Form and Number, and the heart and soul and all the poetry of Natural Philosophy are embodied in the concept of mathematical beauty.

– D'Arcy Wentworth Thompson

Acknowledgements

Test test test

Federico Marotta

Summary

I am of the opinion that every \LaTeX geek, at least once during his life, feels the need to create his or her own class: this is what happened to me and here is the result, which, however, should be seen as a work still in progress. Actually, this class is not completely original, but it is a blend of all the best ideas that I have found in a number of guides, tutorials, blogs and tex.stackexchange.com posts. In particular, the main ideas come from two sources:

- ▶ [Ken Arroyo Ohori's Doctoral Thesis](#), which served, with the author's permission, as a backbone for the implementation of this class;
- ▶ The [Tufte-Latex Class](#), which was a model for the style.

The first chapter of this book is introductory and covers the most essential features of the class. Next, there is a bunch of chapters devoted to all the commands and environments that you may use in writing a book; in particular, it will be explained how to add notes, figures and tables, and references. The second part deals with the page layout and design, as well as additional features like coloured boxes and theorem environments.

I started writing this class as an experiment, and as such it should be regarded. Since it has always been intended for my personal use, it may not be perfect but I find it quite satisfactory for the use I want to make of it. I share this work in the hope that someone might find here the inspiration for writing his or her own class.

Resumen

Contents

Acknowledgements	v
Summary	vii
Resumen	ix
Contents	xi
About the author	1
How to read this document	3
Document structure	4
INTRODUCTION	5
1 Context and motivation	7
2 Research plan	11
2.1 Hypothesis	11
2.2 Objectives	11
2.3 Contributions	11
3 Modelling overview	13
3.1 Performance metrics	13
3.2 First principle modelling	13
3.3 Data-driven modelling	13
3.3.1 Gaussian Process Regression	14
3.3.2 Artificial Neural networks	14
3.3.3 Random Forest	16
3.3.4 Gradient Boosting	16
3.4 Hybrid modelling	16
3.5 Data-driven from first-principles models. Sample generation	16
3.6 Hybrid modelling by means of Finite-State Machines (FSMs)	16
4 Control overview	19
4.1 PID controllers	19
4.2 Hierarchical control	19
5 Optimization overview	21
5.1 NLP problems	21
5.2 MINLP problems	21
5.3 A discussion on constraint handling	21
5.4 Multi-objective optimization	22
5.5 Optimization algorithms	22
OPTIMAL WATER AND ELECTRICITY MANAGEMENT IN A COMBINED COOLING SYSTEM	23
6 Solar thermal energy and water	27
6.1 Concentrated solar thermal	27
6.1.1 Concentrated Solar Power (CSP): Concentrated Solar Power	28
6.1.2 CSP: from the hype to unrealized potential	29
6.2 Cooling and water use	30
6.2.1 Conventional condenser cooling technologies	31
6.2.2 Non-conventional cooling: Combined / hybrid cooling	34
6.2.3 Selection of the cooling technology	37

7 Combined cooling pilot plant at Plataforma Solar de Almería	39
7.1 Plant description	40
7.2 Experimental campaigns	41
7.3 Experimental campaigns for the wet cooling tower	41
7.3.1 Experimental campaign 1	41
7.3.2 Experimental campaign 2	42
7.3.3 Experimental campaign 3	43
7.3.4 Experimental campaigns for the dry cooler	43
8 Modelling of a combined cooling system	45
8.1 Wet cooler	45
8.1.1 Poppe model	46
8.1.2 Samples generation for first-principles to data-driven models	48
8.1.3 Model interface	48
8.2 Dry cooler	49
8.2.1 Physical model	49
8.2.2 Samples generation for first-principles to data-driven models	49
8.2.3 Model interface	49
8.3 Other components	50
8.3.1 Electrical consumption	50
8.3.2 Surface condenser	50
8.3.3 Mixers	51
8.4 Complete system	51
9 Optimization of a combined cooling system	53
9.1 Environment description	55
9.2 Static optimization	55
9.2.1 Dry cooler	56
9.2.2 Wet cooler	57
9.2.3 Combined cooler	57
9.3 Horizon optimization	58
9.3.1 A discussion on solving the optimization problem	59
9.3.2 Proposed solution: Decomposition-based multi-objective optimization with trajectory planning	60
10 Validation in the combined cooling pilot plant	63
10.1 Modelling	63
10.1.1 Wet cooler model alternatives comparison and validation	63
10.1.2 Dry cooler model alternatives comparison and validation	64
10.1.3 Main components modelling conclusions	67
10.1.4 Condenser model validation	69
10.1.5 Complete system model validation	70
10.2 Control and optimization results	72
10.2.1 Choosing an optimization algorithm	72
10.2.2 Comparing the static and horizon optimization strategies	73
10.2.3 Validation at pilot plant	74
11 Annual analysis: ANDASOL-II CSP plant	79
11.1 Limitations	79
11.2 Environment definition	80
11.2.1 Water context	80
11.2.2 Thermal load	80
11.2.3 Costs context	81
11.3 Optimization strategies comparison	81
11.4 Cooling alternatives comparison	84
ENERGY MANAGEMENT IN MED PROCESSES DRIVEN BY VARIABLE ENERGY SOURCES	85
Derived scientific contributions	87
12 Thermal desalination	89

13 SolarMED pilot plant	91
13.1 Heat generation and storage subsystem	91
13.1.1 Solar field	91
13.1.2 Thermal storage	92
13.2 Separation subsystem	92
14 Performance evaluation in Multi-Effect Distillation (MED) processes: standard methodology proposal	95
14.1 Process analysis	97
14.2 Performance metrics	98
14.2.1 Separation metrics	98
14.2.2 Energetic metrics	99
14.2.3 Exergetic metrics	100
14.3 Instrumentation	102
14.3.1 Key Process Variable (KPV)	102
14.3.2 Instrumentation requirements	103
14.3.3 Uncertainty determination	104
14.4 Monitoring and process control	105
14.4.1 Monitoring: steady-state identification	105
14.4.2 Control system	105
14.5 Methodology application in an experimental campaign	107
14.5.1 Implementation results	108
14.5.2 Results analysis	112
15 Hybrid modelling of a solar driven MED system	115
15.1 Introduction	115
15.2 Dynamic modelling. Process variables	115
15.2.1 Solar field	115
15.2.2 Thermal storage	118
15.2.3 Heat exchanger	121
15.2.4 MED	122
15.3 Discrete modelling. Operation state	123
15.3.1 Heat generation and storage subsystem (<i>sfts</i>)	123
15.3.2 Separation subsystem (<i>med</i>)	123
15.4 Complete system model	123
15.4.1 Validation	124
16 Towards the optimal coupling and operation of a solar driven MED system	125
16.1 Introduction	125
16.2 Problem description	125
16.2.1 Implementation discussion	126
16.4 Operation Plan Layer Description	129
16.4.1 Candidate problems generation	129
16.4.2 Update times generation	129
16.5 Operation optimization layer description	131
16.6 Optimization results	132
16.6.1 Choosing an algorithm	132
16.6.2 Choosing a candidate problem	132
16.6.3 Simulation results	133
16.6.4 Performance comparison with alternative strategies	135
CONCLUSIONS AND OUTLOOK	137
Conclusions	139
Outlook and future work	139
Derived scientific contributions	140
Bibliography	141
Alphabetical Index	149

List of Figures

1	A rotated figure	2
2	Condenser outlet temperature controller implementation	5
3	Example figure. Try clicking or scanning the QR code to access the interactive version. [1ex]	3
1.1	“Yes, the planet got destroyed. But for a beautiful moment in time, we created a lot of value for shareholders”	7
1.2	Aerial view of the pilot plants at the Plataforma Solar de Almería (PSA), Spain. The developments presented in this thesis have been developed and validated around two test-rigs: a Combined Cooling System (CCS) and a Solar-driven Multi-Effect Distillation (SolarMED) pilot plants. In the picture, the CCS plant is located on the left side, and the...	9
3.1	ANN model configurations	14
3.2	Considered ANN architectures	15
6.1	Two main Concentrated Solar Thermal (CST) technologies	27
6.2	Solar tower CSP plant. Source: NREL [12]	28
6.3	Levelized Cost of Electricity (LCOE) evolution and capacity predictions	29
6.4	31
6.5	Water consumption comparison between CSP and other thermal power generation technologies. Source: Aseri et al. [27]	31
6.6	32
6.7	Different hybrid/combined coolers configurations	36
7.1	PSA combined cooling system facility	39
7.2	Back view of the WCT	40
7.3	Layout of combined cooling systems pilot plant at PSA.	40
7.4	Example of one experiment at the pilot plant in July with two valid steady-state operating points.	42
8.1	Control volume in the exchange area of a wet cooling tower arrangement.	47
8.2	Inputs-outputs block diagram of the main model components	51
8.3	Complete model diagram of the combined cooling system	52
9.1	Block diagram of the optimization scheme including environment components	54
9.2	Diagram of the dry cooler only cooling problem	56
9.3	Diagram of the wet cooler only cooling problem	57
9.4	Diagram of the combined cooler and condenser problem	58
9.5	Pareto front for a particular problem instance of the combined cooler optimization problem.	58
9.6	Visualization of a constrained search space for two decision variables	59
9.7	Proposed methodology. Decomposition-based multi-objective optimization with trajectory planning	61
10.1	Calibration, tuning, validation and comparison procedure	63
10.2	Experimental results for the Me number as a function of m_w/m_a	64
10.3	Wet Cooling Tower (WCT) samples distribution visualization	65
10.4	WCT Models performance regression	66
10.5	Dry Cooler (DC) samples distribution visualization	67
10.6	DC Models performance regression	68
10.7	Heat transfer coefficient calibration results	69
10.8	Figure caption	71
10.9	Horizon optimization – path selection subproblem. Fitness evolution comparison for four different dates.	73
10.10	Detailed timeseries simulation results. Combined Cooler (CC)-horizon	74
10.11	Implementation of the optimization strategy in the real facility. Hierarchical control	75
11.1	Andasol I, II and III	79

11.2	Spanish electricity mix on July 12, 2024. The peak in photovoltaic generation is clearly visible at midday, while thermosolar generation is more evenly distributed throughout the day. Peak production is majorly from CSP plants with no storage. Data source: Figure elaborated using data extracted from https://www.ree.es/es/datos .	80
11.3	CC static optimization simulation results in three different periods of time	82
11.4	A rotated figure	83
11.5	Annual simulation results for the CC system optimized with static optimization. Results are resampled every 15 days using their mean values. The original frequency results can be found in the interactive version: [1ex]	84
13.1	SolarMED process diagram	91
13.2	MED plant at PSA with open effects for maintenance	93
13.3	· · · · ·	94
14.1	Inputs and outputs variables in an MED process. The dash line delimits the control volume	98
14.2	Piping and Instrumentation Diagram (P&ID) with the required instrumentation, KPVs, and basic control loops (ANSI/ISA 5.1-2022) required in an MED plant	103
14.3	Sensitivity index results for different variables. Useful to assess the impact of the different measured variables uncertainty on the performance metrics. KPVs are shown in bold notation	104
14.4	Diagram of the steady-state identification procedure	106
14.5	· · · · ·	107
14.6	Ryznar Stability Index (RSI) values as a function of temperature and concentration before (left) and after (right) pre-treatment using nanofiltration.	108
14.7	Flowchart of finite state machines for plant start-up (left) and shutdown (right)	109
14.8	Condenser outlet temperature controller implementation	110
14.9	· · · · ·	111
14.10	Temperature and concentration evolution for operation points at each effect in the MED plant. Surface represents the RSI.	113
14.11	Per effect comparison between low and high Top Brine Temperature (TBT) operation points	113
15.1	Solar field process diagram.	116
15.2	Solar field and thermal storage electrical characterization tests.	117
15.3	Solar field flow for different pump configurations and their associated power consumption. [1ex]	118
15.4	· · · · ·	119
15.5	Thermal storage process diagram.	120
15.6	· · · · ·	121
15.7	Heat exchanger process diagram.	122
15.8	· · · · ·	123
15.9	Complete SolarMED model architecture. TODO: Needs to be updated	124
16.1	Decision tree resulting from the combinatorial nature of the integer part of the optimization problem. Text in nodes represents system states.	128
16.2	Proposed optimization strategy architecture	128
16.3	Operation plan layer computation and updates distribution	130
16.4	Fitness evolution for a particular startup-problem	132
16.5	A rotated figure	134

List of Tables

1	MED plant at PSA specifications and nominal operating conditions	4
7.1	Characteristics of instrumentation (^a value of the temperature in °C, ^b of reading, ^c full scale, ^d mean value).	40
7.2	Design of experiments for model comparison.	43
10.1	Bounds and discretization of the model input variables.	64
10.2	Summary table of the prediction results obtained with the different modelling approaches studied.	66
10.3	Bounds and discretization of the model input variables.	67
10.4	Summary table of the prediction results obtained with the different modelling approaches studied.	68

10.5	Static optimization algorithm comparison results	73
10.6	Box-bounds for the decision variables.	75
11.1	ANDASOL-II plant main characteristics	79
13.1	MED plant at PSA specifications and nominal operating conditions	93
13.2	Characteristics of the instrumentation installed at MED-PSA unit (^a value of the measured temperature in °C, ^b of reading, ^c full scale).	93
14.1	RSI values and their interpretation in terms of scaling and corrosion risk [113].	107
14.2	Experimental campaign design specifications	108
14.3	Measured variables and performance metrics for some operation points of the experimental campaign. The values are expressed as mean ± standard deviation with a coverage factor of 2 (95% confidence interval). D is the duration of the steady state period.	112
15.1	Solar Field and Thermal Storage subsystem (sfts) FSM states definitions. \wedge represents the logical AND operator and \forall represents that all meet the condition.	123
15.2	Separation subsystem (med) FSM states definitions. \wedge represents the logical AND operator, \exists represents that at least one meets the condition, and \forall represents that all meet the condition.	123
16.1	Operation plan. Start-up (1) and shutdown (2) degrees of freedom for changes in the operation state.	129

List of Listings

About the author

Un payaso

– Lidia Roca, probablemente

I am currently completing my PhD thesis, with the defense planned for October. My research interests lie primarily in automatic control, optimization, and robotics, especially as applied to solar thermal processes.

I think I am mostly a creative person, but in order to implement those ideas, throughout my work, I've gained experience with a variety of tools and technologies, including Linux, Python, Docker, LaTeX, and the Robot Operating System (ROS). I'm particularly passionate about open science and open source software, and I strive to contribute to communities that value transparency and collaboration.

For my bachelor's thesis, I created a mobile robotics lab in the University of Almería by deploying the [Duckietown project](#). This gave me the opportunity to interact and work with ROS, and since the whole project was deployed using Docker, to learn about containerization technologies. For my master's thesis, work was also software-related, but this time it was about the implementation of a SCADA-like system using Python. During my PhD, I have had four years to really delve into these technologies, so today they are an integral part of my workflow and I am confident to say they've helped me become effective at implementing those (sometimes too) many ideas.



Lidia esto solo lo he copiado
por tener algo, ya lo mejoraré

How to read this document

TL;DR

This preliminary chapter explains how to read this document, mainly the different environment boxes used throughout the manuscript, why the large margins, what is placed in them, and how to use the interactive features of the manuscript. This is an example of a Too Long; Didn't Read (TL;DR) box. It contains an Abstract/Summary of the main point of the chapter and are placed at the beginning of every chapter.

This \LaTeX template is designed with large margins, on the one hand this allows to have shorter lines, which makes for an easier reading experience but most interestingly, it also allows to place additional information in the margins, such as side notes, side citations, figures, tables... your imagination is the limit! Or rather \LaTeX compilation errors and your patience are. Throughout this manuscript I will add side notes¹ to provide additional information and comments that would otherwise be too distracting and verbose to include in the main text, constantly interrupting the flow of the reading. The side notes are not essential to understand the content of the document, but mostly complementary.

1: Like this one! They are like footnotes, but placed in the margin of the page

Boxed environments

Both problem definition boxes (e.g. ref) and model definition boxes (e.g. Model 0.2) are countered environments and can (and will) be referenced in the text.

Problem: Problem definition box example

This is an example of a problem definition box. It is used to formally and concisely define an optimization problem.

$$\min_{\mathbf{x}, \mathbf{e}; \theta} J = f(\mathbf{x}, \mathbf{e}; \theta) = \text{XXXX}$$

with:

$$\begin{aligned} \text{out}_1, \text{out}_2 &= f(\text{in}_1, \text{in}_2, \dots, \text{in}_N) \\ \text{out}_1, \text{out}_2 &= f(\text{in}_1, \text{in}_2, \dots, \text{in}_N) \end{aligned}$$

- ▶ Decision variables

$$\mathbf{x} = [x_1, x_2]$$

- ▶ Environment variables

$$\mathbf{e} = [e_1, e_2, \dots, e_3]$$

- ▶ Fixed parameters

$$\theta = [\theta_1 = X, \theta_2 = Y]$$

subject to:

- ▶ Box-bounds

$$\begin{aligned} \cdot x_1 &\in [\underline{x}_1, \bar{x}_1] \\ \cdot x_2 &\in [\underline{x}_2, \bar{x}_2] \end{aligned}$$

- ▶ Constraints



Figure 3: Example figure. Try clicking or scanning the QR code to access the interactive version.



Table 1: MED plant at PSA specifications and nominal operating conditions

Parameter	Value
Capacity	72 m ³ /day
Number of effects	14
Feed type	Forward feed
Physical arrangement	Vertically stacked
Heat exchanger configuration	90/10 Cu-Ni HTE
Heat source type	Hot water
Top Brine Temperature (TBT)	70 °C
Condenser temperature	35 °C

2: I believe that this is a good way to make the document more accessible and to encourage readers to explore the content in more depth. However, the interactive features are optional and not necessary to understand the content of the document.



3:

厕纸：Like hoarding toilet paper

- $|out_X - out_Y| \leq \epsilon_1$
- $out_X \leq out_Z - \Delta Z$

Model 0.2: Model definition box example

$out_1, out_2 = \text{some cool model}(in_1, in_2, in_3)$

Other boxes

Other boxes are used to highlight important points, or to provide additional information that is not essential to the main text.

In order to make the book more interactive and link-friendly, I have enabled hyperlinks in the PDF. This means that you can click on the references, citations, and links to external resources, and they will take you to the corresponding location. This is standard latex, however to maintain a consistent experience in the physical version, QR codes are inserted in the margin next to the links. The reader is invited to scan them with a QR code reader to access the corresponding online resource². Some figures also include QR codes that link to an interactive (HTML) version of the figure, see Figure 3 as an example.

The additional material as well as the source code of this document are hosted in a [Zenodo repository](#)³. Alternatively, a mirror repository is also available at:

<https://github.com/juan11iguel/my-thesis>

It seems unlikely that both Zenodo and GitHub will go down at a time where this document is still relevant, and if they do, I think there will be more important things to worry about than losing access to the interactive content of this thesis.⁴

Document structure

This document is divided in three parts:

Introduction This first part introduces the context and motivation of the thesis, the research plan, and the contributions. ...

This introductory part is then followed by the two main contributions:

Water mana...

INTRODUCTION

Context and motivation

Hello, here is some text without a meaning. This text should show what a printed text will look like at this place. If you read this text, you will get no information. Really? Is there no information? Is there a difference between this text and some nonsense like "Huardest gefburn"? Kjift – not at all! A blind text like this gives you information about the selected font, how the letters are written and an impression of the look. This text should contain all letters of the alphabet and it should be written in of the original language. There is no need for special content, but the length of words should match the language. Hello, here is some text without a meaning. This text should show what a printed text will look like at this place. If you read this text, you will get no information. Really? Is there no information? Is there a difference between this text and some nonsense like "Huardest gefburn"? Kjift – not at all! A blind text like this gives you information about the selected font, how the letters are written and an impression of the look. This text should contain all letters of the alphabet and it should be written in of the original language. There is no need for special content, but the length of words should match the language. Hello, here is some text without a meaning. This text should show what a printed text will look like at this place. If you read this text, you will get no information. Really? Is there no information? Is there a difference between this text and some nonsense like "Huardest gefburn"? Kjift – not at all! A blind text like this gives you information about the selected font, how the letters are written and an impression of the look. This text should contain all letters of the alphabet and it should be written in of the original language. There is no need for special content, but the length of words should match the language. Hello, here is some text without a meaning. This text should show what a printed text will look like at this place. If you read this text, you will get no information. Really? Is there no information? Is there a difference between this text and some nonsense like "Huardest gefburn"? Kjift – not at all! A blind text like this gives you information about the selected font, how the letters are written and an impression of the look. This text should contain all letters of the alphabet and it should be written in of the original language. There is no need for special content, but the length of words should match the language. Hello, here is some text without a meaning. This text should show what a printed text will look like at this place. If you read this text, you will get no information. Really? Is there no information? Is there a difference between this text and some nonsense like "Huardest gefburn"? Kjift – not at all! A blind text like this gives you information about the selected font, how the letters are written and an impression of the look. This text should contain all letters of the alphabet and it should be written in of the original language. There is no need for special content, but the length of words should match the language.

Hello, here is some text without a meaning. This text should show what a printed text will look like at this place. If you read this text, you will get no information. Really? Is there no information? Is there a difference between this text and some nonsense like "Huardest gefburn"? Kjift – not at all! A blind text like this gives you information about the selected font, how the letters are written and an impression of the look. This text should contain all letters of the alphabet and it should be written in of the original language. There is no need for special content, but the length of words should match the language. Hello, here is some text without a meaning. This text should show what a printed text will look like at this place. If you read this text, you will get no information. Really? Is there no information? Is there a difference between this text and some nonsense like "Huardest gefburn"? Kjift – not at all! A blind text like this gives you information about the selected font, how the letters are written and an impression of the look. This text should contain all letters of the alphabet and it should be written in of the original language. There is no need for special content, but the length of words should match the language. Hello, here is some text without a meaning. This text should show what a printed text will look like at this place. If you read this text, you will get no information. Really? Is there no information? Is there a difference between this text and some nonsense like "Huardest gefburn"? Kjift – not at all! A blind text like this gives you information about the selected font, how the letters are written and an impression of the look.



Figure 1.1: "Yes, the planet got destroyed. But for a beautiful moment in time, we created a lot of value for shareholders"

look. This text should contain all letters of the alphabet and it should be written in of the original language. There is no need for special content, but the length of words should match the language. Hello, here is some text without a meaning. This text should show what a printed text will look like at this place. If you read this text, you will get no information. Really? Is there no information? Is there a difference between this text and some nonsense like "Huardest gefburn"? Kjift – not at all! A blind text like this gives you information about the selected font, how the letters are written and an impression of the look. This text should contain all letters of the alphabet and it should be written in of the original language. There is no need for special content, but the length of words should match the language. Hello, here is some text without a meaning. This text should show what a printed text will look like at this place. If you read this text, you will get no information. Really? Is there no information? Is there a difference between this text and some nonsense like "Huardest gefburn"? Kjift – not at all! A blind text like this gives you information about the selected font, how the letters are written and an impression of the look. This text should contain all letters of the alphabet and it should be written in of the original language. There is no need for special content, but the length of words should match the language.

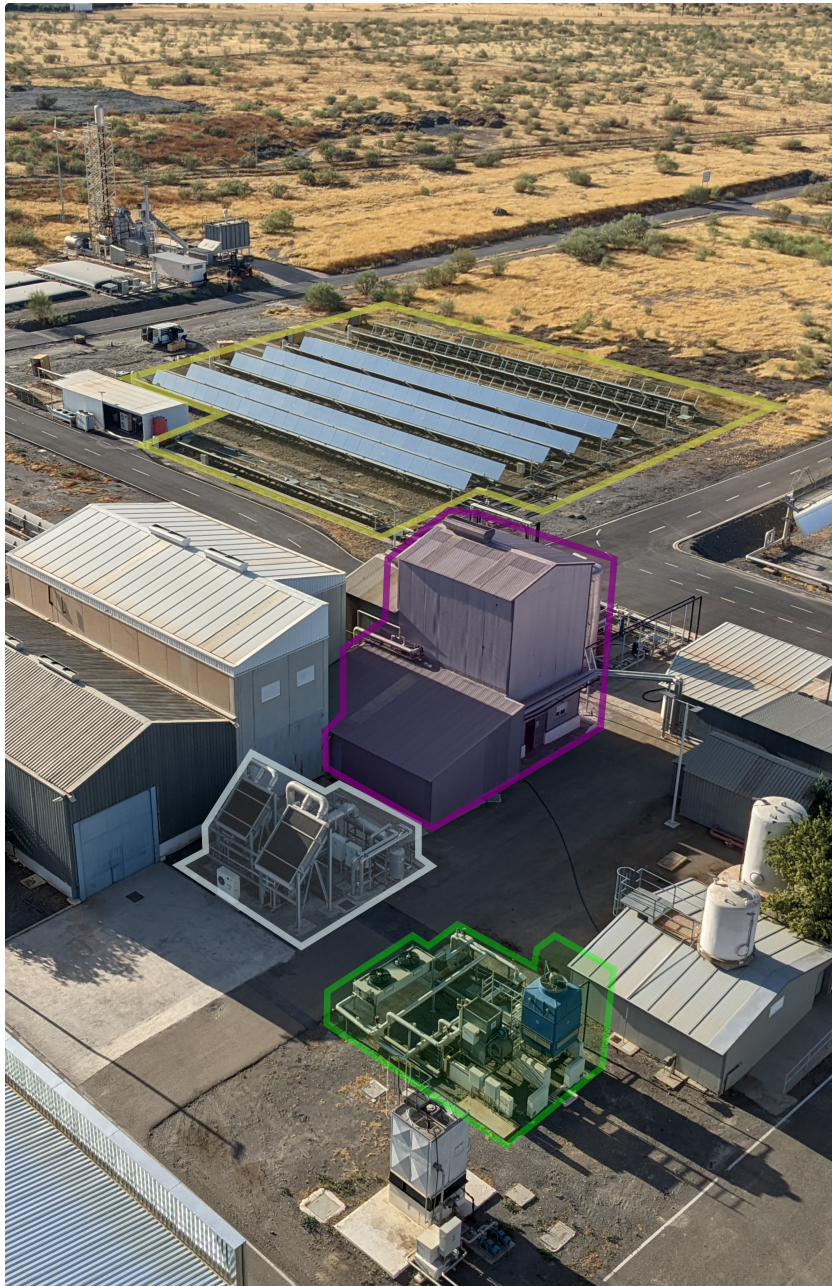


Figure 1.2: Aerial view of the pilot plants at the PSA, Spain.

The developments presented in this thesis have been developed and validated around two test-rigs: a CCS and a SolarMED pilot plants. In the picture, the CCS plant is located on the left side, and the...

asdad

2.1 Hypothesis	11
2.2 Objectives	11
2.3 Contributions	11

2.1 Hypothesis

2.2 Objectives

2.3 Contributions

3.1 Performance metrics

To evaluate the quality of the models fit to the experimental data, four performance metrics were evaluated: coefficient of determination (R^2), Root Mean Squared Error (RMSE), Mean Absolute Error (MAE) and Mean Absolute Percentage Error (MAPE). These metrics are described below.

Coefficient of determination. R^2 measures the proportion of the variance in the predicted variable that can be attributed to the independent variable(s), in this case the considered system inputs. Values close to one indicate a better prediction accuracy. It is calculated as follows:

$$R^2 = 1 - \frac{\sum_{i=1}^n (y_i - \hat{y}_i)^2}{\sum_{i=1}^n (y_i - \bar{y})^2},$$

where y_i is the measured or observed value for the output variable, in the i -th observation, \hat{y}_i is the estimated value of the same variable and n is the total number of observations. Finally, \bar{y} is the mean value of the experimental values.

Root Mean Square Error. RMSE is a statistical measure of the difference between the values predicted by a model and the observed values. It is calculated as the square root of the mean of the squared differences between the predicted and observed values and it has its units.

$$\text{RMSE} = \sqrt{\frac{1}{n} \sum_{i=1}^n (y_i - \hat{y}_i)^2}$$

Mean Absolute Error. It represents the average absolute difference between predicted and actual values.

$$\text{MAE} = \frac{1}{n} \sum_{i=1}^n |y_i - \hat{y}_i|$$

Mean Absolute Percentage Error. As the MAE, it calculates the difference between the predicted and the actual values, but in this case it does so in relative terms:

$$\text{MAPE} = \frac{1}{n} \sum_{i=1}^n \left| \frac{y_i - \hat{y}_i}{y_i} \right| \times 100\%$$

3.2 First principle modelling

3.3 Data-driven modelling

Machine learning algorithms are unique in their ability to obtain models and extract patterns from data, without being explicitly programmed to do so. They

3.1 Performance metrics	13
3.2 First principle modelling	13
3.3 Data-driven modelling	13
3.3.1 Gaussian Process Regression	14
3.3.2 Artificial Neural networks . . .	14
3.3.3 Random Forest	16
3.3.4 Gradient Boosting	16
3.4 Hybrid modelling	16
3.5 DD from FP. Sample generation	16
3.6 Hybrid modelling by means of FSMs	16

are more effective with large volumes of data but can also be applied to build steady state regression models with less information of a process.

3.3.1 Gaussian Process Regression

3.3.2 Artificial Neural networks

Artificial Neural Networks (ANNs), as the name suggests, have a behavior similar to biological neurons. Their structure is formed by a succession of layers, each one composed by nodes (or neurons) and they receive as input the output of the previous layer. This process is subsequently repeated until the final layer which has a number of neurons equal to the number of outputs.

There are important aspects to be considered in the ANN model design, such as the model configuration, the network architecture and the network topology. They are discussed below.

Model configuration. If the model has more than one output, several configurations are available for the implementation of the model as shown in Figure 8.2. The first one is a Multiple Inputs Multiple Outputs (MIMO) configuration, where a single network receives all the inputs and directly produces all predicted outputs. The second one is a cascade structure. This cascading approach involves training a network (*network A* in Figure 8.2 (b)) to predict one output using the available inputs. Subsequently, these inputs, along with the output from the first-output-predicting network, are fed into a second network (*network B* in Figure 8.2 (b)) that is in charge of forecasting the second output. This procedure can be repeated as many times as desired. A potential advantage of this configuration is that it may reduce the experimental data requirements to obtain satisfactory results. A third option is the combination of both configurations, where some networks may predict several outputs, while others are fed some of these outputs as subsequently use them as inputs.

Network architectures. Three network architectures have been implemented and tested:

1. Feed Forward (FF) network - Figure 3.2 (a). This is the base network architecture, where different layers are added sequentially and the flow of information is unidirectional. The transfer function adopted in the hidden layers is the differentiable *Log-Sigmoid*¹, whereas the one employed in the output layer is a linear one with no saturations.
2. Cascade-forward (CF) network - Figure 3.2 (b). It is a variation on the feedforward network since it adds direct connections from the input and hidden layers to the output layer.
3. Radial Basis Function (RBF) network - Figure 3.2 (c). The transfer functions used in the first layer of the RBF network are different, they are local Gaussian like functions. Also, instead of multiplying by the weights, the distance between inputs and weights is computed and the bias is multiplied instead of added [1].

Network topology. Two-layer networks (one hidden and one output layer) can learn almost any input-output relationship, including non-linear ones. Adding more layers can improve the learning for more complex problems. However, increasing the number of layers or neurons per layer increases the training computational requirements, requires more data for a satisfactory model and can lead to overfitting. Therefore, the process is usually started with two layers and then the number of layers is increased if they do not perform satisfactorily [1]. In this study, for the feedforward and cascade-forward architectures, one and two hidden layers have been tested with the following configurations: 5, 10, 20, 5-5, 5-10, 10-5, 10-10. For the case of the RBF, it only has one hidden layer and

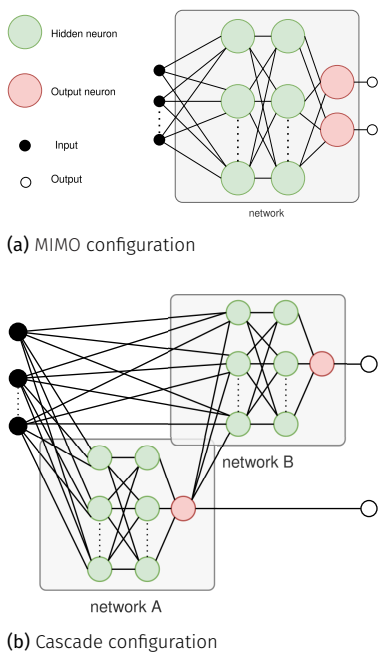


Figure 3.1: ANN model configurations

1: Defined as $\text{logsig}(x) = 1/(1 + e^{-x})$, mapping any real input to a value between 0 and 1.

[1]: Hagan et al. (2014), *Neural Network Design*

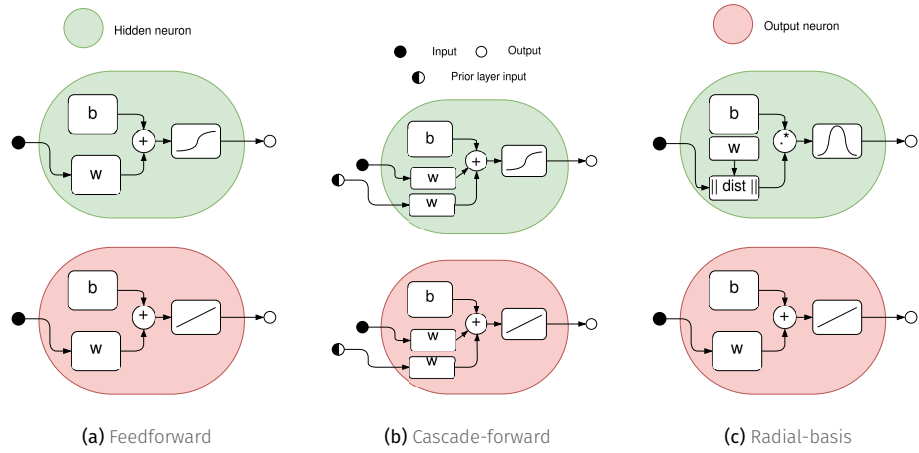


Figure 3.2: Considered ANN architectures

neurons are added sequentially during the training process up to a maximum which is set to 120 neurons.

Training process. The next important aspect to consider is the training process. For the FF and CF networks many Gradient- or Jacobian-based algorithms can be utilized. In this case, the Levenberg-Marquardt backpropagation algorithm [2] has been used. It is a fast algorithm, ideal for multilayer networks with up to a few hundred weights and biases enabling efficient training. The training in this case is done in batches since sequential training is slower and does not produce better results. All data have been normalized applying the z-score normalization method. The criteria established for deciding when to stop the training is the following one: when the performance on the validation set increases (worsens) or when the gradient is below a minimum (1×10^{-7}) for a number of iterations or epochs, or when a maximum number of 1000 epochs is reached. The number of iterations to wait, often referred as patience, is set to 6. Finally, the selected network parameters will be those of the best epoch.

[2]: Beale et al. (2010), "Neural Network Toolbox"

For each network architecture, the training process was repeated a total of ten times (this is the recommended practice if the computational requirements allow it, since it guarantees reaching a global optimum with a high degree of confidence [3]). The optimal architecture and training was selected according to a performance function, which in this case has been the Mean Squared Error (MSE) with the values normalized.

[3]: Hamm et al. (2007), "Comparison of Stochastic Global Optimization Methods to Estimate Neural Network Weights"

In the case of the RBF network, the chosen training method consists in two stages which treats the two layers of the RBF network separately. The first layer weights and biases are tuned based on the orthogonal least squares method [1], while for the second layer are computed in one step using a linear least-squares algorithm. During training, neurons are added to the first layer (in increments of 20) trying to minimize the MSE to some goal, which in this case is set depending on the case study: 10 for the MIMO configuration and 0 ($^{\circ}\text{C}^2$) and 20 (L^2/h^2) for temperature and water lost networks, respectively, for the cascade configuration. Finally, a parameter called spread is used to set the first layer biases. Larger values of this parameter promote a smoother approximation of the training data (more generalization), conversely, lower values provide a more exact fit to the training data. Values from 0.1 to 30 have been tested for this parameter.

[1]: Hagan et al. (2014), *Neural Network Design*

3.3.3 Random Forest

3.3.4 Gradient Boosting

3.4 Hybrid modelling

3.5 Data-driven from first-principles models. Sample generation

One important advantage that first-principles models have over data-driven is their scalability, that is, the ability to adapt a model developed and validated in a pilot-scale system, to a large scale one. This is true for many systems as long as the system configuration remains the same. This allows to study and analyze pilot scale plants and extrapolate the results to industrial sized plants. In addition, these type of model are also capable of predicting the behaviour of the modelled systems in conditions that have not been tested (e.g. different operating or environmental conditions), although the reliability of the model could be lower if these conditions move away from those experimentally used for some parameter calibration.

On the contrary, data-driven models are very specific to the system and operating ranges they are trained for. That is why training/calibrating a data-driven model with data from a first-principles model is a common practice to obtain a model that can be used in a larger range of operating conditions...

The process of generating samples from a first-principles model to train a data-driven model is called sample generation. It consists of running the first-principles model for a set of input parameters, which can be selected randomly or following a specific distribution, and then using the outputs of the first-principles model as the training data for the data-driven model.

The first step is to define the input parameters and their ranges. This can be done by selecting the most relevant parameters for the system and determining their ranges based on the system's operating conditions. The next step is to generate a set of input parameters, which can be done using different methods such as Latin Hypercube Sampling, Monte Carlo Sampling, Sobol Sampling, or simply grid sampling. These methods allow to generate a set of input parameters that cover the entire range of the input parameters and ensure that the generated samples are representative of the system's behaviour. Once the input parameters are defined, the first-principles model is run for each set of input parameters, and the outputs of the model are recorded. Finally, the recorded outputs are used to train the data-driven model.

3.6 Hybrid modelling by means of FSMs

A state machine is a model of behavior composed of a finite number of states and *transitions* between those states. Within each state and transition some *action* can be performed. A state machine needs to start at some *initial state*.

Core concepts description:

- ▶ **State.** A state represents a particular condition or stage in the state machine. It's a distinct mode of behavior or phase in a process.
- ▶ **Transition.** This is the process or event that causes the state machine to change from one state to another.
- ▶ **Action.** Specific operation or task that is performed when a certain event happens i.e. a state is entered, exited, or during a transition.

- ▶ **Model.** A stateful structure that holds information about the state of the machine. It gets updated during transitions and defines actions.
- ▶ **Machine.** This is the entity that manages and controls the model, states, transitions, and actions. It's the conductor that orchestrates the entire process of the state machine.

4

Control overview

The PID control algorithm continuously calculates and adjusts the control inputs based on the error between the desired setpoint and the actual system output, ensuring precise and stable control over various parameters.

4.1 PID controllers 19

4.2 Hierarchical control 19

4.1 PID controllers

4.2 Hierarchical control

Optimization overview

A general expression to define an optimization problem is:

$$\min_{\mathbf{x}, \mathbf{e}; \theta} J = f(\mathbf{x}, \mathbf{e}; \theta) \quad \text{s.t.} \quad g_i(\mathbf{x}) \leq 0, \quad i = 1, \dots, m \quad (5.1)$$

where \mathbf{x} is the vector of decision variables, $f(\mathbf{x})$ is the objective function to be minimized, and $g_i(\mathbf{x})$ are the constraints of the problem. The objective function is a scalar function that maps the decision variables to a real number, representing the cost or performance of the system. The constraints are functions that restrict the feasible region of the problem, defining the set of values that the decision variables can take. The optimization problem is to find the values of the decision variables that minimize the objective function while satisfying the constraints.

Regarding the constraints, they can be categorized in two types depending whether they can be evaluated before evaluating the objective function or not:

- ▶ **Bounds.** These are constraints that limit the range of the decision variables, such as

$$x_i \in [l_i, u_i], \quad i = 1, \dots, n$$

where l_i and u_i are the lower and upper bounds of the decision variable x_i , respectively¹.

- ▶ **Constraints.** These are constraints that restrict the feasible region of the problem, such as

$$g_i(\mathbf{x}) \leq 0, \quad i = 1, \dots, m$$

where $g_i(\mathbf{x})$ are the constraint functions that depend on the decision variables \mathbf{x} , and m is the number of constraints. They can only be known after evaluating the objective function.

5.1 NLP problems

Non-Linear Programming (NLP)

5.2 MINLP problems

Mixed Integer Non-Linear Programming (MINLP)

5.3 A discussion on constraint handling

There are two main approaches to handle constraints in optimization problems:

- ▶ **Penalty methods.** These methods add a penalty term to the objective function to penalize the violation of the constraints. The penalty term is usually a function of the constraint violation, and it is added to the objective function to form a new objective function that is minimized. The penalty term can be linear or non-linear, and it can be adjusted during the optimization process to ensure that the constraints are satisfied. The main advantage of penalty methods is that they allow to handle constraints

5.1 NLP problems	21
5.2 MINLP problems	21
5.3 A discussion on constraint handling	21
5.4 Multi-objective optimization	22
5.5 Optimization algorithms	22

¹: Also known as box-bounds

in a flexible way, and they can be used with any optimization algorithm. However, they can also lead to suboptimal solutions if the penalty term is not properly tuned, and they can also lead to numerical instability if the penalty term is too large.

- ▶ **Constraint handling methods.** These methods handle the constraints directly, by either rejecting solutions that violate the constraints or by modifying the optimization algorithm to ensure that the constraints are satisfied. The main advantage of constraint handling methods is that they guarantee that the constraints are satisfied, and they can also lead to better solutions than penalty methods. However, they can also be more complex to implement, and they can also lead to numerical instability if the constraints are too restrictive. Specific constraint-handling capable algorithms are required to solve these type of problems.

By using inequality constraints, the optimization algorithm is forced to find the best solution that satisfies the constraints, however, in a problem with a horizon window, this would require returning a value of the constraint for each step in the horizon window. Thus, producing a large vector of inequality constraints and increasing the dimension of the problem (*i.e.* its complexity). On the other hand returning a single value for the whole episode gives little information to the algorithm on how to adapt its decision values to satisfy the constraint and thus might be unable² to converge to a solution.

Finally, non constraint-handling capable algorithms can be wrapped with constraint handling methods to solve problems with constraints [4], where they basically implement some type of penalty method.

2: By unable we are referring to requiring an unfeasible amount of objective function evaluations, too much time.

[4]: Farmani et al. (2003), "Self-Adaptive Fitness Formulation for Constrained Optimization"

[5]: Geem et al. (2001), "A New Heuristic Optimization Algorithm"

[6]: Biscani et al. (2020), "A Parallel Global Multiobjective Framework for Optimization: Pagmo"

3: While HS has shown competitive performance, it has also faced criticism—not for its results, but for its metaphor. The musical analogy adds little explanatory value and arguably obscures the algorithm's mechanics. At its core, HS operates similarly to Evolutionary Strategies or Genetic Algorithms, employing concepts like mutation and crossover.

5.4 Multi-objective optimization

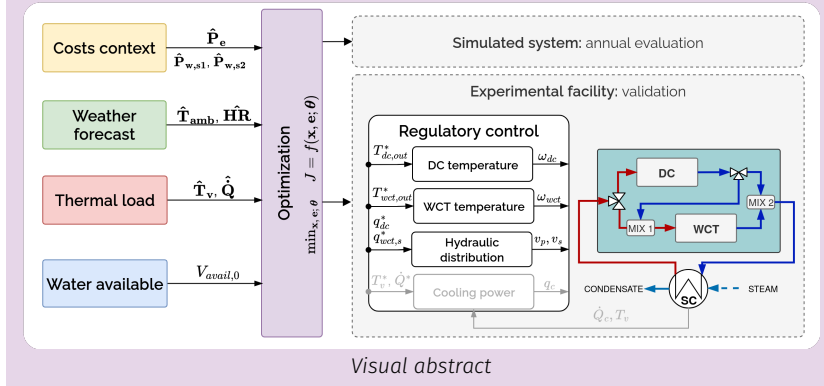
5.5 Optimization algorithms

- ▶ **Improved Harmony Search algorithm (IHS)** [5, 6] is a metaheuristic optimization algorithm inspired by the improvisation process of musicians. In this analogy, each musician represents a decision variable, each note corresponds to a value, and the goal is to create the best possible harmony—analogous to finding the global optimum. In the algorithm, every member of the input population contributes to the search process. At each iteration, a new solution (individual) is generated. If this new solution outperforms the worst individual in the population, it replaces it. The total number of fitness function evaluations equals the number of iterations. An enhanced version of HS introduces dynamic parameters: the probability of selecting values from the decision vector is adjusted linearly, while the mutation rate changes exponentially over time. These improvements aim to balance exploration and exploitation more effectively.³
- ▶ Another

OPTIMAL WATER AND ELECTRICITY MANAGEMENT IN A COMBINED COOLING SYSTEM

TL;DR

In the pursuit of extending the use and feasibility of solar thermal applications, a case study consisting of a commercial 50 MW-8 hours of storage CSP plant, Andasol-II, is analyzed in annual simulations where the cooling solution makes use of the novel proposed CCS. To obtain these results, a model of the CCS has been developed based on the same configuration as the PSA pilot plant. Different optimization strategies based on evolutionary algorithms have been implemented to adapt the system operation to the changing conditions. The strategy has been experimentally validated in the pilot plant and the simulated results show than the proposed scheme can yield ... compared to the DC only and ... with the WCT only alternatives.



Part structure

This part is structured as follows: first in Chapter 6 (Solar thermal energy and water) a context of concentrated solar thermal technologies is provided and their relationship with the water resource, specifically for the case of CSP. Then, the experimental combined cooling system pilot at PSA is presented in Chapter 7. The methodology for modelling and optimizing the operation of the system are described in Chapter ?? and Chapter 9, respectively. Both are validated in the experimental plant as showcased in Chapter 10. Finally, in this part's last chapter, Chapter 11 (Annual analysis: ANDASOL-II CSP plant), describes and analyzes the results of the annual simulations performed for a commercial CSP plant using different cooling alternatives.

Solar thermal energy and water

TL;DR

In the pursuit of eliminating reliance on fossil fuels sources for energy generation and replacing them by renewable sources, CSP has proven to be a reliable contributor. In particular, in providing much needed energy storage, dispatchability and ensuring grid stability.

In this context, water availability emerges not only as a technical constraint but also as a planning and policy issue. CSP deployment in water-stressed regions is strongly dependent on innovative cooling solutions, policy incentives, and careful water resource management to ensure sustainable operation without compromising water security for local communities.

Ideally, negligible raw water would be needed to operate a CSP plant and it should be achieved with no increase in the LCOE. The most water demanding component is the cooling of the power block, and currently this water saving can be achieved with dry cooling and an increase of 7% in the LCOE. A compromise solution can be reached by using hybrid cooling solutions together with water preservation strategies, achieving an 83% decrease in raw water consumption with respect to wet cooling with no reuse and a 5% increase in the LCOE [7].

Further savings can be achieved by optimizing the operation of the combined cooler and take full advantage of its flexibility towards optimal resource management.

6.1 Concentrated solar thermal	27
6.1.1 CSP: Concentrated Solar Power	28
6.1.2 CSP: from the hype to unrealized potential	29
6.2 Cooling and water use	30
6.2.1 Conventional condenser cooling technologies	31
6.2.2 Non-conventional cooling: Combined / hybrid cooling . . .	34
6.2.3 Cooling technology selection	37

6.1 Concentrated solar thermal

CST technologies use heliostats or mirrors to reflect and concentrate solar radiation onto a receiver. There, the radiation is captured as heat, also known as thermal energy. They can be classified in different ways¹, using temperature, two broad groups can be identified.

The first group includes lower-temperature systems operating below 400 °C. These are typically used for applications such as power generation, district heating, cooling, and desalination. It is worth noting that most industrial heat demand lies within this relatively low-temperature range of 100–400 °C [8]. This

1: With some parameters being correlated; for example, higher operating temperatures generally mean higher concentration factors

[8]: Schoeneberger et al. (2020), "Solar for Industrial Process Heat"



(a) Parabolic trough pilot plant at PSA



(b) Gemasolar 20MW-15h central tower CSP plant in Sevilla, Spain. Source: Wikipedia

Figure 6.1: Two main CST technologies. In (a) collector rows positioned facing each other purely for cinematographic purposes

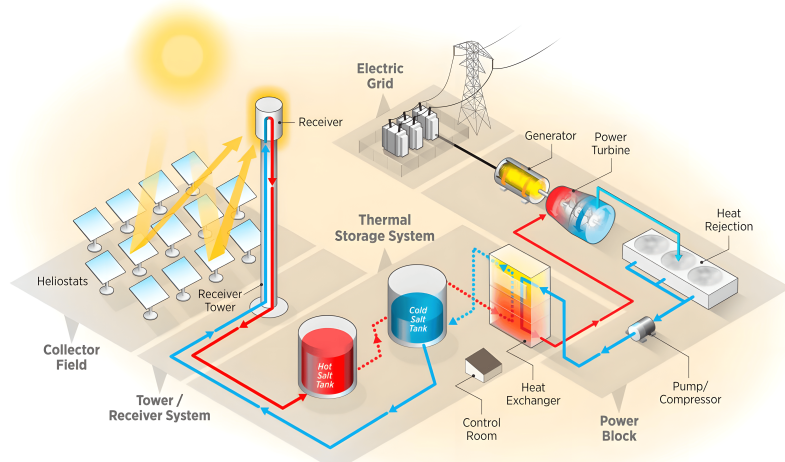


Figure 6.2: Solar tower CSP plant. Source: NREL [12]

2: Flat-plate collectors, though non-concentrating also deserve mention here, as they remain the most widely deployed solar thermal technology [9]

[10]: Thonig et al. (2023), “Concentrating Solar Technology Policy Should Encourage High Temperatures and Modularity to Enable Spillovers”

[11]: Mehos et al. (2020), “Concentrating Solar Power Best Practices Study”

[13]: Pfenninger et al. (2014), “Potential for Concentrating Solar Power to Provide Baseload and Dispatchable Power”

[14]: Binz et al. (2017), “Toward Technology-Sensitive Catching-Up Policies”

[15]: Lilliestam et al. (2021), “The Near- to Mid-Term Outlook for Concentrating Solar Power: Mostly Cloudy, Chance of Sun”

3: In the context of the industrial life-cycle (ILC) [16], the formative phase considers the period in which a technology and its industry and innovation system are still immature and need to grow and develop

[17]: Mir Artigues et al. (2019), *The Economics and Policy of Concentrating Solar Power Gen-*

segment of CST is also the most technically mature. Over the past decades, considerable progress has been made in line-focusing technologies such as parabolic troughs (see Figure 6.1 (a)) and linear Fresnel collectors². Although these systems have reached a high level of development, their potential for significant further cost reduction is relatively limited.

The second group comprises high-temperature systems operating above 600 °C. These rely on point-focusing technologies, most notably central receiver systems (see Figure 6.1 (b)). Still under development, they show promising potential for higher-value applications, including solar-driven chemical processes (such as aviation fuel production) and the provision of high-grade industrial heat in sectors like cement manufacturing [10]. Central receiver technology, however, remains at an earlier stage of commercial maturity. Fewer plants have been built, and many existing installations employ a mix of technical approaches [11].

6.1.1 CSP: Concentrated Solar Power

In a concentrated solar power plant, power is generated with a Rankine-cycle like in a conventional thermal power plant, however, the working fluid is heated up not by combusting/burning a fossil fuel, but as mentioned, by concentrating solar energy.

In a typical CSP plant – Figure 6.2 - *Power block* – the exhaust steam from the turbine is directed to a condenser, where its latent heat of vaporization is transferred to the available cooling medium. By coupling CSP with thermal storage – Figure 6.2 - *Thermal Storage System* – it can generate electricity after sundown or even days later, for example during adverse weather periods. Because of this ability, CSP is one of the few renewable electricity technologies that can generate fully dispatchable or even fully baseload power at very large scale [13].

CSP is an engineering-heavy, complex technology, with each project being different and tailored to both the environment in which it stands and the requirements of each single offtaker [14]. This means, that despite its relative long history, is still in its formative phase [15]³. As CSP is not yet competitive with other new generation, and especially not with operating and depreciated generators, it requires policy support to be economically viable [17]. This is due to its irregular historical development.

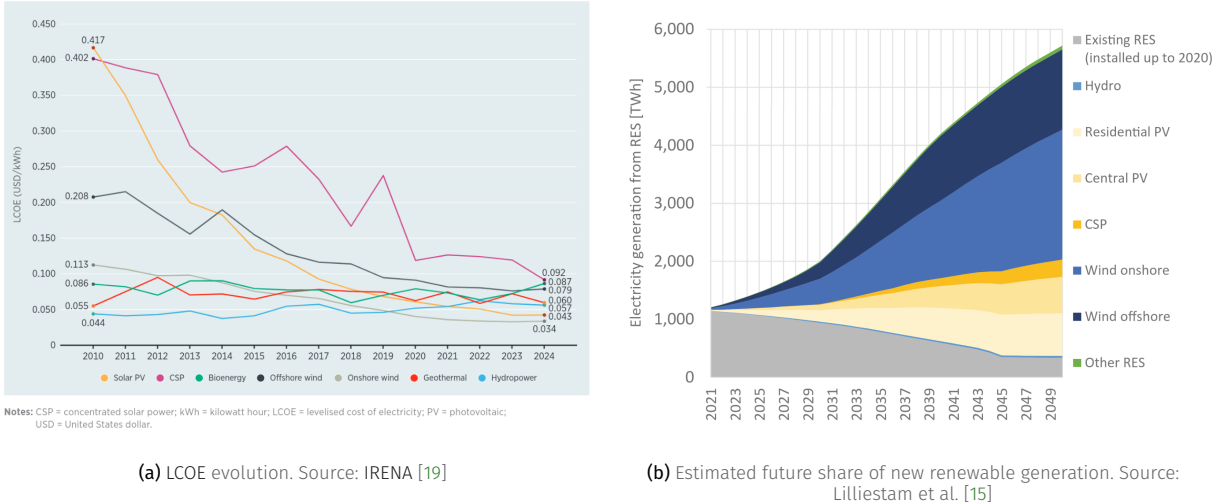


Figure 6.3: LCOE evolution and capacity predictions for different renewable technologies. Share is dominated by variable renewable energies and CSP is the fifth largest contributor, serving as a “gap filler” for the system flexibility of the EU electricity system [20]

6.1.2 CSP: from the hype to unrealized potential

At one point, CSP was seen as the leading alternative for large-scale solar energy. Ambitious visions and bold initiatives—such as the Desertec project—played a key role in generating immediate excitement around the technology. However, the political consequences of raising expectations that were ultimately unmet proved significant. In Europe, this disillusionment contributed to CSP becoming politically sidelined for many years [18]. Additionally, around 2010–2012 the cost crossover with photovoltaic occurred and from there only increased [19]. Many investments shifted from CSP to the more straightforward and profitable Photovoltaic (PV) technology.

The development of CSP has been marked by alternating periods of rapid expansion and sharp decline, largely shaped by national policy support. In the 1980s, California’s incentives led to the construction of nine CSP plants totaling around 350 MW, but the withdrawal of support caused the bankruptcy of Luz in 1991, resulting in a 15-year global pause in new projects. A second growth phase began in 2007 with feed-in tariffs in Spain and temporary backing in the US, leading to the construction of about 50 plants, mostly supplied by Spanish and German companies. However, the end of policy support in both countries around 2013 led to a sharp slowdown, with construction activity in 2016 at just one-third the 2012 level, and many firms exiting the sector. CSP remained commercially active mainly through projects in Morocco and South Africa, although costs increased and future prospects dimmed. Momentum returned in 2016 when China introduced a new feed-in tariff aimed at 5 GW of capacity, sparking renewed global interest. Optimism was further strengthened by major projects launched in Dubai and Morocco in 2018–2019. The near- to mid-term outlook for CSP is very uncertain: there are several positive developments concerning the global value chain and cost development. The market and policy outlook is bleak with the risk of a complete loss in many markets for CSP [15].

Setting realistic targets may ultimately be more effective than raising expectations that cannot be met. CSP remains a valuable technology for the energy transition—though likely at a smaller scale than initially envisioned, and over a longer timeframe. Several studies highlight its potential role in a zero-carbon or near zero power system [21]. For instance, the International Energy Agency (IEA)’s Net Zero by 2050 report projects that the global CSP capacity should reach 73 GW

[18]: Schmitt (2018), “(Why) Did Desertec Fail?”

[19]: IRENA (2025), *Renewable Power Generation Costs in 2024*

[15]: Lilliestam et al. (2021), “The Near- to Mid-Term Outlook for Concentrating Solar Power: Mostly Cloudy, Chance of Sun”

[21]: Bonilla et al. (2022), “Feasibility and Practical Limits of Full Decarbonization of the Electricity Market with Renewable Energy”

[22]: IEA (2021), "Net Zero by 2050 - A Roadmap for the Global Energy Sector"

[23]: IRENA (2024), "World Energy Transitions Outlook 2024: 1.5°C Pathway"

4: See Figure 6.3 (b)

[24]: Lilliestam et al. (2023), "Scaling up CSP"

[19]: IRENA (2025), *Renewable Power Generation Costs in 2024*

5: See Figure 6.3 (a)

[25]: Alliance (2024), *Blue Book of China's Concentrating Solar Power Industry 2024*

6: When wet cooling is used, further explained in the following

[7]: Rohani et al. (2021), "Optimization of Water Management Plans for CSP Plants through Simulation of Water Consumption and Cost of Treatment Based on Operational Data"

by 2030 and 281 GW by 2040 [22]. Likewise, IRENA envisions several hundred gigawatts of CSP by 2050, contributing to grid stability alongside a projected 8500 GW of solar PV and 6000 GW of wind capacity [23]. These projections suggest that CSP can play a complementary role to PV and wind by providing dispatchable, on-demand renewable electricity—further enabling intermittent renewable alternatives⁴. However, even at these more modest levels, CSP deployment would need to accelerate rapidly. To meet the IEA's 2030 target, the global CSP fleet—standing at just 6 GW in 2021—would need to expand more than tenfold in under a decade [24]. So far this is not happening, CSP technology remains niche with only 7 plants coming online in the 2020–2023 period [19] and is unlikely to become a globally important contributor to power system balancing in the next decade [24]. However the winds might be changing: 4 new plants came online in 2024, the costs of new CSP stations have decreased rapidly in the last years, 77% from 2010 to 2024, including a 46% reduction from 2023 to 2024. In terms of LCOE, it means that CSP has improved from 0.402 \$₂₀₂₄/kWh to below 10 cents (0.092 \$₂₀₂₄/kWh) making it competitive with new fossil fuel power stations [19]⁵ and the Chinese CSP project pipeline includes 37 future and ongoing projects, with a total capacity of 4.8 GW [25].

6.2 Cooling and water use

As can be inferred from the previous description, the successful deployment of CSP plants depends on several key factors: high annual direct normal irradiance, adequate land availability, and sufficient water resources. However, while the first two are typically found in arid regions as shown in Figure 6.4, the availability of water is often limited. In such locations, the source of raw water is usually restricted to groundwater or limited surface water bodies such as rivers, lakes, wells, or artificial reservoirs.

A CSP plant consumes water for various purposes, with the most significant demand coming from the cooling of the power block⁶. The power output and efficiency of a thermal power plant are strongly influenced by the operating temperature and pressure conditions at the condenser, which are directly linked to the turbine backpressure, and in turn depend on the cooling system.

In addition to cooling, water is also required for other plant operations, including [7]:

- ▶ Mirror cleaning (1.3% of total water consumption)
- ▶ Boiler blowdown (1.4%)
- ▶ Miscellaneous uses, such as air-cooled condenser (Air-Cooled Condenser (ACC)) bundle cleaning, auxiliary equipment cooling, and general infrastructure and staff needs.

In wet-cooled CSP plants, cooling water accounts for over 95% of the total water consumption, which can be further broken down into evaporation: 77.8% and blowdown and drift: 19.1%.

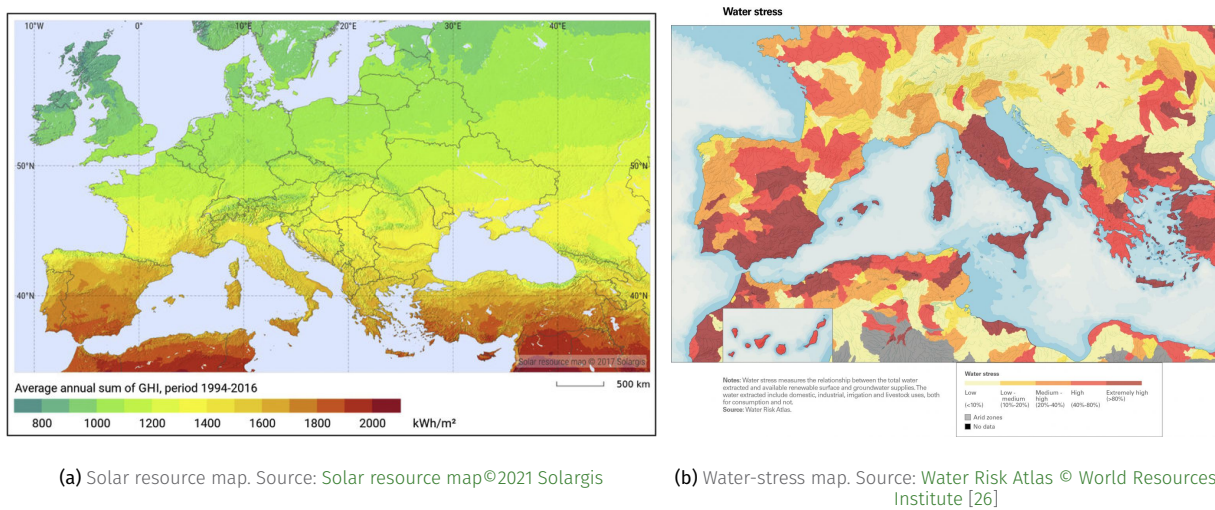


Figure 6.4: Greater potential for solar-powered processes takes place in water-scarce regions

Although CSP plants share a similar power cycle with other thermal power technologies, their water consumption patterns differ (see Figure 6.5). This is due to their unique capacity factor, operating schedule, and particularly their strong dependency on weather conditions, which contrasts with the more stable operation of fossil-fired plants. In contrast, conventional thermal power plants (e.g. coal, gas, or nuclear) are often sited near reliable freshwater sources, such as rivers or lakes, allowing them to utilize wet cooling without severe resource constraints. These plants are not tied to solar availability and can prioritize water access in their location decisions. CSP plants, however, must prioritize solar access and land availability — and thus have less flexibility in selecting sites with abundant water.

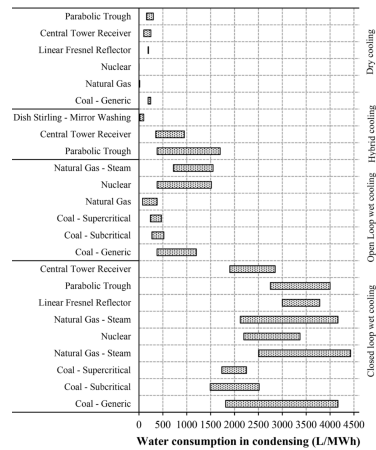


Figure 6.5: Water consumption comparison between CSP and other thermal power generation technologies. Source: Aseri et al. [27]

6.2.1 Conventional condenser cooling technologies

To date, the conventional systems used to remove excess heat from CSP plants are either wet (water-cooled) or dry (air-cooled), each with distinct characteristics and trade-offs regarding water usage, thermal performance, and cost.

Reminder: Cooling thermodynamic concepts

- ▶ The *cooling range* refers to the temperature drop experienced by the cooling water as it circulates through the condenser. The greater the better.
- ▶ The *approach* of the cooling tower is the temperature difference between the circulating water at the condenser inlet (or cooling tower outlet) and the lowest attainable cooling medium temperature, which varies depending on the cooling technology used.
- ▶ The Initial Temperature Difference (ITD) is the temperature difference between the cooler inlet the sink.
- ▶ Terminal Temperature Difference (TTD) represents the difference between the outlet temperatures of the cooling and the cooled fluids.



Figure 6.6: Conventional cooling technologies

Wet cooling

Water has traditionally been used as the cooling medium in wet cooling technology due to its high heat capacity and the possibility of reuse. In power plants, the steam exiting the turbine is condensed in a surface condenser, where cooling water circulates through tubes and absorbs the latent heat of the steam. The warmed cooling water is then returned to the cooling system for heat rejection.

Wet cooling technology requires a substantial amount of water (1.8–4 l/kWh) for condenser cooling, particularly in closed-loop systems that employ wet cooling towers to reject heat from the condenser water to the atmosphere through evaporative cooling [28]. While a small share of heat is removed through sensible air-to-water heat transfer, 80–90% of the cooling is achieved through the latent heat of vaporization [29].

Wet cooling towers function as heat rejection devices by bringing warm water from the condenser into direct contact with air. As part of the water evaporates, it absorbs heat from the remaining liquid, thereby lowering its temperature. The cooled water is then recirculated back to the condenser, completing the loop. This process is highly efficient, but it also leads to water losses from evaporation, drift, and blowdown.

Land availability for cooling systems is often constrained, particularly in central receiver plants where the solar field surrounds the receiver and requires unobstructed space for heliostat placement. For this reason, compact wet cooling designs using forced-draft towers are predominantly employed, such as the example shown in Figure 6.6 (a).

Wet cooling main characteristics

- ▶ Water consumption: 1.8–4 l/kWh [28]
- ▶ Parasitic load: $\approx 0.0165 \text{ kW/KWh}$ or 0.165% average annual consumption [30].
- ▶ Wet cooling consumes similar power along the year but increases its water consumption in the hotter months [31].
- ▶ CSP plants with wet cooling towers consume as much as $1.7 \times 10^6 \text{ m}^3$ per year of operation [7].
- ▶ Greater available approach, since the lowest attainable temperature is

[28]: Meldrum et al. (2013), “Life Cycle Water Use for Electricity Generation”

[29]: Colmenar-Santos et al. (2014), “Water Consumption in Solar Parabolic Trough Plants”

the wet-bulb temperature.

- 55% of CSP plants worldwide make use of wet cooling technology for condenser cooling [32, 33]

Dry cooling

In dry cooling, heat is rejected to the surroundings by convection via extended or finned surfaces or tubes arranged in a row, and each row consists of numerous cells [34]. In this type of cooling, the warm water and the ambient air do not have direct contact with each other (as in wet cooling). But because air is a poor heat transfer medium, the condenser must operate at a higher temperature and pressure to drive heat out efficiently. This sensitivity to ambient air temperature leads to elevated turbine backpressure, specially during hot weather, reducing thermal efficiency and power output compared to wet cooling systems. Dry cooling systems can be broadly categorized as direct or indirect [35].

In direct systems, turbine exhaust steam is delivered straight to an ACC (see Figure 6.6 (b)), where heat rejection to the environment occurs in a single step. The steam is condensed inside finned tubes by ambient air blown across the exterior finned surfaces arranged in A-frame (forced draft) or delta (induced draft) configuration. This process relies on latent heat transfer and can employ either mechanical or natural draft designs. ACCs have been used for nearly 70 years, and were pioneered in regions as diverse as Western Europe, South Africa and the Middle East. The largest ACC units in operation is in South Africa (Medupi) with six 800-MW units on ACCs [36].

In indirect systems, steam first condenses in a separate condenser, which may be either a conventional shell-and-tube surface condenser or a barometric condenser (direct-contact type), where steam meets a spray of cooling water. The resulting warm cooling water is then circulated to an ACHE (see Figure 6.6 (c)) for final heat rejection to the atmosphere. This arrangement introduces an additional heat exchange stage, so the ACHE handles only sensible heat transfer, requiring greater heat exchange surface area but being less sensitive to fluctuations in ambient temperature.

A prominent example of an indirect dry cooling configuration is the Heller system, named after its inventor Prof. H. Heller in Hungary in the 1940's [37, 38]. In the direct-contact Heller system, steam from the turbine condenses in a barometric condenser, and the resulting warm cooling water is cooled in an ACHE before recirculation. Thermal performance is generally comparable to that of an ACC, but mechanically driven Heller systems tend to have higher specific electrical consumption because, in addition to fan power, extra pumping power is required to overcome the jet condenser's added pressure drop [39].

If an indirect-contact surface condenser is used instead of a barometric condenser, the setup is generally less efficient than both ACCs and the direct-contact Heller configuration because it introduces a TTD (TTD \approx 3–4 °C versus \approx 0.3 °C for direct-contact), resulting in lower overall cycle efficiency.

Natural draft dry cooling towers—commonly associated with barometric condenser systems—can only be used in parabolic trough plants. In central receiver systems, their significant size (about 135 m tall) would obstruct the heliostat field. A possible alternative is fan-assisted natural draft systems, which reduce tower height to around 50–70 m while retaining some benefits of natural draft operation [40]. According to Andras et al., Heller systems require approximately the same capital costs but are much cheaper to operate since they do not need to be mechanically driven. They have been operating for decades in 17 power plants including with the largest indirect dry cooled combined cycle power plant with 3x777 MWe dry towers at Gebze-Adapazari combined cycle (Turkey).

[34]: Turchi (2010), *Parabolic Trough Reference Plant for Cost Modeling with the Solar Advisor Model (SAM)*

[35]: Maulbetsch (2004), *Comparison of Alternate Cooling Technologies for U.S. Power Plants: Economic, Environmental, and Other Tradeoffs*

[36]: Maulbetsch (2012), *Economic Evaluation of Alternative Cooling Technologies*

[37]: Jászay (1958), "Indudustrial Review-Aus Der Industrie. The Air-Cooled Condensing Equipment" System Heller" a Comprehensive Survey"

[38]: Balogh et al. (2006), "Heller's Indirect Approach Widens Applicability of Dry Cooling"

[39]: Mil'man et al. (2020), "Air-Cooled Condensing Units in Thermal Engineering (Review)"

[40]: Andras et al. (2005), "Advanced Heller System Technical Characteristics"

Unlike wet cooled plants, the dry cooled plants require minimal waterside infrastructure and other related components. None dedicated to the cooling such as water supply network evaporation ponds, storage ponds, treatment plants for condenser cooling water. As a consequence, for the dry-cooled plants, capital and operation and maintenance costs of these components are negligible [36].

[27]: Aseri et al. (2022), "Condenser Cooling Technologies for Concentrating Solar Power Plants"

[35]: Maulbetsch (2004), *Comparison of Alternate Cooling Technologies for U.S. Power Plants: Economic, Environmental, and Other Tradeoffs*

A recent review on condenser cooling technologies [27] observes that a dry-cooled Parabolic Trough (PT) based plant would deliver 3–10% less annual electricity output and would cost 4% to 10% more than a wet-cooled plant resulting in 2% to 19% increase in LCOE. It was also observed that due to large differences in operating temperature of power cycle (560 °C for Solar Tower (ST) based plants and 391 °C for PT based plants), the reduction in net electricity output for ST based plants is less as compared to PT based plants (Sau et al., 2016). It should be noted that many of these analysis were made for first generation CSP with no thermal storage, which is an outdated technology. The inclusion of thermal energy storage in the dry or hybrid cooling plant (six hours of storage capacity) can reduce the overall penalty of LCOE considerably: 8.1% to 6.3% for dry-cooled as compared to wet-cooled plants [27]. According to Maulbetsch et al. [35], the *break-even* water cost at which wet and dry cooling have the same annual costs (for situations in which the rest of the base case values and assumptions apply) is between 2.00 USD₂₀₀₂/kgal and 3.00 USD₂₀₀₂/kgal.

Dry cooling main characteristics

1. Capital cost ratio ranges from 4.5x at a hot, arid site to about 3.5x at more moderate sites [35].
2. Electrical consumption: 1.5 to 5 times wet cooling, 0.05–0.06 kW/kWh
3. Penalty up to 25% during the hottest hour of the year [35] and 5–6% average annual parasitic consumption [27, 41, 42].
4. Limited approach, constrained by the dry-bulb temperature, worsened if an indirect contact surface condenser is used.
5. 24% of commercial plants make use of this technology [32, 33].

6.2.2 Non-conventional cooling: Combined / hybrid cooling

While energy efficiency has long been a priority, water conservation only began receiving significant attention in recent years. This is reflected in the large number of wet-cooled CSP plants built in the past. Today, some of these plants face growing scrutiny and competition for water resources, as many regions of the world experience prolonged periods of water stress. In response, a third alternative is gaining traction: hybrid or combined cooling technologies, which integrate the advantages of different cooling methods (wet and dry) into a single, innovative system. The concept has been explored since the 1970s [43–46] and regained momentum in the following decades [35, 36], although early studies primarily focused on fossil-fuel and nuclear thermal power plants. Over the past decade, interest sparked in evaluating hybrid cooling solutions specifically for concentrated solar power systems.

Terminology: Combined vs Hybrid Cooling

In the literature, two terms are commonly used to describe cooling systems that integrate both wet and dry components: *hybrid* and *combined*.

Hybrid systems (See Figure ?? (a)) refer to configurations where the dry and wet cooling components are integrated into a single physical unit. An example is a cooling tower with two sections—an upper dry section followed

[43]: Hu (1976), *Engineering and Economic Evaluation of Wet/Dry Cooling Towers for Water Conservation*

[44]: Zaloudek et al. (1976), *Study of the Comparative Costs of Five Wet/Dry Cooling Tower Concepts*

[45]: Loscutoff (1975), *Preliminary Evaluation of Wet/Dry Cooling Concepts for Power Plants*

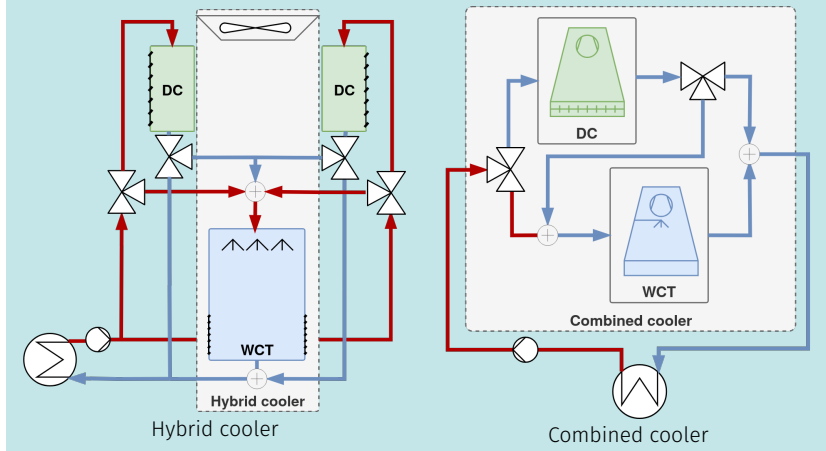
[46]: Wiles et al. (1978), *Description and Cost Analysis of a Deluge Dry/Wet Cooling System*.

by a wet section that can be activated as needed.

Combined systems (See Figure ?? (b)), by contrast, consist of separate, independent dry and wet units connected by a hydraulic circuit. Each component is physically distinct and operates independently.

From a thermodynamic perspective, hybrid and combined systems are functionally equivalent. However, hybrid systems tend to be more compact due to their integrated design, while combined systems offer greater flexibility in component layout and maintenance. Additionally, combined systems are often easier to implement in practice, as the individual dry and wet components are commercially available off the shelf—unlike hybrid units, which may require custom design and manufacturing.

These differences are not all that important, so the two terms can be used interchangeably.



Many heterogeneous hybrid/combined coolers can be found comprising different components with different arrangements:

1. Water-enhanced dry cooling. A dry cooler (usually ACC) switchable to wet (deluge condenser cell). In the deluged condenser configuration, dry-cooling is prioritized until a certain backpressure is reached, when water is sprayed wetting the exchanging surfaces, which now act equivalently to the packing bed in a wet cooling tower [7, 44–47]. The overall heat transfer rates are improved since now the transfer mechanism is air to the water film that evaporates, but air–metal contact is lost, effectively disabling the dry-cooling mechanism. In this configuration is either one or the other. Still, since the cooling system nominal cooling capacity is usually reached by stacking together smaller capacity cells, a parallel configuration could be achieved by keeping some of the cells dry (even having them only dry by design).
 2. Dry cooler (usually ACC) + WCT in parallel [36, 48, 49]. In this configuration part of the vapor is directed to a dry ACC while the rest goes to a surface condenser cooled by a wet cooling tower. Each cooler can be sized independently.
 3. Surface Condenser (SC) + ACHE + WCT in series.
 4. SC + (ACHE+WCT) in series-parallel [50–52]. The series-parallel configuration is interesting since it offers the greatest degree of flexibility, at the cost of adding two heat transfer processes in series at a minimum (SC→ACHE) and three if in series configuration: SC→ACHE→WCT, though this last one is intended and not so problematic since the wet cooling has a higher ITD (difference between outlet temperature from dry cooler and

[7]: Rohani et al. (2021), "Optimization of Water Management Plans for CSP Plants through Simulation of Water Consumption and Cost of Treatment Based on Operational Data"

[44]: Zaloudek et al. (1976), *Study of the Comparative Costs of Five Wet/Dry Cooling Tower Concepts*

[45]: Loscutoff (1975), Preliminary Evaluation of Wet/Dry Cooling Concepts for Power Plants

[46]: Wiles et al. (1978), *Description and Cost Analysis of a Deluge Dry/Wet Cooling System*.

[47]: Golkar et al. (2019), "Determination of Optimum Hybrid Cooling Wet/Dry Parameters

[36]: Maulbetsch (2012), *Economic Evaluation*

[48]: Barigozzi et al. (2011), "Wet and Dry Cooling Systems Optimization Applied to a Modern Waste-to-Energy Cogeneration Heat and

[49]: Barigozzi et al. (2014), "Performance Prediction and Optimization of a Waste-to-Energy Cogeneration Plant with Combined Wet and Dry Cooling System".

[50] Palenzuela et al. (2022). "Experimental

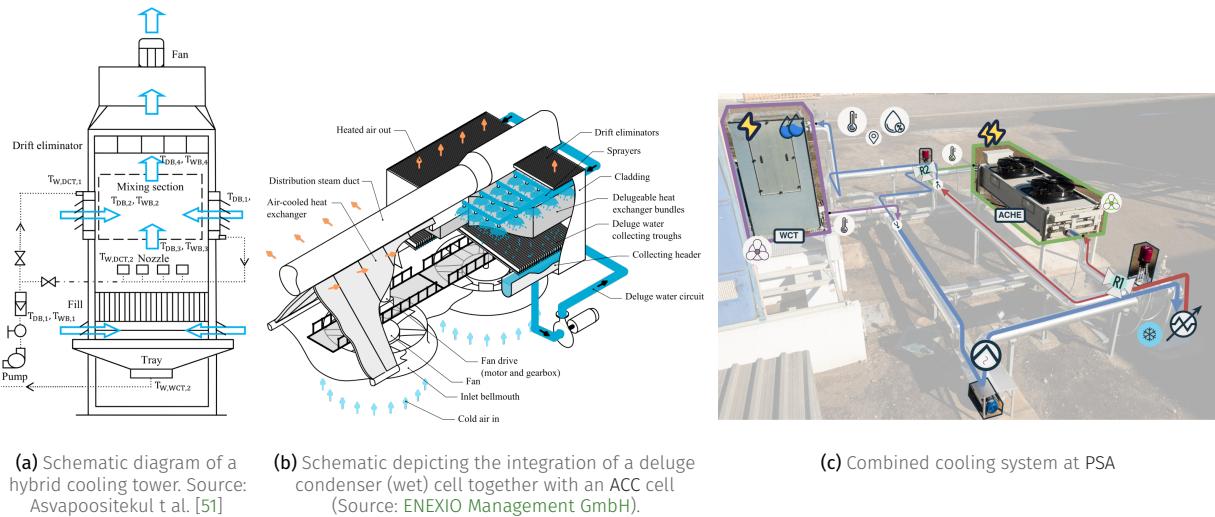


Figure 6.7: Different hybrid/combined coolers configurations

7: Specially in the combined cooler case, in the hybrid alternative it might not be as straightforward

wet bulb temperature). Flexibility is provided by the almost continuous flexible hydraulic configuration: only series, only parallel, any configuration in between or only one of the systems. But also in the design, each cooler can be sized independently⁷. This allows to optimize the system adhoc for each particular deployment by running simulations with the expected operation conditions and prioritizing more the wet or the dry component.

From a literature review a few conclusions can be drawn:

- ▶ Air flow rates are very different between dry and wet systems, so any design needs to allow independent regulation of each. In the combined configuration (separate coolers) this is easily achieved since they have independent fans. On the other hand for hybrid systems curtains?
- ▶ Corrosion might be a problem in the deluged condenser, if so, plastic exchange surfaces might have to be used, further decreasing already low heat transfer coefficients.
- ▶ If dry and wet systems share the condenser *i.e.* the hydraulic circuit. A direct contact jet-condenser type cannot be used, since the power cycle requires high-quality water and large amounts would need to be constantly replenished because of the wet cooler evaporation.
- ▶ If the dry cooler is going to be the main cooling source throughout the year, options that combine an ACHE with a surface condenser, are going to penalize the dry cooling component compared to alternatives like the ACC or Heller system -both with or without delugement or a parallel only configuration.
- ▶ On the contrary, during operation systems that allow combinations of series-parallel configurations provide the greatest potential to adapt the cooling system to the changing operation and ambient conditions. The series configuration is a water conservative configuration while still being able to maintain the required backpressure despite adverse conditions. The parallel configuration maximizes cooling capacity but is more water intensive.

A hybrid cooling technology requires relatively larger infrastructure as it comprises of components of both wet and dry cooling technologies, though much smaller water side infrastructure [7]. Also, the potential for water reuse for a hybrid system according to Rohani et al. [7] can amount to 23% of the total raw water consumption. An important part of this water can be treated and reused

[7]: Rohani et al. (2021), "Optimization of Water Management Plans for CSP Plants through Simulation of Water Consumption and Cost of Treatment Based on Operational Data"

without significantly increasing the production costs: up to 14% reduction with the same production cost or even slightly reduced.

Hybrid/combined systems are a compromise between full-wet and full-dry systems. Due to their heterogeneity depending on the prioritized objective their costs and consumptions can be closer to one or the other. Such systems can be sized for a range of desired water savings. The systems are normally considered for annual water use targets of from 15% to 85% of that used by a wet cooling system. Outside that range, they are normally not economically attractive. When even less water than this is available, water-enhanced dry systems might be the better option [35]. For some configurations (when using indirect dry cooling) they can get more expensive than the standalone ACC alternative [36]. The inclusion of thermal energy storage in the hybrid cooled plant (six hours of storage capacity) can reduce the overall penalty of LCOE from 6.4% to 3.2 compared to wet-cooled plants [27].

[27]: Aseri et al. (2022), "Condenser Cooling Technologies for Concentrating Solar Power Plants"

Hybrid cooling main characteristics

1. Capital cost: 2–3.5x [36]
2. Penalty: 1–3%, 2–8% in LCOE [27],
3. Just one commercial CSP plant makes use of this technology [53]

NOTE: Due to the novelty and heterogeneity of these systems, values can change significantly.

6.2.3 Selection of the cooling technology

Selection of condenser cooling technology can affect the financial as well as technical viability of concentrating solar power (CSP) plants. These differences between technologies are dependent on the environment conditions (local water cost, local temperature, etc). Except for extreme cases: no water availability only dry cooler or plenty water availability throughout the year leading to the immediate decision of a wet cooler, this is not an obvious decision. Dry cooling or hybrid cooling systems are increasingly used in CSP projects, even though they typically come with higher capital costs and reduced thermodynamic performance, particularly in hot weather for the dry only alternative. These systems trade water savings for lower efficiency, making the choice of cooling technology a critical design decision that balances technical, economic, and environmental considerations.

Selecting the cooling technology is not trivial, especially if a hybrid cooler is chosen. The relative capability of the wet and dry systems is the primary determinant of the system cost. This, in turn, depends on: the amount of water available for cooling and the value of plant output during the hottest hours of the year compared to the average value over the entire year. As a general rule, the more water available for cooling, the cheaper and more efficient is the cooling system. If the amount of water available is between 15% and 85% of that required for an all-wet system, the capital cost of a hybrid system will be intermediate between the costs of an all-wet and an all-dry system [35]. Also, environment context and costs structures are strongly dependent on the particular location and affect decision-making. Annual simulations of the different cooling alternatives should be performed using weather data for the particular location, local water availability throughout the year, and performing a techno-economical analysis in order to make an informed decision.

So far most systems make use of either wet cooling (55% worldwide) or dry (24%) [32]⁸, but it is likely that some hybrid cooling configuration would be the optimal choice in most situations where a wet only alternative is used⁹ due to their adaptive nature and flexible operation. Currently, few commercial plants

8: the remaining 21% is unknown, but likely to be either of the conventional technologies

9: and probably in many dry only ones too

makes use of hybrid cooling technologies. An example of a series, integrated, hybrid system providing significant water conservation exists at the San Juan Generating Station in Farmington, New Mexico. It consists of a conventional, shell-and-tube steam condenser coupled to a hybrid tower with an air-cooled dry section on top which discharges into a wet cooling tower beneath. For CSP, the only known plant to make use of this technology is the Crescent Dunes Solar Energy Project, a 110 MW concentrated solar power station equipped with 1.1 GWh of molten-salt thermal energy storage. This plant makes use of the described parallel configuration [53]. Also, within the *MinWaterCSP* project, a full scale pilot hybrid plant consisting of an air cooled deluged condenser was successfully built and tested in Stellenbosch, South Africa [54].

[53]: (), SPX Awarded Contract to Supply Parallel Condensing System For Crescent Dunes Solar Energy Project near Tonopah, Nevada

[54]: GmbH (2020), Blog #29 – Full Scale Testing in Stellenbosch, South Africa | MinwaterCSP

TL;DR

In this chapter a detailed description of the combined cooling pilot plant at PSA is provided including a P&ID diagram and the methodology followed to perform the experimentation and data-processing. Three experimental campaigns for the WCT with XX, XX and XX different operating points and one for the DC with XX operating points are processed and made openly available in public repositories.

7.1	Plant description	40
7.2	Experimental campaigns	41
7.3	Wet cooling tower	41
7.3.1	Exp 1	41
7.3.2	Exp 2	42
7.3.3	Exp 3	43
7.3.4	Experimental campaigns for the dry cooler	43

Introduction

The combined cooling pilot plant at Plataforma Solar de Almería is a unique facility that integrates a wet cooling tower and a dry cooler in a flexible hydraulic configuration. It allows for the study and validation of different cooling strategies and the development of models.

...

This chapter describes the plant in Section 7.1 (Plant description) and the experimental campaigns carried out in Section 7.2 (Experimental campaigns).

completar esta sección antes del domingo

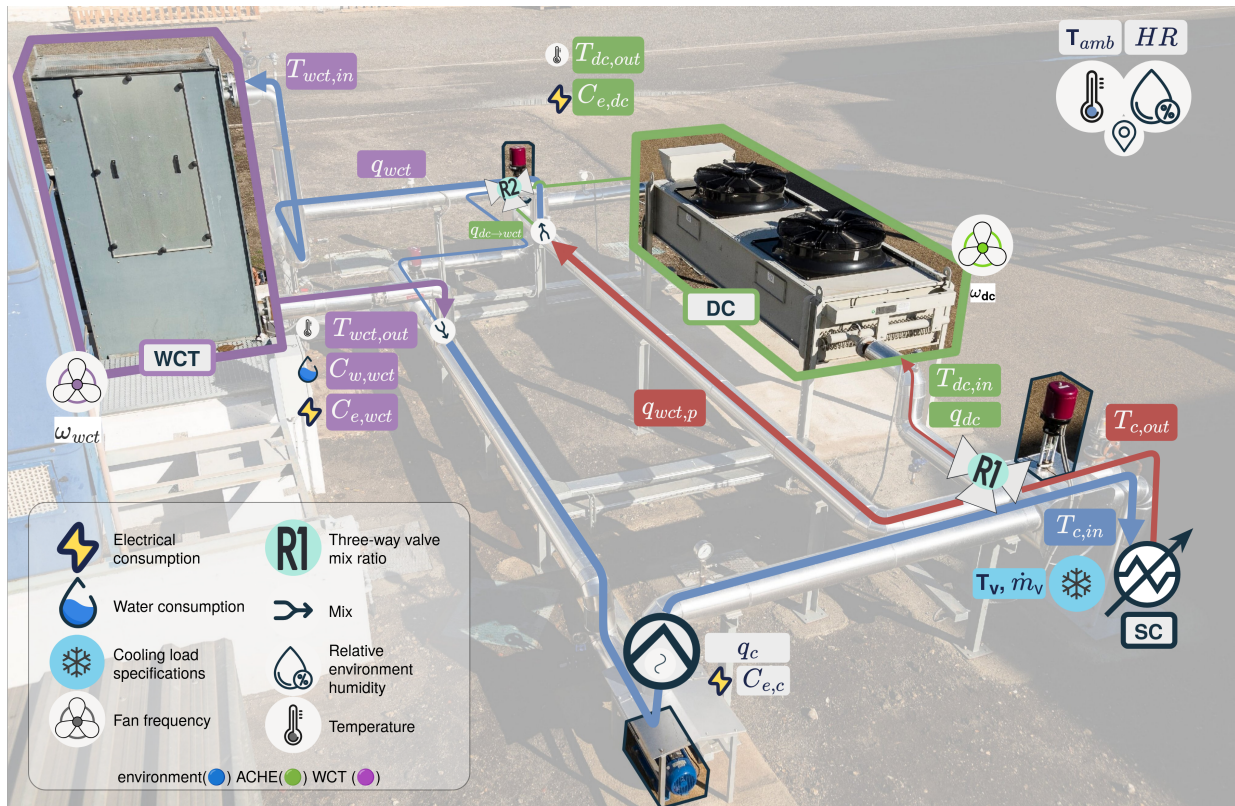


Figure 7.1: PSA combined cooling system facility

7.1 Plant description



Figure 7.2: Back view of the WCT.



The pilot plant of combined cooling systems located at PSA (see the layout in Figure 7.3) consists of three circuits: cooling, exchange and heating. In the cooling circuit (see a picture in Figure 7.2), water circulating inside the tube bundle of a Surface Condenser (SC) can be cooled through a Wet Cooling Tower and/or a Dry Cooling Tower (type Air Cooled Heat Exchanger, ACHE), both with a designed thermal power of 204 kW_{th}. In the exchange circuit, a saturated steam generator of 80 kW_{th} (on the design point), generates steam at different pressures (in the range between 82 mbar and 200 mbar), which is in turn condensed in the surface condenser. In this way, the steam transfers its latent heat of condensation to the refrigeration water, that is heated. Finally, in the heating circuit, a solar field with a thermal power of 300 kW_{th} at the design point, provides the energy required by the steam generator, in the form of hot water. It is a unique, very flexible, fully instrumented and versatile facility, able to operate in different operation modes: series and parallel mode, conventional dry-only mode (all water flow is cooled through the dry cooling tower) and wet-only mode (all water flow is cooled through the wet cooling tower). The instrumentation related to the WCT is described in Table Table 7.1. Note that the sensors measuring the air velocity and temperature and relative humidity at the outlet area of the wet cooling tower have not been installed in the plant. Portable sensors were used instead in some experiments, as described in Section ??.

In regards to operational aspects of the system, note that the cooling water and air flow rates at the experimental facility (\dot{m}_w and air, \dot{m}_a , respectively), are modified with the Pump 1 and the fan frequency percentage SC-001, respectively (see Figure 7.3).

Table 7.1: Characteristics of instrumentation (^a value of the temperature in °C, ^b of reading, ^c full scale, ^d mean value).

Measured variable	Instrument	Range	Measurement uncertainty
Water temperature (TT-001, TT-006)	Pt100	0 - 100 °C	0.03 + 0.005·T ^a
Cooling water flow rate (FT-001)	Vortex flow meter	9.8 - 25 m ³ /h	± 0.65 % o.r. ^b
Water flow rate (FT-004)	Paddle wheel flow meter	0.05 - 2 m ³ /h	± 0.5 % of F.S ^c + 2.5 % o.r
Ambient temperature	Pt100	-40 - 60 °C	± 0.4 @20 °C
Relative humidity	Capacitive sensor	0 - 98%	± 3 % o.r @20 °C
Air velocity	Impeller anemometer	0.1-15 m s ⁻¹	± 0.1 m s ⁻¹ + 1.5 % o.r
Outlet air temperature	Pt100	-20-70°C	±0.5°C
Outlet air humidity	Capacitive sensor	0-100%	± 2%

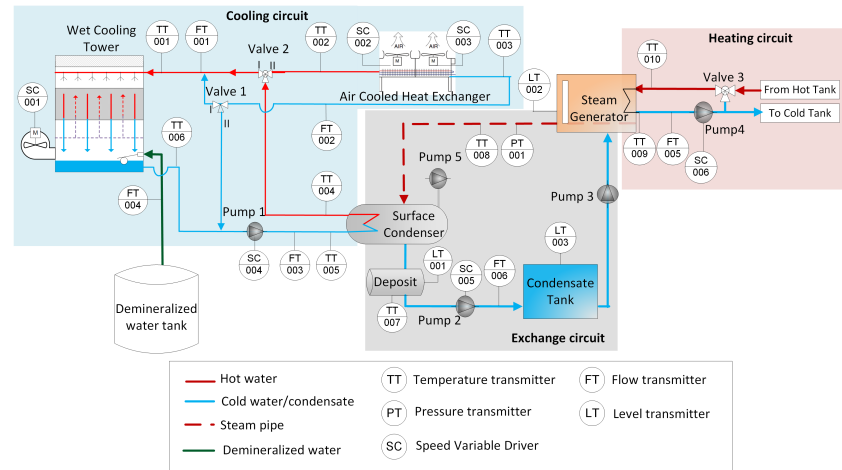


Figure 7.3: Layout of combined cooling systems pilot plant at PSA.

7.2 Experimental campaigns

With the aim of characterizing and developing models for this novel facility, over the years several experimental campaigns have been carried out. In particular, three different experimental campaigns have been performed to characterize the WCT specifically, while a campaign was also carried out to characterize the DC.

7.3 Experimental campaigns for the wet cooling tower

A total of 132 steady-state experimental points have been obtained. These data cover a large variety of ambient conditions (different seasons, days and nights) and thermal loads (from 27 kW to 207 kW). The objective of the experimental campaigns is to develop and validate two modelling strategies for the performance evaluation of the WCT¹.

The normative framework followed to carry out the experiments, in order to ensure stable conditions, has been the standards UNE 13741 [55] and the Spanish CTI [56]. These standards specify the test duration and the allowed variations of the most representative ambient and operating magnitudes (water flow rate, heat load, cooling tower range, wet-bulb and dry-bulb temperatures and wind velocity) during the tests. Although the duration of the test should not be less than one hour according to the standards, due to the low capacity of the WCT in the PSA pilot plant and the operational experience, the duration of the tests has been reduced to up to 30 minutes. Once stable conditions are maintained during the defined interval time, the average and deviations values of each measurement are calculated in order to check that they are within the allowable limits of the norm, which finally lead to a valid steady-state operating point.

Figure 7.4 shows the main variables involved in one of the experiments performed at the pilot plant at constant air flow rate ($f_{fan}=25\%$). As can be observed, there are two time intervals in this case, in which the process is at stationary conditions according to the normative framework mentioned. In order to process the results of the experimental tests and identify valid time intervals, such as the ones shown in this example, a function has been implemented in the MATLAB environment. This function identifies whether the standard criteria is met and calculates the mean values of the required variables.

The data from the different experimental campaigns is available at [\[palenzuela_steadystate_2024a, 57\]](#).

1: See Section 8.1 (Wet cooler)

[55]: UNE (2004), *Thermal Performance Acceptance Testing of Mechanical Draught Series Wet Cooling Towers*

[56]: CTI (2000), *Code Tower, Standard Specifications. Acceptance Test Code for Water Cooling Towers*

7.3.1 Experimental campaign 1 – Exp 1

This campaign was specifically designed for the calibration of the physical model. In total, 19 experimental tests were performed at the combined cooling pilot plant at PSA. The physical model focuses on the calculation of the Merkel number which, according to the literature ASHRAE [58], is not a constant value. Instead, it varies depending on the operating conditions (water-to-air mass flow ratio, \dot{m}_w/\dot{m}_a). Therefore, the experimental campaign has been designed to cover different water-to-air mass flow ratios. Both variables, the water and the air flow rates, were varied within the allowable range for plant operation. In the case of the water flow rate, it ranged from 8 m³/h to 22 m³/h, and in the case of the air mass flow rate, it was modified by changing the fan frequency from 12.5 Hz to 50 Hz (fan frequency percentage, f_{fan} , from 25 % to 100 %). The magnitudes required to experimentally determine the air mass flow rate (air velocity and air temperature and relative humidity) were measured at the outlet area of the

[palenzuela_steadystate_2024a, 57](#): Serrano et al. (2024), "Wet Cooling Tower Performance Prediction in CSP Plants"

[58]: Ashrae (2004), "HVAC Systems and Equipment"

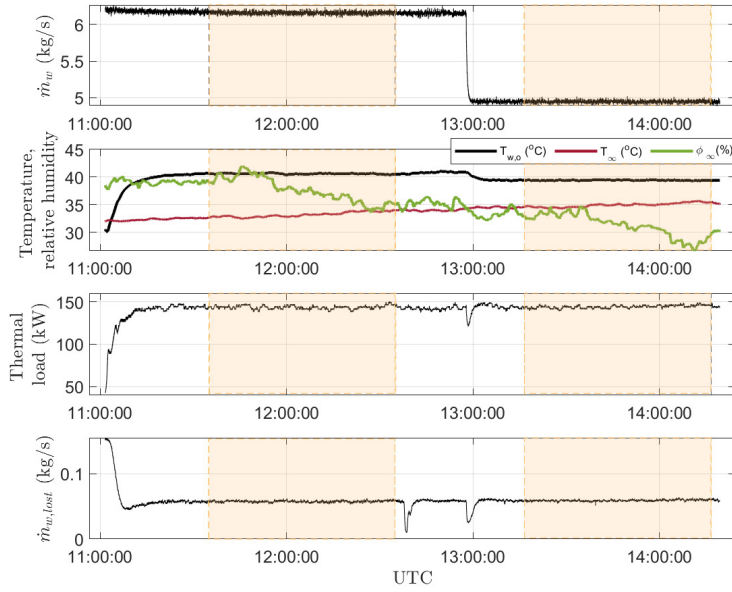


Figure 7.4: Example of one experiment at the pilot plant in July with two valid steady-state operating points.

2: Using the sensors listed in Table 7.1

3: This enables to obtain the air mass flow rate at the outlet of the cooling tower, \dot{m}_w , using the permanent sensors installed in the facility

cooling tower². The outlet area was divided into 9 quadrants and the above mentioned magnitudes were registered at the center of each quadrant. The obtained values were averaged to determine the mean velocity, temperature and relative humidity used in the air mass flow rate calculation.

Following the same experimental procedure, air velocity, temperature and humidity maps were measured for 8 different f_{fan} levels (ranging from 30 % to 100 % in 10 % intervals)³.

The range of air and water mass flow rates are 1.16–4.32 kg/s and 2.17–6.15 kg/s, respectively. Regarding the environmental conditions, these were quite similar for all tests in the campaign: high ambient temperatures (ranging between 32 °C and 41 °C), and low ambient relative humidities (between 13 % and 40 %) since the experiments were carried out during the summer season.

7.3.2 Experimental campaign 2 – Exp 2

The data required for data-driven models depends on several factors such as the complexity of the model and the error allowed or the diversity of the inputs. With the aim of obtaining a reliable model for the WCT, data collected over several years of operation of the combined cooling system have been used for tuning. They are a set of 115 stationary data covering the following operating ranges: ambient temperature, T_∞ , [9-39] °C, ambient humidity, ϕ_∞ , [10-87] %, inlet water temperature, $T_{w,i}$ [33-41] °C, cooling water flow rate, q_w [6-23] m³/h and fan frequency percentage, f_{fan} [21-94] %. The thermal load in these tests varies in the range of [27-178] kW_{th}. The number of steady-state data obtained is a reasonable value when compared to other similar data-driven models of counter-flow cooling towers, as in the case of [59], where 81 experimental points were collected for training and testing⁴

4: Reminder, dataset is available at [palenzuela_steadystate_2024a]

7.3.3 Experimental campaign 3 – Exp 3

With the aim of validating and comparing different modelling approaches, a dataset of 17 tests (different from the ones taken for experimental campaigns 1 and 2) has been compiled. This experimental campaign was designed using a design of experiments based on full factorial design with 4 factors and 2 levels (low and high), whose values are shown in Table 7.2.

An additional test at design operating conditions of the WCT ($T_{b,\infty}=21\text{ }^{\circ}\text{C}$, $T_{w,i}=40\text{ }^{\circ}\text{C}$, $\dot{m}_w=6.9\text{ kg/s}$ and $T_{w,i} - T_{w,o}=7\text{ }^{\circ}\text{C}$) has been also included in this test campaign, where $T_{b,\infty}$ is the ambient wet bulb temperature and $T_{w,o}$ the temperature of the water at the outlet of the WCT.

7.3.4 Experimental campaigns for the dry cooler

Table 7.2: Design of experiments for model comparison.

Variable	Low level	High level
$T_b\text{ (}^{\circ}\text{C)}$	≤ 10	≥ 15
$T_{w,i}\text{ (}^{\circ}\text{C)}$	≤ 37	≥ 39
$\dot{m}_w\text{ (kg/s)}$	≤ 3.3	≥ 5
$T_{w,i} - T_{w,o}\text{ (}^{\circ}\text{C)}$	≤ 7	≥ 8

Modelling of a combined cooling system

TL;DR

This chapter describes the steady-state modelling of the different components of a combined cooling system, mainly a WCT and a DC. Different alternatives are presented: from physical models to data-driven approaches, including the generation of samples for data-driven models trained using data from a physical model. Models are also developed for the other components of the system and finally it is shown how they are integrated into a complete system model. The complete system model interface is defined at Model ?? and a block diagram is presented in Figure 8.3 including all relevant variables.

Introduction

In order to study the potential advantages of making use of a combined cooling system, it is first necessary to develop the modelling of its components. Since the objective is performance prediction, this chapter focuses on the steady state modelling of the combined cooler main components, *i.e.* the WCT and the DC. More specifically, the aim is to compare two modelling strategies: that based on physical equations (Section 3.2) and that based on black box models (Section 3.3) such as ANNs, in order to see which one is more suitable for its integration in the optimization of the complete process.

This chapter presents a comparison between the two modelling approaches, at steady state and with a focus on optimization applications, in terms of predictive capabilities, experimental and instrumentation requirements, execution time, implementation and scalability. A sensitivity analysis is performed to further analyze and compare each case study. It also presents and evaluates all relevant aspects of interest in the development of such models, specifically for ANNs, model configuration, architecture and topology are discussed. Other system components are also described in Section 8.3 (Other components) and finally their integration is discussed in Section 8.4 (Complete system).

8.1 Wet cooler

In the case of the models based on physical equations, the analysis of wet cooling towers has its origin in [60], in which the theory for their performance evaluation was developed. Merkel proposed a model based on several assumptions to simplify the heat and mass transfer equations to a simple hand calculation. However, these assumptions mean that Merkel's method does not reliably represent the physics of the heat and mass transfer process in a cooling tower. This was already stated by Bourillot [61] who concluded that the Merkel method is simple to use and can correctly predict cold water temperature when an appropriate value of the coefficient of evaporation is used. However, it is insufficient for the estimation of the characteristics of the warm air leaving the fill and for the calculation of changes in the water flow rate due to evaporation. Jaber and Webb [62] developed the equations necessary to apply the effectiveness-NTU¹ method directly to counterflow or crossflow cooling towers. This approach is particularly useful in the latter case and simpler compared to a more conventional numerical procedure. Notice that the effectiveness-NTU

8.1 Wet cooler	45
8.1.1 Poppe model	46
8.1.2 Samples generation for first-principles to data-driven models	48
8.1.3 Model interface	48
8.2 Dry cooler	49
8.2.1 Physical model	49
8.2.2 Samples generation for first-principles to data-driven models	49
8.2.3 Model interface	49
8.3 Other components	50
8.3.1 Electrical consumption	50
8.3.2 Surface condenser	50
8.3.3 Mixers	51
8.4 Complete system	51

Ahora mismo esta introducción es demasiado parecida al TL;DR, hay que distinguirla

[60]: Merkel (1925), "Verdunstungskühlung"

[61]: Bourillot (1983), "Hypotheses of Calculation of the Water Flow Rate Evaporated in a Wet Cooling Tower"

[62]: Jaber et al. (1989), "Design of Cooling Towers by the Effectiveness-NTU Method"

1: The effectiveness-NTU method estimates how well a heat exchanger transfers heat by comparing the actual heat transfer to the maximum possible, using a parameter, Number of Transfer Units (NTU), that reflects its size and flow characteristics.

[63]: Poppe et al. (1991), "Berechnung von Rückkühlwerken"

[64]: Kloppers et al. (2005), "A Critical Investigation into the Heat and Mass Transfer Analysis of Counterflow Wet-Cooling Towers"

[65]: Cutillas et al. (2021), "Energetic, Exergetic and Environmental (3E) Analyses of Different Cooling Technologies (Wet, Dry and Hybrid) in a CSP Thermal Power Plant"

[59]: Hosoz et al. (2007), "Performance Prediction of a Cooling Tower Using Artificial Neural Network"

2: The notation $n_1 \dots n_l$ represents the architecture of the ANN model, where l is the number of layers and n_i are the nodes in each one of the layers.

[66]: Gao et al. (2013), "Artificial Neural Network Model Research on Effects of Cross-Wind to Performance Parameters of Wet Cooling Tower Based on Level Froude Number"

[67]: Song et al. (2021), "A Novel Approach for Energy Efficiency Prediction of Various Natural Draft Wet Cooling Towers Using ANN"

3: ANN uses as input f_{fan} whereas Poppe's model uses \dot{m}_a .

[68]: Navarro et al. (2022), "Critical Evaluation of the Thermal Performance Analysis of a New Cooling Tower Prototype"

method is based on the same simplifying assumptions as the Merkel method. On the other hand, Poppe and Rögner [63] developed the Poppe method. They derived the governing equations for heat and mass transfer in a wet cooling tower and did not make any simplifying assumptions as in the Merkel theory, which makes it a very precise model. As a matter of fact, predictions from the Poppe formulation have resulted in values of evaporated water flow rate that are in good agreement with full scale cooling tower test results [64]. This model has already been used for the evaluation of the thermal performance of solar power plants using different condensation systems (wet, dry and hybrid system), as can be found in Cutillas et al. [65].

In the case of black box models, numerous authors in the literature have designed ANN models for WCT with different objectives, such as performance prediction, simulation and optimization. One of the first works in this area is the one described in [59] where an ANN model was developed to predict the performance of a forced-counter flow cooling tower at lab scale. In this case, the input variables were the dry bulb temperature, the relative humidity of the air stream entering the tower, the temperature of the water entering the tower, the air volume flow rate and the cooling water mass flow rate. The outputs of this model were the heat rejection rate at the tower, the mass flow rate of water evaporated, the temperature of the cooling water at the tower outlet, the dry bulb temperature and the relative humidity of the air at the outlet of the tower. The results obtained with a 5-5-5² ANN demonstrated that wet cooling towers at lab-scale can be modelled using ANNs with a high degree of accuracy. There are also ANN models for Natural Draft Counter-flow Wet Cooling Towers (NDWCT) at lab-scale, such as the one proposed by [66]. In this case, the authors used a 4-8-6 ANN structure and considered some additional variables, such as air gravity, wind velocity, heat transfer coefficients and efficiency as outputs. All these works can be useful to validate the model development methodology but may fail predicting the performance of WCT at larger scale. In this sense, special attention deserves the study carried out by [67] where an 8-14-2 ANN model was proposed to predict the performance (the cooling number and the evaporative loss proportion) of NDWCTs at commercial scale. The model is based on 638 sets of field experimental data collected from 36 diverse NDWCTs used in power plants. It is a very challenging work since it covers samples from a wide range of tower sizes and capacities being the Mean Relative Error (MRE) below 5 %.

From the literature review, it can be stated that there are works based on Poppe and ANN models that evaluate the main output variables of WCTs. Nevertheless, to the author knowledge, there are no studies focused on the comparison between both modelling strategies. Also lacking is a comprehensive analysis of the different aspects that affect the models development and performance.

The static models presented in this section have been developed to predict two main outputs, the water temperature at the outlet of the WCT, $T_{w,or}$ and the water consumed due to evaporation losses, $\dot{m}_{w,lost}$. The inputs variables required by both modelling approaches, Poppe model and ANN models, are: the cooling water flow rate (\dot{m}_w), the water temperature at the inlet of the WCT ($T_{w,i}$), the ambient temperature (T_∞), the ambient relative humidity (ϕ_∞) and the frequency percentage of the fan (f_{fan}) (or its equivalence in air mass flow rate³, \dot{m}_a).

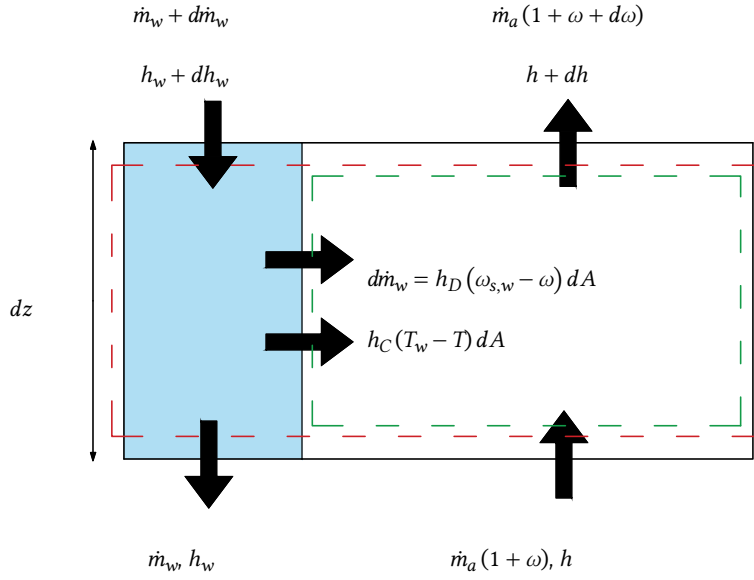
8.1.1 Poppe model

The well-known Merkel number is accepted as the performance coefficient of a wet cooling tower [68]. This dimensionless number is defined in Equation 8.1, and it measures the degree of difficulty of the mass transfer processes occurring in the exchange area of a wet cooling tower.

$$Me = \frac{h_D a_V V}{\dot{m}_w}, \quad (8.1)$$

where h_D is the mass transfer coefficient, a_V is the surface area of exchange per unit of volume and V is the volume of the transfer region.

The Merkel number can be calculated using the Merkel and Poppe theories for the performance evaluation of cooling towers. On the one hand, the Merkel theory [60] relies on several critical assumptions, such as the Lewis factor (Le) being equal to 1, the air exiting the tower being saturated with water vapour and it neglects the reduction of water flow rate by evaporation in the energy balance. On the other hand, the Poppe theory [63], which is the one used in this work, do not consider simplifying assumptions, thus being the one most usually preferred. In this theory, the authors derived the governing equations for heat and mass transfer in the transfer region of the wet cooling tower (control volume shown in Figure 8.1) assuming a one dimensional problem. In this figure, the red and green dashed lines indicate the fill and air-side control volumes, respectively.



[60]: Merkel (1925), "Verdunstungskühlung"

[63]: Poppe et al. (1991), "Berechnung von Rückkühlwerken"

Figure 8.1: Control volume in the exchange area of a wet cooling tower arrangement.

Following the detailed derivation process and simplification of the previously-mentioned governing equations described in [68], the major following equations for the heat and mass transfer obtained, according to the Poppe theory, are:

$$\frac{d\omega}{dT_w} = \frac{c_{p_w} \frac{\dot{m}_w}{\dot{m}_a} (\omega_{s,w} - \omega)}{(h_{s,w} - h) + (Le - 1) [(h_{s,w} - h) - (\omega_{s,w} - \omega) h_v] - (\omega_{s,w} - \omega) h_w} \quad (8.2)$$

$$\frac{dh}{dT_w} = c_{p_w} \frac{\dot{m}_w}{\dot{m}_a} \left[1 + \frac{(\omega_{s,w} - \omega) c_{p_w} T_w}{(h_{s,w} - h) + (Le - 1) [(h_{s,w} - h) - (\omega_{s,w} - \omega) h_v] - (\omega_{s,w} - \omega) h_w} \right] \quad (8.3)$$

$$\frac{dMe}{dT_w} = \frac{c_{p_w}}{(h_{s,w} - h) + (Le - 1) [(h_{s,w} - h) - (\omega_{s,w} - \omega) h_v] - (\omega_{s,w} - \omega) h_w}, \quad (8.4)$$

where the quantity referred to as Me in Eq. 8.4, is the Merkel number calculated according to the Poppe theory. The above described governing equations can be solved by the fourth order Runge-Kutta method to provide the evolution of

[68]: Navarro et al. (2022), "Critical Evaluation of the Thermal Performance Analysis of a New Cooling Tower Prototype"

[58]: Ashrae (2004), "HVAC Systems and Equipment"

the air humidity ratio, air enthalpy and Merkel number inside the transfer area of the cooling tower (fill). Once these profiles are known, the amount of water lost due evaporation can be calculated as per Eq. Equation 8.6. Refer to [68] for additional information concerning the calculation procedure.

$$Me = \frac{h_D a_v V}{\dot{m}_w}, \quad (8.5)$$

$$\dot{m}_{w,lost} = \dot{m}_a (\omega_{a,o} - \omega_{a,i}) \quad (8.6)$$

It is important to mention that the Merkel number varies with the operation conditions and its value can be obtained using a correlation with the water-to-air mass flow ratio as an independent variable. One of the proposed correlations in ASHRAE [58] is:

$$Me = c (\dot{m}_w / \dot{m}_a)^{-n} \quad (8.7)$$

4: See Section 10.1.1 (Wet cooler model alternatives comparison and validation)

where the constants c and n can be obtained from the fitting of experimental data⁴.

8.1.2 Samples generation for first-principles to data-driven models

The first pair of input variables for the WCT sample generation are the wet bulb temperature (T_{wb}) and the difference between this temperature and the system inlet temperature (ΔT_{wb-in}). The wet bulb temperature is used instead of the ambient temperature or the relative humidity, because as it can be derived from the physical model, it is the most relevant thermodynamic variable for the wet cooling tower performance. Using both the ambient temperature and the relative humidity would lead to a larger than necessary input space with many duplicate samples, as the wet bulb temperature is a function of both variables. The second pair of input variables are the cooling water flow rate (q_{wct}) and, following the reasoning from the physical model, the air to water mass flow ratio ($\dot{m}_a / \dot{m}_{wct}$), since it is a key parameter in defining the operating conditions of the tower. From the resulting 2D grid, valid combinations are obtained by calculating the air mass flow rate and finding if a valid fan speed can be obtained using an air mass flow rate to fan speed empirical correlation.

Finally, all valid thermodynamic and operational combinations are merged into a comprehensive sample set, enabling detailed system evaluations across a realistic and constrained input space.

8.1.3 Model interface

Model 8.1: Wet cooling tower

$$T_{wct,out}, C_{w,wct} = \text{wct model}(q_{wct}, \omega_{wct}, T_{amb}, HR, T_{wct,in})$$

Model 8.2: Wet cooling system model

$T_{wct,out}, C_e, C_w, T_{c,in}, T_{c,out} = \text{wcs model}(q_{wct}, \omega_{wct}, T_{amb}, HR, T_{wct,in})$
 $T_{c,in}, T_{c,out} = \text{condenser model}(q_c, \dot{m}_v, T_v)$
 $T_{wct,out}, C_{w,wct} = \text{wct model}(q_{wct}, \omega_{wct}, T_{amb}, HR, T_{c,out})$
 $C_{e,c} = \text{electrical consumption}(q_c)$
 $C_{e,wct} = \text{electrical consumption}(\omega_{wct})$
 $C_e = C_{e,wct} + C_{e,c}$
 $C_w = C_{w,wct}$

8.2 Dry cooler

8.2.1 Physical model

a

Pendiente de basarse en el artículo del modelo físico del DC con Elxe

8.2.2 Samples generation for first-principles to data-driven models

Similar to the wet cooling tower case, setting absolute values for both the inlet temperature and the environment temperature will lead to many unfeasible combinations ($T_{dc,in} \leq T_{db}$). So instead, values are generated for the temperature difference, therefore, a 2D grid is constructed using combinations of ambient/dry-bulb temperature (T_{amb}) and the difference between inlet and ambient temperature ((ΔT_{amb-in})). For each valid temperature pair ($T_{amb}, T_{dc,in}$), additional independent variables (q_{dc}, ω_{dc}) are combined via a Cartesian product, resulting in a full multidimensional grid of plausible operating points. This systematic procedure ensures a dense and uniform sampling across all relevant input dimensions. Finally, infeasible combinations are filtered based on physical constraints.

8.2.3 Model interface

Model 8.3: Dry cooler

$T_{dc,out} = \text{dc model}(q_{dc}, \omega_{dc}, T_{amb}, T_{dc,in})$

Model 8.4: Dry cooling system model

$$\begin{aligned}
 T_{dc,out}, C_e, T_{c,in}, T_{c,out} &= \text{dcs model}(q_{dc}, \omega_{dc}, T_{amb}, T_{dc,in}) \\
 T_{c,in}, T_{c,out} &= \text{condenser model}(q_c, \dot{m}_v, T_v) \\
 T_{dc,out} &= \text{dc model}(q_{dc}, \omega_{dc}, T_{amb}, T_{c,out}) \\
 C_{e,c} &= \text{electrical consumption}(q_c) \\
 C_{e,dc} &= \text{electrical consumption}(\omega_{dc}) \\
 C_e &= C_{e,dc} + C_{e,c}
 \end{aligned}$$

8.3 Other components

8.3.1 Electrical consumption

Electrical consumption is modelled with polynomial regressions of order 3 from experimental data:

Model 8.5: Electrical consumption

$$\begin{aligned}
 C_e &= \text{electrical consumption model}(x) \\
 C_e &= p_1 \cdot x^3 + p_2 \cdot x^2 + p_3 \cdot x + p_4
 \end{aligned}$$

where C_e represents the electrical consumption, and x is the input variable (e.g., the recirculated cooling water flow rate, particular cooler fan speed, etc.). The coefficients p_i correspond to a polynomial regression and must be calibrated individually for each component.

8.3.2 Surface condenser

The surface condenser is a heat exchanger that condenses steam into water, assuming that all the vapor that enters the condenser (at saturated conditions), leaves it as saturated liquid, it can be modelled by applying the first law of thermodynamics, which states that the heat lost by the steam (*released*) is equal to the heat gained by the cooling water (*absorbed*), and equal to the heat transferred by the condenser heat transfer surfaces (*transferred*).

Model 8.6: Surface condenser

$$T_{c,in}, T_{c,out} = \text{condenser model}(\dot{m}_c, T_v, \dot{m}_v)$$

$$LMTD = \frac{T_{c,out} - T_{c,in}}{\ln\left(\frac{T_v - T_{c,in}}{T_v - T_{c,out}}\right)}$$

$$\dot{Q}_{released} = \dot{m}_v \cdot (h_{sat,vap} - h_{sat,liq})$$

$$\dot{Q}_{absorbed} = \dot{m}_c \cdot c_p(T_{c,out} - T_{c,in})$$

$$\dot{Q}_{transferred} = U \cdot A \cdot LMTD$$

$$U = \dots$$

The condenser area (A) is a constant parameter

where $T_{c,in}$ and $T_{c,out}$ are the cooling water inlet and outlet temperatures, respectively, \dot{m}_c the cooling water mass flow rate, T_v vapour temperature and \dot{m}_v its mass flow rate and $h_{sat,vap}$ and $h_{sat,liq}$ are the specific enthalpies of the steam at the inlet and outlet of the condenser, respectively. \dot{Q} represents the heat transfer rate i.e. the thermal power.

8.3.3 Mixers

The mixers outlet flow ($q_{mix,out,i}$) and temperature ($T_{mix,out,i}$) can be determined with a simple mass and energy balances from its inlets streams ($q_{mix,in}$, $T_{mix,in}$):

Model 8.7: Mixer model

$$q_{mix,out}, T_{mix,out} = \text{mixer model}(q_{mix,in,1}, T_{mix,in,1}, q_{mix,in,2}, T_{mix,in,2}) \quad (8.8)$$

$$q_{mix,out} = q_{mix,in,1} + q_{mix,in,2} \quad (8.9)$$

$$T_{mix,out} = T_{mix,in,1} \cdot \frac{c_p(T_{mix,in,1})}{c_p(T_{out,i})} \frac{q_{mix,in,1}}{q_{mix,out,i}} + \\ T_{mix,in,2} \cdot \frac{c_p(T_{mix,in,2})}{c_p(T_{out,i})} \frac{q_{mix,in,2}}{q_{mix,out,i}} \quad (8.10)$$

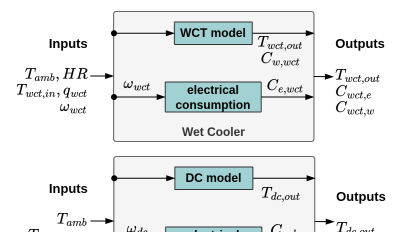
where $c_p(\cdot)$ is the specific heat, which can be assumed to be the same for the mixing temperature differences of this type of system.

8.4 Complete system

The complete model of the combined cooling system integrates the models of the WCT and DC, along with the surface condenser and the mixers, as defined in Model 8.8 (Complete system)⁵. The full diagram, including all variables, is shown in Figure 8.3.

To solve the system, the condenser model is evaluated first, providing the inlet temperature for the dry cooler. Once the dry cooler is solved, the resulting temperatures allow for solving the wet cooling tower. Finally, the mixers are evaluated to determine the final outlet temperature of the combined cooler, which should match the condenser's inlet temperature.

5: Although the electrical consumption for cooling water recirculation is attributed to the condenser in this model, other components—particularly the hydraulic circuit and the dry cooler—also contribute significantly to circulation resistance



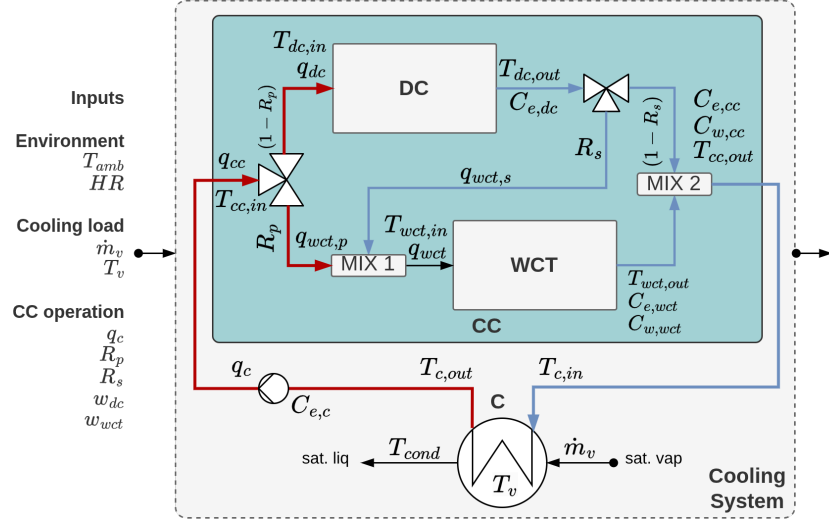


Figure 8.3: Complete model diagram of the combined cooling system

Model 8.8: Combined cooling system

$T_{cc,out}, C_e, C_w, T_{c,in}, T_{c,out} = \text{ccs model}(q_c, R_p, R_s, \omega_{dc}, \omega_{wct}, T_{amb}, HR_i, T_v, \dot{m}_v)$
 $T_{cc,in} = T_{c,out}$
 $T_{dc,in} = T_{cc,in}$
 $q_{dc} = q_c \cdot (1 - R_p)$
 $q_{wct,p} = q_c \cdot R_p$
 $q_{wct,s} = q_{dc} \cdot R_s$
 $T_{dc,out}, C_{e,dc} = \text{dc model}(q_{dc}, \omega_{dc}, T_{amb}, T_{dc,in})$
 $q_{wct}, T_{wct,in} = \text{mixer model}(q_{wct,p}, T_{cc,in}, q_{wct,s}, T_{dc,out})$
 $T_{wct,out}, C_{e,wct}, C_{w,wct} = \text{wct model}(q_{wct}, \omega_{wct}, T_{amb}, HR, T_{wct,in})$
 $T_{c,in}, T_{c,out} = \text{condenser model}(q_c, \dot{m}_v, T_v)$
 $q_{cc}, T_{cc,out} = \text{mixer model}(q_{wct}, T_{wct,out}, q_{dc}, T_{dc,out})$
 $C_{e,c} = \text{electrical consumption}(q_c)$
 $C_{e,dc} = \text{electrical consumption}(\omega_{dc})$
 $C_{e,wct} = \text{electrical consumption}(\omega_{wct})$
 $C_e = C_{e,dc} + C_{e,wct} + C_{e,c}$
 $C_w = C_{w,wct}$

Optimization of a combined cooling system

TL;DR

This chapter describes optimization problems for a combined cooling system, a DC and a WCT as well as different optimization strategies propositions to solve them. The objective is to minimize the daily cost of operation made up by the electricity and water costs, while ensuring the cooling demand is met. The key challenge is to manage the available water resource, since there is a limited amount of cheap rainwater available and any excess water required must be purchased at a significantly higher cost. From the alternatives, this can only be effectively achieved by the shrinking horizon optimization strategy applied to the combined cooler for which an implementation methodology is proposed.

9.1 Environment description	55
9.2 Static optimization	55
9.2.1 Dry cooler	56
9.2.2 Wet cooler	57
9.2.3 Combined cooler	57
9.3 Horizon optimization	58
9.3.1 Problem discussion	59
9.3.2 Proposed solution	60

Introduction

Over the years, various studies have compared wet and dry cooling systems for CSP plants. Most of these works are limited to studying the effect of some operating parameters via a sensitivity analysis [49, 51, 52, 69–71]. Nonetheless, several have focused on improving cooling system performance through optimization of the individual component operation. Among them, the works from Martín et al. stand out. In [31] they were the first to optimize the year-round operation of a CSP system not only considering the cooling side but also integrating the power block. The problem was formulated as a multiperiod NLP problem with air flow rate and outlet temperature as decision variables for the cooling system. They showed that the obtained complex problem can feasibly be solved and an average water consumption of 2.1 l/kWh was obtained with the least efficient month amounting to 2.5 l/kWh. In [41] the same strategy was applied this time for a dry cooling alternative (ACC) and formulating the optimization as a multiperiod MINLP problem. This integer extension to the problem was done to account for the addition of a new decision variable: the discrete number of units and fans that make up the ACC *i.e.* their active state. The problem was solved via relaxation of the integer variables and after evaluating the annual operation they found the optimized dry cooler consumed around 5% of the total generated power compared to 3.44% of the wet alternative, and increasing a cent the LCOE (0.16 vs 0.15 €/kWh, respectively). A limitation of both studies is the use of monthly average values, which masks the significant daily temperature variations—often exceeding 10°C—that coincide with peak power production and can have a substantial impact on cooling system performance.

Two distinct configurations can be found in the literature where a discussion is made about its operation strategy: water-enhanced dry cooling and parallel configuration. Rohani et al. [7] and Golkar et al [47]. In the latter, Rohani et al. implement a thorough model of water streams in a CSP plant that was experimentally validated. Different scenarios and cooling alternatives were analyzed and each of them was simulated for a year of operation. In the hybrid configuration the operation strategy consisted on always prioritizing the dry sections up until a set value in the condenser pressure was reached, in which case the wet units activated. This strategy offers a simple and robust solution but leaves a lot of performance on the table. Water will be left unused despite potentially being available to prioritize the more expensive dry cooler operation. While Golkar et al [47] delved more in the design and sizing of the hybrid cooler

[49]: Barigozzi et al. (2014), “Performance Prediction and Optimization of a Waste-to-Energy Cogeneration Plant with Combined Wet and Dry Cooling System”

[51]: Asvapoositkul et al. (2014), “Comparative Evaluation of Hybrid (Dry/Wet) Cooling Tower Performance”

[52]: Hu et al. (2018), “Thermodynamic Characteristics of Thermal Power Plant with Hybrid (Dry/Wet) Cooling System”

[69]: Afzand et al. (2020), “Thermodynamic Performance and Water Consumption of Hybrid Cooling System Configurations for Concentrated Solar Power Plants”

[70]: Mdallal et al. (2024), “Modelling and Optimization of Concentrated Solar Power Using Response Surface Methodology”

[71]: Tang et al. (2013), “Study on Operating Characteristics of Power Plant with Dry and Wet Cooling Systems”

[31]: Martín et al. (2013), “Optimal Year-Round Operation of a Concentrated Solar Energy Plant in the South of Europe”

[41]: Martín (2015), “Optimal Annual Operation of the Dry Cooling System of a Concentrated Solar Energy Plant in the South of Spain”

Realmente lo que proponen no es nada nuevo, exactamente esa operación ya se propuso por ejemplo en wiles_description_-1978 y zaloudek_study_1976

[7]: Rohani et al. (2021), “Optimization of Water Management Plans for CSP Plants through Simulation of Water Consumption and Cost of Treatment Based on Operational Data”

by application of a genetic algorithm, it then applied a very similar operation strategy.

In Maulbetsch et al. [36], a parallel combined system is analyzed, where the operation strategy is set as follows: At some temperature, the condensing pressure achieved will raise above a desired limit. For ambient temperatures above that level, both systems are operated at full design fan power. When the condensing pressure is below that limit, the capacity of the wet section is reduced to maintain it while the dry section is operated at full capacity. At lower temperature where the dry section can maintain the condensing pressure by itself, the wet system is no longer operated. Finally, at even lower temperatures, the fan power is gradually reduced on the dry section.

One inherent limitation that no optimization strategy can fully overcome is the seasonal mismatch between temperature and water availability. In many locations, ambient temperatures are lowest—favoring dry cooling—during times of the year when water is most abundant—favoring wet cooling. The opposite occurs during hot, dry summer periods, when cooling demand is highest but water becomes a scarce resource. Many studies report annual water savings figures, but this does not offer a complete picture and can be misleading, as it may mask poor performance during critical periods. Reducing water use during times of abundance, while failing to achieve significant savings during water-scarce periods, does not represent an optimal solution—even if total annual water consumption appears lower. Significant cost savings can be achieved with increasing water availability, either from the specification of a smaller condenser or by lowering operating turbine exhaust pressures (increasing the wet ratio). In conclusion, there remains significant potential for improved water management through optimized system operation, particularly when resource availability is explicitly considered in the decision-making process:

- ▶ Humidity is higher at night where ambient temperatures are lower, partially alleviating the limitations of the dry system and making it less unfavorable.
- ▶ Take full advantage of the cheaper and more efficient wet cooling when water is plentiful.
- ▶ Consider the availability of alternative water sources and their dynamic costs.
- ▶ When using a combined cooling system its operation is not trivial but inherently becomes more complex; thus requiring an operation strategy to, at a minimum, robustly satisfy the cooling demand, but preferably also minimize the cost of operation.

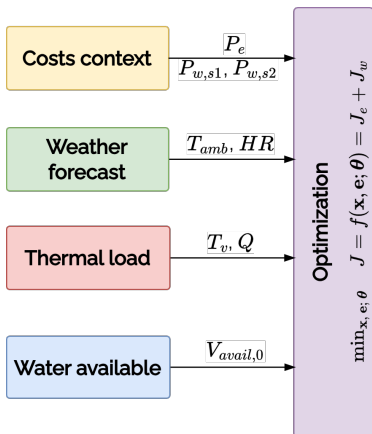


Figure 9.1: Block diagram of the optimization scheme including environment components

This chapter analyzes the optimization of different cooling system configurations, focusing on their two primary resource consumptions: electricity and water. The optimization problems are formulated to minimize the total cost of cooling a thermal load, with cost defined as the combined use of these two resources. The thermal load is treated as an external requirement and is therefore excluded from the decision space. This work addresses existing limitations in the literature and presents, for the first time, an actual optimization of the operation of a combined cooling system in the context of CSP applications.¹

The chapter is structured as follows: first, the environment definition is presented in Section 9.1 (Environment description), which includes a description of the variables taking part in the costs context, weather forecast, thermal load, and water resource availability. Next the two optimization strategies are presented, first a static optimization in Section 9.2 (Static optimization) where the dry cooler, wet cooler and combined cooler static problems are defined; followed by a shrinking horizon optimization approach in Section 9.3 (Horizon optimization) where the combined cooler is optimized over a prediction horizon. This last section includes a discussion on the problem nature and then presents the proposed methodology to solve it.

1: Although the proposed methodology is applicable to any system requiring thermal load cooling, particular emphasis is placed on water resource availability, given its critical importance in solar thermal applications. See Section 6.2 (Cooling and water use)

9.1 Environment description

The environment for the optimization problems described in this section includes the following components and is visualized in Figure 9.1:

1. **Costs context** The cooling system has mainly two associated operational costs: electricity (J_e) and water use (J_w). For the electricity the sale price of electricity (P_e) is used since whatever is consumed by the cooling system, it is electricity that cannot be sold to the market in the case of a system that produces electricity like a CSP plant, and it is electricity that needs to be purchased at market price in the case of any other system.
As for the water, two sources are considered, water price from source 1 is referred as $P_{w,s1}$ and $P_{w,s2}$ for source 2. Source 1 is cheaper than source 2.
2. **Weather forecast** The only two weather variables that have an impact on the cooling system are the ambient temperature (T_{amb}) and the relative humidity (HR) since they set the dry and wet bulb temperatures.
3. **Thermal load** The thermal load is defined either by a vapor flow rate (\dot{m}_v) or a thermal power (\dot{Q}), which enters the condenser at a temperature T_v ²
4. **Water resource availability** Two sources of water are available, one of them, the cheaper one coming from a dam is limited in volume (V_{avail}). The cheaper source (s_1) is prioritized until it is depleted, then the alternative source (s_2) is used:

$$C_{w,s1,i} = \frac{\min(V_{avail,i}, C_{w,i} \cdot T_s)}{T_s} \quad (9.1)$$

$$C_{w,s2,i} = C_{w,i} - C_{w,s1,i} \quad (9.2)$$

$$V_{avail,i} = V_{avail,i-1} - C_{w,s1,i} \cdot T_s \quad (9.3)$$

2: Vapor can also be referred as steam, usually steam is used when the vapor performs work, like in a turbine.

where i represents the step, at every step the amount used from each source is estimated and the source 1 availability is updated accordingly. C_w represents the flow rate of water consumed and T_s is the sample time at which steps are computed.

9.2 Static optimization

Static optimization problems are defined in a particular time, given an environment, and decisions do not take into account prior states or decisions, neither consider the effect on future state.

From a process perspective this also characterizes the cooling process, except for the water resource availability, being the only variable that depends on the previous state, *i.e.* is not static. Each time a static problem is evaluated, it begins with a specific initial water volume ($V_{avail,0}$) for that step. After solving the problem, this volume must be updated before proceeding to the next step. As a result, evaluating multiple consecutive steps requires a sequential approach.

Reminder: Optimization problem definition

The general optimization function is defined as:^a

$$\min_{\mathbf{x}, \mathbf{e}; \theta} J = f(\mathbf{x}, \mathbf{e}; \theta) \quad \text{s.t.} \quad g_i(\mathbf{x}) \leq 0, \quad i = 1, \dots, m$$

where \mathbf{x} is the decision vector, \mathbf{e} represents the environment, and θ contains the fixed parameters.

^a See Section ?? (??)

In order to streamline the problem formulation, a general combined cooling system model is used for every scenario. This unified model incorporates both the dry and wet coolers, as well as the shared surface condenser. For cases where only one cooler is used, the other can be effectively disabled by setting its associated variables to zero and configuring the hydraulic circuit to prevent water circulation through it.

9.2.1 Dry cooler

3: Achieved by setting $R_p = 0$ and $R_s = 0$

In the first case study, the optimization focuses exclusively on the dry cooler. Consequently, all variables and terms associated with the wet cooler, as well as water resource management, are omitted from the formulation, making the problem completely static³. This configuration is illustrated in Figure 9.2 and the problem is defined as follows:

Problem: DC - static

See Section ?? (??) for a detailed description of the dry cooler and Section 8.3.2 (Surface condenser) for the condenser model.

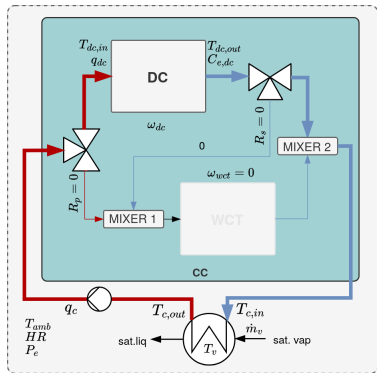


Figure 9.2: Diagram of the dry cooler only cooling problem

4: In order to better comprehend why mismatches between cooler and condenser can exist, the reader is referred to Section 8.4 (Complete system)

$$\min_{\mathbf{x}, \mathbf{e}; \theta} J = f(\mathbf{x}, \mathbf{e}; \theta) = C_e \cdot P_e$$

with:

$$T_{dc,out}, C_e, T_{c,in}, T_{c,out} = dcs \text{ model}(q_c, \omega_{dc}, T_{amb}, T_v, \dot{m}_v)$$

► Decision variables

$$\mathbf{x} = [q_c, \omega_{dc}]$$

► Environment variables

$$\mathbf{e} = [T_{amb}, P_e, T_v, \dot{m}_v]$$

► Fixed parameters

$$\theta = [R_p = 0, R_s = 0, \omega_{wct} = 0]$$

subject to:

► Box-bounds

- $\omega_{dc} \in [\underline{\omega}_{dc}, \bar{\omega}_{dc}]$
- $q_c \in [\underline{q}_c, \bar{q}_c]$

► Constraints

- $|T_{dc,out} - T_{c,in}| \leq \epsilon_1$
- $T_{c,out} \leq T_v - \Delta T_{c-v,min}$
- $|Q_{dc} - Q_{c,released}| \leq \epsilon_2$

The cost of cooling (J) is equivalent to the cost of electricity (J_e), which in turn is the product of the electricity price (P_e) and the electricity consumption (C_e). Only two decision variables are defined, the cooling water recirculation flow rate (q_c) and the dry cooler fan speed (ω_{dc}). Any two pair of values for these variables that satisfy the bounds do not necessarily yield a feasible solution, that is why three constraints are introduced, the first one ensures that the outlet cooler temperature matches the inlet condenser temperature (since they are directly connected, they must be the same), the second one ensures that the condenser outlet temperature respects the minimum temperature difference with the vapor temperature, and the last one ensures that the cooling duty of the dry cooler matches the one of the condenser⁴.

9.2.2 Wet cooler

Conversely to the dry cooler, the wet cooler optimization problem is configured by setting $R_p = 1$, effectively disabling the dry cooler. In this case, water associated variables are included in the problem formulation:⁵

Problem: WCT – static

$$\min_{\mathbf{x}, \mathbf{e}; \theta} J = f(\mathbf{x}, \mathbf{e}; \theta) = J_e + J_w$$

with:

$$J_e = C_e \cdot P_e$$

$$J_w = C_{w,s1} \cdot P_{w,s1} + C_{w,s2} \cdot P_{w,s2}$$

$$C_{w,s1} = \min((V_{avail}, C_w \cdot T_s)/T_s)$$

$$C_{w,s2} = C_w - C_{w,s1}$$

$$T_{wct,out}, C_e, C_w, T_{c,in}, T_{c,out} = \text{wcs model}(q_c, \omega_{wct}, T_{amb}, HR, T_v, \dot{m}_v)$$

- Decision variables

$$\mathbf{x} = [q_c, \omega_{wct}]$$

- Environment variables

$$\mathbf{e} = [T_{amb}, HR, P_e, P_{w,s1}, P_{w,s2}, V_{avail}, T_v, \dot{m}_v]$$

- Fixed parameters

$$\theta = [R_p = 1, R_s = 0, \omega_{dc} = 0]$$

subject to:

- Box-bounds

- $w_{wct} \in [w_{wct}, \bar{w}_{wct}]$
- $q_c \in [q_c, \bar{q}_c]$

- Constraints

- $|T_{wct,out} - T_{c,in}| \leq \epsilon_1$
- $T_{c,out} \leq T_v - \Delta T_{c-v,\min}$
- $|Q_{wct} - Q_{c,released}| \leq \epsilon_2$

In this version of the problem, the decision vector is composed by the recirculation flow rate, but now the fan speed of the wet cooler (ω_{wct}) is included. The cost of cooling now includes the cost of water (J_w) and its availability is updated using the water consumption (C_w) as described in Equations (9.1)–(9.3). The environment now includes the air relative humidity and water prices.

5: See Section 8.1 (Wet cooler) for a detailed description of the wet cooler and condenser model.

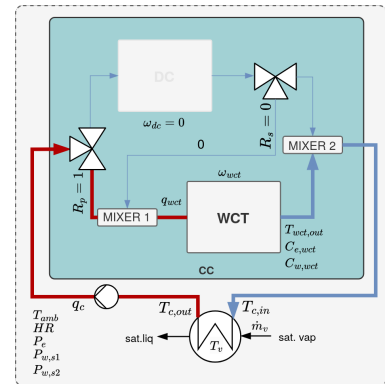


Figure 9.3: Diagram of the wet cooler only cooling problem

9.2.3 Combined cooler

The last static optimization problem is the combined cooler, which incorporates both the dry and wet coolers, as well as the condenser. Here the hydraulic distribution is not fixed but is part of the decision variables, allowing the optimization to determine the optimal distribution between the two coolers. The problem is defined as follows:⁶

6: See Section 8.4 (Complete system) for a detailed description of the combined cooler and condenser model.

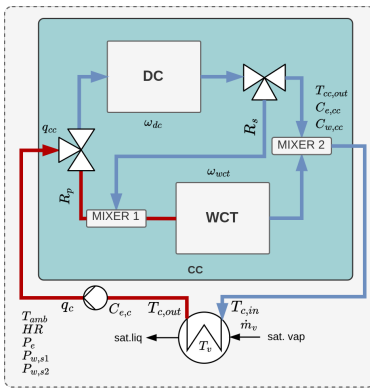
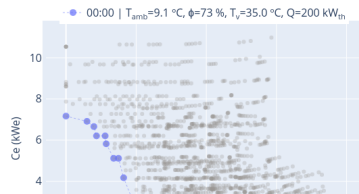


Figure 9.4: Diagram of the combined cooler



Add a background color antes del domingo

Reminder: Pareto front

When dealing with multiple objectives where no single solution is optimal, but improvements in one objective lead to trade-offs in others, a set of points is obtained that represents the best trade-offs between the objectives—known as a Pareto front^a.

^a See Section 5.4 (Multi-objective optimization)

7: Bold notation is used to indicate that the variable is an array and not a single value, e.g. \mathbf{x}

$\forall i = 1 \dots n_{steps}$ is a notation to indicate that a condition must be held at every step i in the optimization horizon (n_{steps})⁷

Problem: CC - static

$$\min_{\mathbf{x}, \mathbf{e}; \theta} J = f(\mathbf{x}, \mathbf{e}; \theta) = J_e + J_w$$

with:

$$J_e = C_e \cdot P_e$$

$$J_w = C_{w,s1} \cdot P_{w,s1} + C_{w,s2} \cdot P_{w,s2}$$

$$C_{w,s1} = \frac{\min(V_{avail}, C_w \cdot T_s)}{T_s}$$

$$C_{w,s2} = C_w - C_{w,s1}$$

$$T_{cc,out}, C_e, C_w, T_{c,in}, T_{c,out} = ccs \text{ model}(q_c, R_p, R_s, \omega_{dc}, \omega_{wct}, T_{amb}, HR, T_v, \dot{m}_v)$$

- Decision variables

$$\mathbf{x} = [q_c, R_p, R_s, \omega_{dc}, \omega_{wct}]$$

- Environment variables

$$\mathbf{e} = [T_{amb}, HR, P_e, P_{w,s1}, P_{w,s2}, V_{avail}, T_v, \dot{m}_v]$$

subject to:

- Box-bounds

- $\omega_{dc} \in [\underline{\omega}_{dc}, \bar{\omega}_{dc}]$
- $\omega_{wct} \in [\underline{\omega}_{wct}, \bar{\omega}_{wct}]$
- $q_c \in [q_c, \bar{q}_c]$
- $R_p \in [0, 1]$
- $R_s \in [0, 1]$

- Constraints

- $|T_{cc,out} - T_{c,in}| \leq \epsilon_1$
- $T_{c,out} \leq T_v - \Delta T_{c-v, \min}$
- $|Q_{cc} - Q_{cc, \text{released}}| \leq \epsilon_2$

Figure 9.5 illustrates the various ways a combined cooler can meet a specific cooling load under identical environmental conditions. The optimal operating points—the Pareto front—are highlighted in the figure. The background color represents the distribution of cooling power: green indicates a greater contribution from the dry cooler, while purple indicates a greater contribution from the wet cooler. Notably, only the leftmost point relies exclusively on the dry cooler. Moving even slightly to the right results in a rapidly increasing contribution from the wet cooler.

9.3 Horizon optimization

The problem structure is very similar to the static alternative, the main difference is that now the decision and environment vectors are composed not from the expected value for the optimization step, but an array of values from the current optimization step (i) until the end of the prediction horizon (n_{steps})⁷:

Problem: CC - horizon

$$\min_{\mathbf{x}, \mathbf{e}; \theta} J = f(\mathbf{x}, \mathbf{e}; \theta) = \sum_{i=1}^{n_{steps}} (J_{e,i} + J_{w,i}) \cdot T_s$$

with:

for $i = 1 \dots n_{steps}$:

$$\begin{aligned} J_{e,i} &= C_{e,i} \cdot P_{e,i} \\ J_{w,i} &= C_{w,s1,i} \cdot P_{w,s1,i} + C_{w,s2,i} \cdot P_{w,s2,i} \\ C_{w,s1,i} &= \frac{\min(V_{avail,i}, C_{w,i} \cdot T_s)}{T_s} \\ C_{w,s2,i} &= C_{w,i} - C_{w,s1,i} \\ V_{avail,i} &= V_{avail,i-1} - C_{w,s1,i} \cdot T_s \\ T_{cc,out,i}, C_{e,i}, C_{w,i}, T_{c,out,i} &= f(q_{c,i}, R_{p,i}, R_{s,i}, \omega_{dc,i}, \omega_{wct,i}, T_{amb,i}, HR_i, T_{v,i}, \dot{m}_{v,i}) \end{aligned}$$

- Decision variables

$$\mathbf{x} = [\mathbf{q}_c, \mathbf{R}_p, \mathbf{R}_s, \omega_{dc}, \omega_{wct}]$$

where $x = [x_{1,1}, \dots x_{1,n_{steps}}, \dots, x_{n_x,n_{steps}}]$

- Environment variables

$$\mathbf{e} = [\mathbf{T}_{amb}, \mathbf{HR}, \mathbf{P}_e, \mathbf{P}_{w,s1}, \mathbf{P}_{w,s2}, \mathbf{V}_{avail,0}, \mathbf{T}_v, \mathbf{m}_v]$$

where $e = [e_{1,1}, \dots e_{1,n_{steps}}, \dots, e_{n_e,n_{steps}}]$

subject to:

- Box-bounds

- $\mathbf{w}_{dc} \in [\underline{w}_{dc}, \bar{w}_{dc}]$
- $\mathbf{w}_{wct} \in [\underline{w}_{wct}, \bar{w}_{wct}]$
- $\mathbf{q}_c \in [q_c, \bar{q}_c]$
- $\mathbf{R}_p \in [0, 1]$
- $\mathbf{R}_s \in [0, 1]$

- Constraints, $\forall i = 1 \dots n_{steps}$:

- $|T_{cc,out,i} - T_{c,in,i}| \leq \epsilon_1$
- $T_{c,out,i} \leq T_{v,i} - \Delta T_{c-v,min}$
- $|Q_{cc,i} - Q_{c,released,i}| \leq \epsilon_2$

This formulation allows for an arbitrary long prediction horizon, however, since forecasts for each variable in the environment are needed, it will be limited to a number of steps where reliable predictions can be obtained. On this work water availability is allocated daily, so the prediction horizon is established until the end of the operation day and it starts from the current time when the optimization is launched.

9.3.1 A discussion on solving the optimization problem

As defined, the CCS problem decision vector is composed by five variables that are direct inputs on the process⁸. But as mentioned, not any five values for these variables will yield a feasible solution, in the real system this translates to the fact that a stable operation *i.e.* steady-state would never be reached for that set of inputs. To check for feasible operation the three mentioned constraints are introduced, however, this increases the complexity of the solution space significantly, since the solution space will not be continuous, but as seen in Figure 9.6, it will be formed by islands of feasible solution space regions separated by infeasible regions. This means that finding a feasible solution is not trivial, and the optimization algorithm will need to explore the solution space-a global search algorithm-in an attempt to find the global minimum.

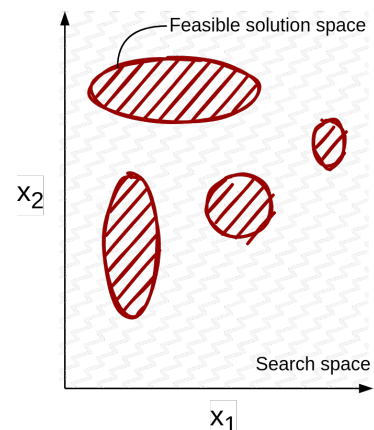


Figure 9.6: Visualization of a constrained search space for two decision variables

9: Tried algorithms include: Algoritmos probados de pygmo y Poner Gaussian también

[72]: Wales et al. (1997), "Global Optimization by Basin-Hopping and the Lowest Energy Structures of Lennard-Jones Clusters Containing up to 110 Atoms"

10: Alternative wording: Pareto front chaining, multi-step Pareto optimization, path planning on Pareto surfaces.

For one single step, most global search algorithms with multiple runs⁹ were able to consistently find the global optima, this was not the case for local gradient-based algorithms, which were very sensible to the initial conditions and often converged to local minima, even when coupled with other techniques, such as Generalized Monotonic Basin Hopping [72], they struggled to consistently escape these local optima.

The problem becomes significantly more complex when the prediction horizon is extended, the decision vector grows five-fold for each additional step in the prediction horizon, and the optimization algorithm is tasked with finding a feasible solution for this much larger decision vector, in a very complex solution space, at once for all steps. The chances of finding a feasible solution decrease significantly, and this was reflected in the failure to find a single feasible solution. Even when providing an initial guess composed by the static problem solutions for each step in a 24 steps horizon, the returned solution was that same initial guess.

9.3.2 Proposed solution: Decomposition-based multi-objective optimization with trajectory planning

A two-level optimization strategy is proposed to solve a multi-step decision problem¹⁰. At each step of the prediction horizon, a multi-objective optimization problem is independently solved, yielding a Pareto front. A global optimization problem is then formulated to select a path through the sequence of Pareto fronts, minimizing a cumulative objective (*i.e.*, cost), akin to a pathfinding or Traveling Salesman Problem (TSP)-like over Pareto-optimal points.

The methodology is illustrated in Figure 9.7 and its components are described in the following sections.

Solving the multi-objective optimization problems

To limit the complexity of the problem, the decision space can be reduced by one by variable by analyzing how the complete model is solved and described in Section 8.4 (Complete system); firstly, the condenser can be solved just by using the recirculation flow rate (q_c), it follows the dry cooler by adding the first valve ratio (R_p) and dry cooler fan speed (ω_{dc}). The only remaining component to solve is the wet cooler. The wet cooler inlet conditions ($q_{wct}, T_{wct,in}$) can be determined by using the second valve ratio (R_s). As for the outlet conditions, from the condenser evaluation, its inlet temperature is known and it sets the value of the combined cooler outlet temperature ($T_{cc,out}$), which in turn is the result of the mixing from the DC and WCT outlet temperatures ($T_{dc,out}$ and $T_{wct,out}$, respectively).

The result of this analysis is that the wet cooler fan speed is not a decision variable anymore, but an output of the model, which can be computed by inverting the wet cooler model, where an outlet temperature is provided as input, and the fan speed is computed as an output. Summarizing, the decision vector can be reduced from five to four variables.¹¹

$$\mathbf{x} = [q_c, R_p, R_s, \omega_{dc}]$$

11: This reasoning works only for a system with this particular configuration, a different combined cooler layout would require a different analysis.

12: *i.e.* within its bounds $\omega_{wct} \in [\underline{\omega}_{wct}, \bar{\omega}_{wct}]$

More importantly, now the optimization algorithm does not need to find a set of five inputs that produce a feasible solution in a complex solution space, but only four values from which a feasible wet cooling tower fan speed exists¹², thus greatly simplifying the problem.

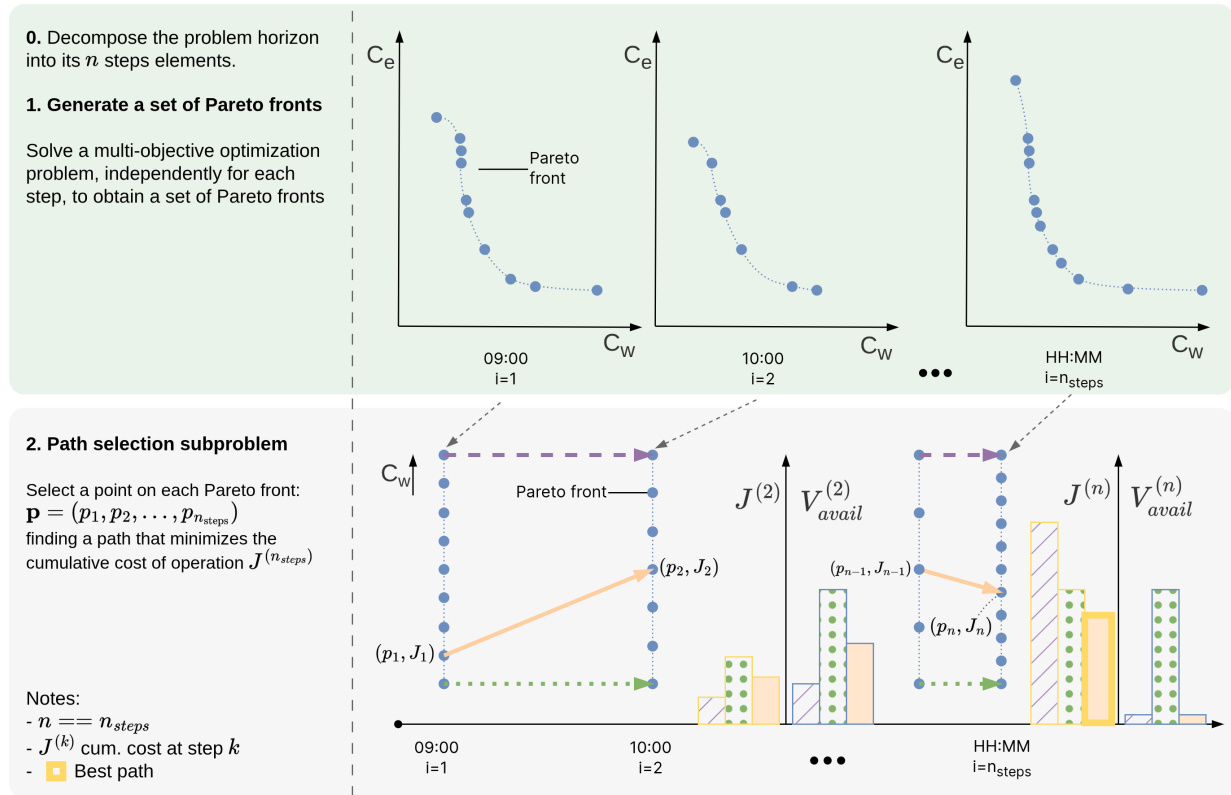


Figure 9.7: Proposed methodology. Decomposition-based multi-objective optimization with trajectory planning. Blue-dots (-) represent points on the Pareto front. In step 2, three paths are illustrated: a water-greedy dash-purple (- -) path, a water-conservative green-dotted path (..) and a compromise-approach solid-orange path (-).

A straightforward approach to solve the multi-objective optimization is to do a grid-search over the decision space, evaluating the model for every combination of decision variables, and then storing only the points for which a feasible ω_{wct} exists. This approach is not recommended for large decision spaces, but for the four-dimensional decision space and with a model that can be evaluated in fractions of a second, it is feasible.

Next, the Pareto front is computed from the feasible points, which are evaluated in terms of the two consumptions: electricity (C_e) and water (C_w). By definition, the Pareto front is the set of points that cannot be improved in one objective without worsening the other, and it is computed by checking for each point if there is another point that is better in both objectives, and if so, it is removed from the set of feasible points. The remaining points form the Pareto front. This process is repeated for each step in the prediction horizon, resulting in a set of Pareto fronts, one for each step, as visualized in Figure 9.7-1.

Path selection subproblem

The path selection subproblem is a combinatorial optimization problem over a layered weighted directed graph, where each layer corresponds to a time step in the prediction horizon, and each node in a layer represents a point on the corresponding Pareto front. The objective is to find a path $\mathbf{p} = (p_1, p_2, \dots, p_{n_{\text{steps}}})$, where p_i is the selected node at time step i , that minimizes the total cumulative cost along the path (J). The problem can be formulated as:

$$\min_{\mathbf{p}} \quad J = \sum_{i=1}^{n_{\text{steps}}-1} C_{\text{transition}}(p_i, p_{i+1})$$

Each transition cost $C_{\text{transition}}(p_i, p_{i+1})$ depends on both consumptions (*i.e.* electricity and water consumption) of the nodes p_i and p_{i+1} , as well as a dynamic price function that depends on the path history. Specifically, the transition cost is correlated to the current resource availability ($V_{\text{avail},i}$)¹³ and will depend on the current state of the system, which is a function of the previous decisions. This is a very simple calculation that can be computed almost instantly, and it is the only information needed to compute the transition costs between two points in the Pareto front:

$$C_{\text{transition}}(p_i, p_{i+1}) = P_e(i) \cdot C_e(p_{i+1}) + P_w(i) \cdot C_w(p_{i+1})$$

where:

- ▶ $C_e(p_{i+1}), C_w(p_{i+1})$: electricity and water consumption at node p_{i+1}
- ▶ $P_e(i), P_w(i)$: price coefficients for electricity and water at step i , which may be dependent on the previously selected nodes (*i.e.*, the path so far)

Prices $P_e(i), P_w(i)$ depend on prior path decisions, this introduces path-dependency into the cost function, and makes the problem non-trivial to solve via simple shortest path algorithms. The problem could be handled via dynamic programming, graph search (like Dijkstra or A*), or metaheuristics such as genetic algorithms.

The subproblem is illustrated in Figure 9.7–2. Each node represents a point in the Pareto front of a step, and edges represent the transition costs between these points, that is, the cumulative cost so far ($J_{0,i}$). Three paths are illustrated in Figure 9.7–2. The **dash-purple** (- -) path is a path that chooses nodes with a high water use¹⁴, so in the first split it can be seen it achieves the lowest cost of operation, but also leaves the least water available for the next steps, resulting in a higher total cost of operation. On the other hand, the **green-dotted path** (..) chooses the nodes with the lowest water use, this translates in a consistently higher cost of operation and leaving some water available at the end of the horizon. Because of the formulation of the problem, this is sub-optimal since this unused water is considered lost. Finally, the **solid-orangey path** (—) is a compromise between the two, it uses water more efficiently, leaving no water available at the end of the horizon and minimizing the overall cost of operation.

13: See Equations (9.1)–(9.3)

14: In Figure 9.7, nodes are ordered with increasing values of C_w from bottom to top.

Validation in the combined cooling pilot plant

To Do

After the chapter is complete, find and replace all mentions to RBF, ANN, RMSE and all other acronyms with the acronym with \gls.

10.1 Modelling

The two main components of the system (WCT and DC) are modelled with different approaches and compared in detail. Afterward, the integration of the selected modelling approach with the rest of the system components (Section 8.3) is validated in Section 10.1.5 (Complete system model validation).

10.1.1 Wet cooler model alternatives comparison and validation

Physical model

As previously mentioned¹, three experimental campaigns have been performed, shown in Figure 10.1 as Exp 1, Exp 2, and Exp 3. Exp 1 corresponds to the Poppe model calibration campaign and it was designed for the calibration of the first principles model. The aims of such campaign was to fit a function (mapping) that relates the air mass flow rate at the outlet of the tower, \dot{m}_a , with the frequency of the fan, f_{fan} :

$$\dot{m}_a = -0.0014f_{fan}^2 + 0.1743f_{fan} - 0.7251. \quad (10.1)$$

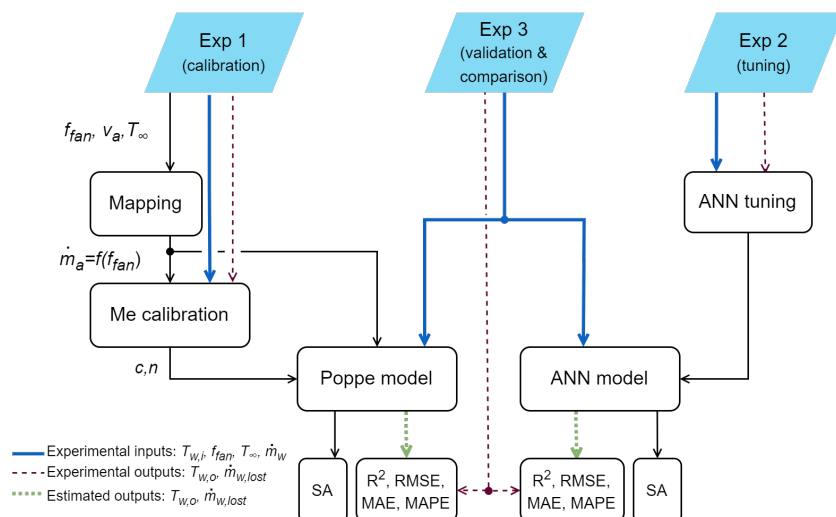
and to calibrate a WCT performance coefficient: the Merkel number, Me. Figure 10.2 shows the variation of the Merkel number as a function of the water-to-air mass flow ratio (\dot{m}_w/\dot{m}_a) using data from Exp1. As can be seen, the Me decreases with \dot{m}_w/\dot{m}_a values following a linear trend on log-log scale.

10.1 Modelling	63
10.1.1 Wet cooler model alternatives comparison and validation	63
10.1.2 Dry cooler model alternatives comparison and validation	64
10.1.3 Main components modelling conclusions	67
10.1.4 Condenser model validation	69
10.1.5 Complete system model validation	70
10.2 Control and optimization results	72
10.2.1 Choosing an optimization algorithm	72
10.2.2 Comparing the strategies	73
10.2.3 Validation at pilot plant	74

1: See Section 7.3 (Experimental campaigns for the wet cooling tower)

Lidia, aquí la correlación no usa la temperatura ambiente

Make text in figure larger



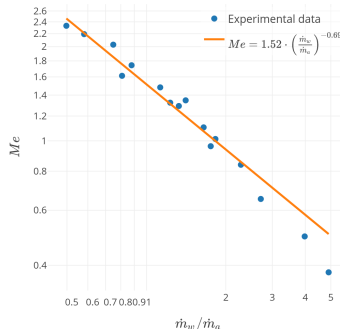


Figure 10.2: Experimental results for the Me number as a function of \dot{m}_w/\dot{m}_a .

Table 10.1: Bounds and discretization of the model input variables.

x	Units	lb	ub	n
T_{amb}	°C	3	50	7
ΔT_{amb-in}	°C	3	30	7
q_{dc}	m ³ /h	0.00	1.00	5
ω_{dc}	%	11.00	9918	10
ω_{wct}	%	21.00	93.42	10

2: Described in Section 3.1

Following the correlation for the Merkl number of a wet cooling tower described in Section 8.1.1, the parameters c and n obtained from the data fitting are 1.516 and 0.693, respectively.

Data-driven

In order to generate the data-driven from first-principles alternative, the most relevant input variables identified in Section ?? are discretized using a fixed number of resolution steps for each variable, within ranges based on expected operating conditions, as defined in Table 10.1.

Figure 10.3 shows the generated input space distribution. The upper plot shows the frequency distribution of the samples while the lower one the actual values per input, where the x-axis represents the samples and the y-axis the values for each of the input variables.

Prediction capabilities

Tabla tocha añadiendo casos (GPR, DD from FP, RF, GB)

The results of each modelling alternative and its comparison can be visualized in Figure ?? and Table 10.4. The results of each modelling alternative and its comparison can be visualized Figure ?? shows the results obtained with the models using Exp 3. It shows the perfect fit together with the results obtained with Poppe's model, MIMO FF, cascade CF, and MIMO RBF. In Table 10.4, the performance of the studied modelling approaches are included for the different performance metrics². T represents the performance metric value for the training / calibration dataset (Exp 1 or Exp 2 depending on the case), and V for the validation and comparison one (Exp 3). In all cases the model representing each alternative is in the best case scenario, *i.e.* maximum number of points available. On the other hand, s.u. indicates that the units of the column are the same as from the source variable.

Comparing both modelling approaches (see Figure ??), it can be outlined that both models provide a good prediction of the output variables, falling most of the discrepancies (errors) within the uncertainty range. Poppe's model provides a better prediction of the outlet temperature, obtaining an RMSE of 0.33 °C and an R^2 of 0.98. In comparison, the best ANN alternative (RBF MIMO) has a slight worse performance with an RMSE of 0.51 °C and $R^2 = 0.95$. In terms of water consumption, the physical model has a better prediction accuracy in terms of RMSE and R^2 (8.5 l/h and 0.97) compared to 11.24 l/h and 0.95 for the best ANN model (cascade CF). It can be stated that, although the results are better for the physical model (specially in the case of the outlet temperature prediction), both approaches produce valid results with high accuracy levels.

Incluir gráfica comparativa de evolución de RMSE (incluyendo GPR) para argumentar por qué GPR es mejor no solo en términos de error, si no también en requerimiento de datos.

10.1.2 Dry cooler model alternatives comparison and validation

Physical model

Data-driven

In order to generate the data-driven from first-principles alternative, the most relevant input variables identified in Section 8.2.2 are discretized using a fixed number of resolution steps for each variable, within ranges based on expected operating conditions, as defined in Table 10.3. and Section ?? (??) visualizes the

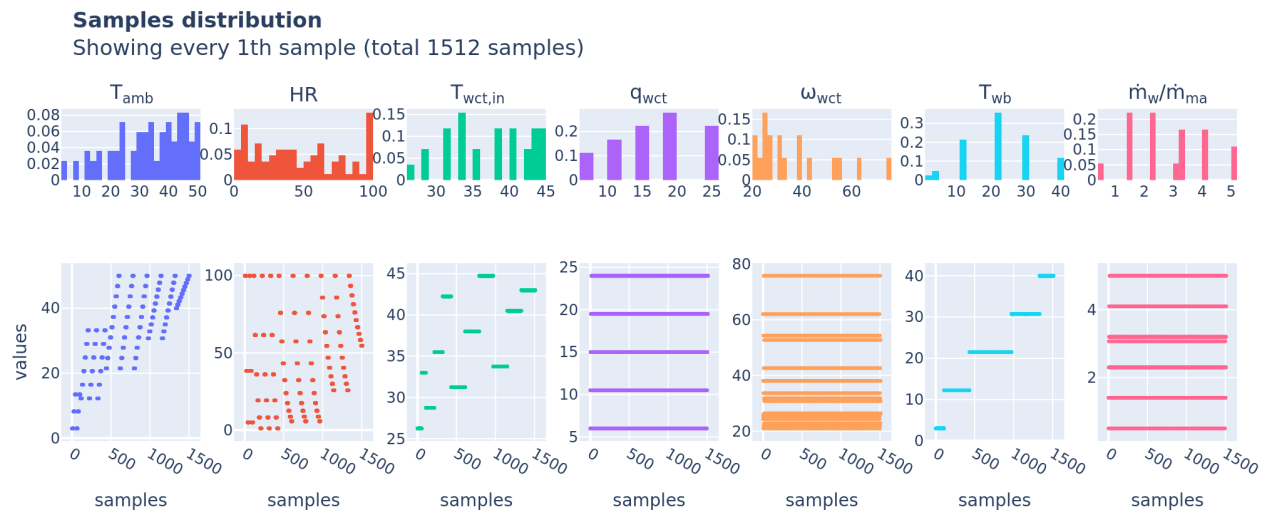


Figure 10.3: Data-driven from first-principles. Samples distribution visualization.



generated input space distribution where it can be appreciated that the samples are well distributed across the entire input space.

Figure 10.4: WCT models performance comparison between the different modelling approaches.

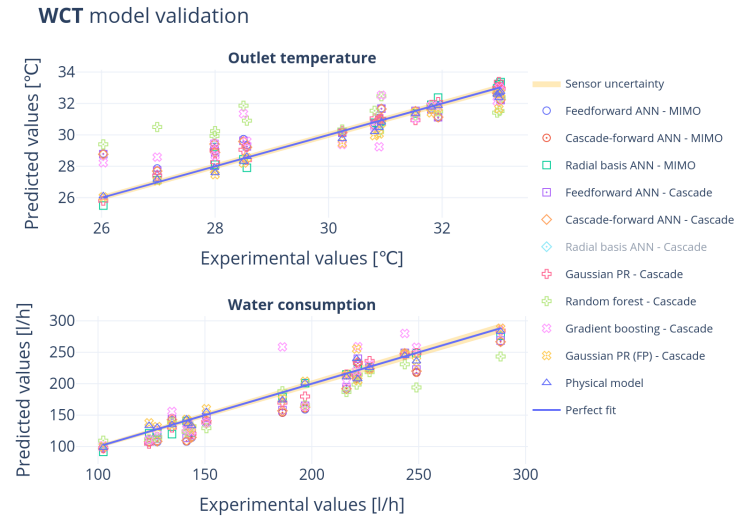


Table 10.2: Summary table of the prediction results obtained with the different modelling approaches studied.

Predicted variable	Modelling alternative	Model config	Topology	Performance metric								Evaluation time (s)	
				R ² (-)		RMSE (s.u.)		MAE (s.u.)		MAPE (%)			
				T	V	T	V	T	V	T	V		
$T_{wet,out}$ (°C)	Physical model	-	-	-	0.98	-	-	-	0.27	-	0.87	6.288	
	Feedforward ANN	MIMO	20-2	0.90	0.81	0.60	0.97	0.42	0.67	1.36	2.36	0.004	
	Cascade-forward ANN	MIMO	10-10-2	0.90	0.82	0.60	0.93	0.44	0.65	1.42	2.27	0.005	
	Radial basis ANN	MIMO	34-2	0.97	0.97	0.34	0.41	0.21	0.28	0.66	0.94	0.007	
	Feedforward ANN	Cascade	20-1	0.90	0.82	0.60	0.93	0.43	0.65	1.41	2.26	0.011	
	Cascade-forward ANN	Cascade	10-10-1	0.90	0.83	0.60	0.92	0.43	0.64	1.40	2.24	0.010	
	Radial basis ANN	Cascade	92-1	0.97	-1.44	0.33	3.45	0.10	2.12	0.32	7.43	0.009	
	Gaussian PR	Cascade	N/A	0.99	0.97	0.20	0.37	0.15	0.26	0.47	0.89	0.001	
	Random forest	Cascade	N/A	0.75	0.30	0.96	1.85	0.60	1.46	2.03	5.05	0.078	
	Gradient boosting	Cascade	N/A	1.00	0.68	0.00	1.24	0.00	0.95	0.01	3.29	0.015	
C_w (l/h)	Gaussian PR (FP)	Cascade	N/A	1.00	0.94	0.32	0.54	0.15	0.41	0.52	1.32	0.105	
	Physical model	-	-	-	0.97	-	8.47	-	6.74	-	3.74	6.288	
	Feedforward ANN	MIMO	20-2	0.92	0.83	14.77	21.58	11.98	18.64	9.91	10.75	0.004	
	Cascade-forward ANN	MIMO	10-10-2	0.92	0.84	15.47	20.90	12.51	17.84	10.48	10.22	0.005	
	Radial basis ANN	MIMO	34-2	0.99	0.97	5.58	9.34	3.81	7.47	3.23	4.68	0.007	
	Feedforward ANN	Cascade	20-1	0.92	0.88	15.00	18.45	11.97	15.77	10.20	8.92	0.011	
	Cascade-forward ANN	Cascade	10-10-1	0.92	0.85	15.01	20.34	12.11	17.66	10.00	10.18	0.010	
	Radial basis ANN	Cascade	33-1	0.99	0.93	4.99	14.28	3.45	10.14	2.68	6.22	0.009	
	Gaussian PR	Cascade	N/A	0.99	0.95	4.74	12.00	3.61	9.96	3.09	6.32	0.001	
	Random forest	Cascade	N/A	0.89	0.80	17.35	23.23	10.51	18.51	7.58	9.73	0.078	
	Gradient boosting	Cascade	N/A	1.00	0.77	0.24	25.07	0.07	17.21	0.05	9.55	0.015	
	Gaussian PR (FP)	Cascade	N/A	0.98	0.95	10.85	11.63	4.81	8.14	3.74	4.52	0.105	

Prediction capabilities

Tabla tocha añadiendo casos (GPR, DD from FP, RF, GB)

Experimental data requirements

10.1.3 Main components modelling conclusions

This section presents a comparison between two modelling alternatives: data-driven and first-principles. It applies to wet cooling towers and dry coolers, specifically to ACHE. The main conclusions obtained during the investigation and final recommendations can be summarized as follows:

Wet cooling tower

Regarding the prediction of the output variables, in the case of the outlet water temperature, both models reported good results, with low errors falling within the uncertainty range of the experimental equipment. Nonetheless, the physical model performs better than the best data-driven alternative (MIMO RBF): $R^2 = 0.98$ and RMSE= 0.33 °C compared to $R^2 = 0.95$ and RMSE= 0.51 °C, respectively.

For the predictions of water consumption, it was shown that the Poppe model accurately predicts this variable, with results of $R^2 = 0.97$ and RMSE= 8.47 l/h. The best ANN alternative (cascade CF) achieves close results with an $R^2 = 0.95$ and RMSE= 11.24 l/h.

However, the Poppe model reached such reliable prediction levels with a much lower number of tests, needing only 2. In comparison, the ANN alternatives need more data, at least 10 (with a good distribution over the operating range) for the FF and CF ANN models.

Table 10.3: Bounds and discretization of the model input variables.

x	Units	lb	ub	n
T_{amb}	°C	3	50	7
$\Delta T_{amb-dc,in}$	°C	3	30	7
q_{dc}	m³/h	6	24	7
$T_{dc,in}$	°C	25	45	-
ω_{dc}	%	11	99.18	6

completar esta sección antes del domingo

Samples distribution

Showing every 1th sample (total 798 samples)

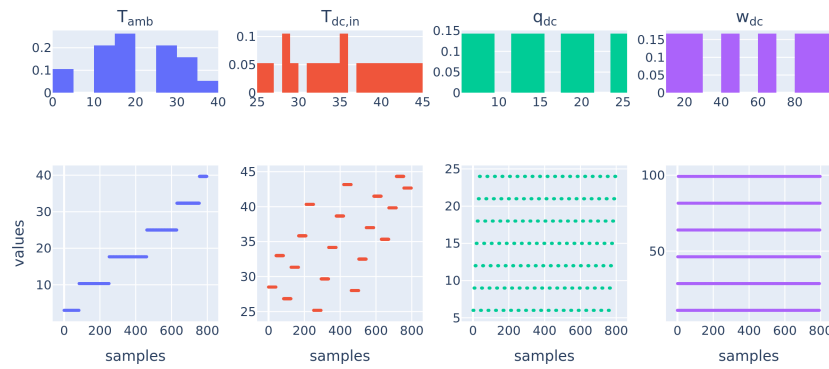


Figure 10.5: Data-driven from first-principles. Samples distribution visualization.



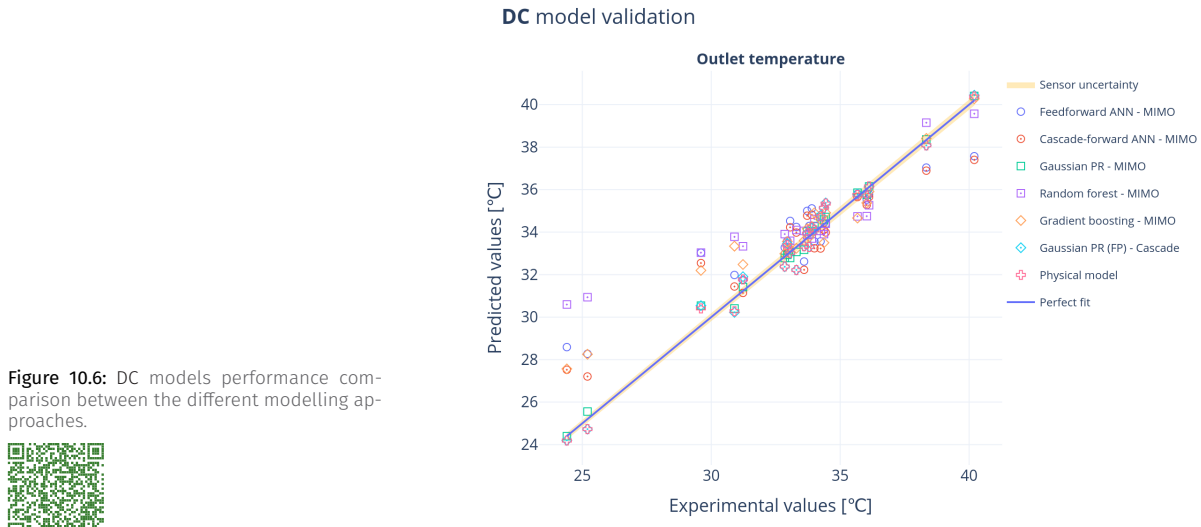


Figure 10.6: DC models performance comparison between the different modelling approaches.



Table 10.4: Summary table of the prediction results obtained with the different modelling approaches studied.

Predicted variable	Modelling alternative	Model config	Topology	Performance metric								Evaluation time (s)	
				R ² (-)		RMSE (s.u.)		MAE (s.u.)		MAPE (%)			
				T	V	T	V	T	V	T	V		
T _{dc,out} (°C)	Physical model	-	-	-	0.98	-	0.50	-	0.42	-	1.28	0.035	
	Feedforward ANN	-	20-1	0.77	0.78	1.42	1.62	1.13	1.18	3.29	3.85	0.005	
	Cascade-forward ANN	-	10-10-1	0.78	0.85	1.39	1.37	1.12	1.02	3.23	3.24	0.007	
	Gaussian PR	-	N/A	0.99	0.99	0.24	0.32	0.19	0.25	0.56	0.77	0.005	
	Random forest	-	N/A	0.84	0.61	1.19	2.17	0.72	1.36	2.05	4.69	0.022	
	Gradient boosting	-	N/A	1.00	0.86	0.00	1.31	0.00	0.86	0.00	2.92	0.035	
	Gaussian PR (FP)	-	N/A	1.00	0.98	0.03	0.53	0.02	0.44	0.07	1.35	0.002	

Air-cooled heat exchanger

Conclusions and recommendations

For the proposed optimization strategy in Section ?? (??), a fast, reliable model that can be scaled to different system sizes is required.

On the one hand, the first-principle models execution time is much higher than the data-driven alternatives, which is a significant drawback when it comes to the optimization strategy, where the model is evaluated many times in a short period of time. On the other hand, the data-driven counterparts are only applicable to the conditions and the particular system with which they are developed.

Conversely, one of the main strengths of both physical models presented in this chapter, is their ability to predict the operation of the coolers regardless of the conditions tested; while the data-driven execution time is faster by orders of magnitude, it can be vectorized and its execution time is more constant regardless of the input conditions.

Therefore, as combining a wet cooler and a dry cooler into a combined cooler offers potential advantages compared to the individual systems, combining both modelling approaches is the chosen solution to model the system. The best performing data-driven model, the Gaussian-Process Regression (GPR) is calibrated using data from the first-principle models, where physical models are adapted dynamically to the required scale and finally the data-driven model can be generated. This approach provides a way of having on-demand models that

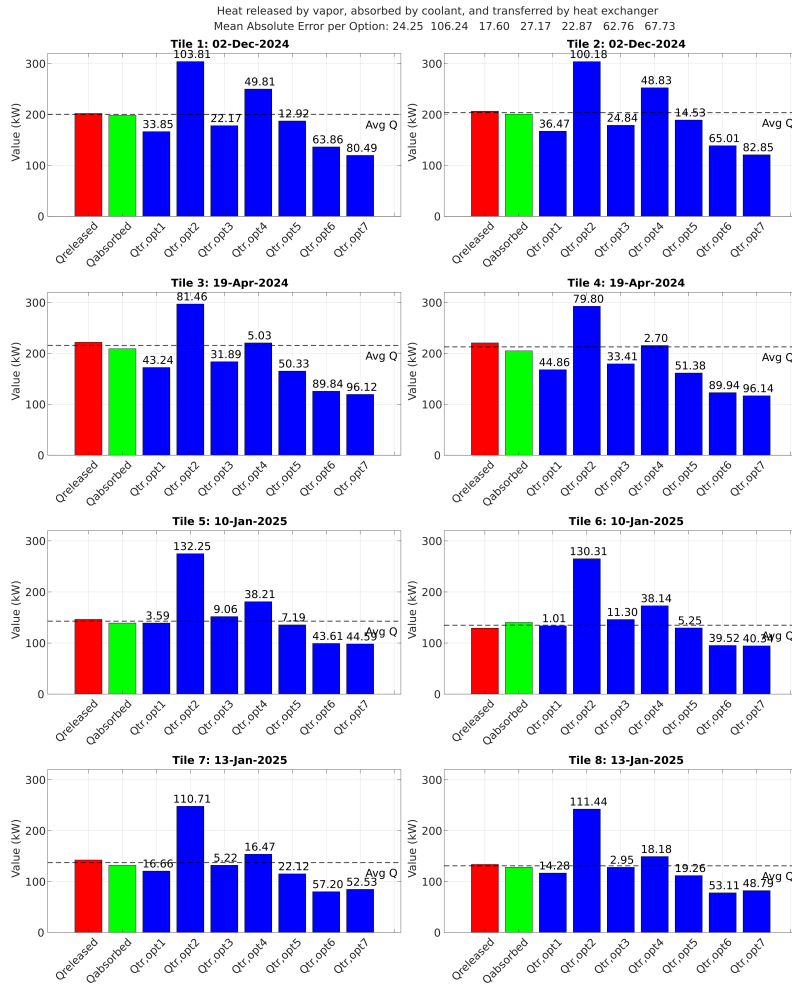


Figure 10.7: Heat transfer coefficient calibration results

can be adapted to the particular case study, while still being fast and efficient in terms of computational resources.

10.1.4 Condenser model validation

For the surface condenser³ a physical model is used, with the heat transfer coefficient as the only parameter to calibrate. Seven different alternative estimations of the heat transfer coefficient were calculated, using the data from the experimental campaign described in Section ?? (??). They are as follows:

1. Empirical correlation using the condenser flow rate (q_c) and the vapor temperature (T_v) as inputs.
2. Empirical correlation using the cooling water inlet temperature ($T_{c,in}$) and T_v as inputs.
3. Empirical correlation using the flow rate per condenser tube ($q_{c,tube} = q_c/n_{tubes} = q_c/24$) and the cooling water inlet temperature.
4. Nominal value from the manufacturer, which equals 1.838 W/m²°C
5. Calibra_Uexp_original
6. Calibra_Uexp_recortado

The results of the calibration are shown in Figure 10.7, where the y-axis shows the thermal power obtained and the x-axis holds different bars for the different heat transfer coefficient estimation methods, with bars also for the experimental

3: See Section ?? (??)

Estos qué son? Generar una nueva versión de la figura una vez se seleccionen los métodos finales

heat released by the vapor and absorbed by the coolant. As can be seen in the figure. The shown results are for steady-state conditions with the condenser in an equilibrium state ($Q_{\text{released}} \approx Q_{\text{absorbed}}$), and with a large variation in the condenser conditions (120 to 200 kW, the whole operating range of the condenser). The results show that the heat transfer coefficient obtained with the method 3 is the one that best fits the experimental data, with a MAE of 17.6 kW and a maximum error of 33.41 kW (15%).

10.1.5 Complete system model validation

a completar una vez se tengan resultados experimentales, hay que implementar la función para generar la visualización

Esto, o bien se hace comparando puntos en estático cuando todo el sistema está en estacionario, o en la gráfica de validación de la estrategia de optimización se muestra también una línea con las predicciones del modelo. Y después una tabla con cada una de las salidas del sistema, mostrando el error entre cada una de las predicciones del modelo (cada vez que se evalúa la optimización), en comparación al valor real obtenido en la planta.

Cuando haya un cambio en la planificación, las predicciones de predicciones antes a conocerse el cambio, cambiar su color a un gris para mostrar que esas predicciones ya no son válidas pues han cambiado las condiciones.

Figure 10.8 shows the model validation results for the complete system model. Different plots are shown for the main output variables⁴. Solid lines represent the measured variables in the real facility, while the different markers represent the predictions generated at different times. The plots also include a right-axis to display a metric error, specifically the MAPE of the predictions with respect to the measured values. The error is shown with a bar for each prediction.

The results show that the model is able to predict the main output variables of the system with a good accuracy. As expected the errors compound over time, specially after the change in the operation schedule at XX:XX. Nonetheless, the model is able to adapt after a new evaluation including the change and overall predictions below XX% of error are achieved.

4: C_w , $T_{dc,out}$, etc

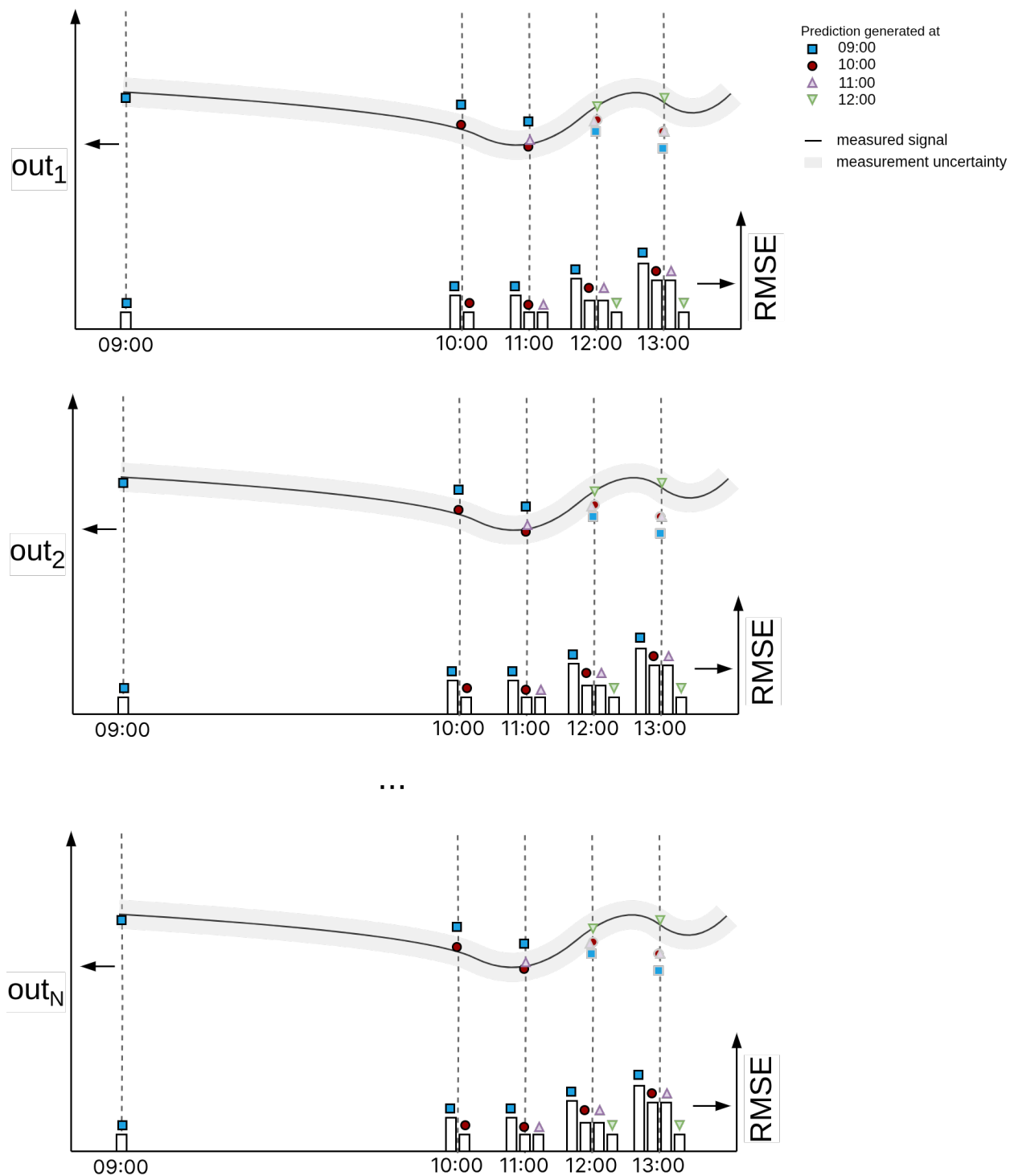


Figure 10.8: Figure caption.



10.2 Control and optimization results

Once the models of the main components of the system have been validated, the next step is to validate the optimization strategy proposed in Section ?? (??). First, an optimization algorithm is chosen by comparing different alternatives in Section 10.2.1 (Choosing an optimization algorithm). Then, the two proposed variants for the combined cooler are compared in simulation for one operation day in the simulated pilot plant in order to see which one performs better in Section 10.2.2 (Comparing the static and horizon optimization strategies). Finally, two validation scenarios are tested in the real facility, one where a regular operation schedule is followed throughout the operation, and a second one where planned changes are introduced in the operation schedule, in order to validate how the optimization strategy adapts to changing conditions.

10.2.1 Choosing an optimization algorithm

Static problems

For every static optimization problem (referencias a problemas) three different algorithms are tested: (N+1)-ES Simple Evolutionary algorithm with self-adaptive Constraint Handling (SEA-CSTR), IHS and Differential Evolution with self-adaptive Constraint Handling algorithm (DE-CSTR). For each alternative the same number of objective function evaluations are given (800) but they are distributed differently depending on the algorithm:

- ▶ SEA-CSTR and DE-CSTR make use of the Self-Adaptive Constraint handling algorithm (CSTR-SA) wrapper algorithm, which allows them to the constrained problems. 10 iterations are performed for this wrapper algorithm, leaving 80 iterations to spare for the inner algorithm.
- ▶ For all alternatives, three values are tested for the initial population size: 50, 100 and 400 individuals⁵.
- ▶ Depending on the algorithm only one individual is evolved (IHS and (N+1)-ES Simple Evolutionary algorithm (SEA)) or the whole population (Differential Evolution algorithm (DE)). This means that 800 generations are available for IHS, 80 generations for SEA-CSTR and for DE-CSTR, 1 generation is available for the population of 50 individuals, while only the initial generation is for the population of 100 and 400 individuals.

5: The initial population fitness evaluation is not counted for the budget of objective function evaluations

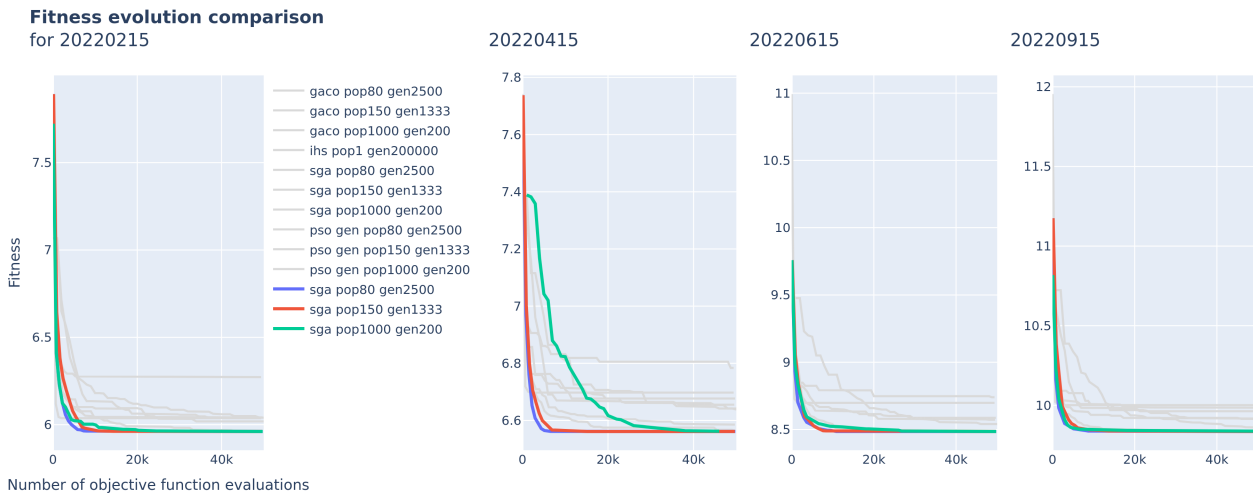
Table X shows the results obtained, in terms of fitness at different stages in the evolution. From the results it can be seen that for all alternatives the best performing and most consistent algorithm is ...

Horizon optimization. Path selection

A methodology similar to the static comparison is used. This time the algorithms evaluated are: Generalized Ant Colony Optimization algorithm (GACO), IHS, Simple Genetic Algorithm (SGA) and Particle Swarm Optimization algorithm (PSO). Three different population sizes are tested (80, 150 and 1000) if the particular algorithm evolves more than one individual; the number of generations is calculated accordingly so that all alternatives have the same budget of objective function evaluations, equal to 200k evaluations⁶. The results are visualized in Figure 10.9, where there are different plots for different dates, the y-axis represents the fitness and the x-axis shows the number of objective function evaluations. The results show that consistently the SGA outperforms the alternatives, and particularly, the smaller population size (80) configuration followed very closely by the 150 population size configuration.

6: Only up to 50k evaluations is shown in the figure for clarity

System	Algorithm	Parameters			Average fitness per obj. fun. evaluations			
		pop size	gen	wrapper algo iters	0	50	150	800
DC	IHS	50	800	N/A	1.28 ± 0.82	1.05 ± 0.29	0.80 ± 0.10	0.77 ± 0.09
		100	800	N/A	0.92 ± 0.18	0.87 ± 0.14	0.81 ± 0.11	0.77 ± 0.10
		400	800	N/A	0.81 ± 0.11	0.80 ± 0.11	0.79 ± 0.10	0.77 ± 0.10
	SEA	50	80	10	1.19 ± 0.28	0.95 ± 0.11	0.79 ± 0.10	0.77 ± 0.09
		100	80	10	0.92 ± 0.13	0.86 ± 0.10	0.80 ± 0.10	0.77 ± 0.09
		400	80	10	0.82 ± 0.10	0.80 ± 0.10	0.78 ± 0.10	0.77 ± 0.09
WCT	IHS	50	1	10	1.06 ± 0.40	0.97 ± 0.18	0.83 ± 0.10	1.04 ± 1.04
		100	0	10	0.95 ± 0.16	0.95 ± 0.16	0.95 ± 0.95	0.95 ± 0.95
		400	0	10	0.83 ± 0.10	0.83 ± 0.10	0.83 ± 0.10	0.83 ± 0.83
	SEA	50	800	N/A	0.24 ± 0.08	0.18 ± 0.04	0.10 ± 0.00	0.07 ± 0.00
		100	800	N/A	0.12 ± 0.02	0.11 ± 0.01	0.08 ± 0.00	0.07 ± 0.00
		400	800	N/A	0.07 ± 0.00	0.07 ± 0.00	0.07 ± 0.00	0.07 ± 0.00
CC	SEA	50	80	10	0.25 ± 0.04	0.16 ± 0.01	0.07 ± 0.00	0.06 ± 0.00
		100	80	10	0.17 ± 0.03	0.11 ± 0.00	0.07 ± 0.00	0.06 ± 0.00
		400	80	10	0.07 ± 0.00	0.07 ± 0.00	0.07 ± 0.00	0.06 ± 0.00
	SEA	50	1	10	0.29 ± 0.07	0.17 ± 0.02	0.09 ± 0.00	0.07 ± 0.07
		100	0	10	0.11 ± 0.00	0.11 ± 0.00	0.11 ± 0.11	0.11 ± 0.11
		400	0	10	0.07 ± 0.00	0.07 ± 0.00	0.07 ± 0.00	0.07 ± 0.07
CC	IHS	50	1000	N/A	0.77 ± 0.12	0.80 ± 0.11	0.77 ± 0.11	0.59 ± 0.11
		100	1000	N/A	0.70 ± 0.12	0.78 ± 0.10	0.82 ± 0.15	0.61 ± 0.13
		400	1000	N/A	0.79 ± 0.19	0.82 ± 0.21	0.80 ± 0.22	0.65 ± 0.16
	SEA	50	100	10	0.92 ± 0.13	0.86 ± 0.14	0.74 ± 0.16	0.51 ± 0.10
		100	100	10	0.88 ± 0.16	0.82 ± 0.16	0.75 ± 0.21	0.62 ± 0.16
		400	100	10	0.84 ± 0.21	0.80 ± 0.18	0.74 ± 0.21	0.69 ± 0.19
CC	SEA	50	2	10	0.83 ± 0.16	0.79 ± 0.13	0.73 ± 0.14	0.56 ± 0.13
		100	1	10	0.82 ± 0.17	0.80 ± 0.13	0.77 ± 0.10	0.64 ± 0.13
		400	0	10	0.73 ± 0.16	0.73 ± 0.16	0.73 ± 0.16	0.73 ± 0.73

Table 10.5: Static optimization algorithm comparison results**Figure 10.9:** Horizon optimization – path selection subproblem. Fitness evolution comparison for different algorithms in four different dates.

10.2.2 Comparing the static and horizon optimization strategies

TODO

Poner la figura de resultados del horizonte para SOLO un día detallado aquí (más días hace que no se distingan bien las barras, tampoco se puede poner el pareto). Debe incluir la distribución hidráulica en barras comparando estático con horizonte, el frente de pareto del horizonte, y la comparativa de coste acumulado.

Comentar la figura, sobre el frente de pareto que se muestra, cómo la estática al principio abusa del agua y para el final del día aumenta muchos sus costes,

La figura es provisional. Actualizar la figura con cambios mencionados

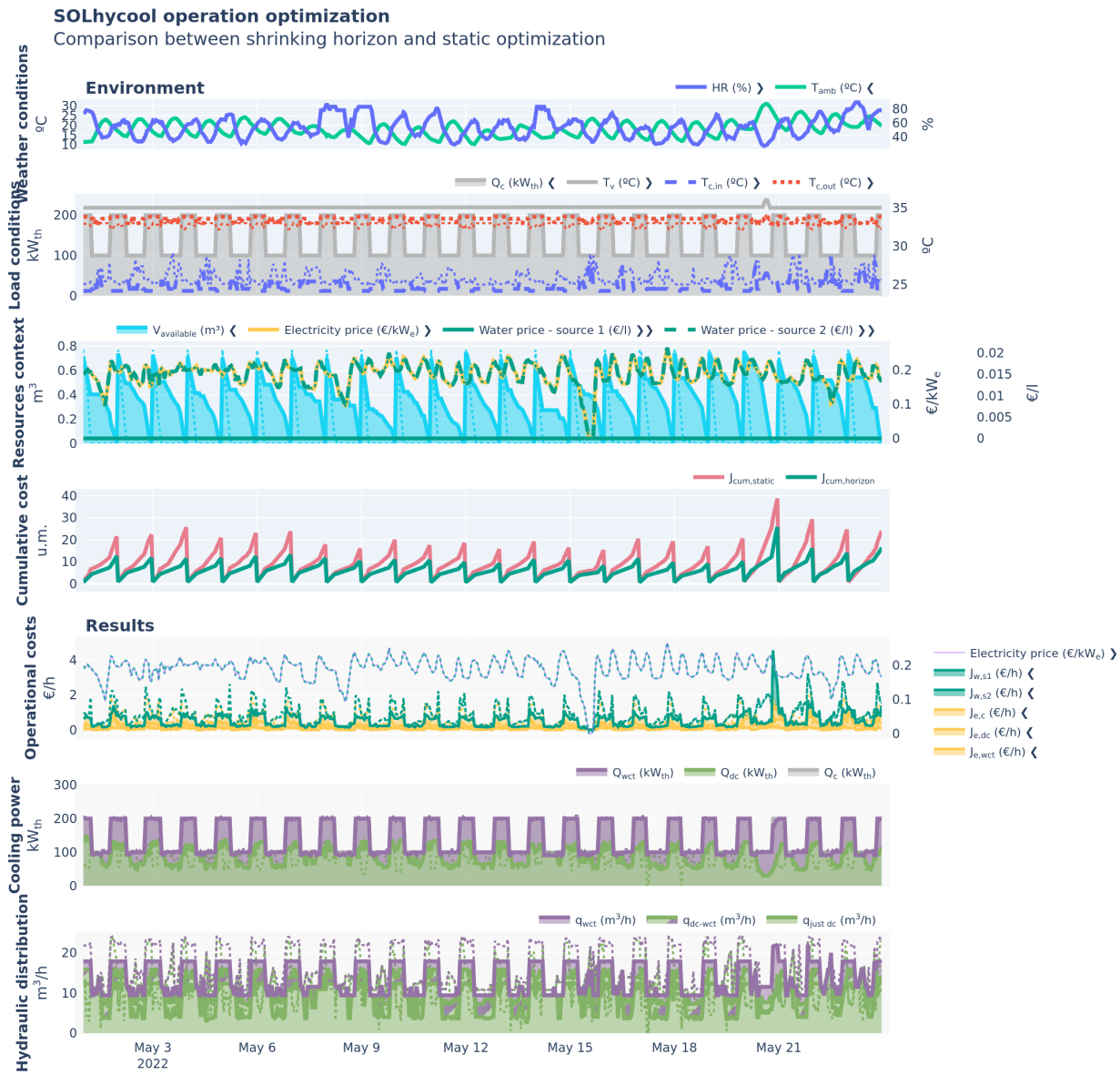


Figure 10.10: Detailed simulation results for the horizon optimization compared to the static alternative.



etc.

10.2.3 Validation at pilot plant

A hierarchical control strategy has been implemented in order to validate the optimization strategy in the real facility. Figure ?? shows a diagram of the methodology, where the left side represents the upper layer with the proposed

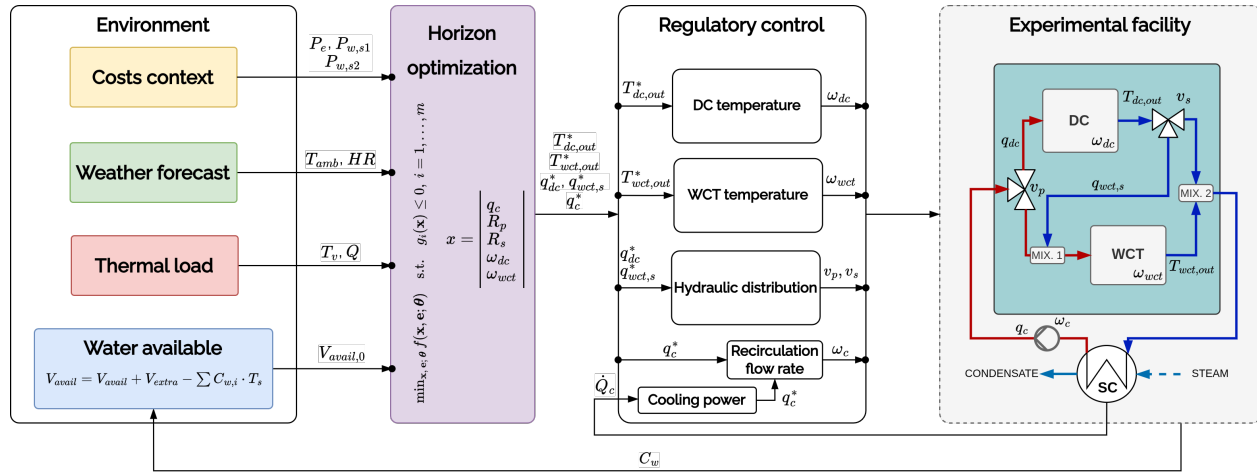


Figure 10.11: Implementation of the optimization strategy in the real facility. Hierarchical control

shrinking horizon optimization⁷ and the right side shows the low-level regulatory control layer, which directly interfaces with the actuators and sensors of the facility.

Environment. To generate the environment for the optimization, weather forecasts using the OpenWeather API [openweather_api] were used, for the electricity costs data from the 2022 spanish grid was used, updating the year to the one in which the experiment was performed, and the water cost was set to $C_{w,s1} = X$ and $C_{w,s2} = Y$. For the thermal load a profile was generated by setting a constant vapor temperature of $T_v = 45^\circ\text{C}$ while an arbitrary cooling power was generated considering the heat availability from the flat-plate collector field, which is the heat source of the system, for the particular day. Finally, an initial value for the water availability was set to $V_{avail,0} = 0.5 \text{ m}^3$, and from there it is updated by reading the actual system consumption online.

Optimization layer. The optimization algorithm is run every 30 minutes, and generates a new set of results for the remaining operation time. The results of the optimization are then passed to the regulatory control layer by setting them as setpoints for the low-level control. The box-bounds for the decision variables are shown in Table 10.6.

Control layer. Four controllers are implemented in this layer...

Table 10.6: Box-bounds for the decision variables.

7: \mathbf{x} See Section ??	Units	lb	ub
q_c	m^3/h	5.22	24.15
R_p	-	0.00	1.00
R_s	-	0.00	1.00
openweather_%i	%	11.00	99.18
ω_{wct}	%	21.00	93.42

aiuda Lidia!

In order to validate the optimization strategy, several tests were performed over different days. In particular Figure ?? visualizes one test carried out in the 1st August to analyze in this section. The objective of the test was twofold. For the first part of the test a set operation plan was established:

- \dot{Q} = Ramp up from 150 to 200 kW from 08:40 until 10:00, and hold the 200 kW value until the end of the test (13:00).
- $T_v = 45^\circ\text{C}$. Held constant throughout the experiment (08:40 – 13:00)

The objective was to validate that the optimized operation based on the provided predictions was effectively able to correctly manage resources and cool the thermal load with the predicted associated consumptions. During operation of a CSP plant changes to the operation plan can arise in response to changes in electricity market dynamics, or other unforeseen environment circumstances. At 10:20 a change is introduced in the operation plan to simulate this behavior, the thermal load was ramped down with a similar (inverse) profile to the initial one. This allows to verify the adaptability of the proposed strategy to changing conditions and is the second objective of the test.

The operation strategy was as follows:

- ▶ Before the test and while the system starts up by generating vacuum in the surface condenser, the optimization layer was evaluated to have an initial perspective on the day operation and expected consumptions. If the operator was satisfied the provided values were used as reference and manually set to bring the system into stable operation after gradually increasing the thermal load.
- ▶ The optimization sample time was 20 minutes, it takes around that time to compute and is evaluated every 40 minutes.
- ▶ The thermal load was designed to change every 40 minutes, this means that for each optimization evaluation, two setpoint changes are provided to the regulatory control layer per optimization evaluation and thus predictions must be valid for those at least 40 minutes.
- ▶ For every optimization layer evaluation, first the environment is updated and then is provided as input to the optimization evaluation (see Figure 10.11).
- ▶ The low-level control layer has available the operation strategy for the whole horizon provided by the upper layer and following its schedule updates its setpoints.

Figure ?? is divided in several sections. In general solid lines represent measured (experimental) values, while the thin-dashed equivalent (same color) is the predicted value by the upper-optimization layer. This predicted value is provided by the latest evaluated optimization. The upper section of the figure displays the environment evolution (weather conditions, load conditions and resources context). They are followed by a comparison between predicted and actual results for: (a) distribution between cooling systems, in terms of flows (*hydraulic distribution*) and in terms of the assigned cooling power (*cooling power distribution*) and (b) individual cooler outputs in terms of temperature profile and water consumption in the wet cooler case. Finally, the bottom of the plot shows the low-level control layer performance for each control loop: coolers outlet temperature and flows.

In Figure ?? – *Hydraulic Distribution*, several sequentially added bars are shown. The first bar corresponds to the experimental value, while the remaining bars represent the predicted hydraulic distributions from successive optimization evaluations: the second bar comes from the first evaluation, the third from the second, and so on.

From the results, a few observations can be made:

- ▶ Overall a very good agreement between the optimization layer predicted operation and the experimental values can be observed. It can be seen than as long as the environment, specifically the thermal load, does not change, the generated operation strategy is valid for hours. Particularly, the initial evaluation at XX:XX. In another test (not shown) where the thermal load does not change throughout the day the initial optimization held valid until the end of operation.
- ▶ The dry system is very sensitive to the ambient temperature when operating in its limits. Less than half-degree prediction error in the ambient temperature (0.4 °C between 09:04 and 09:17) translates in a 15% difference between the expected and the actual fan speed.
- ▶ When both systems are operating, if the dry cooler falls short in its cooling allocation, the wet cooler can compensate for the dry cooler shortcoming on its cooling allocation. However, as can be seen at the beginning of the test (09:04 – 09:17), when only the dry cooler is used and does so in its limits (Figure ?? - DC outlet temperature loop - Control signal) it can happen that the load is undercooled resulting in a higher condenser pressure (in terms of temperature, +1-2 °C can be observed, which would

translate in a penalty in the power produced by the turbine). A low-level supervisory controller should be set in place to prevent this.

- ▶ To avoid using the alternative more expensive alternative water source, the optimization prioritized the use of the dry cooling (as far as being dry-only as long as the ambient temperature and demanded thermal load allowed it 09:20) to conserve water until the end of operation. After the operation plan change, the lower expected load gives more room for adjustment and the optimization increases the load through the wet system from 0-40% to about 50% (Figure ?? - Hydraulic distribution and Cooling power distribution).
- ▶ The restricted availability of the water resource, means that the optimizations strategy always prioritizes water savings either by dry-only operation, or combined operation using a series configuration, at no point the parallel configuration is used despite progressively increased electricity cost (*Resources context – P_e*).
- ▶ The good agreement between upper and lower layer, means that the upper layer predicted controlled variables values could be used by the low-level control, for example, in a static feed-forward action.
- ▶ From the initial optimization evaluation, the low-level control layer has available an operation strategy for the whole horizon. This makes the strategy robust in the case the optimization is not evaluated again, or not evaluated on time.

TL;DR

This chapter presents the annual simulation results for different cooling systems: a WCT, a DC and the presented CC optimized with static optimization and with horizon optimization. They provide cooling to the power block of the XX hours storage–CSP plant ANDASOL-II with an off-peak operation strategy. Results for the case study report a specific cooling cost of XX, XX and XX for the WCT, DC and CC, respectively, compared to the 5 L/kWh figure provided by the developer.

11.1	Limitations	79
11.2	Environment definition	80
11.2.1	Water context	80
11.2.2	Thermal load	80
11.2.3	Costs context	81
11.3	Comparison	81
11.4	Cooling alternatives comparison	84

Introduction

A modeling framework has been developed to simulate and optimize the operation of various cooling systems, with a particular focus on the proposed combined cooling system. This methodology has been validated using data from a pilot plant. In this chapter, the objective is to apply the framework to a specific case study: a CSP plant.

As previously mentioned, CSP plants are among the most water-intensive power generation technologies [28], a concern that is especially relevant in the arid regions where they are typically located. To assess the performance-water use and operational costs- of different cooling systems, the proposed methodology is applied to a real-world case study through an annual simulation. The case study examined is the Andasol-II CSP plant.

In the south-east of Spain, near Guadix and next to the Sierra Nevada mountain range (see Figure 11.1), thanks to the region high altitude (1100 m) and the semi-arid climate, the site has exceptionally high annual direct insolation (2260 W/m²) and thus is ideal for solar projects. This is why the first parabolic trough power plant in Europe, Andasol-I, was built there in 2008. One year later Andasol-II followed, located in the immediate neighbourhood and with almost identical construction. It has a rated output of 50 MW with 7.5 hours¹ of thermal storage, providing electricity for up to 200,000 people. More specifications are available in Table 11.1.

According to the developer, Andasol-II vaporizes 870 000 m³/year, or in specific units 5 l/kWh.

11.1 Limitations

1. The combined cooler analyzed has a 50% split in nominal cooling power of the WCT and DC components compared to the standalone cooling systems. Different ratios could be analyzed and one would probably be a better fit for the particular case study. This in itself is a design optimization problem that is not addressed in this thesis.
2. An ACHE is used for the DC, but other options could be considered, such as an ACC.



Figure 11.1: Andasol (I and II) aerial view.
Andasol is the “one generation”
Source: https://en.wikipedia.org/wiki/File:Andasol_5.jpg

1: This means that if fully charged, it can produce the nominal rated power of the turbine for that duration

Table 11.1: ANDASOL-II plant main characteristics

Technology	Parabolic Trough
Solar Resource	2260 W/m ²
Nominal Capacity	50 MW
Status	Operational
Start Year	2009
Considerar mover esto al apartado de trabajos futuros	
TF Inlet Temperature	293°C
TF Outlet Temperature	393°C
Power Cycle	Steam Rankine
Turbine Efficiency	38.1%
Cooling Type	Wet
Storage Type	Molten salts
Storage Capacity	7.5 Hours – 1 GWh

Source: Institute for Advanced Sustainability Studies (IASS) and others, 2022; data by Lilliestam@IASS, Thonig@IASS, Zang@CAS, Gilmanova@CAS and others. Licensed under a Creative Commons Attribution 4.0 International License.

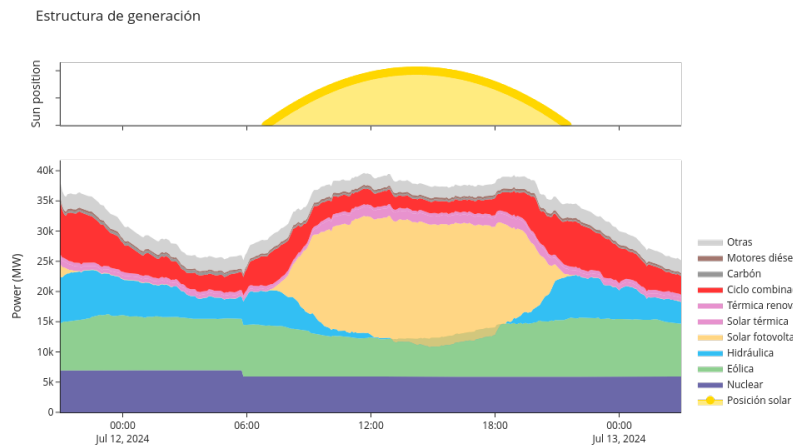


Figure 11.2: Spanish electricity mix on July 12, 2024. The peak in photovoltaic generation is clearly visible at midday, while thermosolar generation is more evenly distributed throughout the day. Peak production is majorly from CSP plants with no storage.

Data source: Figure elaborated using data extracted from <https://www.ree.es/es/datos>

11.2 Environment definition

11.2.1 Water context

Obtaining accurate water availability data is challenging. Unlike resources such as electricity—where demand, supply, and prices are readily available—water availability data is often lacking. Water prices are not standardized; they vary from region to region, and even within the same region, depending on the source and the specific agreements in place.

2: See Section ?? (??)

<empty citation>

meteonorm_

For the simulation scenario, two sources of water are considered². The first source is rainwater or water from a dam, which is assumed to be available at a constant price of XX [<empty citation>]. To create a representative dataset, water availability is modeled as a function of precipitation data, which can be obtained from hourly Typical Meteorological Year (TPY) data [meteonorm_]. A linear model is fitted to relate maximum precipitation to maximum available water, and when there is no precipitation, water availability is set to zero. The data is then resampled every 15 days, and the daily volume of available water is calculated by dividing the resampled fortnightly volume by 15. This approach accounts for the presence of water reservoirs and some degree of management capacity.

The alternative source is regenerated water³ is not limited in volume.

11.2.2 Thermal load

Traditionally, thermal power plants were designed and operated to generate electricity only when solar energy was available. This approach remained common until the rapid rise in competitiveness of PV plants, which offer significantly lower generation costs. In response, concentrated solar power plants began integrating thermal energy storage systems to enable dispatchable power generation. Today, 21 out of 51 CSP plants in Spain—approximately 42%—have thermal storage capacities exceeding two hours [15, 32, 33]. This enables them to produce electricity even when solar input is unavailable.

However, many of these plants still follow traditional operating patterns, generating most of their electricity during peak solar hours⁴. This strategy is increasingly seen as suboptimal and is likely to be phased out as the electric grid becomes saturated with PV generation⁵.

[15]: Lilliestam et al. (2021), “The Near- to Mid-Term Outlook for Concentrating Solar Power: Mostly Cloudy, Chance of Sun”

[32]: Thonig et al. (2023), CSPGuru 2023-07-01

[33]: Bonilla et al. (2024), “CSP Data: A Data Discovery Web Application of Commercial CSP Plants”

4: The storage is primarily used to extend generation past sunset.

5: This trend is already observable in Spain during the summer months; see Figure 11.2

In this work, a different operational strategy is adopted: the plant is configured to generate electricity during off-peak solar hours, typically in the evening when electricity demand is at its highest. This is achieved by shifting the plant's production to align with these peak demand periods.

A model of the Andasol-II plant, developed by Bartolomé et al. [[empty citation](#)], was configured to follow this production strategy and simulated over an entire year. The resulting thermal load profile represents the demand to be met by the cooling system. The simulation used the same weather dataset as that employed for modeling the cooling system.

[empty citation](#)

11.2.3 Costs context

Electricity. The spanish grid operator Red Eléctrica de España (REE) provides an API⁶ to access the electricity market prices. A python script was developed to systematically download monthly data⁷ for each month in the desired year. The data is fetched in hourly intervals and saved in JSON format, then every file is read and joined into a single dataset resulting in prices for the whole year.

Water. Rainwater has a constant lower price of XX. This price was obtained considering that the plan has access to the same water than the irrigation community of the area [[empty citation](#)]. The alternative source, *i.e.* regenerated water, is considerably more expensive, and its price is linked to the electricity price, specifically by a factor of XX⁸.



6:

<https://api.esios.ree.es>

7: Longer periods would result in silent errors in the API

[empty citation](#)

8: This value includes a scaling factor to normalize the values

Simulation data and parameters information

Weather data	Hourly weather data from TPY of Guadix (Spain) for the year. Data was obtained from ...
Thermal load	Hourly thermal load data from the power block of ANDASOL-II CSP plant from a simulation model.
Electricity price	Spanish electricity market from 2022.
maximum available water	The maximum available water for ...
active water source	...

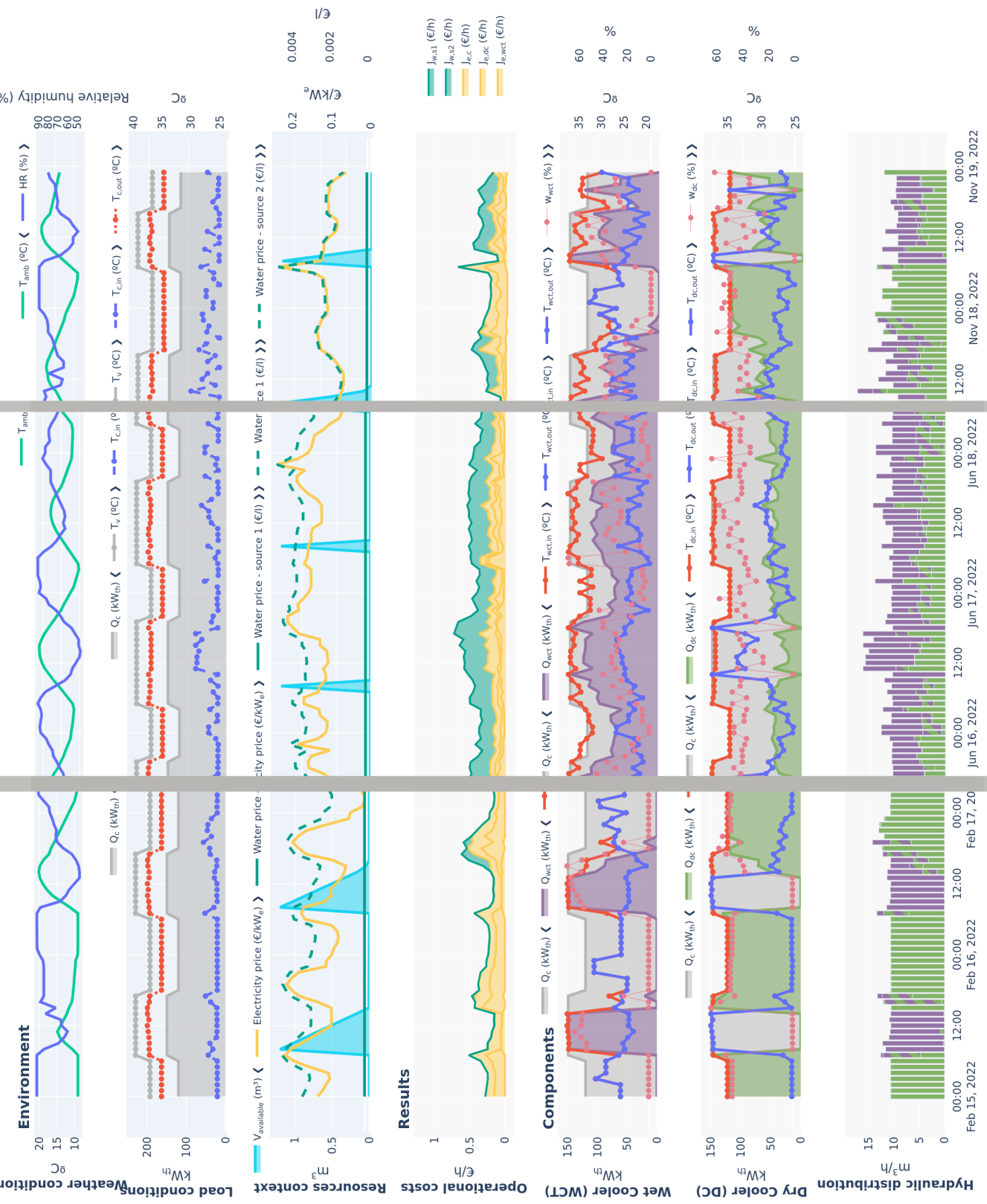
The full environment dataset is available at



11.3 Optimization strategies comparison

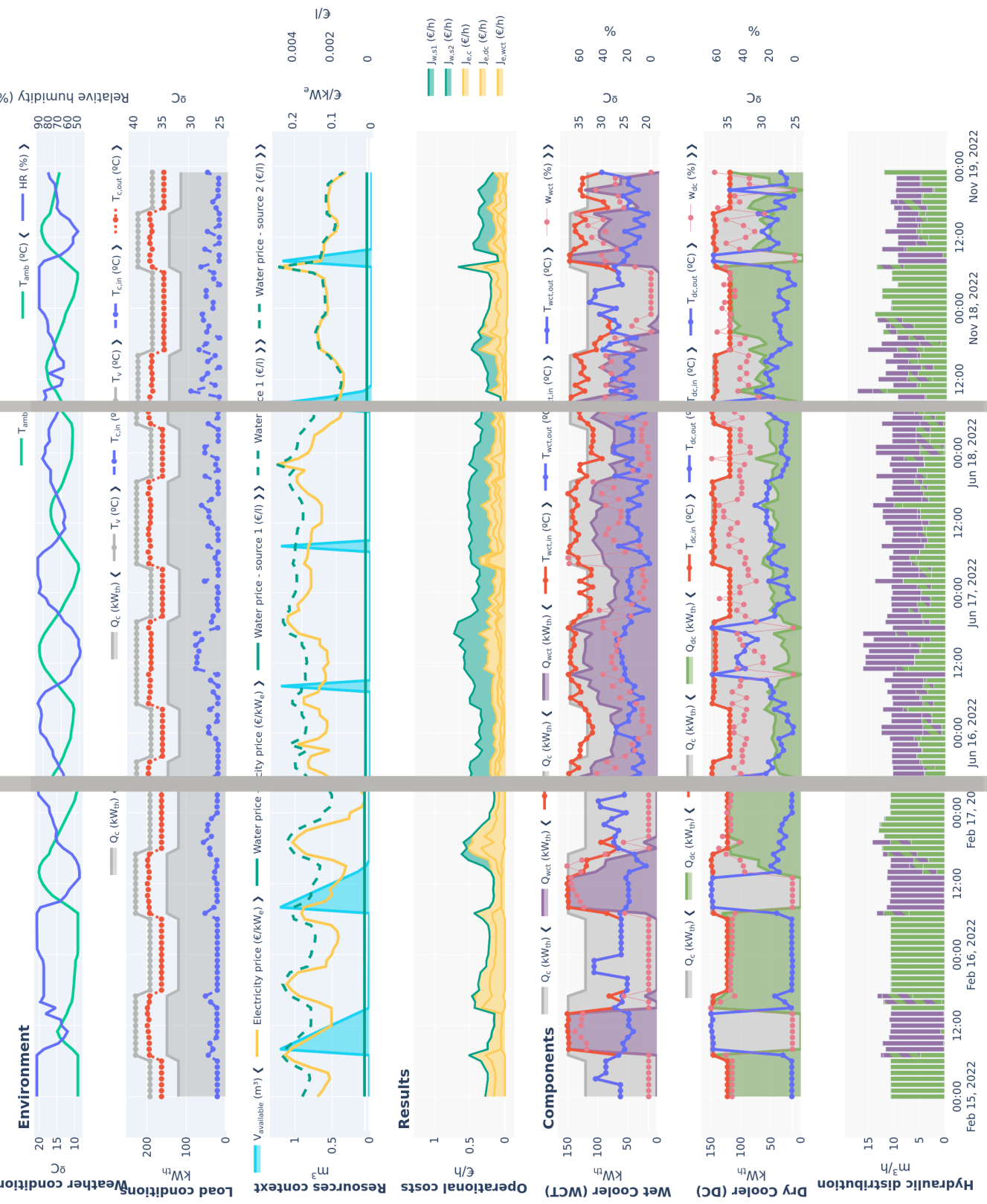
SOLhycool operation optimization

Evaluation results



SOLhycool operation optimization

Evaluation results



11.4 Cooling alternatives comparison

Fusionar las gráficas de resultados anuales remuestreados para que incluyan todas las alternativas. Cambiar fondo para cada sistema

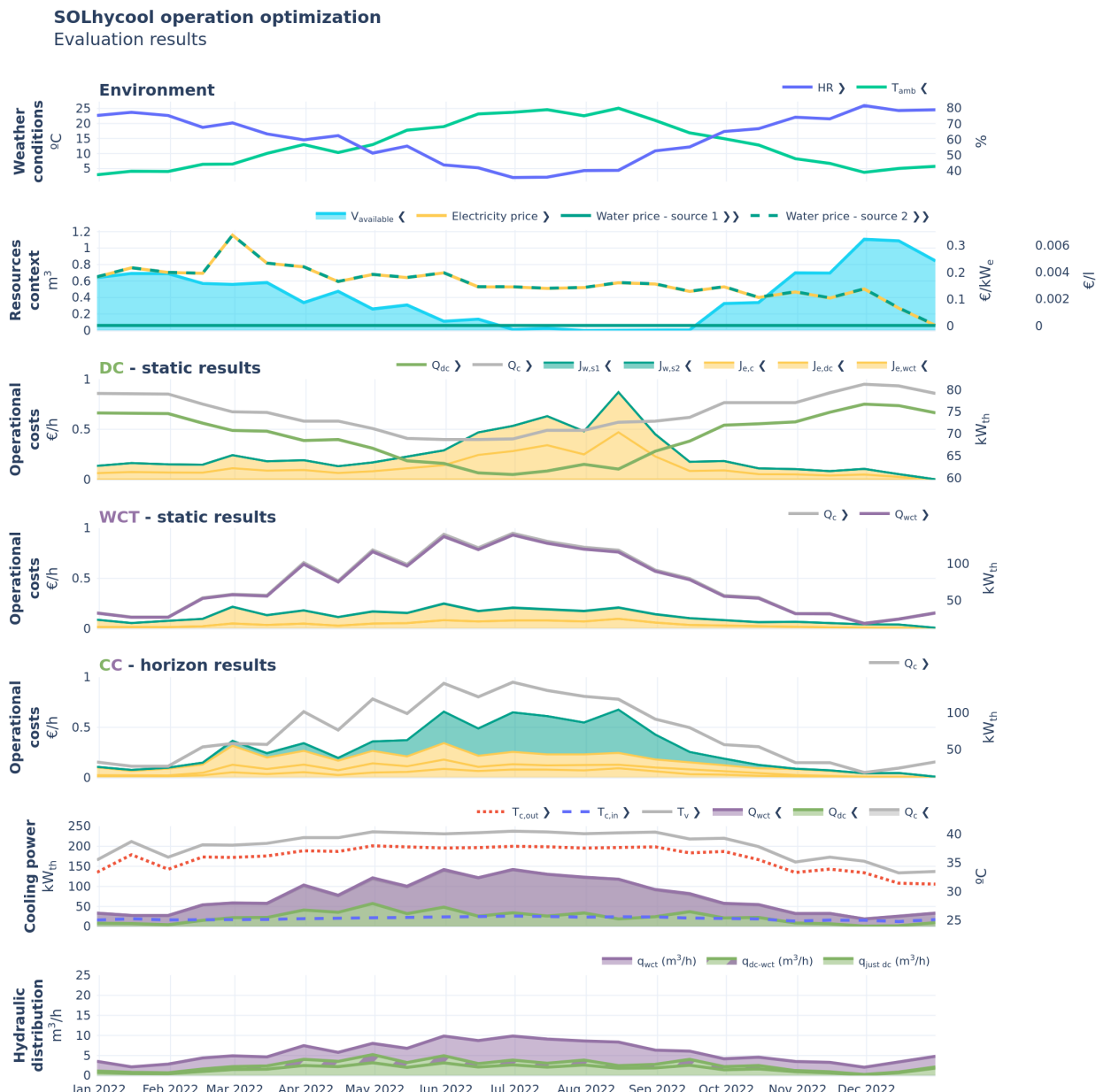


Figure 11.5: Annual simulation results for the CC system optimized with static optimization. Results are resampled every 15 days using their mean values. The original frequency results can be found in the interactive version:



Añadir gráfica de barras comparando coste por kWh refrigerado

Añadir gráfica de barras comparando distribución de potencia térmica por componente y distribución hidráulica por componente para cc-static y cc-horizon

One caveat that no optimization strategy will ever be able to overcome is that in most locations, ambient temperatures are lowest (favoring the dry system) at times with the most annual water availability (favoring the wet one). The inverse is true in the hot-dry summer season where water will inherently be a scarce resource. Still as shown, there is a lot of margin for improved water management via system optimization with integrated dry and wet systems. Additionally, CSP systems should consider not operating in the hottest hours of the summer days - when water is scarce and enough power generation from other renewables is

ENERGY MANAGEMENT IN MED PROCESSES DRIVEN BY VARIABLE ENERGY SOURCES



Esta sección no está terminada. Siquieres puedes echarle un ojo para ver la estructura y cómo encaja con el resto pero no merece la pena revisarla en detalle en el estado actual.

TL;DR

...

a

Add visual abstract

Derived scientific contributions

Part structure



Esta sección no está terminada. Siquieres puedes echarle un ojo para ver la estructura y cómo encaja con el resto pero no merece la pena revisarla en detalle en el estado actual.

Desalination is increasingly recognized as a key strategy to address global freshwater scarcity, driven by the combined pressures of climate change and population growth. Regions already facing drought and water stress, such as parts of Spain, are expected to see growing dependence on desalinated water to meet rising demand. While desalination technologies—particularly membrane-based systems like Reverse Osmosis (RO)—have seen rapid expansion, the energy intensity of the process remains a major challenge. To mitigate this, efforts have focused on improving energy efficiency and integrating renewable energy sources such as solar or geothermal heat. In particular, thermal desalination technologies like MED are gaining renewed interest due to their compatibility with low-exergy heat sources (e.g. waste heat) and the ability to treat high-salinity brines. These thermal processes also align better with circular economy approaches, allowing the concentration of brine and the recovery of valuable minerals such as lithium or magnesium, an emerging field known as brine mining.

 WORK IN PROGRESS   

Esta sección no está terminada. Si puedes echarle un ojo para ver la estructura y cómo encaja con el resto pero no merece la pena revisarla en detalle en el estado actual.

13.1 Heat generation and storage subsystem	91
13.1.1 Solar field	91
13.1.2 Thermal storage	92
13.2 Separation subsystem	92

The SolarMED system is an MED plant that receives its thermal energy from a solar field connected to a two-tank thermal storage system. It is one of the experimental facilities located in PSA as can be seen in Figure 1.2.

The different components are interconnected as depicted in Figure 13.1: a flat plate collector solar field which is the heat source, a pressurized hot water two-tank thermal storage system, and an MED plant which uses this heat to separate seawater into fresh water and brine. The solar field and thermal storage circuits are separated by a heat exchanger. Two subsystems are differentiated: the **sfts** subsystem and the thermal load that makes use of this heat for some useful application, in this case, to produce separation by means of the MED: the separation subsystem.

A esta figura quitar colores de decision variable and environment

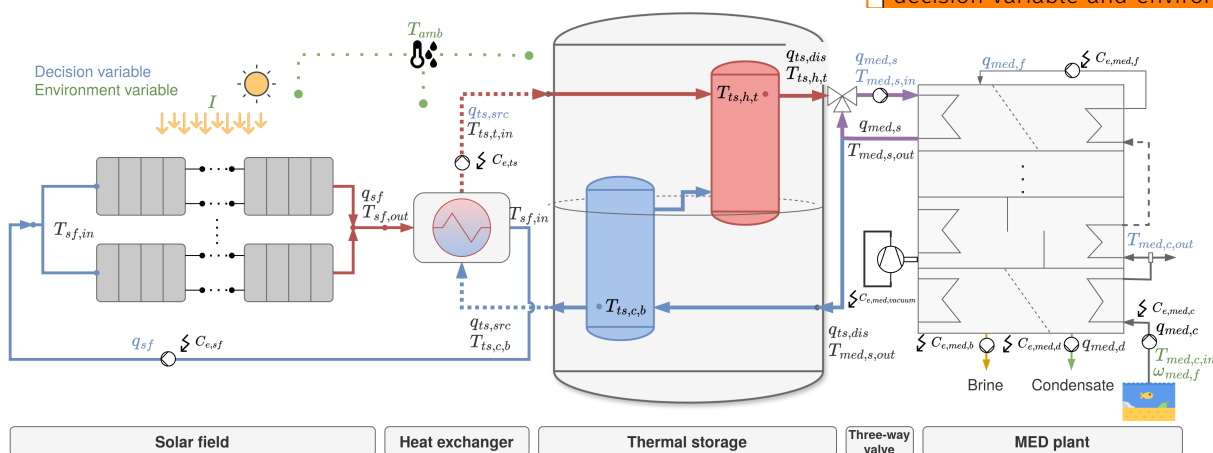


Figure 13.1: SolarMED process diagram

13.1 Heat generation and storage subsystem

Two pressurized water tanks coupled to a solar field composed of static flat plate collectors.

13.1.1 Solar field

The solar field is basically a converter of electrical to thermal energy conditioned to the availability of solar irradiance. It has a total aperture area of 606 m^2 and can generate a maximum thermal power of 323 kW_{th} with a 1000 W/m^2 solar irradiance. It is composed of 4 loops each with 2 rows of collectors...

The parameters are the collector aperture (A_c (m^2)), number of parallel collectors in each loop ,number of serial connections of collectors rows (n_s), number of parallel tubes in each collector (n_t) and the length of the collector inner tube (L_t). Their values are shown in Table ??.

13.1.2 Thermal storage

1: See Figure 13.1 - *Thermal storage*

The thermal storage system¹ consists on a two-tank system designed to ensure thermal stratification. It has a total capacity of 40 m³. One of the tanks (the red tank in the diagram) operates at a higher temperature, receiving heat from the energy source and delivering it to the load. The return flow from the load enters the bottom of the cold tank (blue tank in the diagram) before circulating back to the hot tank, where it absorbs heat from the source.

13.2 Separation subsystem

patricia

The MED pilot plant was built in 1988 within the Solar Thermal Desalination project [REF]. It is a 14 effect, vertically stacked, forward-feed plant initially built to use low-pressure saturated steam as heat source for the first effect and later replaced to use hot water within the XXX project in 2005. An image of the facility in its current state can be seen in Figure 13.2It has been operated in different experimental campaigns and configurations robustly for more than two decades, as can be seen in Figure 13.3, which shows the operation history of the plant (starting from 2009). The campaign from 2009 to 2012 focused on ... [patricia] while the campaign from 2015 to 2016.... Finally, within the research work presented in this thesis, a new campaign was performed to validate a standardization methodology proposal and experimentally characterize the behaviour of the system at higher temperatures. This is explained in detail in the following chapter (Chapter 14 (Performance evaluation in MED processes: standard methodology proposal)).

Some particularities of this system are explained hereinafter:

- ▶ VFDs are used to control all flow rates in the system: heat source, cooling, feed, brine and distillate.
- ▶ As mentioned, the external heat source driving the process, is hot water from a thermal storage system. Water is drawn from one of the tanks and mixed with the water at the outlet of the first effect through a three-way valve, allowing independent regulation of flow and temperature.
- ▶ The inland location of this experimental plant is another particularity of the system. A fixed amount of seawater (30 m³), stored in a reservoir, is available to be used in the process and replenished as needed. The effluents from the plant are mixed in a different reservoir (5 m³), and returned to the feed in a close loop operation. Because water exits the process at a higher temperature than when it enters, this type of operation implies an ever-increasing heat sink temperature. A wet cooling tower, installed between the two reservoirs, is used to mitigate this effect.
- ▶ The previous particularity leads to a significant variation in the inlet water temperature from day to day and also within the same day depending on the operation conditions. To ensure the stability of the condenser (i.e. a constant vapor pressure and outlet cooling water temperature), the cooling flow rate is regulated. This allows to have a stable system representative of a real plant operating under normal conditions. However, this can lead to variable electrical consumption of the cooling pump.

- The vacuum system of the plant is based on two hydro-ejectors and a pump. The pump is operated always at fixed speed and its electrical consumption has been characterized with measurements under various conditions as being near-constant and independent of the operation conditions. Its associated nominal power is 5 kW_e.
- The salinity of the feedwater is checked before every test measuring its conductivity with a conductivity meter (see Table ??).

A summary of its main specifications is shown at Table Table 14.1.

The facility's instrumentation is shown in Table 13.2. As can be seen, Platinum temperature transducer, 100 ohms at 0 °C (PT100) sensors are used to measure all liquid temperatures (TT01..TT05), while a PT1000 sensor is used to measure the ambient temperature (TT06). The pressure inside the first effect and condenser (PT01 and PT02, respectively) is measured by two different pressure transducers which fundamentally differ in their measurement range. To monitor the power consumption of the system, various subsystems have been individually instrumented using a power meter (JT01..JT04). Conductivity is measured using a portable conductivity meter (CT01, CT02), to which a calibration is periodically performed to convert conductivity to salinity. Flow rates (FT01..FT04) are measured using different types of flowmeters depending on the characteristics of the fluid being evaluated. Electromagnetic flowmeters are used for conductive fluids, while vortex flowmeters are used for non-conductive fluids. All sensors transmit a 4–20 mA analog signal that is converted to digital by Analog-to-Digital Converter (ADC) converters.



Figure 13.2: MED plant at PSA with open effects for maintenance

Table 13.1: MED plant at PSA specifications and nominal operating conditions

Parameter	Value
Capacity	72 m ³ /day
Number of effects	14
Feed type	Forward feed
Physical arrangement	Vertically stacked
Heat exchanger configuration	90/10 Cu-Ni HTE
Heat source type	Hot water
Vacuum system	Hydro-ejectors
Heat source flow rate	12 L/s
Feed water flow rate	8 m ³ /h
Brine rejection	5 m ³ /h
Distillate production	3 m ³ /h
Cooling flow rate at condenser	8-20 m ³ /h (10-25 °C)
Thermal power consumption	190 kW
Top Brine Temperature (TBT)	70 °C
Condenser temperature	35 °C

Measured variable	Instrument	Model	Range	Measurement uncertainty
Water temperature, TT01..TT04	PT100 Class A	SEDEM OF112871	0 - 100 °C	± 0.15 + 0.002·T ^a
Distillate flow rate, FT03	Vortex flow meter	ABB TRIO-WIRL VT4	1.6 - 18 m ³ /h	± 0.75% o.r. ^b
Hot water flow rate, FT01	Electromagnetic	Endress+Hauser Proline Promag 50P	2.42 - 78.33 L/s	± 0.5% o.r.
Feedwater flow rate, FT02	Electromagnetic	Proline Promag P 300	21 - 66 m ³ /h	± 0.5% o.r.
Ambient temperature, TT05	PT1000	-	-40 - 60 °C	± 0.15 + 0.002·T
Pressure, PT01	Pressure capacitive	Endress+Hauser Cerabar T-PMC131	0 - 1 bar	± 0.5% FS ^c
Pressure, PT02	Piezoresistive sensor	WIKA S-10	0 - 0.6 bar	± 0.5% FS
Level, LT01, LT02	Magnetic level gauge	IGEMA NA7-50	0-750 mm	± 5 mm
Power, JT01..JT04	Power meter Class 1	Circutor CM31	0-7 kW	±1% o.r.
Conductivity, CT01..CT02	Conductivity meter	Prominent Portamess 911	0.1 μS/cm - 1000 mS/cm	± 0.5% o.r. < 500 mS/cm ± 1% o.r. ≥ 500 mS/cm

Table 13.2: Characteristics of the instrumentation installed at MED-PSA unit (^a value of the measured temperature in °C, ^b of reading, ^c full scale).

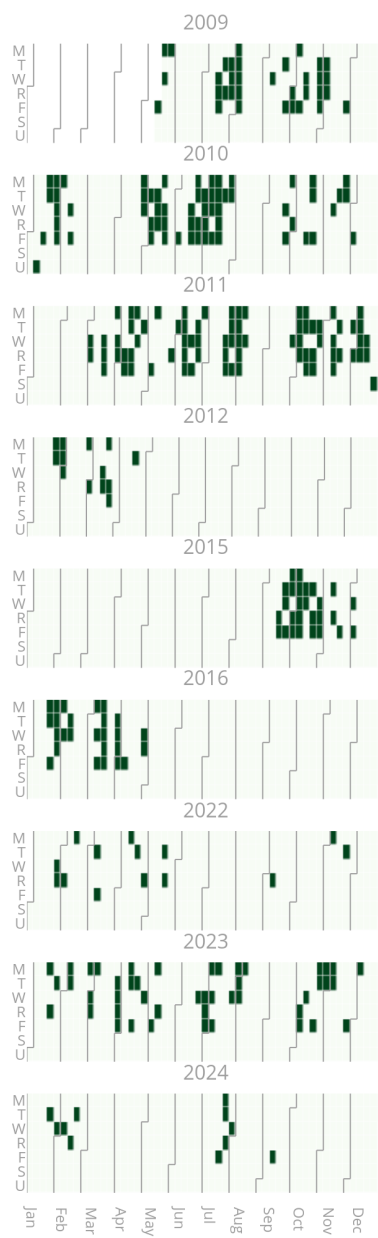


Figure 13.3: Operation history of the pilot plant.



TL;DR

This chapter presents a standardized method for evaluating the performance of MED processes, which can also be extended to other thermal separation technologies. The method addresses key aspects such as instrumentation requirements, process control, and the suitability of performance metrics, including the uncertainties associated with their determination. Additionally, an algorithm has been developed for the automatic detection of steady-state operation, enhancing the reliability and robustness of evaluations under variable conditions. Experimental results confirm that the proposed method is both robust and reliable, enabling fair comparisons of MED processes across different operating scenarios.

The experimentation includes the evaluation of the process at high TBTs. The results are analyzed using different performance metrics and the scale formation risk is estimated by the RSI. The results show that the MED process can be operated at high TBTs without significant scale formation and achieve higher concentrations, but without significant improvements in thermal performance and limited reconcentration capacity if no changes to its design are made.

14.1	Process analysis	97
14.2	Performance metrics	98
14.2.1	Separation metrics	98
14.2.2	Energetic metrics	99
14.2.3	Exergetic metrics	100
14.3	Instrumentation	102
14.3.1	KPV	102
14.3.2	Instrumentation requirements	103
14.3.3	Uncertainty determination .	104
14.4	Monitoring and process control	105
14.4.1	Monitoring: steady-state identification	105
14.4.2	Control system	105
14.5	Methodology application and results	107
14.5.1	Implementation results	108
14.5.2	Results analysis	112

Introduction

The future of MED in desalination and brine concentration applications depends on the technical development of the process and its integration with other technologies [73, 74]. The performance of this technology and how it is evaluated plays an important role in this development.

Although efforts have been made to propose performance metrics to evaluate the multi-effect evaporation process, there is neither consensus in which metrics are the most suitable [75] nor standards on how to evaluate the experimental process. The only standard existing in MED is not related to performance evaluation, but to cost structures and determinants [76].

For the performance evaluation of MED processes, originally, the index Gain Output Ratio (GOR) was used for plants operating with steam as external energy source. In order not to be limited to steam-driven systems and to take into account sensible heat sources, a new performance index was defined: the Performance Ratio (PR) [77, 78], which is currently the most widely adopted for MED performance evaluation although it is constrained by using a reference enthalpy of 2326 kJ equivalent to 1000 BTU. In [79], a variation of this metric called the Waste Heat Performance Ratio (PR_{WH}) was suggested to account for the potential of low-grade waste heat sources. Another widespread thermal performance metric that has been used in MED is the Specific Thermal Energy Consumption (STEC) and its electrical equivalent, the Specific Electrical Energy Consumption (SEEC). However, there are certain limitations in the aforementioned metrics that challenge making a fair comparison between desalination systems that use different energy sources *i.e.* electrical and thermal¹. Furthermore, the ability of thermal energy to perform work changes with its temperature, so it is essential to consider the quality of the thermal energy used in desalination processes. This limitation of traditional energetic metrics was showcased in Bouma et al. [81] where they compared four different configurations of MED plants: a low temperature MED configuration (LT-MED), a MED unit incorporating Thermal

[73]: Ghenai et al. (2021), "Performance Analysis and Optimization of Hybrid Multi-Effect Distillation Adsorption Desalination System Powered with Solar Thermal Energy for High Salinity Sea Water"

[74]: Son et al. (2020), "Pilot Studies on Synergistic Impacts of Energy Utilization in Hybrid Desalination System"

[75]: Burgess et al. (2000), "Solar Thermal Powered Desalination: Membrane versus Distillation Technologies"

[76]: Pinto et al. (2017), "Desalination Projects Economic Feasibility"

[77]: Mistry et al. (2011), "Entropy Generation Analysis of Desalination Technologies"

[78]: EL-Dessouky et al. (2002), *Fundamentals of Salt Water Desalination*

[79]: Christ et al. (2014), "Thermodynamic Optimisation of Multi Effect Distillation Driven by Sensible Heat Sources"

1: the value of 1 kWh electric differs from that of 1 kWh thermal in terms of their ability to produce work, as the latter is constrained by the Carnot efficiency [80]

[81]: Bouma et al. (2020), "Metrics Matter"

Vapor Compression (MED-TVC), a MED unit using nanofiltration (NF-LT-MED) for feedwater pretreatment, and a combination of TVC and nanofiltration. Although the STEC values favored the use of TVC, a more rigorous analysis revealed that the most efficient systems were those that used lower temperature heat sources (LT-MED and NF-LT-MED).

[82]: Darwish et al. (2006), "Multi-Effect Boiling Systems from an Energy Viewpoint"

[83]: Shahzad et al. (2019), "A Standard Primary Energy Approach for Comparing Desalination Processes"

[80]: Lienhard et al. (2017), "Thermodynamics, Exergy, and Energy Efficiency in Desalination Systems"

[84]: Brogioli et al. (2018), "Thermodynamic Analysis and Energy Efficiency of Thermal Desalination Processes"

[85]: Spiegler et al. (2001), "El-Sayed, Y.M."

[86]: Sharqawy et al. (2011), "On Exergy Calculations of Seawater with Applications in Desalination Systems"

[87]: Sharqawy et al. (2010), "Formulation of Seawater Flow Exergy Using Accurate Thermo-dynamic Data"

[88]: Mistry et al. (2012), "Effect of Nonideal Solution Behavior on Desalination of a Sodium Chloride (NaCl) Solution and Comparison to Seawater"

[89]: Mistry et al. (2013), "Generalized Least Energy of Separation for Desalination and Other Chemical Separation Processes"

[90]: Thiel et al. (2015), "Energy Consumption in Desalinating Produced Water from Shale Oil and Gas Extraction"

[91]: Valenzuela et al. (2014), "Optical and Thermal Performance of Large-Size Parabolic-Trough Solar Collectors from Outdoor Experiments"

[92]: Prahla et al. (2018), "Protocol for Characterization of Complete Solar Concentrators Using Photogrammetry or Deflectometry"

[93]: Bayón et al. (2019), "Development of a New Methodology for Validating Thermal Storage Media"

Some authors have carried out exergy analyzes to overcome the limitations aforementioned of energy performance metrics. Darwish et al. [82] proposed two new metrics: Specific Fuel Energy and Equivalent Specific Work. The first compares the energy used for the desalination process that could otherwise be used for energy generation in a turbine for which it was assumed a value for the efficiency of the power plant. The second sets the work potential of the extracted steam as a baseline, considering the desalination plant separation efficiency and adding the energy consumption for pumping. The problem of this study is that it is limited to cogeneration schemes (joint electricity and water production) and would not be useful in the case of desalination with low-temperature sources. Shahzad et al. [83] developed an approach based on the second law of thermodynamics, which is also useful only for cogeneration schemes. They proposed a common metric called the Standard Universal Performance Ratio to compare desalination processes using different kinds of energy, which is based on conversion of different types and grades of energies to standard primary energy. In this case, conversion factors were proposed to convert the derived energy input to the standard primary energy. Other authors have performed exergy analyses for stand-alone desalination processes, as is the case of Lienhard et al. [80] and Brogioli et al. [84], who considered desalination processes as a black box and the ideal work or the thermodynamic limit for the separation of dissolved salts in seawater as the Carnot work.

The problem with the exergy analyses is that they are more complex [85] due to the need to consider several aspects not present in simple energetic metrics: definition of dead state and control volume [86], chemical exergy modeling of seawater [87, 88] and minimum energy reference (least and minimum work of separation) [89, 90]. Probably because of their complexity, they have not been widespread in the performance evaluation of practical setups. Also, none of the works published so far in the scientific literature addresses specifically the exergetic evaluation when using non-conventional energy sources such as waste heat.

Two important requirements for an accurate and reliable performance assessment, yet to be dealt with in thermal desalination, are the steady state identification and the uncertainty of both the direct measurement and that associated with the performance metric determination. With respect to the former, it is highly recommended to use automatic procedures that increase the reliability of the measurements. The steady state evaluation carried out manually so far by qualified operators [91–93], leads to high time consumption and full dependence on the operators' attention, leading to potential unreliable identifications. With respect to the latter, it allows for a more comprehensive and nuanced approach to performance evaluation, since it increases the robustness of the evaluation while providing information on the reliability of the results. Therefore, there is a gap in the establishment of standard methodologies that include all the necessary requirements for the reliable assessment of the performance of thermal desalination processes. This chapter aims to address this gap by proposing a method with potential for a broader application in other thermal desalination processes. The method is applied and validated in an experimental MED plant as part of a high TBT experimental campaign.

This chapter is structured as follows: first in the Section 14.1 (Process analysis) a process analysis focused on performance evaluation is done to clearly define the scope of the evaluation and the inputs and outputs of the process. Then in Section 14.2 (Performance metrics), the performance metrics are defined, including separation, energetic, and exergetic. Section 14.3 (Instrumentation)

is related to the instrumentation of the system: KPVs, instrumentation requirements and uncertainty determination for both direct measurement and derived metrics. Section 14.4 (Monitoring and process control) presents the proposed steady state identification algorithm for stable operation monitoring and the controllers to be implemented. Finally, in Section 14.5 (Methodology application in an experimental campaign) the proposed methodology is applied to a case study: a pilot MED plant evaluated in a TBT experimental campaign. The results from the campaign are also analyzed in this section.

14.1 Process analysis

Metrics are defined based on some criteria, and this criteria is of paramount importance because resources and efforts are invested in optimizing the process in its direction. In order to adequately define these criteria, it is important to have an overall perspective of the process: defining its inputs and useful outputs, from a qualitative point of view, as well as a clear delineation of the scope of the evaluation.

Metrics can be related either to the operation – isolated MED operation or considering primary energy [81] – or to the design of the system². This chapter focuses on the operation of an isolated MED system.³

Application. Two applications are distinguished:

- ▶ **Seawater desalination.** The objective is to obtain fresh water. The level of separation achieved is a secondary (not useful) output.
- ▶ **Brine concentration.** The objective is to extract resources from the brine in order to valorize it. Here, the level of separation is a crucial factor to consider.

External heat source type. Two types of external heat sources are distinguished:⁴

- ▶ **Process heat.** Process heat is the heat utilized by a system and its associated costs are related to the amount of energy consumed.
- ▶ **Waste heat.** Waste heat is the heat utilized by a system that would otherwise be lost to the environment. It has no associated costs to the amount of heat used, though there are other costs associated with its use [94, 95]⁵. Here the paradigm is different as described by Christ et al [79, 96, 97], the goal is to maximize the amount of product by maximizing the utilization of the waste source.

Process vs waste heat take on efficiency

In a process heat driven system, between two plants that produce the same amount of useful product, the most efficient one is the one that uses the least external heat to do so, whereas in a waste heat driven system, the two plants would be considered as efficient since the unused heat would be wasted to the environment. A more intuitive definition would be:

Given two plants that consume the same waste heat, the most efficient one is the one that produces more product with the available heat.

Based on the above considerations, Figure 14.1 shows the control volume of the MED process with the inputs and outputs used for the definition of the performance metrics. From left to right, seawater (including cooling water, c , and feed, f) enters the control volume at the seawater intake conditions ($T_{c,in}$). The cooling water is rejected at $T_{c,out}$. On the right side, the distillate and the brine are discharged from the MED system at temperatures $T_{d,out}$ and $T_{b,out}$ and mass fractions w_d and w_b , respectively. The temperatures of all these outlet streams,

2: e.g. specific area [78]

[81]: Bouma et al. (2020), "Metrics Matter"

3: It is as if an already built system is provided, so decision over its design parameters and energy source conditions is not an available degree of freedom, only optimization in its operational variables.

4: The use of electrical work will always be desired to be minimized, so the distinction is not needed.

[94]: Mistry et al. (2013), "An Economics-Based Second Law Efficiency"

[95]: Christ et al. (2017), "Techno-Economic Analysis of Geothermal Desalination Using Hot Sedimentary Aquifers"

5: e.g. a less efficient system will require a larger heat exchanger area to extract more energy from the waste source, directly increasing the cost of the system

[79]: Christ et al. (2014), "Thermodynamic Optimisation of Multi Effect Distillation Driven by Sensible Heat Sources"

[96]: Christ et al. (2015), "Application of the Boosted MED Process for Low-Grade Heat Sources — A Pilot Plant"

[97]: Christ et al. (2015), "Boosted Multi-Effect Distillation for Sensible Low-Grade Heat Sources"

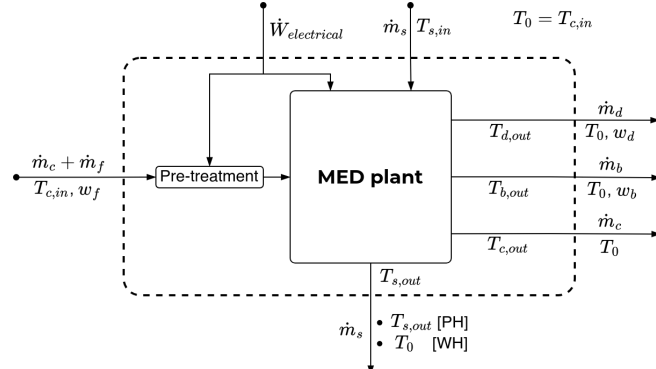


Figure 14.1: Inputs and outputs variables in an MED process. The dash line delimits the control volume

6: It is heat that is lost to the environment, no additional work can be feasibly extracted from these streams

from a qualitative (*i.e.* exergetic) point of view, are useless and thus considered to be at T_0 when leaving the control volume⁶.

From top to bottom, the energy sources for the system are depicted. Electrical work is depicted as $\dot{W}_{electrical}$ and it may include pumping, vacuum system, and feed water pretreatment, among others. The heat source is represented by the subscript (s) and as shown in the figure, it enters the MED plant at $T_{s,in}$ and leaves it at $T_{s,out}$ after releasing part of its energy. When leaving the control volume, $T_{s,out}$ value depends on the type of heat source:

- ▶ Process heat (PH). The value of $T_{s,out}$ does not change. In case steam is used, the primary energy driver is the latent heat of phase change and $T_{s,out}$ is usually similar to or equal to $T_{s,in}$. In case a sensible heat source is used, the driving force is the temperature difference and $T_{s,out}$ is between $T_{s,in}$ and T_0 .
- ▶ Waste heat source (WH). In this case, $T_{s,out}$ is considered to be at the sink conditions, T_0 , since this heat is not reused but lost to the environment.

14.2 Performance metrics

A performance metric is a quantitative measure used to evaluate the effectiveness or efficiency of a system. It provides objective information that can be used to monitor progress, identify areas for improvement, and inform decision making. A metrics division in three categories is proposed: separation, energetic, and exergetic metrics. A detailed description of each of them within each category is presented below.

14.2.1 Separation metrics

[98]: Jones et al. (2019), "The State of Desalination and Brine Production"

[99]: Palenzuela et al. (2015), *Concentrating Solar Power and Desalination Plants*

The Recovery Ratio (RR) represents the flow ratio of unit of distillate produced per unit of feed and is very useful in seawater brine concentration applications [98]. It is related to electricity consumption, since the lower the RR the higher the feed pumping needs are for the same distillate production [99]. It is determined as follows:

$$RR = \frac{\dot{m}_d}{\dot{m}_f} \times 100 [\%], \quad (14.1)$$

where \dot{m}_d is the mass flow rate of distillate and \dot{m}_f is the feedwater mass flow rate, both in kg/s.

An equivalent metric is the concentration factor, which accounts for how many times the brine is concentrated with respect to the feed concentration:

$$CF = \frac{w_b}{w_f} = \frac{\dot{m}_f}{\dot{m}_f - \dot{m}_d} [-], \quad (14.2)$$

where w_b is the brine concentration and w_f is the feedwater concentration, both in g/kg.

Apart from the already known previous metrics, a new one is proposed in this work that can be useful for seawater brine concentration applications. This metric is called Reconcentration Index (RI), and it allows to determine how close the separation achieved (RR) is to the theoretical maximum recovery ratio (RR_{max}). It is defined as:

$$RI = RR/RR_{max} [-], \quad (14.3)$$

where RR_{max} is calculated as follows [90]:

$$RR_{max} = w_{w,f} \left(1 - \frac{b_{NaCl,f}}{b_{NaCl,sat}} \right) \times 100 [\%], \quad (14.4)$$

[90]: Thiel et al. (2015), "Energy Consumption in Desalinating Produced Water from Shale Oil and Gas Extraction"

where $w_{w,f}$ is the water mass fraction in the feed (which is $1 - w_{sol,f}$, where $w_{sol,f}$ is the mass fraction of the solutes in the feed) and $b_{NaCl,f}$ is the molality of sodium chloride in the feed, in mol_{NaCl}/kg_w (both can be obtained from a feedwater chemical analysis). On the other hand, $b_{NaCl,sat}$ is the molality of sodium chloride at saturation conditions (see Section ?? for more details of its estimation)⁷.

⁷: sodium chloride is the only solute considered, as it sets the concentration limit being the solute in seawater with the highest concentration and the greatest solubility [90]

14.2.2 Energetic metrics

The energetic metrics are metrics that consider only the first law of thermodynamics (*i.e.* quantity). They are: GOR, STEC, and SEEC and are described in the following.

Regarding the GOR, a universal definition of this metric that avoids the limitations of some of the commonly used definitions mentioned⁸ is the ratio between the energy in the form of latent heat required to vaporize all the distillate produced and the external thermal energy contributed to the system (Eq. 14.5) [100].

$$GOR = \frac{\dot{m}_d \cdot \Delta h_{avg}}{\dot{Q}_{in}} \quad (14.5)$$

⁸: Limited to steam or 1000 BTU as arbitrary conversion factor

[100]: Lienhard V et al. (2012), "SOLAR DESALINATION"

where Δh_{avg} is the latent heat of vaporization at the average vapor temperature between the first effect and the last effect, in kJ/kg, and \dot{Q}_{in} is the external thermal energy consumption required to drive the process, in kW. It is determined by \dot{m}_s (mass flow rate of the external energy source supplied in the first effect, in kg/s) and Δh_s , which can be calculated as $h_{s,in} - h_{s,out}$ (in case of sensible heat) or as $h_{s,sat,vap} - h_{s,sat,liq}$ (in case of latent heat of phase change at saturation conditions from vapor to liquid at temperature $T_{s,in}$).

In case waste heat is used as external thermal energy source for the MED system, \dot{Q}_{in} is determined with \dot{m}_s and Δh but referred to the lowest temperature of the system ($T_{c,in}$).

Another performance index widely used in thermal desalination is the STEC. For desalination applications, it is defined as the input heat to the system per unit

of product (distillate). This index has units of energy per fraction of volume and its expression is shown in Eq. 14.6.

$$STEC = \frac{\dot{m}_s \cdot (h_{s,in} - h_{s,out})}{\dot{m}_d} \cdot \rho_d \cdot \frac{1 \text{ kWh}}{3600 \text{ kJ}} \left[\frac{\text{kWh}_{\text{th}}}{\text{m}^3} \right]. \quad (14.6)$$

For brine concentration applications, it is named as $STEC_{bc}$ and it is determined as the energy required (in kJ) per unit of feed (in kg) (i.e. \dot{m}_f in the denominator) [101].

Both STEC and GOR are equivalent and are related via Eq. 14.7.

$$STEC = \frac{2326 \text{ kJ/kg}}{GOR} \cdot \rho_d \cdot \frac{1 \text{ kWh}}{3600 \text{ kJ}}, \quad (14.7)$$

where ρ_d is the density of the distillate in kg/m^3 .

For the cases in which waste heat source is used as energy source, a variation of the STEC is proposed: the waste heat STEC. For desalination applications, it is determined as follows:

$$STEC_{wh} = \frac{\dot{m}_s \cdot (h_{s,in} - h_{c,in})}{\dot{m}_d} \cdot \rho_d \cdot \frac{1 \text{ kWh}}{3600 \text{ kJ}} \left[\frac{\text{kWh}_{\text{th}}}{\text{m}^3} \right]. \quad (14.8)$$

As before, for brine concentration applications, \dot{m}_d would be replaced by \dot{m}_f in the denominator.

Another important index in desalination is the SEEC, which represents the total electrical consumption of the plant and its auxiliary systems per unit of distillate water produced. These are the subsystems that should be considered:

- ▶ J_s . External energy source
- ▶ J_f . Feed pumping
- ▶ J_c . Cooling
- ▶ J_d, J_b . Discharge extractions
- ▶ J_{vacuum} . Vacuum system
- ▶ J_{aux} . Auxiliary consumptions. Represents any additional power that the system may require to function (e.g., electrical consumption for the feedwater pretreatment such as nanofiltration)

For desalination applications, the following equation is used for the calculation of this metric:

$$SEEC = \frac{\sum_{i=1}^N (J_i)}{\dot{m}_d} \left[\frac{\text{kWh}_e}{\text{m}^3} \right], \quad (14.9)$$

where J_i is the electrical consumption of the i_{th} subsystem. In the case of brine concentration applications, the index is called $SEEC_{bc}$ and the denominator would be replaced by \dot{m}_f .

14.2.3 Exergetic metrics

Exergy is the maximum amount of work achievable when a system is brought into equilibrium from its initial state to a reference state (known as the dead state and represented by the subscript "0") [86, 102]. This reference state is usually established for desalination applications as the seawater intake temperature

$(T_{c,in})$. In contrast to the energetic metrics, it considers not only the first law of thermodynamics (quantity), but also the second law (quality).

The most widespread exergetic metric is the second law efficiency (η_{II}) [80], which accounts for irreversible losses within a system. It is calculated as the ratio of the useful exergy output of a system ($\dot{E}x_{out,useful}$) to the exergy input given to the system ($\dot{E}x_{in}$) (a further explanation of how to determine the different exergy flows can be found in Section ?? (??)):

$$\eta_{II} = \frac{\dot{E}x_{out,useful}}{\dot{E}x_{in}} \times 100 [\%]. \quad (14.10)$$

Considering exergy losses, which are the sum of exergy destroyed in each individual component ($\dot{E}x_{destroyed}$) and exergy losses due to discharge streams in disequilibrium to the environment ($\dot{E}x_{streams}$), the previous equation can be written as follows:

$$\eta_{II} = 1 - \frac{\dot{E}x_{destroyed} + \dot{E}x_{streams}}{\dot{E}x_{in}} \times 100 [\%]. \quad (14.11)$$

For brine concentration applications and in case waste heat is used, the metric is called $\eta_{II,wh}$ and $\eta_{II,bc}$, respectively, to distinguish between the type of application and external energy source.

Another useful metric is the Specific Exergy Consumption (SEXC), which was firstly referenced as specific consumed available energy in [82]. Similarly to SEEC and STEC, it accounts for the exergy input to the system per unit of distillate produced (Eq. 14.12) and it is determined as follows [81]:

$$SEXC = \frac{\dot{E}x_{in}}{\dot{m}_d} \left[\frac{\text{kWh}_{\text{ex}}}{\text{m}^3} \right]. \quad (14.12)$$

It is important to note that the terms $\dot{E}x_{out,useful}$ and $\dot{E}x_{in}$ from the previous exergetic metrics are determined depending on what is considered as useful exergy leaving the process and what is deemed as exergy input to the system.⁹

Useful exergy output . The useful exergy output of the system ($\dot{E}x_{out,useful}$) depends on what is considered the valuable product generated by the process. In a separator in which the objective is to separate water and brine, the useful exergy is the chemical exergy of separation. As discussed in [80], for seawater desalination applications, where the valuable product is fresh / pure water, the chemical exergy of separation corresponds to that of a reference ideal separator that achieves the *minimum separation work* ($\dot{W}_{least}^{min} = \dot{W}_{least}|_{RR \rightarrow 0}$). The objective is to minimize the required energy consumption to produce fresh / pure water, regardless of how much separation takes place ($RR \rightarrow 0$), so $\dot{E}x_{out,useful} = \dot{W}_{least}^{min}$.

On the other hand, in brine concentration applications, since the objective is to maximize the separation achieved, the separator takes into account the amount of separation achieved ($\dot{W}_{least}|_{RR}$), and $\dot{E}x_{out,useful} = \dot{W}_{least}|_{RR}$ [90]. The definition and determination of the least and minimum least work of separation can be found in Section ??.

Exergy input . The exergy input ($\dot{E}x_{in}$) is determined according to the type of external heat source. In case process heat is used, the exergy input is determined as:

$$\dot{E}x_{in} = \dot{E}x_{s,in} - \dot{E}x_{s,out} + \sum_i \dot{E}_i, \quad (14.13)$$

[80]: Lienhard et al. (2017), "Thermodynamics, Exergy, and Energy Efficiency in Desalination Systems"

[82]: Darwish et al. (2006), "Multi-Effect Boiling Systems from an Energy Viewpoint"

[81]: Bouma et al. (2020), "Metrics Matter"

9: It mirrors the qualitative analysis presented in Section 14.1

[80]: Lienhard et al. (2017), "Thermodynamics, Exergy, and Energy Efficiency in Desalination Systems"

[90]: Thiel et al. (2015), "Energy Consumption in Desalinating Produced Water from Shale Oil and Gas Extraction"

where $\dot{E}x_{s,in}$ and $\dot{E}x_{s,out}$ are the exergy flows associated with the thermal energy source at the inlet and outlet, respectively.

When using waste heat sources, the exergy input is determined as:

$$\dot{E}x_{in} = \dot{E}x_{s,in} - \dot{E}x_{s,out}^{wh} + \sum_i \dot{E}_i, \quad (14.14)$$

where $\dot{E}x_{s,out}^{wh}$ is the outlet heat source exergy flow, which is evaluated at temperature T_0 (dead state).

14.3 Instrumentation

14.3.1 KPV

The KPVs are those variables that uniquely define an operating point, which is obtained by averaging all monitored variables when stable operation is achieved. In other words, any change in the key variables is associated with a different operating point, since the plant outputs are affected accordingly. The following selected variables apply to any MED plant with any configuration in terms of seawater flow direction, tube arrangement in tube bundles, or effect layout [99]. They are represented in Figure 14.2 and described hereinafter:

- ▶ Heat source flow rate (\dot{m}_s - FT01), inlet temperature and pressure ($T_{s,in}$ and $P_{s,in}$ - TT01 and PT03) for sensible heat sources, and just FT01 and TT01 if saturated steam is used (otherwise steam quality needs to be estimated). They determine the hot side conditions, which usually take place in the first effect that is at the highest temperature and pressure. If multiple effects receive external heat sources, each one has to be monitored.
- ▶ Feed water flow rate (\dot{m}_f - FT02), which affect the overall plant operation conditions. A precise and stable input feed flow rate ensures consistent heat transfer rates, residence times, and separation efficiencies.
- ▶ Distillate flow rate (\dot{m}_d - FT03). It is a basic variable that gives information about the production of the system. As long as this output variable is stable, it can be assumed that the sum of it plus the brine flow rate is equal to the feed flow rate.
- ▶ Condenser pressure / temperature ($P_{v,c}$ - PT02 / $T_{v,c}$) or condenser outlet temperature ($T_{c,out}$ - TT02). The stability of any of these variables, together with that of the distillate production, establish a stable heat sink.
- ▶ Effect pressure / temperature ($P_{v,1}$ - PT01 / $T_{v,1}$) or heat source outlet temperature ($T_{s,out}$ - TT05), which is always required in case that sensible heat source is considered as the external energy source. The stability of this output variable determines a stable hot side. In case other effects, apart from the first one, receive external heat sources, each one has to be monitored.
- ▶ Feed water salinity (w_f - CT01). It affects the overall plant operation conditions since any stream with different salinity would have different thermodynamic properties (i.e. boiling point elevation) and therefore, different energy requirements to perform the separation.
- ▶ Condensate salinity (w_d - CT02). This variable together with the distillate flow rate gives information on the levels of salt separation from water achieved.
- ▶ Ambient temperature (T_{amb} - TT06). The ambient conditions determine the losses to the environment which can change the results for the, otherwise, same operating conditions.
- ▶ Seawater temperature or condenser inlet temperature ($T_{c,in}$ - TT04). It is another environment variable that sets the minimum achievable temperature in the system.

[99]: Palenzuela et al. (2015), *Concentrating Solar Power and Desalination Plants*

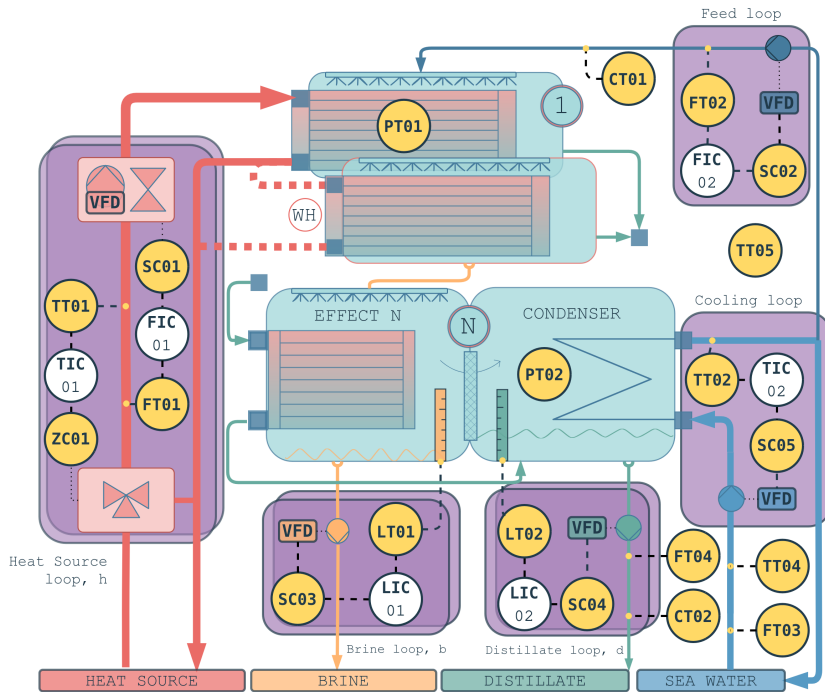


Figure 14.2: P&ID with the required instrumentation, KPVs, and basic control loops (ANSI/ISA 5.1-2022) required in an MED plant

- Last effect (L_b - LT01) and condenser (L_d - LT02) levels. In the case of the final condenser, it is a vessel in which the vapor coming from the final effect condenses, producing distillate that is continuously extracted from the system. The stability in this vessel is achieved when the extraction rate is equal to the condensate production rate. A higher extraction rate would eventually lead to unstable production, while a lower extraction rate would cause an increase in the vapor pressure, which would lead to induced lower production caused by misoperation. A stable level throughout the operation can ensure that the extraction and production rates (\dot{m}_d) are in balance. In the case of the last effect, it is important to keep the level as low as possible in order to avoid brine contamination in the final condenser.

14.3.2 Instrumentation requirements

The installed instrumentation must measure magnitudes such as flow rate (mass or volumetric), temperature, pressure, water conductivity, level, and power. First, it is important to account for the influence of the quality of each measured variable on the reliability of the performance metrics, which is determined by a sensitivity analysis.

Reminder: How to interpret Sensitivity Analysis (SA) results

The results are different sensitivity indices such as total sensitivity indices (total-order), first-order sensitivity indices (first-order), and interaction sensitivity indices (second-order). First-order measures the direct effect of an input variable on the output, excluding interaction effects with other variables, while the second-order measures specifically these interaction effects. Finally, total-order indices account for the total effect of an input variable, including both direct and interaction effects.^a

^a More in Chapter ?? (??)

All KPVs must be monitored regardless of their influence on the performance metric being evaluated because, as mentioned above, the average values of these variables at steady state conditions define an operating point.

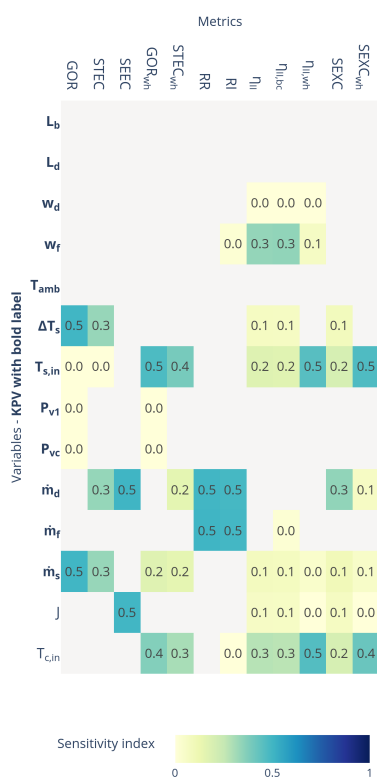


Figure 14.3: Sensitivity index results for different variables. Useful to assess the impact of the different measured variables uncertainty on the performance metric. KPVs are shown in bold notation

[104]: Smith (2013), *Uncertainty Quantification*

Figure 14.3 shows the results obtained from the sensitivity analysis in terms of total-order Sensitivity Index (SI). The closer the SI is to 1, the greater the influence of the variable (shown on the left axis) on the reliability of the performance metric (shown on the top). In other words, the quality of the variable measurement should be higher for variables with a higher SI. The cases where no sensitivity index is obtained indicate that the variable has no effect on the metric.

In general, monitoring of these variables must be performed online for each operating point evaluated. However, some of the variables rarely change and can be measured periodically or offline. This is the case of environment variables such as w_f , w_d , T_{amb} .

Another aspect that deserves careful consideration is the measurement of the temperature of the heat source. To determine the thermal efficiency of the system when a sensible heat source is utilized, it is crucial to accurately measure the temperature difference between the inlet and outlet of this energy source (ΔT_s). Using temperature transmitters with high accuracy rates (i.e. PT100), uncertainties of about 0.5 °C or below 1 % for the absolute temperature can be expected at temperatures exceeding 60 °C. However, when considering the small temperature differences between the inlet and outlet, which can be as low as 2 °C, the resulting relative uncertainty could be up to 25 %. To address this problem, it is recommended that both temperature transmitters are identical and calibrated simultaneously, using the same calibration pattern, which translates into observed values for the uncertainty of the temperature difference in the range of 0.1 °C or 5 %.

On the other hand, the total electrical energy consumption (represented as JT01 in Figure 14.2 can be monitored as global system consumption, or independently per subsystem (J_s , J_c , J_f , J_d , J_b , J_{vacuum} , J_{aux}).

14.3.3 Uncertainty determination

Uncertainty determination is particularly valuable in assessing the reliability and validity of predictions, forecasts, or results evaluation. The framework on which the uncertainty assessment of this paper is based is JCGM 100:2008 [103].

In an uncertainty analysis, the uncertainties of direct measurements must first be determined. The uncertainty of each direct measure (ΔX_i) consists of the sum of two components, as indicated below:

$$\Delta X_i = \Delta X_{sensor} + \Delta X_{control}$$

where:

- ▶ ΔX_{sensor} is the contribution of the sensor, which depends on its accuracy, calibration and conversion errors, and should be available from the instrument datasheet.
- ▶ $\Delta X_{control}$ is the uncertainty attributed to the quality of the control and is estimated using the standard deviation of the measurement throughout the period considered as stable.

On the other hand, when working with derived variables, i.e. quantities that are calculated based on other measured or known quantities, the uncertainty is determined through uncertainty propagation. There are several analytical and numerical methods to propagate uncertainty [104]. One simple approach is the use of first-order Taylor series approximation, obtained calculating the partial derivative of the different direct measurements ($X_i = 1..N$) that take part in the calculation of an output (y):

$$Y = f(X_1, \dots, X_N),$$

$$\Delta Y = \left(\sum_{i=1}^N \left(\left| \frac{\delta Y}{\delta X_i} \right| \Delta X_i \right) \right)^{1/2},$$

where ΔY_i can be expressed in terms of absolute uncertainty, relative, or standard uncertainty [105]. This alternative provides a simple mathematical expression to directly estimate uncertainty. Expressions for the uncertainty estimation of energetic and separation metrics of MED processes with this approach are available in Section ???. However, first-order Taylor series approximation has certain limitations, being the main one that it is not adequate for highly non-linear models, where a higher order Taylor expansion is required, or when uncertainties are far from the mean. Also, when working with complex models, as in the case of exergetic metrics, its expression can not be practically obtainable. For these cases, the recommended approach are numerical methods, specifically the Monte Carlo method [106], which despite its higher computational requirements does not have the aforementioned limitations [107].

[105]: nist (), "NIST Guidelines for Evaluating and Expressing the Uncertainty of NIST Measurement Results Cover"

[106]: (2008), JCGM101:2008. Evaluation of Measurement Data — Supplement 1 to the "Guide to the Expression of Uncertainty in Measurement" — Propagation of Distributions Using a Monte Carlo Method

[107]: Wolff (2007), "Monte Carlo Errors with Less Errors"

14.4 Monitoring and process control

14.4.1 Monitoring: steady-state identification

The evaluation of the system performance must be carried out when the plant is at steady state conditions, that is, when the mass and energy balances are in equilibrium and thus do not change with time; otherwise, erroneous results can be obtained. Steady-state conditions can be identified by observation by qualified and experienced plant operators. However, the use of automatic detection algorithms is recommended for experimental facilities where a wide range of operating conditions are involved. In this work, an automatic detection algorithm has been purposely developed and implemented to identify the steady state of the process. The methodology is based on the idea presented by M. Korbel [108] et al. and consists of combining an algorithm to detect anomalies, such as the wavelet transform [109, 110] (which allows detecting abrupt signal changes and distinguishing between high-frequency noise, transient states and steady states), with a trend detection method to identify smooth ramps as non-steady states. Whereas M. Korbel [108] et al propose a statistical trend detection approach, in this paper the derivative of the signal is used due to its simplicity (only one parameter, the threshold, must be established). A diagram of the steady-state detection procedure is shown in Figure 14.4, where three parameters are mainly required: wavelet transform threshold (y_a), derivative threshold (y_d) and time window duration (T_{ss}). At each k -sample time, a new value is read, and the *Anomaly detection* algorithm is applied (in this case the wavelet transform). If the output is positive (true, no anomaly), the second step is to analyse the *Trend detection*. Only if all elements in the result vector are positive along T_{ss} , is the value considered to be at steady state (ss) conditions. As a final step, the *Global steady state evaluation* identifies a steady-state period if all the values of the N variables involved have been previously classified as ss.

[108]: Korbel et al. (2014), "Steady State Identification for On-Line Data Reconciliation Based on Wavelet Transform and Filtering"

[109]: Jiang et al. (2003), "Application of Steady-State Detection Method Based on Wavelet Transform"

[110]: Jiang et al. (2000), "Industrial Application of Wavelet Transform to the On-Line Prediction of Side Draw Qualities of Crude Unit"

[108]: Korbel et al. (2014), "Steady State Identification for On-Line Data Reconciliation Based on Wavelet Transform and Filtering"

14.4.2 Control system

Figure 14.2 shows the control loops to be implemented in an MED unit, whose subsystems and their control are described below:

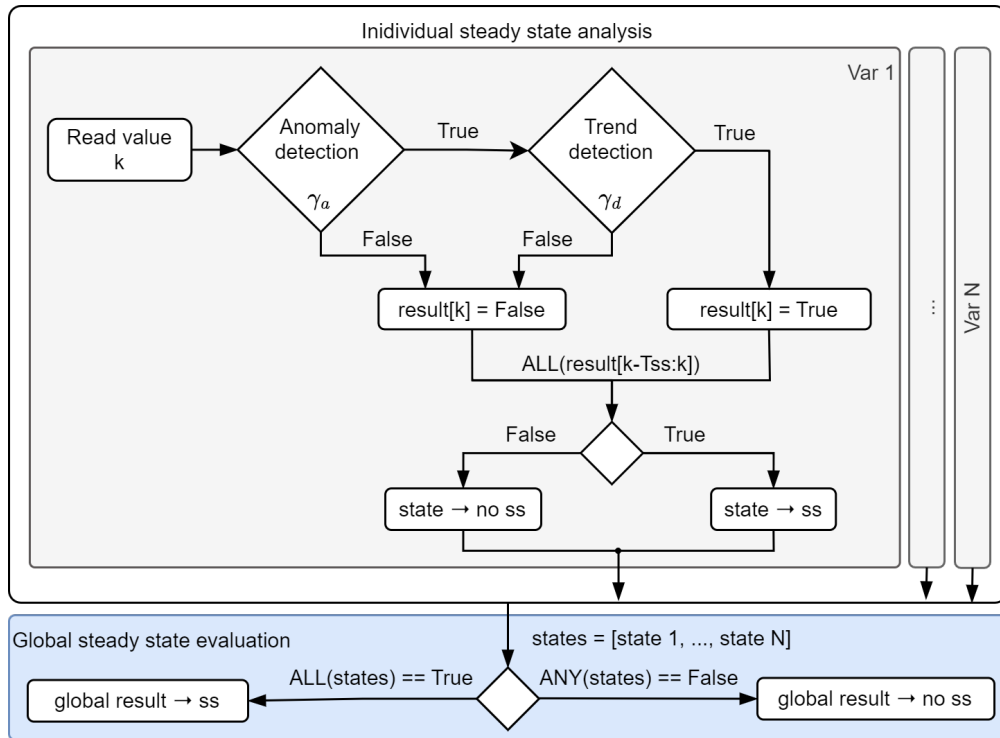


Figure 14.4: Diagram of the steady-state identification procedure

► **Heat source** (*Heat Source loop* in Figure 14.2). Both the inlet temperature (TT01) / pressure (PT03) and the flow rate of the heat source (FT01) must be controlled. It can be done either by direct control over the heat source obtaining heat under the required operating conditions or by performing a transformation. Depending on the heat source characteristics, this transformation involves:

For sensible heat sources, independent variation of temperature and flow rate can be achieved by means of: 1) a mixing three-way valve that mixes part of the return fluid, at temperature TT05, with the inlet fluid, at TT01 by acting over ZC01, the control signal for temperature regulation and; 2) flow (FT01) regulation by acting over the control signal SC01, which can be a Variable Frequency Drive (VFD) or valve. This decoupled regulation is shown in Figure 14.2, where ZC01 represents the control signal for temperature regulation. The flow rate regulation (FT01) is achieved by acting on the selected actuator (SC01), which can be a VFD or a valve¹⁰. For latent heat sources (steam), the pressure-flow-independent regulation is not possible since they are intrinsically coupled variables. In this case, a pressure regulator valve (ZC01) can be used to control either the flow rate (FT01) or the pressure (PT03).

► **Cooling** (*Cooling Loop* in Figure 14.2). The pressure inside the condenser (PT02) or the condenser outlet temperature (TT02) can be controlled by regulating the cooling flow rate (FT03), being the cooling water inlet temperature (TT04) a disturbance. This control loop (TIC02) consists in turn in two control loops (cascade control [111]), where an outer loop sets a reference flow rate value to achieve the desired condenser outlet temperature (or pressure), and an inner loop (not shown in Figure 14.2) acts on SC05 (VFD's frequency) to achieve the desired flow rate. Direct regulation of condenser outlet temperature using the VFD is also valid in case the measurement of the cooling flow rate is not available.

► **Brine extraction** (*Brine loop* in Figure 14.2). The brine level in the last

10: It should be noted that this decoupling is at the expense of energy losses in the mixing process

[111]: Åström et al. (1995), *PID Controllers: Theory, Design, and Tuning*

14.5 Methodology application in a high TBT experimental campaign at the pilot plant

effect (**LT01**), or in all effects if a parallel feed configuration is used, is controlled by the brine flow rate (see control loop **LIC01** in Figure 14.2). In this case, the controller can act directly on the VFD frequency (**SC03**) to avoid the need for an additional flow meter.

- ▶ **Distillate extraction** (*Distillate loop* in Figure 14.2). As in the previous case, the distillate level (**LT02**) is controlled by acting on the control variable (**SC04**).
- ▶ **Feedwater** (*Feed loop* in Figure 14.2). The feed water flow rate is regulated by the **FIC02** control loop, using a VFD (**SC02**) and a flow meter (**FT02**).

A standard method for performance evaluation of thermal separation processes

1. Define the KPVs (Section 14.3.1)
2. Select the required performance metrics to be evaluated according to the application and type of energy source(s) (Section 14.1).
3. Define the required instrumentation of the KPVs and of any additional variables needed for the target performance metrics (Section 14.3.2).
4. Define the uncertainty associated with the measurement and that associated with the performance metric determination (Section 14.3.3)
5. Implement the required actuators and integrate them into a control system to ensure the stability of the plant operation (Section 14.4.2).
6. Identify a time window where stable operation is achieved (Section 14.4.1).

14.5 Case study: methodology application in a high TBT experimental campaign at the pilot plant

Reminder: Performance of a thermal separator

The performance of a thermal process, such as MED, is dictated by the Carnot cycle [84], which sets the theoretical maximum efficiency for any heat engine. The efficiency of the Carnot cycle is limited by the temperature difference between the hot and cold sinks, which determine the amount of thermal energy that can be converted into useful (separation) work.

An approach to bring the MED closer to its thermodynamic limit can be achieved by raising the TBT, which allows to increase the number of effects [112] while maintaining an optimal temperature drop across them¹¹. This leads to an improvement in the thermal performance of traditional desalination or an increase of the concentration factors that can be achieved, potentially enabling applications such us brine mining, introduced in Chapter 12 (Thermal desalination).

In practice, the TBT in the MED system is limited to 70°C. As shown in Figure 14.6, higher TBTs increase the risk of precipitation of divalent ions, which tend to form incrustations on the heat exchange surfaces. These deposits reduce heat transfer efficiency, as noted in [78]. For un-treated feedwater (Figure 14.6 - left) this risk of precipitation is present at almost any temperature due to its composition¹². A nanofiltration pre-treatment¹³ is used to selectively remove the divalent ions while leaving relatively unaffected the components to be separated in the MED process, *i.e.* NaCl. This allows the operation of MED processes at higher TBTs or higher feed concentration, with only severe scaling above 80°C and ≈ 100 g/kg as shown in Figure 14.6 - right.

To showcase the application and usefulness of the proposed methodology, a case study consisting on the application of the methodology to an experimental campaign at the SolarMED pilot plant is presented. The campaign was designed

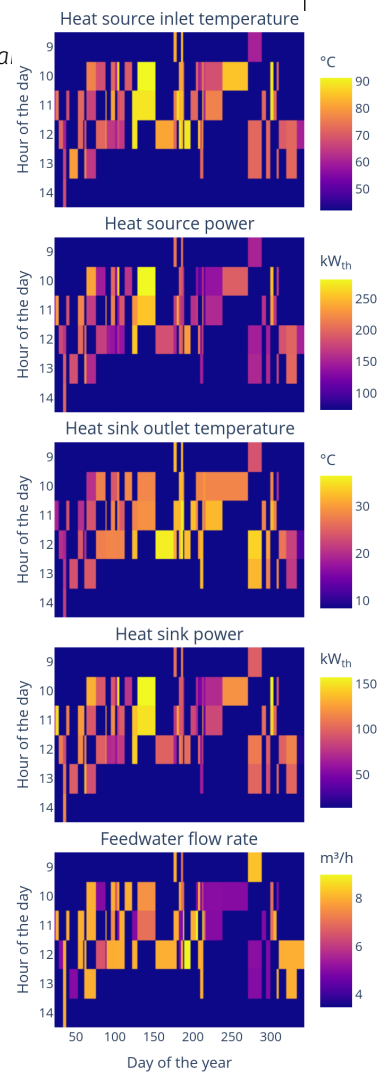


Figure 14.5: Visualization of the different process inputs values during the experimental campaign.



11: With limitations, on each effect a considerable exergy is destroyed. It has been shown that around XX effects is the limit ...

Table 14.1: RSI values and their interpretation in terms of scaling and corrosion risk [113].

RSI > 9	Severe corrosion
7.5 < RSI < 9	Heavy corrosion
7 < RSI < 7.5	Significant corrosion
6 < RSI < 7	Stable water
5 < RSI < 6	Moderate to light scaling
4 < RSI < 5	Severe scaling

12: Figure 14.6 - seawater in center bar plot

13: Figure 14.6 - pretreated water in center bar plot

to evaluate the performance of the MED process under different operating conditions (see Table 14.2 and Figure 14.5), with the aim of improving its thermal performance and assessing the feasibility of using higher TBTs.

14.5.1 Implementation results

Table 14.2: Experimental campaign design specifications

Variable	Unit	Range
$T_{s,in}$	°C	60-89
q_s	l/s	7-14
$T_{c,out}$	°C	20-40
q_f	m ³ /h	5-9
w_f	g/kg	40

The experimental facility at PSA is a complex system of considerable size for a pilot plant. It includes over 100 variables, between inputs and monitored outputs. Additionally, due to the large number of target operating points, each experimental campaign requires a significant number of test days. Achieving a valid steady state takes approximately 20–30 minutes, not including the transition time between operating points. On a good day, 3–4 stable operating points can be reached; on a bad day, due to for example unfavorable environmental conditions, none may be achieved. This makes the duration of experimental campaigns complex and extensive as illustrated in Figure 13.3, making it highly suitable for extensive subsystem automation. The following sections describe the implementation of the methodology, which is showcased in Figure 14.9 for one particular test and further discussed in the following.

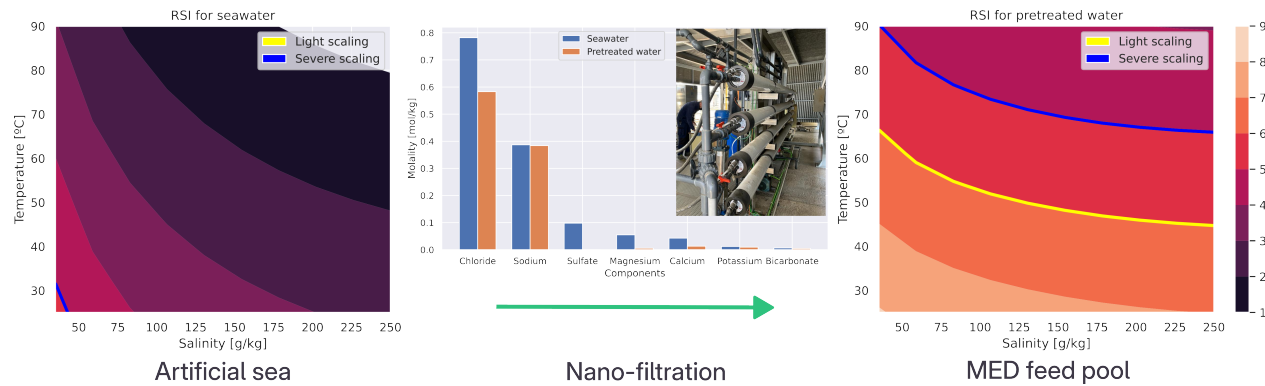


Figure 14.6: RSI values as a function of temperature and concentration before (left) and after (right) pre-treatment using nanofiltration.

Monitoring and control system

Finite state machines. Each day of operation requires starting up and shutting down the system, making it a repetitive and sufficiently complex process that requires an experienced operator. Manual management of the process leads to errors that cause setbacks or, in the worst cases, premature failures in the facility: contamination of the condenser with brine due to erratic draining of the last effect, accumulation of scale on the surfaces of heat exchangers due to rapid cooling after shutdown, pumps cavitating because they are not stopped when the water flow at the intake ceases, etc. For this reason, two finite state machines have been implemented to manage the startup and shutdown of the facility. These have been designed to perform a sequence of operations that take the plant from an initial state to a final state following proper operating practices. A diagram of the process is shown in Figure 14.7.

The machines are responsible for managing the activation and deactivation of devices as well as controllers. Additionally, they set reference values for these based on a previously established configuration and evaluate whether the reference has been reached before proceeding to the next step. They also adjust certain parameters of the control system (level control) and restore the initial values once the task is completed.

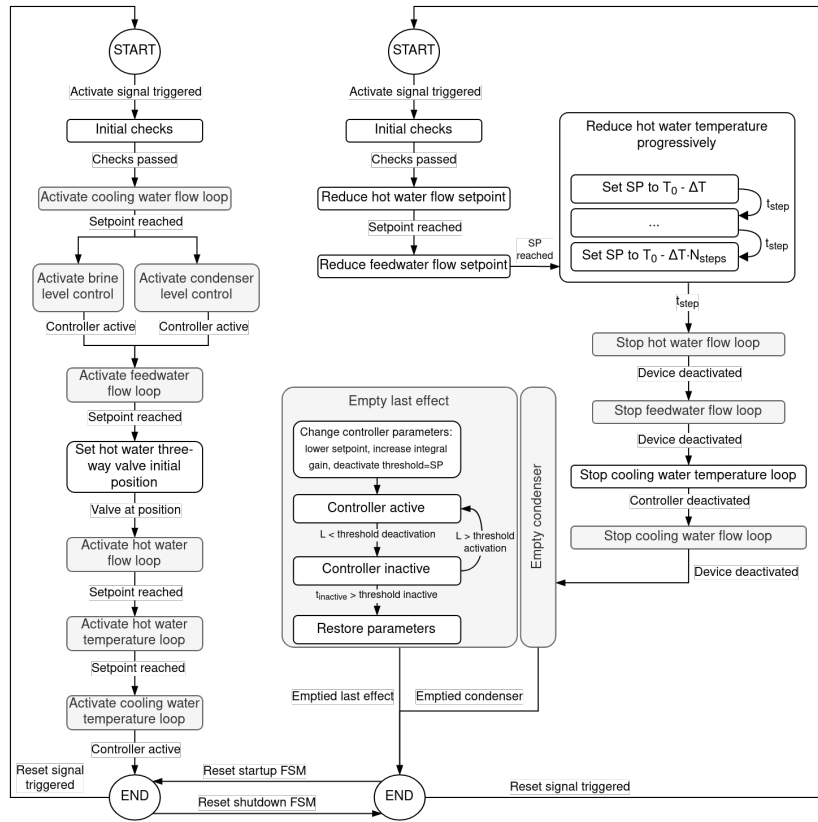


Figure 14.7: Flowchart of finite state machines for plant start-up (left) and shutdown (right)

In Figure 14.9 the activation sequence can be visualized at the beginning of the test (09:49–10:00): extractions → cooling → feedwater and heat source. The Flows are activated in about two minutes followed by another minute for the inlet temperature. Then the system is left to stabilize. At 09:52 the delay between activating the feedwater and it reaching the last effect is completed and the brine extraction pump starts operating. Pressures, temperatures and the distillate level in the system progressively evolve up to 10:00 when the conditions are changed for the first operation point for the day. The distillate level control action is delayed further until 10:04 when the first distillate is produced.

Regarding the shutdown procedure, the two most delicate processes are the cooling of the first effect (which has the highest scaling potential if not done properly) and the complete draining of the last effect and condenser. For the gradual cooling of the first effect, after the plant shutdown signal, the hot water temperature is reduced in 5-minute steps starting from the last recorded value until a final temperature of 50°C is reached. To drain the levels, a reference value well below the normal operating level is set, and the controller parameters are changed to more aggressive ones. Additionally, the device is deactivated each time the reference is reached and is not reactivated until the level reaches a specified value. This activation and deactivation process continues while the feedwater finishes draining from the upper effects of the plant. Once the control system has been deactivated for longer than a preset time, the plant shutdown procedure is considered complete, and the level controller parameters are restored.

This procedure can be observed in Figure 14.9 starting from 13:07. After a decrease in flow rates, the first effect heat load is progressively decreased until 13:34. From this time, pumps are stopped and the extraction cycles begin as can be noted by the high oscillations in the *Electrical consumption – J_b* and *J_d* and *Levels*.

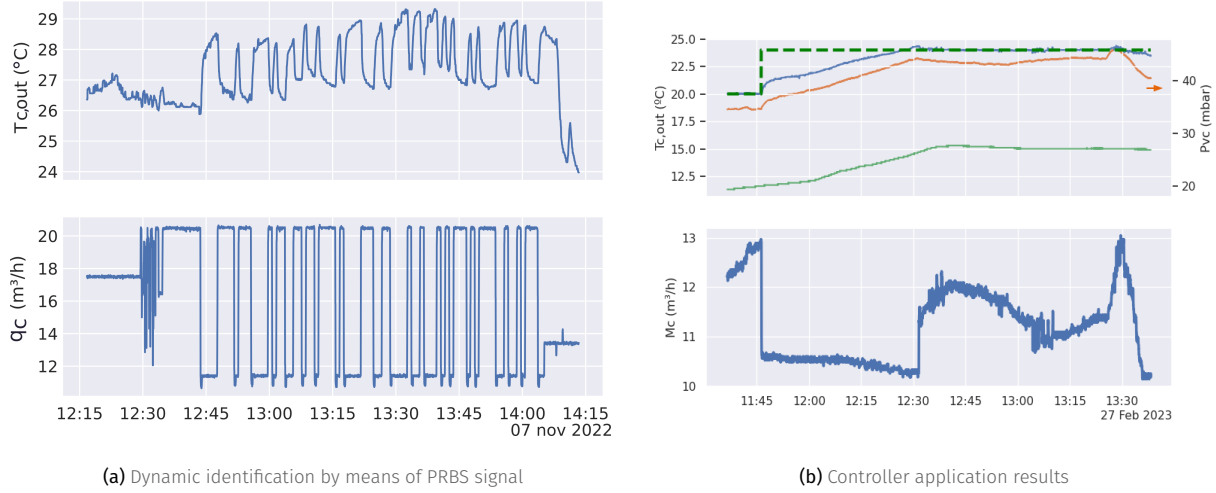


Figure 14.8: Condenser outlet temperature controller implementation. On (b) the perturbation (inlet temperature) is shown with a solid-green line, while the output (condenser outlet temperature) is shown with a solid-blue line. The reference is a thick dashed-green line.

Steady state identification. The steady state identification algorithm has been implemented in the control system. It allows the automatic detection of stable operation points. This is done by monitoring the KPVs and applying the algorithm described in Section 14.4.1. In Figure 14.9, steady state periods are highlighted with a yellow background, which indicates that the algorithm has detected a stable operation point. Two are detected, the first one from 11:00 to 11:55 and the second one from 12:16 to 12:59.

Control. In terms of control, a Proportional-Integral-Derivative controller (PID) control has been implemented to effectively regulate and maintain the desired setpoints of the subsystems mentioned in Section 14.4.2. This approach enables the system to respond quickly to changes, minimize steady state errors, reject disturbances, and enhance overall performance and reliability. Figure 14.8 shows the development procedure for one of the main loops, the condenser outlet temperature control. To tune the controller, the system was excited with a Pseudo-Random Binary Sequence (PRBS) signal (a), obtaining an ARX model ($n_a = 20$, $n_b = 49$, $n_k = 5$, 96.38% fit) using the *System Identification Toolbox* from MATLAB, this allowed to extract an approximate first-order dynamic with which to tune the controller. Figure 14.8 (b) shows the controller performance for a particular test. Initially, the control signal (q_c) increases to compensate for the trend observed in the condenser inlet temperature. At 11:45 the setpoint¹⁴ is changed to 24 °C, to which the controller immediately adapts by decreasing its input and allowing the temperature to increase. The system progressively evolves towards the new setpoint, reached at 12:30 the controller then maintains the desired temperature compensating for other - not shown in the figure - disturbances. A similar situation can be observed in the showcased test of Figure 14.9 – Temperatures and Flows. For the first operation point (11:00 onwards), the continuously increasing inlet temperature ($T_{c,in}$) is compensated by the controller, which increases the cooling flow rate to maintain the condenser outlet temperature at the setpoint. For the second operation point (12:16) the higher outlet temperature setpoint and turning on of the cooling tower allowing the inlet temperature to stabilize permits the controller to reduce the cooling flow rate and remain relatively unchanged.

14: i.e. reference

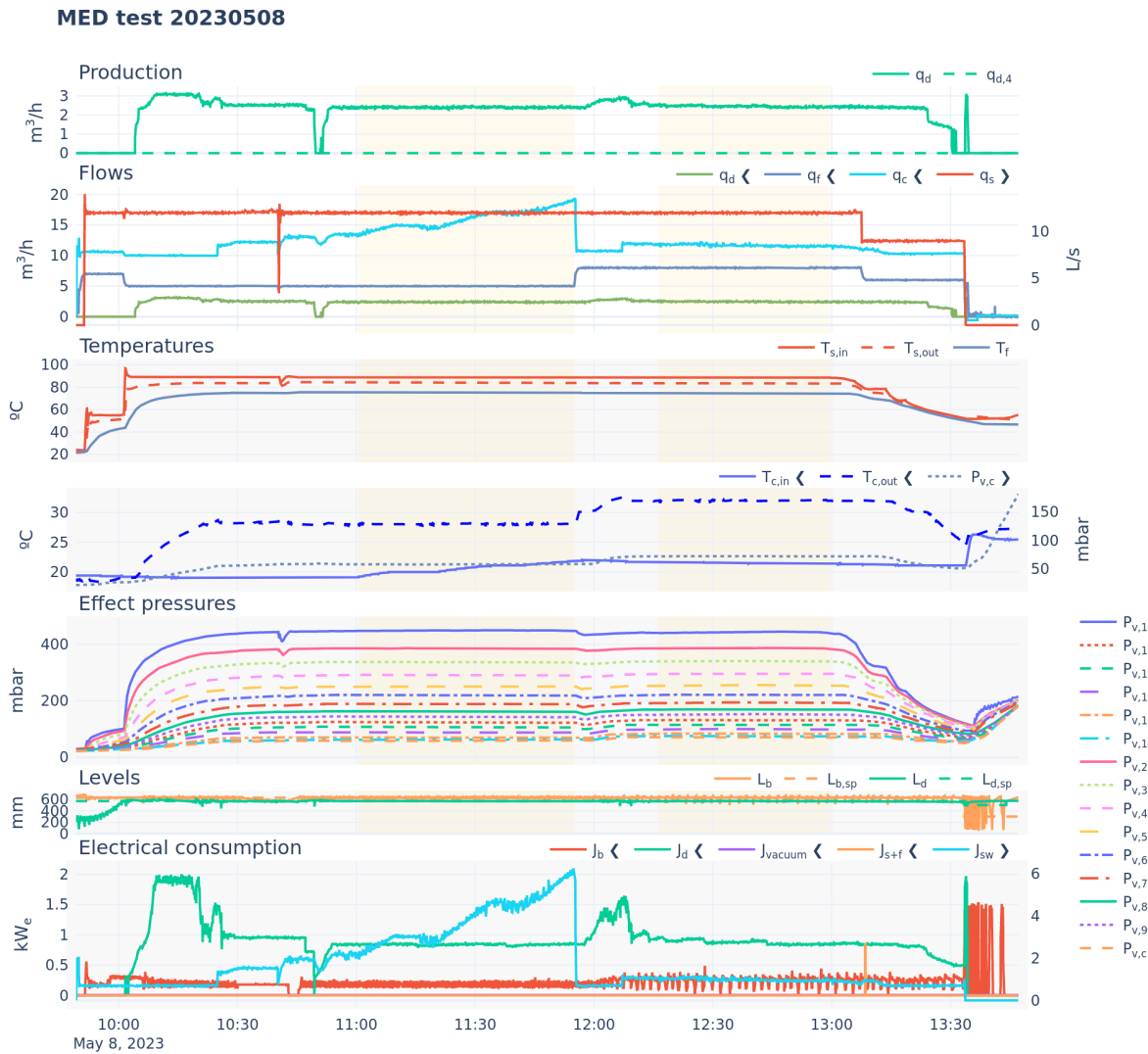


Figure 14.9: Test results. Several days available in interactive version



Reproducibility and the effect of the steady state duration

The operation points pairs 1–2 and 3–4 in Table 14.3 are the same test, *i.e.* the same operating conditions, but performed on different days. Particularly for 1–2, the duration of the steady state is significantly different (16 and 76 minutes, respectively). The obtained performance metrics are similar, with almost identical values for the energetic and separation metrics. Slight differences, but still within the uncertainty margin are observed in metrics influenced by electrical consumption—which vary between tests due to differences in the cooling water inlet temperature: 17 (1) vs 13 (2) m^3/h for the cooling water flow rate, translates into a 0.3% difference in second law efficiency and 0.1 KWh_e for SEEC. Inlet condenser temperature conditions are more similar in 3–4 (22.6 vs

Table 14.3: Measured variables and performance metrics for some operation points of the experimental campaign. The values are expressed as mean \pm standard deviation with a coverage factor of 2 (95% confidence interval). D is the duration of the steady state period.

	Test date (UTC)	D (min)	Performance metrics						
			GOR (-)	STEC (kW _{th})	SEEC (kW _e)	RR (-)	RI (-)	η_{II} (%)	SEXC (kWh _{ex} /m ³)
1	20230331 12:15	16	11 \pm 1	60 \pm 6	3.9 \pm 0.2	29 \pm 1	0.35 \pm 0.02	8.0 \pm 0.6	10.9 \pm 0.8
2	20230418 12:22	76	11 \pm 1	59 \pm 6	4.0 \pm 0.2	29 \pm 2	0.35 \pm 0.02	7.7 \pm 0.6	11.3 \pm 0.9
3	20230329 13:10	24	10.1 \pm 0.7	66 \pm 5	3.9 \pm 0.2	30 \pm 2	0.35 \pm 0.02	6.9 \pm 0.4	12.7 \pm 0.8
4	20230414 12:51	27	10.2 \pm 0.7	65 \pm 5	3.9 \pm 0.2	30 \pm 2	0.36 \pm 0.02	6.8 \pm 0.4	12.8 \pm 0.8
5	20230511 11:23	32	8.1 \pm 0.4	81 \pm 4	3.2 \pm 0.2	44 \pm 2	0.52 \pm 0.02	4.6 \pm 0.3	17.8 \pm 0.9
6	20230414 11:49	18	11 \pm 1	59 \pm 5	3.8 \pm 0.2	47 \pm 3	0.56 \pm 0.03	7.2 \pm 0.5	11.9 \pm 0.9
7	20230508 11:00	54	7.0 \pm 0.4	93 \pm 6	3.7 \pm 0.2	48 \pm 3	0.57 \pm 0.03	3.9 \pm 0.3	21 \pm 1

	Measured variables										
	$T_{c,in}$ (°C)	$T_{c,out}$ (°C)	q_s (L s ⁻¹)	q_f (m ³ h ⁻¹)	q_d (m ³ h ⁻¹)	$T_{s,out}$ (°C)	$T_{c,in}$ (°C)	w_f (mS cm ⁻¹)	w_d (μS cm ⁻¹)	q_c (m ³ h ⁻¹)	J (kW)
1	64.0 \pm 0.8	28.1 \pm 0.6	12.0 \pm 0.2	8.0 \pm 0.1	2.4 \pm 0.1	61.1 \pm 0.7	24.5 \pm 0.7	67.4 \pm 0.7	8.00 \pm 0.08	17 \pm 1	(8.0 \pm 0.2) \times 10 ³
2	64.0 \pm 0.7	28.0 \pm 0.6	12.0 \pm 0.3	8.0 \pm 0.1	2.3 \pm 0.1	61.2 \pm 0.7	23 \pm 1	67.4 \pm 0.7	8.00 \pm 0.08	13 \pm 2	(8.1 \pm 0.2) \times 10 ³
3	68.0 \pm 0.7	28.0 \pm 0.6	12.0 \pm 0.2	8.0 \pm 0.1	2.4 \pm 0.1	64.8 \pm 0.7	22.6 \pm 0.6	67.4 \pm 0.7	8.00 \pm 0.08	13.8 \pm 0.8	(8.1 \pm 0.2) \times 10 ³
4	68.0 \pm 0.7	27.9 \pm 0.8	12.0 \pm 0.3	8.0 \pm 0.1	2.4 \pm 0.1	64.8 \pm 0.6	21.4 \pm 0.8	67.4 \pm 0.7	8.00 \pm 0.08	10.9 \pm 0.9	(8.1 \pm 0.2) \times 10 ³
5	88.9 \pm 0.9	29 \pm 1	12.0 \pm 0.3	7.0 \pm 0.1	3.1 \pm 0.1	83.8 \pm 0.9	22 \pm 1	64.7 \pm 0.6	8.00 \pm 0.08	20.1 \pm 0.3	(7.9 \pm 0.3) \times 10 ³
6	68.0 \pm 0.7	28.0 \pm 0.5	12.0 \pm 0.3	5.0 \pm 0.1	2.4 \pm 0.1	65.2 \pm 0.7	20.8 \pm 0.6	67.4 \pm 0.7	8.00 \pm 0.08	10.1 \pm 0.4	(7.9 \pm 0.3) \times 10 ³
7	89.0 \pm 0.7	28.1 \pm 0.6	12.0 \pm 0.3	5.0 \pm 0.1	2.4 \pm 0.1	84.4 \pm 0.8	21 \pm 2	64.5 \pm 0.7	8.00 \pm 0.08	16 \pm 3	(7.8 \pm 0.3) \times 10 ³

21.4 °C), making differences for all metrics negligible.

Thus, it can be stated that the proposed methodology provides reproducible results and that the quality of stable operation and the ability to correctly identify it are of greater importance than the specific duration of the steady state.

14.5.2 Results analysis

In Table 14.3 operation points 4-5 and 6-7 compare low and high TBT operation. Two of them (4 and 6) receive heat at 68°C, while they differ in the feedwater flow rate (q_f), one (4) with a higher value (8 m³/h) and the other (6) at a lower one (5 m³/h). The other two operation points receive heat at 89°C and similar feedwater flow rate¹⁵. The first two operation points result in an approximate TBT of 61.5°C while the last two operation points have an approximate TBT of 79.2°C. This operation points selection is made to compare the performance of the plant at low and high TBT operation with otherwise equivalent conditions.

Performance analysis. The first immediate observation is that contrary to what stated in the introduction, the performance of the plant does not improve with higher heat source temperatures, on the contrary it decreases: GOR -20% and -36% for the low (4-5) and high (6-7) q_f scenario, respectively. Results are even worse in terms of second law efficiency: -32% and -46%, respectively, since higher quality heat is being destroyed. In summary, more energy, of better quality is being consumed to produce distillate less efficiently

This can be explained by the fact that the increase in the heat source temperature is not taken advantage of by introducing more effects, which would provide the increase in efficiency.

On the other hand, the concentration achieved does increase significantly for the high q_f scenario, with a 47% increase in the recovery ratio. This is not the case for the low q_f scenario, where the recovery ratio is similar to the low temperature operation point. A possible explanation is presented hereinafter.

Using a physical model of the plant¹⁶, a better insight into the inner working of the plant can be obtained. The model is based on the energy and mass balances of the system, and it is used to estimate different outputs at the effect level, such as the temperature and pressure of the vapor, the distillate production, and the brine concentration. This allows to analyze the temperature and concentration

15: Equal between 4 and 5, slightly different but comparable between 6 and 7

comprobar números

16: See Section ??

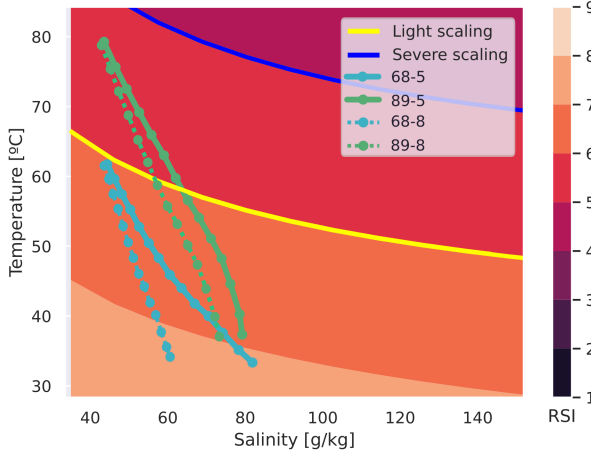


Figure 14.10: Temperature and concentration evolution for operation points at each effect in the MED plant. Surface represents the RSI.

evolution and visualize it as shown in Figure 14.10. According to the RSI, the high temperature operation points (5, 7) do get into the light scaling zone for the first 7 effects, while the low temperature operation points (4, 6) remain in the stable water zone for all effects.

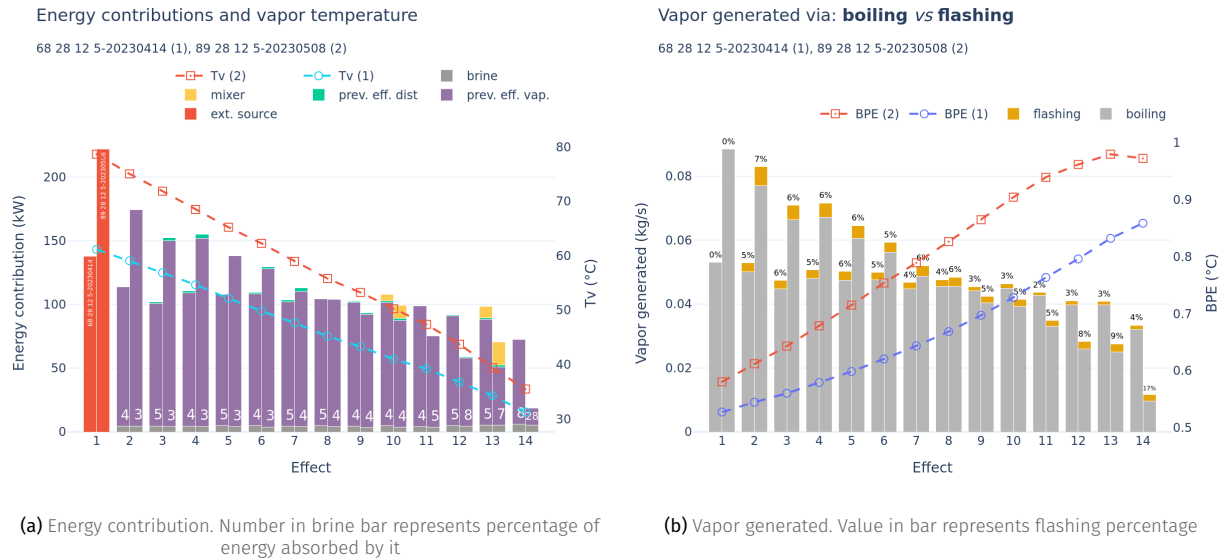


Figure 14.11: Per effect comparison between low and high TBT operation points

A per effect comparison can also be made in terms of energy contribution for vapor generation. This is shown in Figure 14.11 (a) for the low q_f scenario. In the first effect a stark difference between low and high operation can be seen, with almost double the power released, producing almost double the vapor (Figure 14.11 – (b)). However this difference is not maintained in the following effects, but an opposite trend is observed. Effect 8 is the crossing point and from there on the low temperature operation point produces more vapor. Another interesting comparison is the mixer energy contribution, the higher temperature of the distillate produced in the first effects becomes a significant contributor in the later effects, with a greater impact compared to the low temperature operation. Thus, distillate distribution is more effective when

total plant temperature differences are higher.

An explanation as to why vapor generation seems limited and thus the achieved concentration, can be the Boiling Point Elevation (BPE) of the brine (see Figure 14.11 (b)), which is a function of temperature and concentration, increasing with the latter. This means that the temperature difference between the brine and the vapor is reduced, and, which in turn reduces the boiling driving force. In the visualized case, the final BPE value for the low-temperature operation is reached by effect 9 of the high temperature one. In an MED plant, the vapor generated in the previous effect is the driving force for the next effect (Figure 14.11 – (a)), low vapor production on one effect means a diminished force for heat transfer in the next one, which in turn reduces the vapor production on that effect. It is an exponential decay process. That is why despite the larger energy availability in the first effects, the better balanced effects of the low temperature operation turns out to ultimately produce similar levels of separation [114].

[114]: Lienhard V (2019), "Energy Savings in Desalination Technologies"

In this figure, it can be seen than flashing takes a more relevant role in vapor generation in the latter effects of the high temperature alternative, since it is not affected by BPE (8,9 and 17% of the total vapor generated in effects 12, 13 and 14, respectively). This indicates that maybe flashing is a good alternative to increase the vapor production in the latter stages of a thermal brine concentrator plant.

Remark 14.5.1 A MED-MSF hybrid could be a good alternative to increase the brine concentration in the last effects, where the vapor production is limited by the BPE. Another option worth exploring is variable geometry effects, in order to increase temperature differences and maintain vapor production at higher concentrations.

Scaling assessment. To assess whether scaling occurred during high-temperature operation, control tests were conducted both before the high-temperature tests and repeated after about 30 hours of operation. In Table 14.3 the same operation points used to validate the reproducibility¹⁷, i.e.: 1-2 and 3-4 can be used to draw conclusions. Aside from the mentioned differences in metrics influenced by electrical consumption, the performance metrics values are consistent across tests, suggesting that the system is operating efficiently without significant fouling or scaling.

17: Section 14 (Reproducibility and the effect of the steady state duration)

Incluir una gráfica de los coeficientes de transferencia para ambos tests?

15.1 Introduction

The behavior of the SolarMED process can be abstracted into two components, a continuous and a discrete one. Each component is described and validated in the respective Section 15.2 (Dynamic modelling. Process variables) and Section 15.3 (Discrete modelling. Operation state) sections. Then, they are combined to create a complete model of the SolarMED process in Section 15.4 (Complete system model).

15.2 Dynamic modelling. Process variables

The dynamic behavior of the SolarMED determines the values of the process variables. This behavior is modelled by a set of models for each component of the SolarMED system. A discrete representation of the system is used, where the process variables are sampled at a fixed sample time, T_s , and systems are described by a set of difference equations. This is the case for most cases, but for some, even though this modelling component represents the dynamic behavior of the system, some models described in the following sections are steady-state models. This can lead to discrepancies between the model predictions and the actual system behavior, particularly during transient events. However, this is not deemed a significant limitation since the model is intended to be used for an optimization approach where the model sample rate is in the order of minutes, and inputs for slower component dynamics are changed sparingly, typically starting from 30 minutes and above, more than enough time for the system to reach steady state.

15.2.1 Solar field

The solar field is basically a converter of electrical to thermal energy dependent on the irradiance availability. The main outputs, in terms of operation of the solar field, are the thermal power obtained ($Q_{sf}(kW_{th})$), at what temperature that heat is obtained ($T_{sf,out}$) and the electricity needed to do so ($C_{e,sf}(kW_e)$).

The diagram illustrates the individual loops that make up the field. In the model, it is assumed that all loops have equal flow rates and temperatures (*i.e.*, a balanced flow distribution with similar collectors)¹. As a result, the system can be simplified to a single loop with a collector area equal to the sum of the collector areas of the individual rows of collector loops.

A first-principles based on the one presented in Ampuño et al. [115] is used to model the solar field. The model has two types of parameters: dynamic and constant. The dynamic parameters are the thermal loss coefficient ($H \left(\frac{J}{s \cdot ^\circ C} \right)$) which relates power losses to the environment and the collector conversion factor ($\beta(m)$) encompassing the collector transmisitivity and absorstancce. It determines the amount of irradiance that is transferred to the working fluid. These two dynamic parameters are calibrated using experimental data. The constant parameters are the ones defined in Table ??.

15.1	Introduction	115
15.2	Dynamic modelling	115
15.2.1	Solar field	115
15.2.2	Thermal storage	118
15.2.3	Heat exchanger	121
15.2.4	MED	122
15.3	Discrete modelling	123
15.3.1	Heat generation and storage subsystem (sfts)	123
15.3.2	Separation subsystem (med)	123
15.4	Complete system model	123
15.4.1	Validation	124

1: Which is the case in the experimental facility for loops 2 to 5, the ones used

[115]: Ampuño et al. (2018), “Modeling and Simulation of a Solar Field Based on Flat-Plate Collectors”

Model 15.1: Solar field

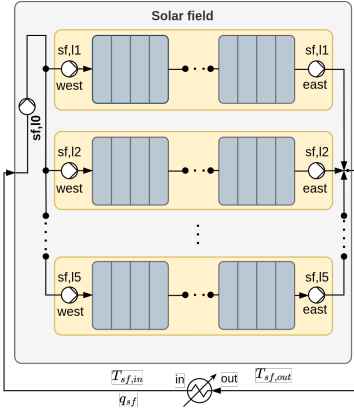


Figure 15.1: Solar field process diagram.

[116]: Ampuño et al. (2019), "Apparent Delay Analysis for a Flat-Plate Solar Field Model Designed for Control Purposes"

2: Transport delays are a common feature in dynamic systems, where the response of the system to an input is not instantaneous, but rather delayed by a certain amount of time. This delay can be caused by various factors, in this particular system, is due to the time it takes for the water to flow through the solar field and reach the temperature sensors. The apparent delay is the result of adding up the individual - different delays of each collector cell

[117]: Normey-Rico et al. (1998), "A Robust Adaptive Dead-Time Compensator with Application to A Solar Collector Field"

3: In reverse order, from newest to oldest

$$T_{\text{out}}(k) = \text{sf model}(T_{\text{out},k-1}, \mathbf{T}_{\text{in},k-n:k}, q_{k-n:k}, I_k, T_{\text{amb},k}; \beta, H, \theta)$$

$$L_{\text{pipe},eq} = \frac{T_s}{A_{\text{pipe},eq}} \sum_{k=0}^n q_{sf}[k] \quad \text{Equivalent pipe length [m]}$$

$$L_{eq} = n_{c,s} \cdot L_t \quad \text{Eq. collector tube length [m]}$$

$$c_f = n_{c-loop} \cdot n_{tub-c} \quad \text{Conversion factor [-]}$$

$$K_1 = \beta / (\rho \cdot c_p \cdot A_{cs}) \quad \text{Solar contribution [K·m²/J]}$$

$$K_2 = H / (L_{\text{pipe},eq} \cdot A_{cs} \cdot \rho \cdot c_p) \quad \text{Environment losses [1/s]}$$

$$K_3 = 1 / (L_{\text{pipe},eq} \cdot A_{cs} \cdot c_f) \cdot (1/3600) \quad \text{Heat absorbed [h/(3600·m³·s)]}$$

$$\begin{aligned} T_{\text{out}}(k) &= T_{\text{out}}(k-1) + \left(\right. \\ &\quad + K_1 \cdot I \\ &\quad - K_2 \cdot (\bar{T} - T_{\text{amb}}) \\ &\quad - K_3 \cdot q_{k-n_d} (T_{\text{out},k-1} - T_{\text{in},k-n_d}) \\ \left. \right) \cdot T_s \end{aligned}$$

The main difference with respect to the model presented in [115] is how the apparent transport delay is modelled [116]². In this implementation, the transport delay is simplified to a single steady state parameter based on the work presented in Normey-Rico et.al [117] since delays vary less than 30% from this nominal value.

The number of delay samples depends on the model sample time, and a system parameter called the equivalent length. For this work, the following procedure was followed to estimate it:

1. Using a reference test with a fixed sample time, T_s , the number of delay samples (n_d) was manually fitted to the data, by visually inspecting the response of the system to a step change in the input flow.
2. Estimate the equivalent length of the solar field by taking the average flow rate (\bar{q}_{sf}) across the delay samples span³, and divide it by a fixed parameter: the solar field pipe equivalent cross-sectional area ($A_{\text{pipe},eq}$).

$$\bar{q}_{sf} = \frac{\sum_{k=-n_d}^{k=0} q(k)/n_d}{n_d}$$

$$L_{\text{pipe},eq} = \frac{\bar{q}_{sf} \times T_s \times n_d}{A_{\text{pipe},eq}}$$

3. With this equivalent length ($L_{\text{pipe},eq}$), the number of delay samples can be estimated for any sample time T_s and flows vector \mathbf{q}_{sf} by iteratively adding the distance that flow travels at each sample time until the equivalent length is reached.

Electrical consumption

Definition 15.2.1 Step train test. Variations in the VFD pump speed from a minimum to a maximum value, with fixed increments.

The AQUASOL solar field is composed by a set of pumps that recirculate the water through the solar field. The pumps are controlled by VFDs that allow to vary the flow rate through the solar field. A main recirculation pump (P_{l0}) is responsible for the primary flow, while additional pumps (P_{l1}, P_{l2} , etc.) are used in the individual loops to either increase the total flow rate or to operate with the isolated loop. This redundancy means that the same flow rate can be achieved with different pump configurations.

Then, prior to modelling the electrical consumption of the solar field, a prior step is to characterize the electrical consumption of the system. This is done by determining the relationship between flow rate and power consumption for every configuration and to find the best configuration, that is, the one that minimizes the electrical consumption across the range of flow rates that the solar field operates at.



Figure 15.2: Solar field and thermal storage electrical characterization tests.



In order to characterize the electrical consumption of the solar field, a series of tests were performed as can be seen in Figure 15.2. The tests were carried out in two different dates since they have to be performed early, before the

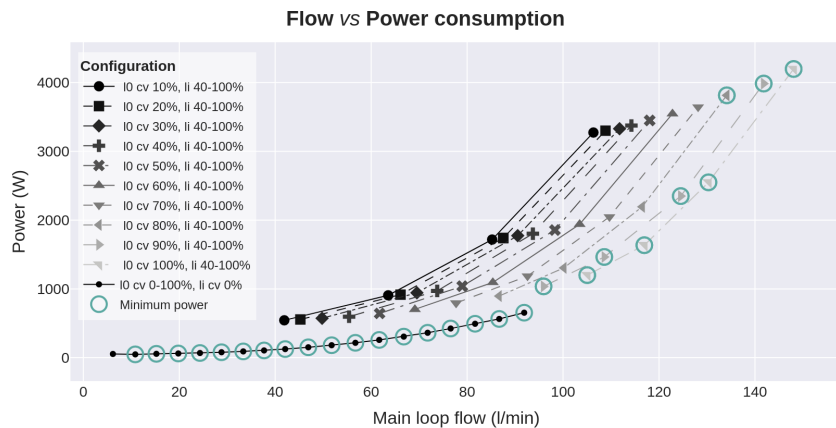


Figure 15.3: Solar field flow for different pump configurations and their associated power consumption.



4: observe the trend in Figure 15.2 - Temperatures

5: In Figure 15.2, from 20240927 07:35 to 08:20

solar field is irradiated by the sun and the field heats up⁴. In the first day, step trains are applied to the main loop and individual isolated loops (20240925 07:15 - 08:30). On the second day, different speeds levels were set for the main recirculation pump (10% - 100%, 10% increments) while step trains were applied to the individual loops (40% - 100%, 20% increments)⁵.

Figure 15.3 shows the relationship between flow rate and power consumptions for different configuration and pump speeds. Up to 90 l/min the best configuration is to just use the main recirculation pump. Above this flow rate, the main pump is used in combination with the individual loops. First a combination of main pump from 85 to 100% and individual loops at their 40% minimum speed, then the main pump at 100% and individual loops at increasing values up to 100%. With this selection, a two degree order polynomial regression is fitted to the data, as shown in Figure ??.

Summarizing, the electrical consumption of the solar field is modelled as a function of the flow rate through the solar field from a minimum value of XX m³/h to a maximum value of YY m³/h. This is achieved as a result of the combination of the main recirculation pump and the individual loops.

Model 15.2: Solar field electrical consumption

$$C_{e,sf} [kW_e] = sf \text{ electrical consumption} (q_{sf} [m^3/h])$$

$$C_{e,sf} = -8.48 \cdot 10^{-2} \cdot q_{sf}^3 + 2.29 \cdot 10^{-1} \cdot q_{sf}^2 + -8.72 \cdot 10^{-4} \cdot q_{sf} + 1.3 \cdot 10^{-5}$$

Validation

15.2.2 Thermal storage

A first-principles model of a two-tank thermal storage system, developed to capture the key thermodynamic and fluid dynamic phenomena governing energy transfer and stratification. The system is based on the design principles outlined by Duffie and Beckman[118], and consists of two thermally insulated tanks: a hot tank and a cold tank, each serving distinct roles in the thermal cycle. In normal operation, heat is extracted from the bottom of the cold tank, and after being heated, it is injected into the top of the hot tank. The load extracts heat from the top of the hot tank, and returns it to the bottom of the cold tank, completing

[118]: Duffie et al. (2013), "Energy Storage"



Figure 15.4: Solar field model validation for a particular test.



the cycle. The tanks are connected from top of the cold tank to the bottom of the hot tank, allowing for recirculation of the fluid between the two tanks.

The governing model equations and boundary conditions to simulate the transient thermal behavior of the storage system, including mass and energy balances, heat transfer mechanisms, and the stratification dynamics are shown in Model 15.3.

Similar to the solar field model, it has two parameters that need to be calibrated using experimental data and are considered dynamic and constant design parameters defined in Table ???. The dynamic parameters are the thermal loss coefficient (H_i ($\frac{J}{s \cdot C}$)) which relates heat losses to the environment and the volume of each of the considered control volumes (V_i). Three types of volumes are defined: the inner volume, the top volume and the bottom volume:

- ▶ Top volume (V_T): can receive external heat, and have heat extracted from it. It interacts with the inner volume that it interfaces with.
- ▶ Bottom volume (V_B): can also have external interactions, and exchanges with the inner volume above it.
- ▶ Inner volume (V_i): is any volume that is not the top or bottom, that is, is surrounded by other volumes with which it exchanges heat and mass by inner recirculation.

Esto debería probablemente ir en la parte de la instalación

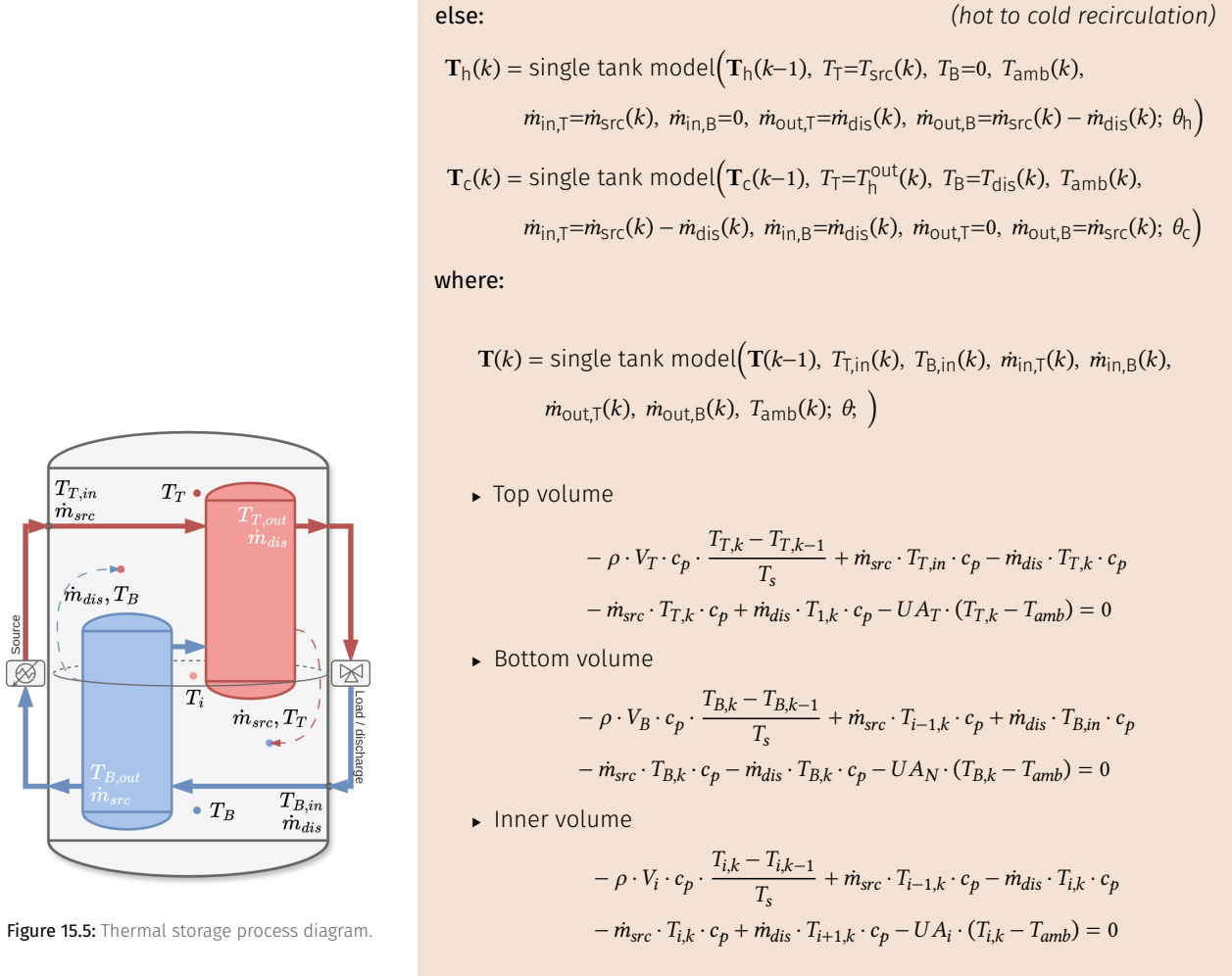
Model 15.3: Thermal storage

$$\mathbf{T}_h(k), \mathbf{T}_c(k) = \text{thermal storage model}(\mathbf{T}_h(k-1), \mathbf{T}_c(k-1), T_{src}(k), \\ T_{dis}(k), \dot{m}_{src}(k), \dot{m}_{dis}(k), T_{amb}(k); \theta_h; \theta_c)$$

if $\dot{m}_{dis}(k) > \dot{m}_{src}(k)$: *(cold to hot recirculation)*

$$\mathbf{T}_c(k) = \text{single tank model}(\mathbf{T}_c(k-1), T_T=0, T_B=T_{dis}(k), T_{amb}(k), \\ \dot{m}_{in,T}=0, \dot{m}_{in,B}=\dot{m}_{dis}(k), \dot{m}_{out,T}=\dot{m}_{dis}(k) - \dot{m}_{src}(k), \dot{m}_{out,B}=\dot{m}_{src}(k); \theta_c)$$

$$\mathbf{T}_h(k) = \text{single tank model}(\mathbf{T}_h(k-1), T_T=T_{src}(k), T_B=T_c^{out}(k), T_{amb}(k), \\ \dot{m}_{in,T}=\dot{m}_{src}(k), \dot{m}_{in,B}=\dot{m}_{dis}(k) - \dot{m}_{src}(k), \dot{m}_{out,T}=\dot{m}_{dis}(k), \dot{m}_{out,B}=0; \theta_h)$$



Three temperature sensors are available in the experimental facility, so three volume divisions are used to model the thermal storage. The model is based on

Electrical consumption

The first step train given in Figure 15.2 - 20250925 at 06:50 - 07:15 is used to characterize the electrical consumption of recirculating water ($q_{ts,src}$) in the thermal storage circuit. The electrical consumption is modelled as a function of the flow rate through the thermal storage from a minimum value of XX m³/h - XX kW_e to a maximum value of YY m³/h - YY kW_e.

Model 15.4: Thermal storage electrical consumption

$$C_{e,ts} [kW_e] = ts \text{ electrical consumption} (q_{ts,src} [m^3/h])$$

$$C_{e,ts} = 4.88 \cdot 10^{-1} \cdot q_{ts,src}^2 + -6.95 \cdot 10^{-3} \cdot q_{ts,src} + 0.01$$

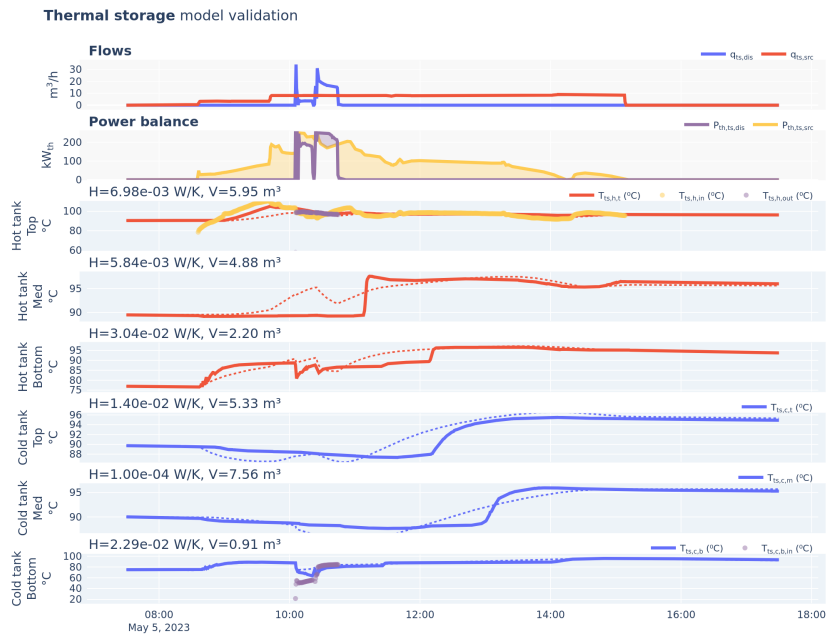


Figure 15.6: Thermal storage model validation for a particular test.



Validation

15.2.3 Heat exchanger

The solar field and thermal storage are interfaced by a Heat Exchanger (hex), particularly a counter-flow heat exchanger. The component is modelled using a first-principles steady state model based on the effectiveness-NTU method[119, 120].

[119]: Çengel et al. (2015), *Heat and Mass Transfer*

[120]: Kays et al. (1958), *Compact Heat Exchangers*

Modelling considerations [119]:

- ▶ It has been assumed that the rate of change for the temperature of both fluids is proportional to the temperature difference; this assumption is valid for fluids with a constant specific heat, which is a good description of fluids changing temperature over a relatively small range. However, if the specific heat changes, the Logarithmic Mean Temperature Difference (LMTD) approach will no longer be accurate.
- ▶ It has also been assumed that the heat transfer coefficient (U) is constant, and not a function of temperature.
- ▶ No phase change during heat transfer.
- ▶ Changes in kinetic energy and potential energy are neglected.

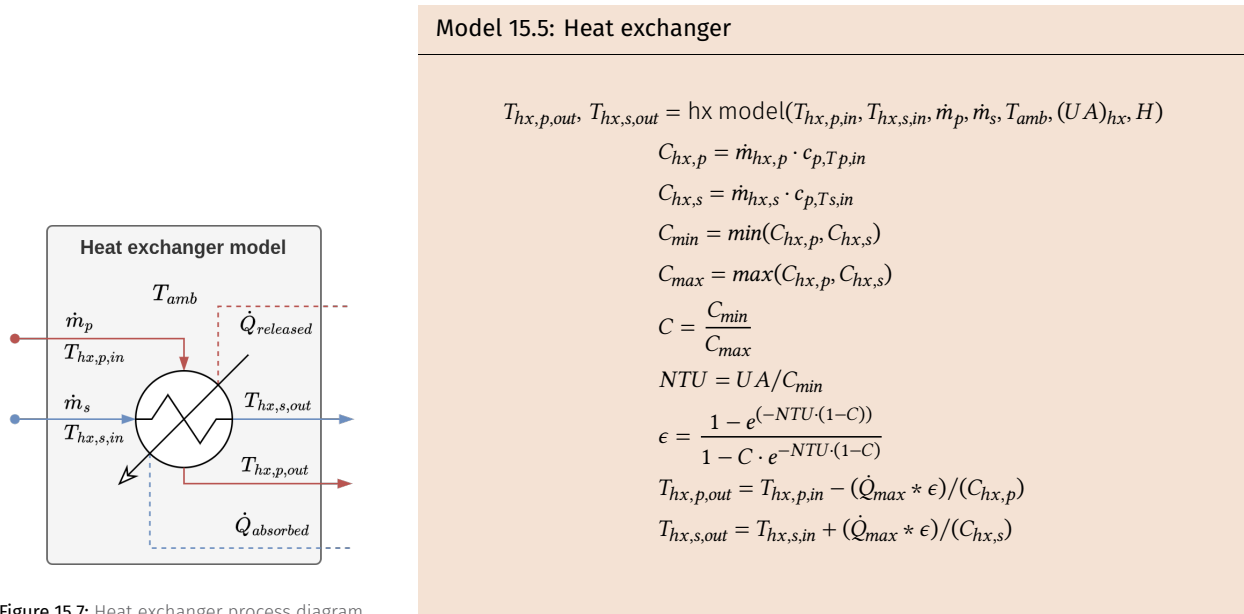


Figure 15.7: Heat exchanger process diagram.

Where p references the primary circuit (solar field side) and s the secondary circuit (thermal storage side). As shown in the Model 15.5, first the heat capacity C is determined in order to calculate the effectiveness (ϵ) of the heat exchanger. Finally, after determining the maximum heat transfer rate (\dot{Q}_{max}), the outlet temperatures can be obtained.

Validation

In order to calibrate the two parameters of this model (UA and H), one experimental test used where the parameters are varied in order to minimize the error between the model and the experimental data. The obtained values are shown in Table ?? and the dynamic behavior of the model is shown in Figure ???. It can be seen than the model performs fairly well even in transient conditions, with a mean absolute error of XX% and a coefficient of determination R^2 of YY%.

Several more tests are evaluated and the performance obtained is shown in Table ???. On average, the model has a mean absolute error of XX% and a coefficient of determination R^2 of YY%. The model is able to predict the outlet temperatures of the heat exchanger with a good accuracy, even in transient conditions, which is a good indication of the model's reliability.

15.2.4 MED

The MED is modelled statically, that is, considering that changes in the system operating conditions happen at a slow enough rate that the dynamic behavior between stable states can be neglected, and thus, only those stable states are considered. The model is a data driven one, specifically a GPR model calibrated using data from an experimental campaign in the pilot plant⁶.

6: Referencia a donde se mencione o algún artículo de Patricia

Electrical consumption

Validation

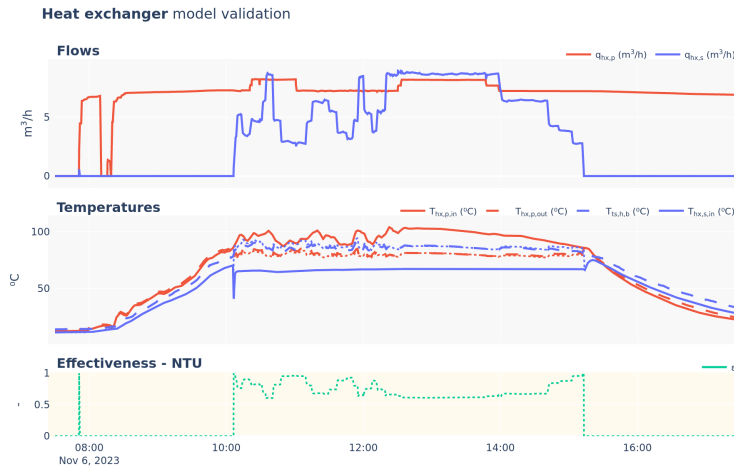


Figure 15.8: Heat exchanger model validation for a particular test.



15.3 Discrete modelling. Operation state

The second modelling component defines the discrete state of the system, that is, its *operation state*. This component is modelled by means of FSMs.

Reminder: FSMs

A finite state machine is a model of behavior composed of a finite number of states and *transitions* between those states. Within each state and transition some *action* can be performed^a.

^a See Section 3.6 (Hybrid modelling by means of FSMs) for a more detailed description.

The complete system is divided into two subsystems: the heat generation and storage subsystem and the separation subsystem.

15.3.1 Heat generation and storage subsystem (**sfts**)

This subsystem encompasses the Solar Field (**sf**) and the Thermal Storage (**ts**). The subsystem can be modelled with a simple FSM as shown in Figure ??, where the states are defined based on whether water is being recirculated in each circuit. Four states are defined as shown in Table 15.1.

15.3.2 Separation subsystem (**med**)

15.4 Complete system model

Aquí describir cómo se combinan los componentes en función del estado del sistema y cómo ello depende de las máquinas de estado finito.

To refer to the operational state of the system, a three digit number is used, where the first two digits represent the **sfts** state and the last one the **med** state. For example, the state **005** represents an inactive **sfts** subsystem with an active **med**. **101** represents a warming-up solar field while vacuum is being generated in the MED system.

Table 15.1: **sfts** FSM states definitions. \wedge represents the logical AND operator and \forall represents that all meet the condition.

State	Name	Condition
0	Off	$\forall q == 0$
1	Generating vacuum	$\text{med}_{\text{vac}} == 2$
2	Idle	$\forall q == 0 \wedge \text{med}_{\text{vac}} == 1$
3	Starting-up	$\forall q > q \wedge \text{med}_{\text{vac}} \geq 1 \wedge \forall T > T$
4	Shutting down	$\exists q < q$
5	Active	$\forall q > q \wedge \text{med}_{\text{vac}} \geq 1 \wedge \forall T > T$

Table 15.2: **med** FSM states definitions. \wedge represents the logical AND operator and \forall represents that all meet the condition.

State	Name	Condition
0	Off	$\forall q == 0$
1	Generating vacuum	$\text{med}_{\text{vac}} == 2$
2	Idle	$\forall q == 0 \wedge \text{med}_{\text{vac}} == 1$
3	Starting-up	$\forall q > q \wedge \text{med}_{\text{vac}} \geq 1 \wedge \forall T > T$
4	Shutting down	$\exists q < q$
5	Active	$\forall q > q \wedge \text{med}_{\text{vac}} \geq 1 \wedge \forall T > T$

Hello, here is some text without a meaning. This text should show what a printed text will look like at this place. If you read this text, you will get no information. Really? Is there no information? Is there a difference between this text and some nonsense like “Huardest gefburn”? Kjift – not at all! A blind text like this gives you information about the selected font, how the letters are written and an impression of the look. This text should contain all letters of the alphabet and it should be written in of the original language. There is no need for special content, but the length of words should match the language. Hello, here is some text without a meaning. This text should show what a printed text will look like at this place. If you read this text, you will get no information. Really? Is there no information? Is there a difference between this text and some nonsense like “Huardest gefburn”? Kjift – not at all! A blind text like this gives you information about the selected font, how the letters are written and an impression of the look. This text should contain all letters of the alphabet and it should be written in of the original language. There is no need for special content, but the length of words should match the language.

15.4.1 Validation

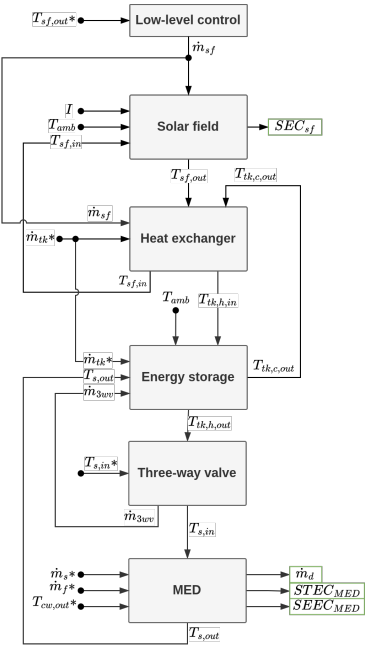


Figure 15.9: Complete SolarMED model architecture. TODO: Needs to be updated

TL;DR

This chapter describes a method to develop an operational strategy enabling the seamless integration of a solar driven MED system in an autonomous and optimal manner, including decisions on when to start or stop each subsystem and how to regulate them during operation.

The method is based on a hierarchical control approach consisting of three layers, where the upper operation plan solves a MINLP problem. Results for a week long simulation of the system are compared against two alternative strategies: a baseline operation and only operation optimization strategies show that the proposed method is able to significantly increase the water production by XX % by taking full advantage of the solar resource and flexibility of the thermal storage.

16.1	Introduction	125
16.2	Problem description	125
16.2.1	Implementation discussion .	126
16.3	Proposed strategy	128
16.4	Operation Plan Layer Description	129
16.4.1	Candidate problems generation	129
16.4.2	Update times generation . .	129
16.5	Operation optimization layer description	131
16.6	Optimization results	132
16.6.1	Choosing an algorithm . . .	132
16.6.2	Choosing a candidate problem	132
16.6.3	Simulation results	133
16.6.4	Performance comparison with alternative strategies	135

16.1 Introduction

LRoca, Carballo, Juan Diego

16.2 Problem description

The behavior of the SolarMED process is controlled by acting on two components, a discrete (operation state) and a continuous one (process variables).

The goal is to design an operational strategy that enables the seamless integration of both subsystems in an autonomous and optimal manner, including decisions on when to start or stop each subsystem and how to regulate them during operation. Therefore, considering the whole system as a MINLP optimization problem¹ that aims to maximize the water production while minimizing the (electrical) consumption of the system. Decisions on when to operate the system are weighted considering an optimization horizon, approximating the operation strategy of the system to the optimum:²

Problem: SolarMED

$$\min_{\mathbf{x}, \mathbf{e}; \theta} \quad J = f(\mathbf{x}, \mathbf{e}; \theta) = \sum_{i=1}^{n_{steps}} (J_{e,i} - J_{w,i})$$

with:

for $i = 1 \dots n_{steps}$:
 $J_{w,i} = q_{d,i} \cdot P_{w,i}$ if valid operation else 0
 $J_{e,i} = C_{e,i} \cdot P_{e,i}$
 $q_{d,i}, C_{e,i}$, valid operation = solarmed model($x_{c,i}, x_{p,i}, \dots$)

- Decision variables

$$\mathbf{x} = [\mathbf{med}_{mode}, \mathbf{sfts}_{mode}, \mathbf{qsf}, \mathbf{qts,src}, \mathbf{qmed,s}, \mathbf{qmed,f}, \mathbf{T}_{med,s,in}, \mathbf{T}_{med,c,out}]$$

1: See Section 5.2 (MINLP problems)

2: In general q represents flow rates while T are temperatures. Figure 13.1 can be consulted for subscript reference.

$\forall i = 1 \dots n_{steps}$ is a notation to indicate that a condition must be held at every step i in the optimization horizon (n_{steps}).
 Bold variables represent vectors.

where $\mathbf{x}_{nx \times \sum n_{updates,xi}} = [x_{1,i}, \dots, x_{1,n_{updates,x_1}}, \dots, x_{n_x,n_{updates,x_{n_x}}}]$

- ▶ Environment variables

$$\mathbf{e} = [\mathbf{I}, \mathbf{T}_{\text{amb}}, \mathbf{P}_e, \mathbf{P}_w]$$

where $\mathbf{e} = [e_{1,1}, \dots, e_{1,n_{steps}}, \dots, e_{n_e,n_{steps}}]$

- ▶ Fixed parameters ??

$$\theta = [R_p = 1, R_s = 0, \omega_{dc} = 0]$$

subject to:

- ▶ Box-bounds

- $\text{med}_{\text{mode}} \in [0, 1] \subset \mathbb{Z}$
- $\text{sfts}_{\text{mode}} \in [0, 1] \subset \mathbb{Z}$
- $q_{sf} \in [q_{sf}, \bar{q}_{sf}] \subset \mathbb{R}$
- $q_{ts,src} \in [q_{ts,src}, \bar{q}_{ts,src}] \subset \mathbb{R}$
- $q_{med,s} \in [q_{med,s}, \bar{q}_{med,s}] \subset \mathbb{R}$
- $q_{med,f} \in [q_{med,f}, \bar{q}_{med,f}] \subset \mathbb{R}$
- $T_{\text{med,s,in}} \in [T_{\text{med,s,in}}, \bar{T}_{\text{med,s,in}}] \subset \mathbb{R}$
- $T_{\text{med,c,out}} \in [T_{\text{med,c,out}}, \bar{T}_{\text{med,c,out}}] \subset \mathbb{R}$

valid operation conditions, $\forall i = 1 \dots n_{steps}$:

- ▶ $T_{sf,out} \leq \bar{T}_{sf,out}$

Where the objective is to minimize the cumulative cost of operation (J). Fresh water ($q_{med,d}$) sold (J_w) at price P_w is the negative term while electrical consumptions (C_e) at price P_e make up the positive cost term (J_e). The benefit (B) of operation is simply the inverse of the cost of operation.

The environment is represented by the vector \mathbf{e} , which includes the global solar irradiance (\mathbf{I}), ambient temperature (\mathbf{T}_{amb}), and the prices of water (\mathbf{P}_w) and electricity (\mathbf{P}_e).

The decision vector \mathbf{x} is composed of the decision variables for both the discrete and the continuous space. Two decision variables are defined to manipulate the discrete state of each subsystem defined in Section 15.3: med_{mode} and $\text{sfts}_{\text{mode}}$. These binary ($\subset \mathbb{Z}$) variables establish whether the particular subsystem is active ($x_i = 1$) or inactive ($x_i = 0$). This is directly related to the operation state of the particular subsystem³⁴ and accounted for in the models by the integrated finite-state machines as explained in Section 15.3. For the continuous space, the decision variables include the ones that define the operating conditions (i.e. operation point) of the MED system, and the two recirculation flow rates that determine the conditions of the heat source ($q_{sf}, q_{ts,src}$).

3: As defined in Tables 15.1 and 15.2

4: Once the values for these decision variables are provided, the low-level control layer is in charge of safely transitioning between operation states e.g. $\text{med}_{\text{mode}} : 0 \rightarrow 1$, med state: off → generating vacuum → starting-up → active

16.2.1 Implementation discussion

On the constraint handling

The reader might notice that no constraints are explicitly defined in the problem definition. This is because the constraints are implicitly defined in the model equations, which are used to evaluate the objective function. This design decision is motivated to avoid the need for a constraint-handling capable optimization algorithm, limiting the choice for an already complex MINLP problem⁵. Specifically, two aspects demand further consideration:

5: See Section 5.3 (A discussion on constraint handling) for a more detailed discussion on the topic

1. The decision value for the MED outlet condenser temperature ($T_{med,c,out}$) is not a direct input to the system, but rather a setpoint to be followed by a low-level control loop by manipulating the cooling water flow rate ($q_{med,c}$). This input might saturate and thus not be able to achieve the desired setpoint. In this case, a new value for the decision variable is computed, which is the minimum value that can be achieved (with $\overline{q_{med,c}}$).

In this case, the value used in the SolarMED and the output from the optimization to the low-level control layer would be the validated value for $T_{med,c,out}$. No additional actions are needed.

2. In the solar field, in order to not constantly interrupt the evaluation due to the solar field temperature going above $\overline{T}_{sf,out}$ (120 °C), the model saturates this temperature when going above and sets a flag. The limitation of this approach is that when there is low energy demand from the load, and likely because it favors energy transfer in the heat exchanger⁶, the optimizer tends to minimize the solar field flow, and systematically lets the solar field outlet temperature reach the limit. To avoid this situation, the positive term of the objective function is nullified in iterations where the constraint is not met.

Here, in order to ensure *valid operation* the fitness function is manipulated to de-incentivize decision variable values that lead to unfeasible operation.

6: greater temperature difference in primary side instead of greater mass flow rate with its associated increase in pumping power

On the prediction horizon

The problem is designed as an optimization problem with a shrinking horizon. The horizon size should be large enough so that decisions on how to operate the system are made with perspective, taking into account how they will affect the system in the future, but not so large that current decisions have no impact on the far future, and making the problem dimensionality become unmanageable.

For this case study, this parameter should be chosen based on the hours of capacity of the thermal storage to operate the MED system.

The thermal storage capacity is XXX which allows the system to operate with no supply from the solar field for up to XX hours. This means that depending on the charge state of the thermal storage, the system could start operation independently of the irradiance conditions, or operate at different levels of temperature. Considering this the optimization horizon, in time units, chosen was 36 hours. This means that if the optimization is evaluated at 5:00 on day 1, the fitness function is evaluated until 19:00 of day 2 *i.e.* including the end of operation for day 2.

Reminder: Shrinking horizon optimization

An optimization where the horizon end is fixed, and as time progresses, the start of the horizon moves forward.⁹

⁹ See Chapter 5 (Optimization overview)

On solving the optimization problem

Solving the optimization problem for this MINLP formulation presents significant challenges due to the combinatorial nature of the integer decision variables [121]. As shown in Figure 16.1, each combination of integer decisions, such as the operational modes of the separation subsystem (med_{mode}) and the solar field thermal storage subsystem ($sfts_{mode}$), leads to a different system trajectory along the prediction horizon⁷.

[121]: Grossmann (2021), Advanced Optimization for Process Systems Engineering

The number of possible operation trajectories increases exponentially with both the number of integer variables (n_{xi}) and the number of decision updates ($n_{updates,xi}$), following the expression⁸:

$$n_{problems} = n_{xi}^{n_{updates,xi}}. \quad (16.1)$$

7: This will be referred to as: **operation plan**

8: For example: $n_{updates,xi} = 6 \rightarrow n_{problems} = 64$, $n_{updates,xi} = 24 \rightarrow n_{problems} = 16\,777\,216$

This exponential growth makes the search space extremely large and complex.

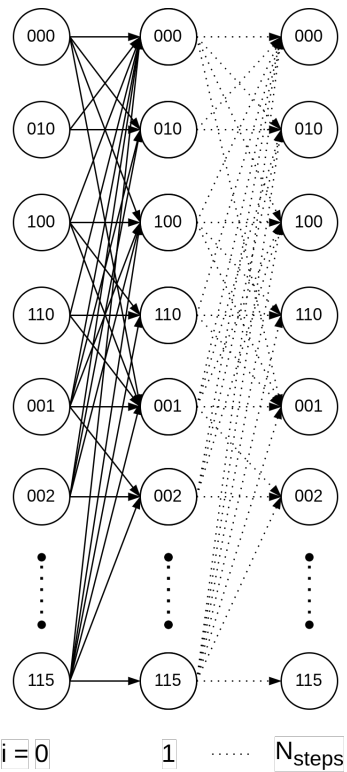


Figure 16.1: Decision tree resulting from the combinatorial nature of the integer part of the optimization problem. Text in nodes represents system states.

An important design consideration when solving the optimization problem is whether the sequence of integer decisions (*i.e.*, operational mode transitions over time) is predefined or whether the optimization algorithm is allowed to explore the decision tree freely and determine the optimal sequence. The latter case requires more computational effort but allows for potentially better-performing solutions by dynamically adjusting to system conditions.

On the decision variables update frequency

Apart from the integer decision variables, if a fixed decision variable update frequency is chosen for all continuous decision variables, the size of the decision vector for a large horizon like the one chosen can become large with diminishing returns. Instead, a new design parameter is introduced: the number of decision variable updates ($n_{updates,x_i}$) for each decision variable in the optimization problem.

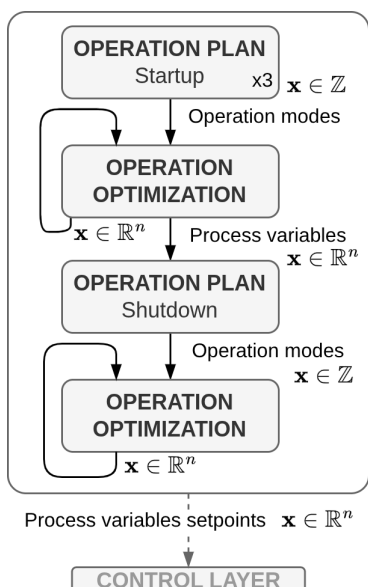
Thus, the decision vector is formed by each individual decision variable repeated as many times as updates for it:

$$X_{nx \times \sum n_{updates,xi}} = [x_{1,k}, \dots, x_{1,n_{updates,x_1}}, \dots, x_{n_x,n_{updates,x_n}}]$$

The number of updates of the decision variable ($n_{updates,x_i} \in [1, n_{steps}]$) can be chosen individually. More updates are assigned to variables regulating faster dynamics ($q_{sf}, q_{ts,src}$), and these updates of the decision variables are evenly distributed throughout the active period of the subsystem within the horizon. This is a crucial design consideration since otherwise the limited number of updates would be assigned to long inactive periods (between end of operation in day 1 and start on day 2).

It also means that the continuous component of the decision vector can only be assigned timestamps after the integer part is defined. Once timestamps are associated with each decision variable, the decision vector values can be resampled to match the desired sampling time of the optimization problem. This is done by forward filling [122] the values of the decision vector until the next update time.

16.3 Proposed optimization strategy



A hierarchical control approach (see Figure 16.2) was chosen consisting of three layers: operation plan, operation optimization, and control. This scheme was chosen for two main reasons. On the one hand, the time scales of the different aspects of the operation of the system (operation mode changes, process variables setpoint changes, regulatory control, respectively) can differ substantially. Secondly, it allows to abstract process complexity from the more computationally demanding upper layers by allocating it into the downstream layers. The operation plan layer makes decisions for the *operation modes*, the operation optimization layer sets the setpoints given to the continuous *process variables* that are to be followed by the low-level regulatory control layer.

Both operation plan and operation optimization layers share the same underlying problem structure, the difference being that the operation plan layer evaluates a predefined library of $n_{problems}$ combinations of the binary decision variables med_{mode} and $sfts_{mode}$ twice; once to decide the operation start, and another to end operation. The operation optimization layer periodically solves a single NLP problem with the selected values for these two variables fixed. They are further described in the following sections.

Figure 16.2: Proposed optimization strategy architecture

16.4 Operation Plan Layer Description

This layer determines the integer decision variables of the MINLP problem, namely, the sequence of operation modes producing an operation plan. To make the problem computationally tractable, only a limited number of combinations, $n_{problems}$, are evaluated. This transforms the mixed-integer problem into a simpler form by moving the integer variables from the decision to the environment space. In effect, the original MINLP is decomposed into a library of nNLP problems that are individually evaluated⁹.

To improve robustness, the layer can be evaluated multiple times (n_{evals}) under different scenarios—typically reflecting variations in forecasted environmental conditions. The final operation plan is selected as the best compromise across these scenarios.

The time required to perform this layer's computation is denoted $\Delta t_{eval,plan}$.

The number of updates available for each integer variable $n_{updates,xi}$ will be interchangeably referred to as Degrees of Freedom (DoF).

9: MINLP → nNLP

16.4.1 Candidate problems generation

Given the available computational resources and the complexity of the objective function, it has been found feasible to evaluate in the order of $n_{problems} \sim 100$ candidate combinations. This constraint informs how many DoF (*i.e.* number of updates available for the operation modes) can be defined by using Equation 16.1. The particular design choice for the number of updates per subsystem is shown in Table 16.1. In total, 101 distinct operation plans are generated for the start-up evaluation and 144 for the shutdown¹⁰.

Subsystem	Degrees of freedom				$n_{problems}$	
	Day 1		Day 2			
	Start	Stop	Start	Stop		
Evaluation: Start-up (1)	sfts	3	3	1	1	
	med	3	3	1	1	
Evaluation: Shutdown (2)	sfts	-	3	2	144	
	med	-	3	2	144	

10: Notice the total number does not match exactly Equation 16.1 since special cases are added (subsystem inactive)

Table 16.1: Operation plan. Start-up (1) and shutdown (2) degrees of freedom for changes in the operation state.

16.4.2 Update times generation

Up to this stage the operation plans generated just consist of a list of ones and zeros for each subsystem, indicating whether the subsystem is active or inactive in the particular update. The next step is to assign the operation mode updates to specific time instants, which then can be resampled to match the desired sampling time of the optimization problem¹¹.

In order to maintain the solution close to the optimal one, while keeping the number of problems reasonable, decision updates are distributed throughout the prediction horizon at strategic time instants. Since the case study system is fundamentally a solar process, the operation is strongly dependent on the irradiance availability, and thus operation changes are likely to take place at the start and end of the solar day.

The operation mode updates are distributed temporally as shown in Figure 16.3 (b) depending on the number of updates available (DoF). These update times are dependent on the solar irradiance profile and are bounded by lower- and upper-level thresholds. Depending on the plan action (start-up or shutdown), they are named early-late start or early-late stop thresholds, respectively.

In Figure 16.3 (b) up to three DoF are visualized. If only one update is available, the update time is set at the mean of the early and late thresholds. If two DoF are available, for the sfts subsystem, they are placed halfway between the

11: As with the continuous component of the decision vector, this is done by forward filling [122] the values of the decision vector until the next update time. This is also known as *Last Observation Carried Forward*

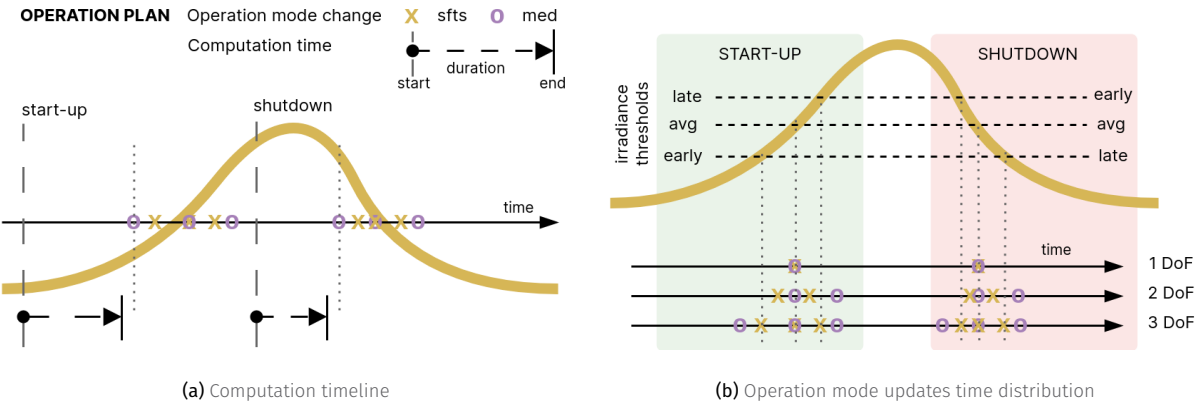


Figure 16.3: Operation plan layer computation and updates distribution. The yellow line represents the irradiance illustrating the solar day.

early threshold and the mean, and the late threshold and the mean, respectively. For the MED subsystem, updates are delayed. Finally, with three DoF, updates for the `sfts` subsystem are placed at the early, mean and late thresholds, while for the MED subsystem, the leftmost and rightmost updates are shifted to the left and right, respectively. If more updates for the particular action are available *i.e.* DoF, additional thresholds can be added.

Given a number of updates per subsystem and the update times assigned. The potential operation time change candidates are defined as:

$$t_{mode-change,candidates} = [t_0, t_1, \dots, t_{max(n_{updates}, \forall x_i)}]$$

Ordered in ascending order, where t_0 is the earliest potential operation change time and $t_{\max(n_{updates,V_i})}$ is the latest potential operation change time. Based on this definition, the earliest potential subsystem start-up would be at $t_{\uparrow,candidates}(0)$. Similarly, the earliest potential shutdown would be at $t_{\downarrow,candidates}(0)$.

Start-up

The most important aspect of this evaluation is to find the right time to bring the subsystems online, and secondary is to provide a preliminary estimate for their shutdown timing.

This is the first evaluation of the proposed methodology (see Figure 16.2) and is computed ahead of the first potential operation mode change (Figure 16.3 (a) - start-up), with enough lead time to complete the analysis before any potential change in operation mode ($t_{\text{candidates}}(0)$):

$$t = t_{\uparrow, \text{candidates}}(0) - (\Delta t_{\text{eval, plan}} \times n_{\text{evals}})$$

Being the earliest evaluation, it has the longest prediction horizon and thus the highest predicted variables uncertainty. As a counterpart, as shown in Figure 16.3 (a), this early evaluation start allows sufficient computation time, even several hours in advance, to perform several evaluations. Specifically three evaluations (n_{evals}) are performed: a nominal scenario with the forecasted environmental conditions, a pessimist one with a 20% decrease in the expected solar irradiance and finally an optimist one with a 20% increase in the expected solar irradiance.

Shutdown

A second evaluation is performed later in the day (see Figure 16.2), before system shutdown. This aims to determine the most suitable time to stop operations using the most recent system state information. It includes DoF regarding the operation schedule for the following day, allowing the shutdown decision for day 1 to account for its impact on the start and end times of day 2¹².

12: See Table 16.1

Only one evaluation is performed, as the uncertainty in the prediction horizon is significantly lower than in the start-up evaluation. It is evaluated in parallel to the operation optimization layer and just before the earliest expected shutdown time of the subsystems from Section 11 (Start-up), $t_{\downarrow, \text{candidates}}(0)$, considering subsystem shutdown.

$$t = t_{\downarrow, \text{candidates}}(0) - (\Delta t_{\text{eval, plan}} \times \text{somenumber})$$

Once computed the integer decision are updated in this layer. The faster the computation the better, since it will allow the operation optimization layer to optimize operation for the actual shutdown time and adapt accordingly.

16.5 Operation optimization layer description

As mentioned, this middle layer establishes the setpoints for the continuous process variables, *i.e.* the continuous part of the MINLP problem. The operation optimization layer evaluates periodically, with a sample time $T_{\text{eval, optim}}$, a NLP problem where the integer decision variables are fixed to the values provided by the operation plan layer¹³. It uses the latest available state of the system and environment predictions to evaluate the objective function.

13: It is exactly equivalent to the operation plan layer problem, just making $n_{\text{problems}} = 1$

The layer computation time is named $\Delta t_{\text{eval, optim}}$.

SolarMED optimization methodology

1. Generate operation mode change candidates based on the available updates per subsystem and irradiance thresholds.
2. Before the first potential operation change and considering the evaluation time, $t = t_{\uparrow, \text{candidates}}(0) - (\Delta t_{\text{eval, plan}} \times n_{\text{evals}})$, evaluate the operation plan layer to establish the operation start of the subsystems and an estimation of when to stop.
3. Before the established startup and considering the layer evaluation time, $t = t_{\uparrow} - \Delta t_{\text{eval, optim}}$, start evaluating the operation optimization layer periodically ($T_{\text{eval, optim}}$) to establish the setpoints for the continuous process variables.
4. Before the earliest subsystem projected shutdown and considering the operation optimization layer evaluation time, $t = t_{\downarrow, \text{candidates}}(0) - \Delta t_{\text{eval, plan}}$, evaluate the operation plan layer, in parallel to the operation optimization layer, to establish the shutdown time of the subsystems.
5. Continue evaluating the operation optimization layer periodically ($T_{\text{eval, optim}}$) until the last subsystem is shutdown.



Figure 16.4: Fitness evolution for a particular startup-problem

16.6 Optimization results

16.6.1 Choosing an algorithm

Once the optimization problem(s) is defined, an algorithm must be chosen that explores the solution space and finds a decision vector that minimizes the objective function.

The solution space has proven to be non-convex, with many local minimums (poor results were obtained when using local-gradient-based algorithms). The size of the decision vector depends on the active periods duration, around 120 elements. In addition, simulation of two days of operation (even when inactive periods are skipped) requires 5-10 seconds of computation time. Algorithm parallelization capabilities are of no use in this case, since many candidate problems will already be evaluated in parallel. The objective is then to find a global large-scale optimization algorithm that can find near-optimal solutions with 200 to 300 objective function evaluations (totaling 2-4 hours of computation time). In order to find the best algorithm, one of the candidate problems is arbitrary chosen and a library of global-evolutionary optimization algorithms is used from the PyGMO open-source Python library, specifically: Differential Evolution (DE), Self-adaptive DE (SADE), (N+1)-ES Simple Evolutionary Algorithm (SAE), Covariance Matrix Adaptation Evolution Strategy (CMA-ES) and Particle Swarm Optimization (PSO). Evolution results are shown in Fig.??, showcasing that for this particular problem the best alternative is the (N+1)-ES Simple Evolutionary Algorithm.

16.6.2 Choosing a candidate problem

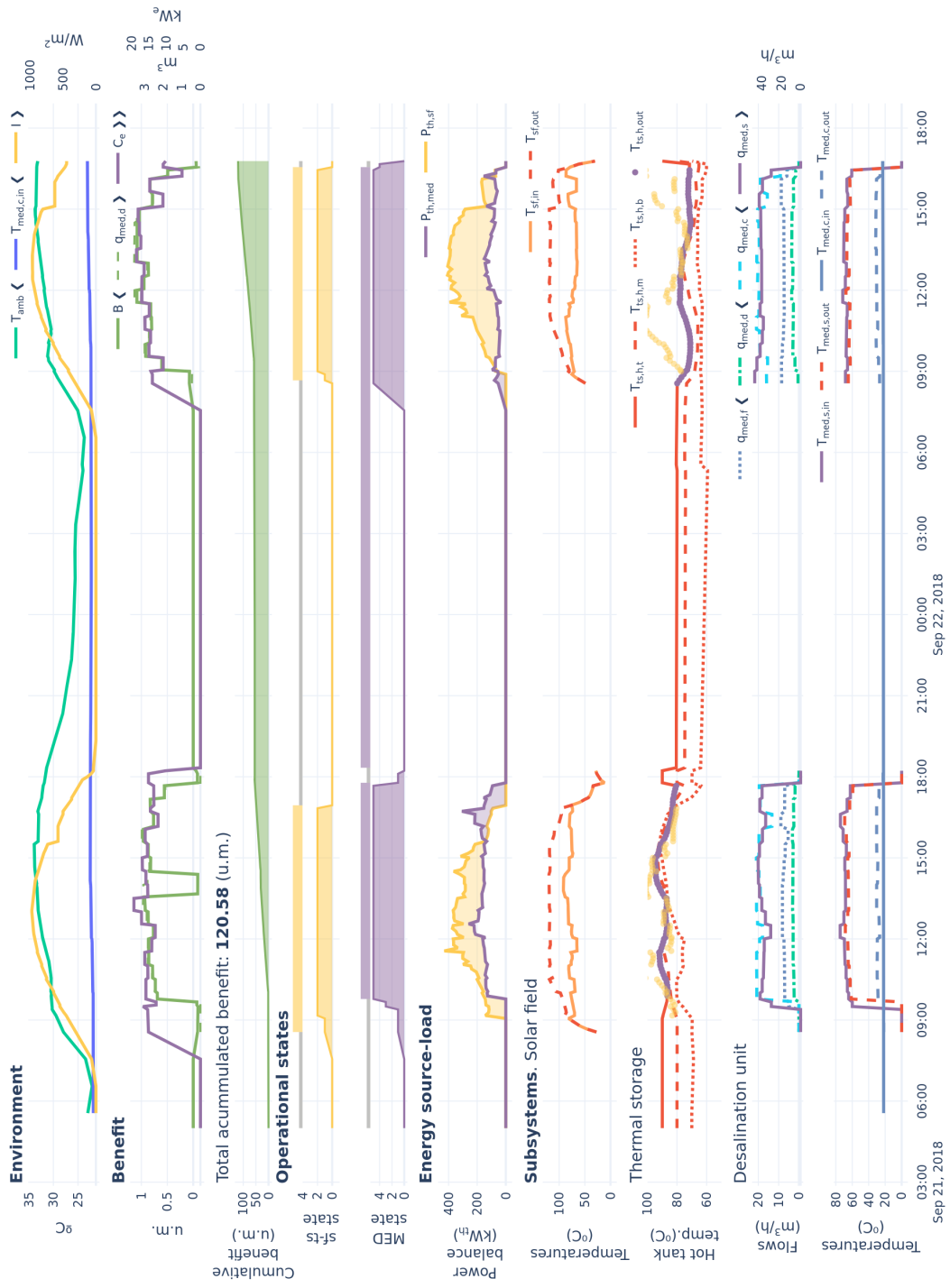
Once an algorithm was chosen, all $n_{problems}$ were evaluated where the algorithm is only required to choose values for the process variables (continuous). The results of this evaluation are shown in Fig.??, 101 problems were evaluated and visualized is their fitness evolution as a function of objective function evaluations. Problems 8, 18 and 48 resulted in the best fitness after the evolution process and their operation plan can be visualized in Fig. ??.

16.6.3 Simulation results

Figure ?? shows results for the simulated system in a total of X days. Where the first two days present favorable - sunny - conditions, followed by a cloudy day, and finishing with a sunny day (Figure ?? - *Environment*).

Solar MED optimal coupling

Evaluation results



16.6.4 Performance comparison with alternative strategies

baseline operation and just operation optimization

CONCLUSIONS AND OUTLOOK

Conclusions

Outlook and future work

Optimal water and electricity management in a combined cooling system

Improved Pareto front computation. In the current optimization implementation, the Pareto front for each step in the optimization horizon is constructed using a grid search over the decision space. This approach can become computationally expensive, especially as the grid resolution increases. Additionally, the Pareto front must be recalculated from scratch at every step, even though the sequential steps are often very similar—cost parameters remain constant, and only the thermal load and weather conditions change, typically with small variations. A more efficient solution would be to use a multi-objective optimization algorithm such as NSGA-II [[<empty citation>](#)], which can transfer evolved populations between successive evaluations, significantly reducing redundant computations.

<empty citation>

Better water management In the current implementation, the primary water source is distributed evenly each day, so the optimization process uses up the entire supply daily. However, a more intelligent daily distribution—essentially, a new optimization problem—could improve water management by allocating different amounts on different days, based on expected weather conditions and predicted generation. This approach would likely be incorporated as a new layer in the hierarchical control structure.¹⁴

Techno-economic analysis. The presented cooling alternatives comparative in this thesis focus on the operation cost of the system, but to get a better picture of the alternatives performance, a techno-economic analysis that includes the capital cost of the system and the expected lifetime of the components should be performed *i.e.* considering all costs associated with the system the plant's lifetime. This is currently being worked on as part of [SOLHycool], where the methodology presented here in terms of operation costs will be integrated in a techno-economic analysis for different case studies.

14: The resulting structure would be: 1. Water allocation, 2. CCS operation optimization, 3. CC regulatory control.

Energy management in MED processes driven by variable energy sources

Alternative configurations for an MED brine concentrator. Configuraciones alternativas para procesos MED para aplicaciones de concentración de salmueras: geometría variable de efectos, fuentes externas en efectos distintos al primero, acoplamiento con MSF para efectos posteriores.

Alternative configurations for solar-driven MED. Configuraciones alternativas para el proceso solar MED (almacenamiento con distintos puntos de carga y descarga, MED con distintos puntos de fuente externa, etc. Incluir diagrama de draw.io con las distintas configuraciones)

The layout configuration of the facility focused on reliability and simplifying operation and maintenance, not strictly on thermodynamic efficiency. The efficiency of the system could be improved:

1. if direct coupling between solar field and thermal storage was used, avoiding the heat exchanger energy transfer associated losses
2. thermal storage allowed charge and discharge from different levels, in order to take advantage of the temperature stratification and avoid fluid mixing

3.

4.

These decisions were made to, on the one hand allow to separate the solar field and thermal storage into two distinct decoupled circuits, providing flexibility, reducing the volume of additives required (only added to the solar field circuit), and operational flexibility (other external loads can be connected to the solar field when the MED is not being operated).

In conclusion this system, although improvable, allows to validate the feasibility of the proposed approach by means of the implementation of a suitable control system, in such a way, that the ideas and techniques presented in this work, could be directly extrapolated to a commercial system just by modifying some of the decision variables to suit the particular implementation.

Derived scientific contributions

1. Publicaciones en revista
2. Contribuciones a congreso
3. Coloquios doctorales
4. Colaboraciones en proyectos de investigación
5. Estancias de investigación
6. Repositorios de código
7. Repositorios de datos
8. Herramientas interactivas
9. Contribuciones a librerías de código abierto?

Bibliography

Here are the references in citation order.

- [1] Martin T. Hagan et al. *Neural Network Design*. Martin Hagan, 2014. 800 pp. (cited on pages 14, 15).
- [2] Mark Hudson Beale, Martin T Hagan, and Howard B Demuth. "Neural Network Toolbox." In: *User's Guide, MathWorks* 2 (2010), pp. 77–81 (cited on page 15).
- [3] Lonnie Hamm, B. Wade Brorsen, and Martin T. Hagan. "Comparison of Stochastic Global Optimization Methods to Estimate Neural Network Weights." In: *Neural Processing Letters* 26.3 (Dec. 1, 2007), pp. 145–158. doi: [10.1007/s11063-007-9048-7](https://doi.org/10.1007/s11063-007-9048-7). (Visited on 03/16/2024) (cited on page 15).
- [4] R. Farmani and J.A. Wright. "Self-Adaptive Fitness Formulation for Constrained Optimization." In: *IEEE Transactions on Evolutionary Computation* 7.5 (Oct. 2003), pp. 445–455. doi: [10.1109/TEVC.2003.817236](https://doi.org/10.1109/TEVC.2003.817236). (Visited on 03/31/2025) (cited on page 22).
- [5] Zong Woo Geem, Joong Hoon Kim, and G.V. Loganathan. "A New Heuristic Optimization Algorithm: Harmony Search." In: *SIMULATION* 76.2 (Feb. 1, 2001), pp. 60–68. doi: [10.1177/003754970107600201](https://doi.org/10.1177/003754970107600201). (Visited on 06/16/2025) (cited on page 22).
- [6] Francesco Biscani and Dario Izzo. "A Parallel Global Multiobjective Framework for Optimization: Pagmo." In: *Journal of Open Source Software* 5.53 (2020), p. 2338. doi: [10.21105/joss.02338](https://doi.org/10.21105/joss.02338) (cited on page 22).
- [7] Shahab Rohani et al. "Optimization of Water Management Plans for CSP Plants through Simulation of Water Consumption and Cost of Treatment Based on Operational Data." In: *Solar Energy* 223 (July 15, 2021), pp. 278–292. doi: [10.1016/j.solener.2021.05.044](https://doi.org/10.1016/j.solener.2021.05.044). (Visited on 06/17/2025) (cited on pages 27, 30, 32, 35, 36, 53).
- [8] Carrie Schoeneberger et al. "Solar for Industrial Process Heat: A Review of Technologies, Analysis Approaches, and Potential Applications in the United States." In: *Energy* 206 (2020), p. 118083. doi: [10.1016/j.energy.2020.118083](https://doi.org/10.1016/j.energy.2020.118083). (Visited on 08/07/2025) (cited on page 27).
- [9] IEA SHC. *Solar Heat Worldwide* 2025. 2025 (cited on page 28).
- [10] Richard Thonig and Johan Lilliestam. "Concentrating Solar Technology Policy Should Encourage High Temperatures and Modularity to Enable Spillovers." In: *AIP Conference Proceedings* 2815.1 (Oct. 6, 2023), p. 050005. doi: [10.1063/5.0149423](https://doi.org/10.1063/5.0149423). (Visited on 06/13/2025) (cited on page 28).
- [11] Mark Mehos et al. "Concentrating Solar Power Best Practices Study." In: (2020). (Visited on 08/05/2025) (cited on page 28).
- [12] Mark Mehos et al. "Concentrating Solar Power Gen3 Demonstration Roadmap." In: (2017). doi: [10.2172/1338899](https://doi.org/10.2172/1338899). (Visited on 08/02/2025) (cited on page 28).
- [13] Stefan Pfenninger et al. "Potential for Concentrating Solar Power to Provide Baseload and Dispatchable Power." In: *Nature Climate Change* 4.8 (Aug. 2014), pp. 689–692. doi: [10.1038/nclimate2276](https://doi.org/10.1038/nclimate2276). (Visited on 08/08/2025) (cited on page 28).
- [14] Christian Binz et al. "Toward Technology-Sensitive Catching-Up Policies: Insights from Renewable Energy in China." In: *World Development* 96 (Aug. 1, 2017), pp. 418–437. doi: [10.1016/j.worlddev.2017.03.027](https://doi.org/10.1016/j.worlddev.2017.03.027). (Visited on 08/08/2025) (cited on page 28).
- [15] Johan Lilliestam et al. "The Near- to Mid-Term Outlook for Concentrating Solar Power: Mostly Cloudy, Chance of Sun." In: *Energy Sources, Part B: Economics, Planning, and Policy* 16.1 (2021), pp. 23–41. doi: [10.1080/15567249.2020.1773580](https://doi.org/10.1080/15567249.2020.1773580) (cited on pages 28, 29, 80).
- [16] Nuno Bento and Charlie Wilson. "Measuring the Duration of Formative Phases for Energy Technologies." In: *Environmental Innovation and Societal Transitions* 21 (Dec. 1, 2016), pp. 95–112. doi: [10.1016/j.eist.2016.04.004](https://doi.org/10.1016/j.eist.2016.04.004). (Visited on 08/08/2025) (cited on page 28).
- [17] Pere Mir Artigues, Pablo del Río González, and Nàtalia Caldés. *The Economics and Policy of Concentrating Solar Power Generation*. Springer Nature, 2019. (Visited on 08/08/2025) (cited on page 28).
- [18] Thomas M. Schmitt. "(Why) Did Desertec Fail? An Interim Analysis of a Large-Scale Renewable Energy Infrastructure Project from a Social Studies of Technology Perspective." In: *Local Environment* 23.7 (July 3, 2018), pp. 747–776. doi: [10.1080/13549839.2018.1469119](https://doi.org/10.1080/13549839.2018.1469119). (Visited on 08/08/2025) (cited on page 29).

- [19] IRENA. *Renewable Power Generation Costs in 2024*. 978-92-9260-669-5. Abu Dhabi, July 22, 2025. (Visited on 08/02/2025) (cited on pages 29, 30).
- [20] Franziska Schöniger et al. "The Need for Dispatchable RES: A Closer Look at the Future Role of CSP in Europe." In: *Renewable Energy Based Solutions*. Ed. by Tanay Sıdkı Uyar and Nader Javani. Cham: Springer International Publishing, 2022, pp. 219–239. doi: [10.1007/978-3-031-05125-8_8](https://doi.org/10.1007/978-3-031-05125-8_8). (Visited on 06/13/2025) (cited on page 29).
- [21] Javier Bonilla et al. "Feasibility and Practical Limits of Full Decarbonization of the Electricity Market with Renewable Energy: Application to the Spanish Power Sector." In: *Energy* 239 (Jan. 15, 2022), p. 122437. doi: [10.1016/j.energy.2021.122437](https://doi.org/10.1016/j.energy.2021.122437). (Visited on 08/09/2025) (cited on page 29).
- [22] IEA. "Net Zero by 2050 - A Roadmap for the Global Energy Sector." In: (2021) (cited on page 30).
- [23] IRENA. "World Energy Transitions Outlook 2024: 1.5°C Pathway." In: (2024) (cited on page 30).
- [24] Johan Lilliestam et al. "Scaling up CSP: How Long Will It Take?" In: *AIP Conference Proceedings* 2815.1 (Oct. 6, 2023), p. 050003. doi: [10.1063/5.0148709](https://doi.org/10.1063/5.0148709). (Visited on 06/13/2025) (cited on page 30).
- [25] China Solar Thermal Alliance. *Blue Book of China's Concentrating Solar Power Industry 2024*. 2024 (cited on page 30).
- [26] Samantha Kuzma et al. "Aqueduct 4.0: Updated Decision-Relevant Global Water Risk Indicators." In: (Aug. 16, 2023). (Visited on 08/09/2025) (cited on page 31).
- [27] Tarun Kumar Aseri, Chandan Sharma, and Tara C. Kandpal. "Condenser Cooling Technologies for Concentrating Solar Power Plants: A Review." In: *Environment, Development and Sustainability* 24.4 (Apr. 2022), pp. 4511–4565. doi: [10.1007/s10668-021-01678-5](https://doi.org/10.1007/s10668-021-01678-5). (Visited on 06/15/2025) (cited on pages 31, 34, 37).
- [28] J Meldrum et al. "Life Cycle Water Use for Electricity Generation: A Review and Harmonization of Literature Estimates." In: *Environmental Research Letters* 8.1 (Mar. 2013), p. 015031. doi: [10.1088/1748-9326/8/1/015031](https://doi.org/10.1088/1748-9326/8/1/015031). (Visited on 06/13/2025) (cited on pages 32, 79).
- [29] Antonio Colmenar-Santos et al. "Water Consumption in Solar Parabolic Trough Plants: Review and Analysis of the Southern Spain Case." In: *Renewable and Sustainable Energy Reviews* 34 (June 1, 2014), pp. 565–577. doi: [10.1016/j.rser.2014.03.042](https://doi.org/10.1016/j.rser.2014.03.042). (Visited on 06/02/2023) (cited on page 32).
- [30] Philipp Habl, Ana Blanco-Marigorta, and Berit Erlach. "Exergoeconomic Comparison of Wet and Dry Cooling Technologies for the Rankine Cycle of a Solar Thermal Power Plant." In: () (cited on page 32).
- [31] Lidia Martín and Mariano Martín. "Optimal Year-Round Operation of a Concentrated Solar Energy Plant in the South of Europe." In: *Applied Thermal Engineering* 59.1 (Sept. 25, 2013), pp. 627–633. doi: [10.1016/j.applthermaleng.2013.06.031](https://doi.org/10.1016/j.applthermaleng.2013.06.031). (Visited on 06/13/2025) (cited on pages 32, 53).
- [32] Richard Thonig, Alina Gilmanova, and Johan Lilliestam. *CSP.Guru* 2023-07-01. Zenodo, July 1, 2023. (Visited on 05/31/2025) (cited on pages 33, 34, 37, 80).
- [33] Javier Bonilla et al. "CSP Data: A Data Discovery Web Application of Commercial CSP Plants." In: (July 2024) (cited on pages 33, 34, 80).
- [34] C. Turchi. *Parabolic Trough Reference Plant for Cost Modeling with the Solar Advisor Model (SAM)*. NREL/TP-550-47605, 983729. July 1, 2010, NREL/TP-550-47605, 983729. doi: [10.2172/983729](https://doi.org/10.2172/983729). (Visited on 08/09/2025) (cited on page 33).
- [35] J Maulbetsch. *Comparison of Alternate Cooling Technologies for U.S. Power Plants: Economic, Environmental, and Other Tradeoffs*. 1005358. Palo Alto, CA: EPRI, Aug. 2004 (cited on pages 33, 34, 37).
- [36] J Maulbetsch. *Economic Evaluation of Alternative Cooling Technologies*. 1024805. Palo Alto, CA: Electric Power Research Institute (EPRI), Jan. 2012. (Visited on 08/09/2025) (cited on pages 33–35, 37, 54).
- [37] T Jászay. "Indusdustrial Review-Aus Der Industrie. The Air-Cooled Condensing Equipment" System Heller" a Comprehensive Survey." In: *Periodica Polytechnica Mechanical Engineering* 2.4 (1958), pp. 389–402 (cited on page 33).
- [38] A. Balogh and J. Budik. "Heller's Indirect Approach Widens Applicability of Dry Cooling." In: *Modern Power Systems* 26.7 (July 2006), ?? (Cited on page 33).
- [39] O. O. Mil'man and P. A. Anan'ev. "Air-Cooled Condensing Units in Thermal Engineering (Review)." In: *Thermal Engineering* 67.12 (Dec. 1, 2020), pp. 872–891. doi: [10.1134/S0040601520120058](https://doi.org/10.1134/S0040601520120058). (Visited on 08/11/2025) (cited on page 33).
- [40] Nalogh Andras and Szabo Aoltan. "Advanced Heller System Technical Characteristics." 2005 (cited on page 33).

- [41] Mariano Martín. "Optimal Annual Operation of the Dry Cooling System of a Concentrated Solar Energy Plant in the South of Spain." In: *Energy* 84 (May 1, 2015), pp. 774–782. doi: [10.1016/j.energy.2015.03.041](https://doi.org/10.1016/j.energy.2015.03.041). (Visited on 06/12/2025) (cited on pages 34, 53).
- [42] Kelly Birkinshaw, Marwan Masri, and Robert L Therkelsen. "Comparison of Alternate Cooling Technologies for California Power Plants Economic, Environmental and Other Tradeoffs." In: (Feb. 2002) (cited on page 34).
- [43] M. C. Hu. *Engineering and Economic Evaluation of Wet/Dry Cooling Towers for Water Conservation*. COO-2442-1. United Engineers and Constructors, Inc., Philadelphia, PA (USA), Oct. 31, 1976. doi: [10.2172/7101949](https://doi.org/10.2172/7101949). (Visited on 08/09/2025) (cited on page 34).
- [44] F. R. Zaloudek et al. *Study of the Comparative Costs of Five Wet/Dry Cooling Tower Concepts*. BNWL-2122. Battelle Pacific Northwest Labs., Richland, WA (USA), Sept. 1, 1976. doi: [10.2172/7101320](https://doi.org/10.2172/7101320). (Visited on 08/09/2025) (cited on pages 34, 35).
- [45] W. V. Loscutoff. *Preliminary Evaluation of Wet/Dry Cooling Concepts for Power Plants*. BNWL-1969. Battelle Pacific Northwest Labs., Richland, Wash. (USA), Dec. 31, 1975. doi: [10.2172/7341661](https://doi.org/10.2172/7341661). (Visited on 08/09/2025) (cited on pages 34, 35).
- [46] L. E. Wiles et al. *Description and Cost Analysis of a Deluge Dry/Wet Cooling System*. PNL-2498. Battelle Pacific Northwest Labs., Richland, WA (USA), June 1, 1978. doi: [10.2172/6700397](https://doi.org/10.2172/6700397). (Visited on 08/10/2025) (cited on pages 34, 35).
- [47] Babak Golkar et al. "Determination of Optimum Hybrid Cooling Wet/Dry Parameters and Control System in off Design Condition: Case Study." In: *Applied Thermal Engineering* 149 (Feb. 25, 2019), pp. 132–150. doi: [10.1016/j.applthermaleng.2018.12.017](https://doi.org/10.1016/j.applthermaleng.2018.12.017). (Visited on 06/21/2025) (cited on pages 35, 53).
- [48] G. Barigozzi, A. Perdichizzi, and S. Ravelli. "Wet and Dry Cooling Systems Optimization Applied to a Modern Waste-to-Energy Cogeneration Heat and Power Plant." In: *Applied Energy* 88.4 (Apr. 1, 2011), pp. 1366–1376. doi: [10.1016/j.apenergy.2010.09.023](https://doi.org/10.1016/j.apenergy.2010.09.023). (Visited on 03/10/2023) (cited on page 35).
- [49] G. Barigozzi, A. Perdichizzi, and S. Ravelli. "Performance Prediction and Optimization of a Waste-to-Energy Cogeneration Plant with Combined Wet and Dry Cooling System." In: *Applied Energy* 115 (Feb. 15, 2014), pp. 65–74. doi: [10.1016/j.apenergy.2013.11.024](https://doi.org/10.1016/j.apenergy.2013.11.024). (Visited on 03/10/2023) (cited on pages 35, 53).
- [50] Patricia Palenzuela et al. "Experimental Assessment of a Pilot Scale Hybrid Cooling System for Water Consumption Reduction in CSP Plants." In: *Energy* 242 (Mar. 1, 2022), p. 122948. doi: [10.1016/j.energy.2021.122948](https://doi.org/10.1016/j.energy.2021.122948). (Visited on 03/10/2023) (cited on page 35).
- [51] Wanchai Asvapoositkul and Mantheerapol Kuansathan. "Comparative Evaluation of Hybrid (Dry/Wet) Cooling Tower Performance." In: *Applied Thermal Engineering* 71.1 (Oct. 5, 2014), pp. 83–93. doi: [10.1016/j.applthermaleng.2014.06.023](https://doi.org/10.1016/j.applthermaleng.2014.06.023). (Visited on 03/10/2023) (cited on pages 35, 36, 53).
- [52] Hemin Hu et al. "Thermodynamic Characteristics of Thermal Power Plant with Hybrid (Dry/Wet) Cooling System." In: *Energy* 147 (Mar. 15, 2018), pp. 729–741. doi: [10.1016/j.energy.2018.01.074](https://doi.org/10.1016/j.energy.2018.01.074). (Visited on 03/10/2023) (cited on pages 35, 53).
- [53] SPX Awarded Contract to Supply Parallel Condensing System For Crescent Dunes Solar Energy Project near Tonopah, Nevada. URL: https://www.powersystemsdesign.com/articles/spx-awarded-contract-to-supply-parallel-condensing-system-for-crescent-dunes-solar-energy-project-near-tonopah-nevada/8/3720?utm_source=chatgpt.com (visited on 08/12/2025) (cited on pages 37, 38).
- [54] Steinbeis 2i GmbH. Blog #29 – Full Scale Testing in Stellenbosch, South Africa | MinwaterCSP. Jan. 27, 2020. URL: <https://www.minwatercsp.eu/blog-29-full-scale-testing-in-stellenbosch-south-africa/> (visited on 08/02/2025) (cited on page 38).
- [55] UNE. *Thermal Performance Acceptance Testing of Mechanical Draught Series Wet Cooling Towers*. manual. UNE. 2004 (cited on page 41).
- [56] CTI. *Code Tower, Standard Specifications. Acceptance Test Code for Water Cooling Towers*. manual. Cooling Technology Institute. 2000 (cited on page 41).
- [57] Juan Miguel Serrano et al. "Wet Cooling Tower Performance Prediction in CSP Plants: A Comparison between Artificial Neural Networks and Poppe's Model." In: *Energy* (May 29, 2024), p. 131844. doi: [10.1016/j.energy.2024.131844](https://doi.org/10.1016/j.energy.2024.131844). (Visited on 05/30/2024) (cited on page 41).
- [58] Ashrae. "HVAC Systems and Equipment." In: *Chapter 36 Cooling Towers*. 2004 (cited on pages 41, 48).
- [59] M. Hosoz, H. M. Ertunc, and H. Bulgurcu. "Performance Prediction of a Cooling Tower Using Artificial Neural Network." In: *Energy Conversion and Management* 48.4 (Apr. 1, 2007), pp. 1349–1359. doi: [10.1016/j.enconman.2006.06.024](https://doi.org/10.1016/j.enconman.2006.06.024). (Visited on 03/08/2023) (cited on pages 42, 46).

- [60] F. Merkel. "Verdunstungskühlung." In: *VDI Zeitschrift Deutscher Ingenieure, Berlin, Alemania* (1925), pp. 123–128 (cited on pages 45, 47).
- [61] C Bourillot. "Hypotheses of Calculation of the Water Flow Rate Evaporated in a Wet Cooling Tower." In: (Aug. 1983) (cited on page 45).
- [62] H. Jaber and R. L. Webb. "Design of Cooling Towers by the Effectiveness-NTU Method." In: *Journal of Heat Transfer* 111.4 (Nov. 1989), pp. 837–843. doi: [10.1115/1.3250794](https://doi.org/10.1115/1.3250794) (cited on page 45).
- [63] M. Poppe and H. Rögner. "Berechnung von Rückkühlwerken." In: *VDI wärmeatlas* (1991), p. Mi 1 (cited on pages 46, 47).
- [64] J.C. Kloppers and D.G. Kröger. "A Critical Investigation into the Heat and Mass Transfer Analysis of Counterflow Wet-Cooling Towers." In: *International Journal of Heat and Mass Transfer* 48.3 (2005), pp. 765–777 (cited on page 46).
- [65] C. G. Cutillas et al. "Energetic, Exergetic and Environmental (3E) Analyses of Different Cooling Technologies (Wet, Dry and Hybrid) in a CSP Thermal Power Plant." In: *Case Studies in Thermal Engineering* 28 (Dec. 1, 2021), p. 101545. doi: [10.1016/j.csite.2021.101545](https://doi.org/10.1016/j.csite.2021.101545). (Visited on 03/27/2024) (cited on page 46).
- [66] Ming Gao et al. "Artificial Neural Network Model Research on Effects of Cross-Wind to Performance Parameters of Wet Cooling Tower Based on Level Froude Number." In: *Applied Thermal Engineering* 51.1 (Mar. 1, 2013), pp. 1226–1234. doi: [10.1016/j.applthermaleng.2012.06.053](https://doi.org/10.1016/j.applthermaleng.2012.06.053). (Visited on 03/08/2023) (cited on page 46).
- [67] Jialiang Song et al. "A Novel Approach for Energy Efficiency Prediction of Various Natural Draft Wet Cooling Towers Using ANN." In: *Journal of Thermal Science* 30.3 (May 2021), pp. 859–868. doi: [10.1007/s11630-020-1296-0](https://doi.org/10.1007/s11630-020-1296-0). (Visited on 03/04/2023) (cited on page 46).
- [68] P. Navarro et al. "Critical Evaluation of the Thermal Performance Analysis of a New Cooling Tower Prototype." In: *Applied Thermal Engineering* 213 (2022), p. 118719. doi: [10.1016/j.applthermaleng.2022.118719](https://doi.org/10.1016/j.applthermaleng.2022.118719) (cited on pages 46–48).
- [69] Faisal Asfand et al. "Thermodynamic Performance and Water Consumption of Hybrid Cooling System Configurations for Concentrated Solar Power Plants." In: *Sustainability* 12.11 (2020). doi: [10.3390/su12114739](https://doi.org/10.3390/su12114739) (cited on page 53).
- [70] Ayman Mdallal et al. "Modelling and Optimization of Concentrated Solar Power Using Response Surface Methodology: A Comparative Study of Air, Water, and Hybrid Cooling Techniques." In: *Energy Conversion and Management* 319 (Nov. 1, 2024), p. 118915. doi: [10.1016/j.enconman.2024.118915](https://doi.org/10.1016/j.enconman.2024.118915). (Visited on 06/17/2025) (cited on page 53).
- [71] Tao Tang et al. "Study on Operating Characteristics of Power Plant with Dry and Wet Cooling Systems." In: *Energy and Power Engineering* 5.4 (4 June 30, 2013), pp. 651–656. doi: [10.4236/epc.2013.54B126](https://doi.org/10.4236/epc.2013.54B126). (Visited on 06/13/2025) (cited on page 53).
- [72] David Wales and Jonathan Doye. "Global Optimization by Basin-Hopping and the Lowest Energy Structures of Lennard-Jones Clusters Containing up to 110 Atoms." In: *The Journal of Physical Chemistry A* 101.28 (July 1, 1997), pp. 5111–5116. doi: [10.1021/jp970984n](https://doi.org/10.1021/jp970984n). (Visited on 06/11/2025) (cited on page 60).
- [73] Chaouki Ghenai et al. "Performance Analysis and Optimization of Hybrid Multi-Effect Distillation Adsorption Desalination System Powered with Solar Thermal Energy for High Salinity Sea Water." In: *Energy* 215 (Jan. 15, 2021), p. 119212. doi: [10.1016/j.energy.2020.119212](https://doi.org/10.1016/j.energy.2020.119212). (Visited on 01/08/2023) (cited on page 95).
- [74] Hyuk Soo Son et al. "Pilot Studies on Synergetic Impacts of Energy Utilization in Hybrid Desalination System: Multi-effect Distillation and Adsorption Cycle (MED-AD)." In: *Desalination* 477 (Mar. 1, 2020), p. 114266. doi: [10.1016/j.desal.2019.114266](https://doi.org/10.1016/j.desal.2019.114266). (Visited on 01/07/2023) (cited on page 95).
- [75] Greg Burgess and Keith Lovegrove. "Solar Thermal Powered Desalination: Membrane versus Distillation Technologies." In: (Jan. 2000) (cited on page 95).
- [76] F. Silva Pinto and R. Cunha Marques. "Desalination Projects Economic Feasibility: A Standardization of Cost Determinants." In: *Renewable and Sustainable Energy Reviews* 78 (Oct. 2017), pp. 904–915. doi: [10.1016/j.rser.2017.05.024](https://doi.org/10.1016/j.rser.2017.05.024). (Visited on 07/27/2023) (cited on page 95).
- [77] Karan H. Mistry et al. "Entropy Generation Analysis of Desalination Technologies." In: *Entropy. An International and Interdisciplinary Journal of Entropy and Information Studies* 13.10 (2011), pp. 1829–1864. doi: [10.3390/e13101829](https://doi.org/10.3390/e13101829) (cited on page 95).
- [78] H. T. El-Dessouky and H. M. Ettouney. *Fundamentals of Salt Water Desalination*. Elsevier, Mar. 20, 2002. 691 pp. (cited on pages 95, 97, 107).
- [79] A. Christ, K. Regenauer-Lieb, and H.T. Chua. "Thermodynamic Optimisation of Multi Effect Distillation Driven by Sensible Heat Sources." In: *Desalination* 336.1 (2014), pp. 160–167. doi: [10.1016/j.desal.2013.12.006](https://doi.org/10.1016/j.desal.2013.12.006) (cited on pages 95, 97).

- [80] John H. Lienhard et al. "Thermodynamics, Exergy, and Energy Efficiency in Desalination Systems." In: *Lienhard via Angie Locknar* (2017). (Visited on 04/04/2022) (cited on pages 95, 96, 101).
- [81] Andrew T. Bouma, Jaichander Swaminathan, and John H. Lienhard V. "Metrics Matter: Accurately Defining Energy Efficiency in Desalination." In: *Journal of Heat Transfer* 142.12 (Oct. 7, 2020). doi: [10.1115/1.4048250](https://doi.org/10.1115/1.4048250). (Visited on 03/22/2023) (cited on pages 95, 97, 101).
- [82] M. A. Darwish, Faisal Al-Juwayhel, and Hassan K. Abdulraheim. "Multi-Effect Boiling Systems from an Energy Viewpoint." In: *Desalination* 194.1 (June 10, 2006), pp. 22–39. doi: [10.1016/j.desal.2005.08.029](https://doi.org/10.1016/j.desal.2005.08.029). (Visited on 06/01/2022) (cited on pages 96, 101).
- [83] Muhammad Wakil Shahzad, Muhammad Burhan, and Kim Choom Ng. "A Standard Primary Energy Approach for Comparing Desalination Processes." In: *npj Clean Water* 2.1 (Jan. 7, 2019), pp. 1–7. doi: [10.1038/s41545-018-0028-4](https://doi.org/10.1038/s41545-018-0028-4). (Visited on 07/23/2024) (cited on page 96).
- [84] Doriano Brogioli, Fabio La Mantia, and Ngai Yin Yip. "Thermodynamic Analysis and Energy Efficiency of Thermal Desalination Processes." In: *Desalination* 428 (Feb. 15, 2018), pp. 29–39. doi: [10.1016/j.desal.2017.11.010](https://doi.org/10.1016/j.desal.2017.11.010). (Visited on 01/05/2023) (cited on pages 96, 107).
- [85] K.S. Spiegler and Y.M. El-Sayed. "El-Sayed, Y.M.: The Energetics of Desalination Processes. Desalination 134, 109-128." In: *Desalination* 134 (Apr. 1, 2001), pp. 109–128. doi: [10.1016/S0011-9164\(01\)00121-7](https://doi.org/10.1016/S0011-9164(01)00121-7) (cited on page 96).
- [86] Mostafa H. Sharqawy, John H. Lienhard V, and Syed M. Zubair. "On Exergy Calculations of Seawater with Applications in Desalination Systems." In: *International Journal of Thermal Sciences* 50.2 (Feb. 1, 2011), pp. 187–196. doi: [10.1016/j.ijthermalsci.2010.09.013](https://doi.org/10.1016/j.ijthermalsci.2010.09.013). (Visited on 03/22/2023) (cited on pages 96, 100).
- [87] Mostafa H. Sharqawy, Syed M. Zubair, and John H. Lienhard. "Formulation of Seawater Flow Exergy Using Accurate Thermodynamic Data." In: *Prof. Lienhard via Angie Locknar* (Nov. 2010). (Visited on 04/13/2023) (cited on page 96).
- [88] Karan H. Mistry and John H. Lienhard V. "Effect of Nonideal Solution Behavior on Desalination of a Sodium Chloride (NaCl) Solution and Comparison to Seawater." In: *Karan Mistry* (Nov. 2012). (Visited on 04/22/2023) (cited on page 96).
- [89] Karan H. Mistry and John H. Lienhard. "Generalized Least Energy of Separation for Desalination and Other Chemical Separation Processes." In: *Entropy. An International and Interdisciplinary Journal of Entropy and Information Studies* 15.6 (2013), pp. 2046–2080. doi: [10.3390/e15062046](https://doi.org/10.3390/e15062046) (cited on page 96).
- [90] Gregory P. Thiel et al. "Energy Consumption in Desalinating Produced Water from Shale Oil and Gas Extraction." In: *Desalination. Energy and Desalination* 366 (June 15, 2015), pp. 94–112. doi: [10.1016/j.desal.2014.12.038](https://doi.org/10.1016/j.desal.2014.12.038). (Visited on 03/06/2023) (cited on pages 96, 99, 101).
- [91] Loreto Valenzuela, Rafael López-Martín, and Eduardo Zarza. "Optical and Thermal Performance of Large-Size Parabolic-Trough Solar Collectors from Outdoor Experiments: A Test Method and a Case Study." In: *Energy* 70 (June 1, 2014), pp. 456–464. doi: [10.1016/j.energy.2014.04.016](https://doi.org/10.1016/j.energy.2014.04.016). (Visited on 07/17/2024) (cited on page 96).
- [92] Christoph Prahl, Christoph Happich, and Jesús Fernández. *Protocol for Characterization of Complete Solar Concentrators Using Photogrammetry or Deflectometry*. WP14 – Task 14.2. DLR, Feb. 2018 (cited on page 96).
- [93] Rocío Bayón and Esther Rojas. "Development of a New Methodology for Validating Thermal Storage Media: Application to Phase Change Materials." In: *International Journal of Energy Research* 43.12 (2019), pp. 6521–6541. doi: [10.1002/er.4589](https://doi.org/10.1002/er.4589). (Visited on 07/17/2024) (cited on page 96).
- [94] Karan H. Mistry and John H. Lienhard. "An Economics-Based Second Law Efficiency." In: *Entropy* 15.7 (7 July 2013), pp. 2736–2765. doi: [10.3390/e15072736](https://doi.org/10.3390/e15072736). (Visited on 03/22/2023) (cited on page 97).
- [95] Alexander Christ et al. "Techno-Economic Analysis of Geothermal Desalination Using Hot Sedimentary Aquifers: A Pre-Feasibility Study for Western Australia." In: *Desalination* 404 (Feb. 17, 2017), pp. 167–181. doi: [10.1016/j.desal.2016.11.009](https://doi.org/10.1016/j.desal.2016.11.009). (Visited on 01/05/2023) (cited on page 97).
- [96] Alexander Christ, Klaus Regenauer-Lieb, and Hui Tong Chua. "Application of the Boosted MED Process for Low-Grade Heat Sources – A Pilot Plant." In: *Desalination. Energy and Desalination* 366 (June 15, 2015), pp. 47–58. doi: [10.1016/j.desal.2014.10.032](https://doi.org/10.1016/j.desal.2014.10.032). (Visited on 01/04/2023) (cited on page 97).
- [97] Alexander Christ, Klaus Regenauer-Lieb, and Hui Tong Chua. "Boosted Multi-Effect Distillation for Sensible Low-Grade Heat Sources: A Comparison with Feed Pre-Heating Multi-Effect Distillation." In: *Desalination. Energy and Desalination* 366 (June 15, 2015), pp. 32–46. doi: [10.1016/j.desal.2014.12.047](https://doi.org/10.1016/j.desal.2014.12.047). (Visited on 01/04/2023) (cited on page 97).
- [98] Edward Jones et al. "The State of Desalination and Brine Production: A Global Outlook." In: *Science of The Total Environment* 657 (Mar. 20, 2019), pp. 1343–1356. doi: [10.1016/j.scitotenv.2018.12.076](https://doi.org/10.1016/j.scitotenv.2018.12.076). (Visited on 06/29/2022) (cited on page 98).

- [99] Patricia Palenzuela, Diego-César Alarcón-Padilla, and Guillermo Zaragoza. *Concentrating Solar Power and Desalination Plants*. Oct. 9, 2015 (cited on pages 98, 102).
- [100] John H. Lienhard V et al. "SOLAR DESALINATION." In: *Annual Review of Heat Transfer* 15 (2012). doi: [10.1615/AnnualRevHeatTransfer.2012004659](https://doi.org/10.1615/AnnualRevHeatTransfer.2012004659). (Visited on 10/17/2024) (cited on page 99).
- [101] Qian Chen et al. "A Zero Liquid Discharge System Integrating Multi-Effect Distillation and Evaporative Crystallization for Desalination Brine Treatment." In: *Desalination* 502 (Apr. 2021), p. 114928. doi: [10.1016/J.DESAL.2020.114928](https://doi.org/10.1016/J.DESAL.2020.114928) (cited on page 100).
- [102] Adrian Bejan. *Advanced Engineering Thermodynamics*. John Wiley & Sons, 2016 (cited on page 100).
- [103] JCGM 100:2008. *GUM 1995 with Minor Corrections. Evaluation of Measurement Data — Guide to the Expression of Uncertainty in Measurement*. Joint Committee for Guides in Metrology, 2008. URL: https://www.bipm.org/documents/20126/2071204/JCGM_101_2008_E.pdf/325dcaad-c15a-407c-1105-8b7f322d651c (cited on page 104).
- [104] Ralph C. Smith. *Uncertainty Quantification: Theory, Implementation, and Applications*. SIAM, Dec. 2, 2013. 400 pp. (cited on page 104).
- [105] nist. "NIST Guidelines for Evaluating and Expressing the Uncertainty of NIST Measurement Results Cover." In: *NIST* (). (Visited on 06/16/2023) (cited on page 105).
- [106] JCGM101:2008. *Evaluation of Measurement Data — Supplement 1 to the "Guide to the Expression of Uncertainty in Measurement" — Propagation of Distributions Using a Monte Carlo Method*. Joint Committee for Guides in Metrology, 2008. URL: https://www.bipm.org/documents/20126/2071204/JCGM_101_2008_E.pdf/325dcaad-c15a-407c-1105-8b7f322d651c (cited on page 105).
- [107] Ulli Wolff. "Monte Carlo Errors with Less Errors." In: *Computer Physics Communications* 176.5 (Mar. 2007), p. 383. doi: [10.1016/j.cpc.2006.12.001](https://doi.org/10.1016/j.cpc.2006.12.001). (Visited on 06/19/2023) (cited on page 105).
- [108] Milan Korbel et al. "Steady State Identification for On-Line Data Reconciliation Based on Wavelet Transform and Filtering." In: *Computers & Chemical Engineering* 63 (Apr. 17, 2014), pp. 206–218. doi: [10.1016/j.compchemeng.2014.02.003](https://doi.org/10.1016/j.compchemeng.2014.02.003). (Visited on 12/14/2022) (cited on page 105).
- [109] Taiwen Jiang et al. "Application of Steady-State Detection Method Based on Wavelet Transform." In: *Computers & Chemical Engineering* 27.4 (Apr. 15, 2003), pp. 569–578. doi: [10.1016/S0098-1354\(02\)00235-1](https://doi.org/10.1016/S0098-1354(02)00235-1). (Visited on 01/03/2023) (cited on page 105).
- [110] Taiwen Jiang, Bingzhen Chen, and Xiaorong He. "Industrial Application of Wavelet Transform to the On-Line Prediction of Side Draw Qualities of Crude Unit." In: *Computers & Chemical Engineering* 24.2 (July 15, 2000), pp. 507–512. doi: [10.1016/S0098-1354\(00\)00520-2](https://doi.org/10.1016/S0098-1354(00)00520-2). (Visited on 12/27/2022) (cited on page 105).
- [111] Karl Johan Åström and Tore Hägglund. *PID Controllers: Theory, Design, and Tuning*. ISA - The Instrumentation, Systems and Automation Society, 1995 (cited on page 106).
- [112] Karan H. Mistry, Mohamed A. Antar, and John H. Lienhard V. "An Improved Model for Multiple Effect Distillation." In: *Desalination and Water Treatment* 51.4–6 (Jan. 1, 2013), pp. 807–821. doi: [10.1080/19443994.2012.703383](https://doi.org/10.1080/19443994.2012.703383). (Visited on 06/01/2022) (cited on page 107).
- [113] John W Ryznar. "A New Index for Determining Amount of Calcium Carbonate Scale Formed by a Water." In: *Journal-American Water Works Association* 36.4 (1944), pp. 472–483 (cited on page 107).
- [114] John H. Lienhard V. "Energy Savings in Desalination Technologies: Reducing Entropy Generation by Transport Processes." In: *Journal of Heat Transfer* 141.7 (May 17, 2019). doi: [10.1115/1.4043571](https://doi.org/10.1115/1.4043571). (Visited on 03/30/2023) (cited on page 114).
- [115] Gary Ampuño et al. "Modeling and Simulation of a Solar Field Based on Flat-Plate Collectors." In: *Solar Energy* 170 (Aug. 1, 2018), pp. 369–378. doi: [10.1016/j.solener.2018.05.076](https://doi.org/10.1016/j.solener.2018.05.076). (Visited on 03/17/2023) (cited on pages 115, 116).
- [116] Gary Ampuño et al. "Apparent Delay Analysis for a Flat-Plate Solar Field Model Designed for Control Purposes." In: *Solar Energy* 177 (Jan. 1, 2019), pp. 241–254. doi: [10.1016/j.solener.2018.11.014](https://doi.org/10.1016/j.solener.2018.11.014). (Visited on 03/15/2023) (cited on page 116).
- [117] Julio E. Normey-Rico et al. "A Robust Adaptive Dead-Time Compensator with Application to A Solar Collector Field1." In: *IFAC Proceedings Volumes*. IFAC Workshop on Linear Time Delay Systems (LTDS '98), Grenoble, France, 6–7 July 31.19 (July 1, 1998), pp. 93–98. doi: [10.1016/S1474-6670\(17\)41134-7](https://doi.org/10.1016/S1474-6670(17)41134-7). (Visited on 02/19/2024) (cited on page 116).
- [118] John A. Duffie and William A. Beckman. "Energy Storage." In: *Solar Engineering of Thermal Processes*. John Wiley & Sons, Ltd, 2013, pp. 373–408. doi: [10.1002/9781118671603.ch8](https://doi.org/10.1002/9781118671603.ch8). (Visited on 07/15/2025) (cited on page 118).

- [119] Yunus A. Çengel and Afshin J. Ghajar. *Heat and Mass Transfer: Fundamentals & Applications*. Fifth edition. New York, NY: McGraw Hill Education, 2015. 968 pp. (cited on page 121).
- [120] William Morrow Kays and Alexander Louis London. *Compact Heat Exchangers: A Summary of Basic Heat Transfer and Flow Friction Design Data*. McGraw-Hill, 1958. 180 pp. (cited on page 121).
- [121] Ignacio E. Grossmann. *Advanced Optimization for Process Systems Engineering*. Cambridge Series in Chemical Engineering. Cambridge: Cambridge University Press, 2021 (cited on page 127).
- [122] Rob J. Hyndman and George Athanasopoulos. *Forecasting: Principles and Practice*. 3rd ed. OTexts, 2021 (cited on pages 128, 129).

Alphabetical Index

preface, ix